COUPLING MATRIX BASED INTEGRATION OF THE ACTIVE COMPONENTS WITH MICROWAVE FILTERS

by

GAO, YANG

A thesis submitted to the University of Birmingham for the degree of Doctor of Philosophy

College of Engineering and Physical Sciences
University of Birmingham
March 2018

UNIVERSITY OF
BIRMINGHAM

University of Birmingham Research Archive

e-theses repository

This unpublished thesis/dissertation is copyright of the author and/or third parties. The intellectual property rights of the author or third parties in respect of this work are as defined by The Copyright Designs and Patents Act 1988 or as modified by any successor legislation.

Any use made of information contained in this thesis/dissertation must be in accordance with that legislation and must be properly acknowledged. Further distribution or reproduction in any format is prohibited without the permission of the copyright holder.

ABSTRACT

This thesis introduces novel integrated millimetre wave components for amplification and filtering. The conventional coupling matrix theory for passive filters is extended to the design of 'filter-amplifiers', which have both filtering and amplification functionalities. The design is based on the coupling matrix theory, and for this approach extra elements are added to the standard coupling matrix to represent the transistor. Based on the specification of the filter and small-signal parameters of the transistor, the active coupling matrices for the 'filter-amplifier' can be synthesised. Adopting the active coupling matrices, the resonators of the filter adjacent to the transistor and the coupling between them are modified mathematically to provide a Chebyshev filter response with amplification. Although the transistor has complex input and output impedances, it can be matched to the filters by choice of coupling structure and resonance frequency. This is particularly useful as the filter resonators can be of a different construction (e.g. waveguide) to the amplifier (e.g. microstrip).

An X-band waveguide filter amplifier and a microstrip filter amplifier are constructed as examples based on the active N+3 coupling matrix. An X-band waveguide filter amplifier using all resonators structure based on the N+4 coupling matrix is also implemented. Elements of the matching network are replaced by waveguide resonators, reducing the integrated device's size, increasing the port to port isolation and providing filtering. For waveguide amplifiers, it is also noted that high-Q waveguide resonators can be employed to offer lower loss impedance matching/filtering functions to the active components. The design methodology is expected to be especially useful at terahertz frequencies where waveguide is the choice of interconnection and low loss filtering and matching are critical.

ACKNOWLEDGEMENTS

I would like to express my sincerest gratitude to Professor Michal J Lancaster for his patient supervising and continuous support during my PhD study at the University of Birmingham. Without his assistance and encouragement, the work presented in this thesis may never have been accomplished.

I would also like to express my appreciation to my co-supervisor Dr Tim Jackson for his useful advice and to my academic advisor Professor Peter Gardener for his valuable suggestions on my PhD work. My appreciation also goes to my colleagues, Dr Jeffrey Powell, Dr Xiaobang Shang, Dr Fred Huang, Dr Wenlin Xia, Dr Cheng Guo and Dr Hao Yang for their encouragement and assistance. I would like to extend thanks to my colleagues in the Emerging Device Technology Research Group at the University of Birmingham.

My great gratitude goes to my family for their support and encouragement.

CONTENTS

CHAPTER 1
INTRODUCTION

1.1 Research Motivation

The terahertz (THz) frequency range covers 300 GHz to 10 THz, with the equivalent wavelength from 1 millimetre to 30 micrometres [1], [2]. Terahertz radiation is of interest in recent academic research as well as industry for its specific properties and wide applications, for example, in security scanning, medical imaging, short range communications, and high-altitude earth atmosphere observation [3], [4].

As the operating frequencies increase to the THz region, the conventional planar circuit is not a good choice due to its high loss. Waveguide based components are of interest where the lowest loss is required, and they are widely employed in submillimetre wave and terahertz applications [5]-[12].

Micromachining technologies have been investigated for various terahertz components at the University of Birmingham recently. Waveguide based THz components such as filters, mixers, triplers have all been demonstrated using a range of micromachining technologies, such as precision milling [5], SU-8 thick resist [6], and laser cutting [6]. Some of these structures are

presented in Fig. 1.1.

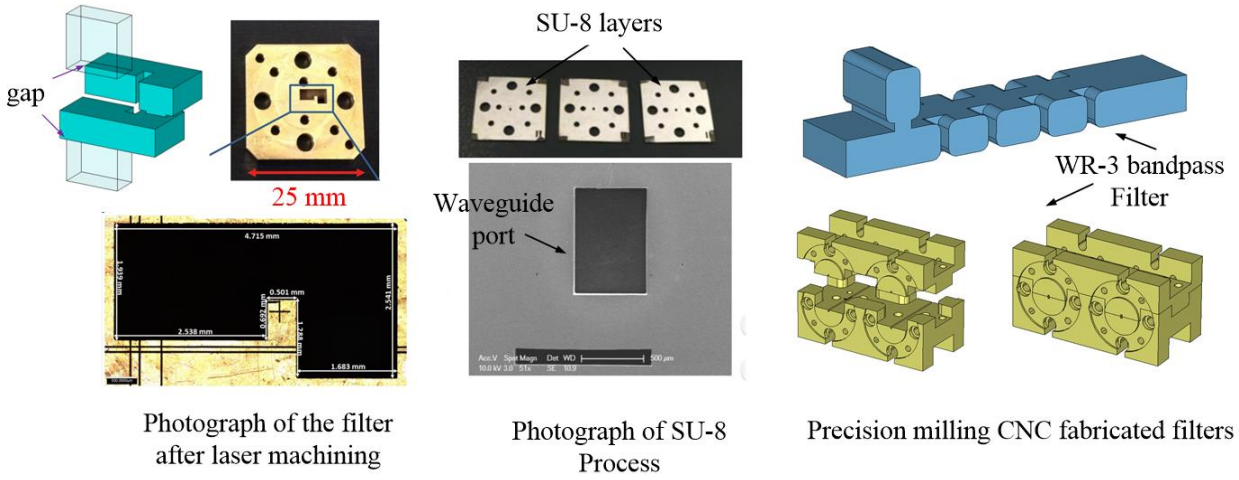

Fig. 1.1 Waveguide components fabricated using micromachining techniques [5], [6].

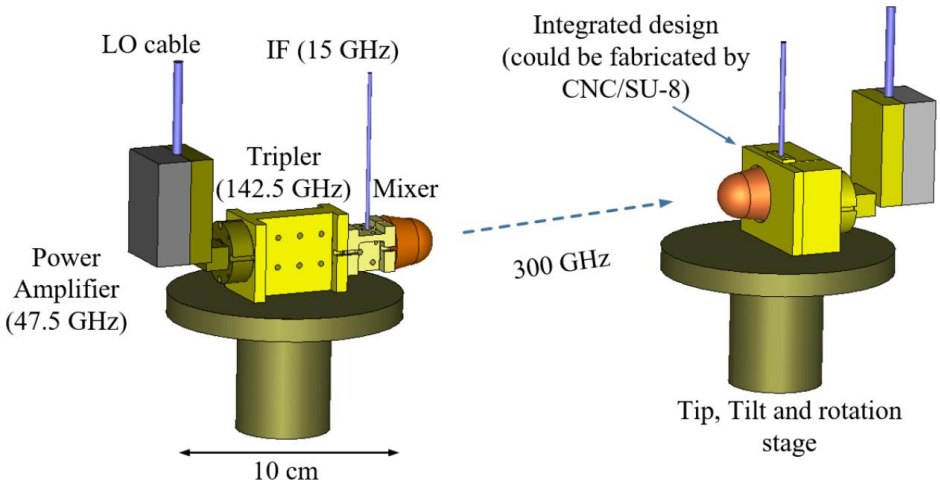

Fig. 1.2 A 300 GHz wireless link [7].

A 300 GHz communication link (Fig. 1.2), using all waveguide structures, has been proposed at Birmingham to demonstrate THz micromachining circuits technology and a practical application [8]. In the system design, waveguide resonators are employed to integrate the different components, essentially removing matching networks and replacing them with filters. This combined filter

matching is applied not only to the passive components including the antenna but also to the amplifier, multiplier and mixer. This thesis provides a detailed investigation of this novel filter amplifier design, and here the amplifier is designed combining with the waveguide structure in order to cascade other waveguide components in the communication system.

For a low noise amplifier, there are criteria achieving optimum performance: (i) impedance matching of the active components, maximum power gain and optimal noise figure, or trade-off between them, are commonly achieved by carrying out the input and output impedance matching of the low noise amplifier. (ii) losses in the matching circuit at the input of the transistor, where ohmic losses impair the overall system in terms of gain and noise performance.

In current amplifier designs, impedance matching circuits, such as matching stubs [1], quarter wavelength transformers [2], coupled lines [13], are widely adopted. However, general matching techniques for the amplifier primarily rely on planar circuits, referring to a common terminal impedance based on the conventional 50 Ω matching condition and it becomes difficult to design waveguide amplifiers using the conventional matching methods. In the waveguide amplifier design described in this thesis, the planner matching structures are transferred into high-Q waveguide resonators reducing the additional losses as well as circuit complexity. There are some filter amplifier examples using the active impedance/admittance inverters [14]-[17] or active resonators [18]-[20], namely active microwave filters. In these design examples, filter and the transistor are combined to form the filter amplifier. Each active inverters and active resonators are constructed by incorporating the transistor into every resonator and inverter. These multiple transistor-resonator structures are more likely realised in the planar circuits because it becomes difficult to construct the active resonators or active inverters with three-dimensional waveguide structures.

Several different types of amplifiers are summarised in Table 1.1. A substrate integrated waveguide filter is co-designed with a power amplifier in [21], and a 90° phase shift filter is addressed to match the output of a power amplifier in [22]. These amplifiers are designed combining the filters, and the design approaches are based on the conventional matching/filtering techniques. Besides, some waveguide amplifiers are also presented: coplanar waveguide lines (CPW) [23], SIW stub line [24], and ridge gaps [25] act as matching network of the amplifiers, respectively. In these examples, the waveguide amplifiers are constructed without a synthesised filter, and the on-chip transistor is combined with the waveguide through planner circuit to waveguide transitions.

TABLE 1.1
AMPLIFIER DESIGN EXAMPLES

Type	Functions	Matching Technique	Structure	Whether using coupling matrix	References
Low noise amplifier	Filtering, amplification	Active inverters	Planner circuit-MMIC	No	[14] [15] [16] [17]
Low noise amplifier	Filtering, amplification	Active resonators	Planner circuit-MMIC	No	[18] [19] [20]
Power amplifier	Filtering, amplification	90° phase shift filter	Planner circuit Microstrip	No	[22]
Power amplifier	Filtering, amplification	SIW filter	Substrate integrated waveguide	*N*+2 coupling matrix	[21]
Low noise amplifier	Amplification	CPW stub lines	Coplanar waveguide	No	[23]
Low noise amplifier	Amplification	SIW stub lines	Substrate integrated waveguide	No	[24]
Low noise amplifier	Amplification	Ridge gaps	Rectangular waveguide	No	[25]

In this thesis, we propose to include active amplifying components into waveguide filters to construct the integrated waveguide filter amplifiers. This demands new amplifier design methodologies suitable for various physical structures. In the thesis, we will introduce novel

waveguide amplifier design approaches which combine high-Q rectangular waveguide resonators with a transistor designing the filter amplifiers. Design examples are discussed and demonstrated at a lower frequency of 10 GHz, but the technique is general and is being applied to the 300 GHz amplifier design. Furthermore, novel N+X (N is the order of the filter) coupling matrices are synthesised to describe the filter amplifiers. The coupling matrices are used to develop the actual physical structure of the waveguide filters and the interface to the transistor. This design methodology is accurate enough to provide good initial values for full wave optimisation of the structures, enabling the optimisation process to be very rapid.

1.2 Thesis Overview

This thesis is formed of 6 chapters, introducing the synthesised novel coupling matrices and their implementation in filter-amplifiers. These chapters are organised as follows.

- Chapter 1 is the research motivation and the thesis overview.
- Chapter 2 introduces the basic concepts of microwave filters and the microwave amplifier. The introduction to microwave filters starts from the polynomials of a filter system, followed by the lump circuit representation of different types of filters. The N×N and N+2 coupling matrices are introduced. A simple microwave amplifier model is introduced using the two-port model described by scattering parameters.
- Chapter 3 synthesises three novel coupling matrices. First, an N+4 coupling is developed to represent cascaded filters separated by transmission lines. The second coupling matrix is the N+3 coupling matrix, describing the filter-amplifier, where the transistor is adjacent to the last resonator of the filter. This N+3 coupling matrix is an active coupling matrix, as the parameters of the transistor are included. The N+3 coupling

matrix characterises the integrated filter-amplifier, achieving a filtering response with gain. The N+3 matrix only describes a filter on the input to the transistor amplifier. Finally, the coupling matrix is generalised to N+4 coupling matrix, describing the transistor coupling in the middle of the resonators providing filters at both input and output. Physical implementations of using these novel coupling matrices are presented in Chapter 4 and Chapter 5.

- Chapter 4 demonstrates a microstrip bandpass filter-amplifier and an X-band waveguide filter-amplifier. The coupling matrix description for the two filter-amplifiers is the same. Procedures of determining the physical dimensions are developed based on the N+3 coupling matrix. The experimental measurements of the fabricated amplifiers show an excellent filtering response with two poles and also a gain.
- Chapter 5 presents the design of an X-band waveguide filter-amplifier. Two waveguide filters are coupled at the input and the output of the transistor, achieving Chebyshev filtering response between the two waveguide ports. This amplifier is designed based on the N+4 coupling matrix. The process of extracting the coupling coefficients and external Q using the N+4 coupling matrix is discussed, followed by the measurements showing two poles in the response in the reflection coefficient at both the input and the output port.
- Chapter 6 makes a conclusion of the thesis and suggestions for future works are also discussed.

REFERENCES

[1] D. Pozar, *Microwave engineering*. Hoboken, NJ: Wiley, 2012.

[2] J. S. Hong and M. J. Lancaster, Microstrip Filters for RF/Microwave Applications. New York, NY, USA: Wiley, 2001.

[3] Guillermo Carpintero; Enrique Garcia-Munoz; Hans Hartnagel; Sascha Preu; Antti Raisanen, "THz Electronics," in *Semiconductor TeraHertz Technology:Devices and Systems at Room Temperature Operation* , 1, Wiley-IEEE Press, 2015

[4] Guillermo Carpintero; Enrique Garcia-Munoz; Hans Hartnagel; Sascha Preu; Antti Raisanen, "Principles of Emission of THz Waves," in *Semiconductor TeraHertz Technology:Devices and Systems at Room Temperature Operation* , 1, Wiley-IEEE Press, 2015

[5] H. Yang, Y. Dhayalan, X. Shang, M. J. Lancaster *et al*., "WR-3 Waveguide Bandpass Filters Fabricated Using High Precision CNC Machining and SU-8 Photoresist Technology," *IEEE Trans. THz Sci. Techn.*, vol. 8, no. 1, pp. 100-107, Jan. 2018.

[6] X. Shang, P. Penchev, M. J. Lancaster *et al*., "*W* -Band Waveguide Filters Fabricated by Laser Micromachining and 3-D Printing," *IEEE Trans. Microw. Theory Techn.*, vol. 64, no. 8, pp. 2572-2580, Aug. 2016.

[7] C. Guo, M. J. Lancaster, X. Shang, *et al*. "Fabrication Technologies for Sub-Millimeter Wave to THz Applications" European Microwave Week, 2017.

[8] http://gow.epsrc.ac.uk/NGBOViewGrant.aspx?GrantRef=EP/M016269/1

[9] M. Abdolhamidi and M. Shahabadi, "X-Band Substrate Integrated Waveguide Amplifier," in IEEE *Microw. Compon. Lett.*, vol. 18, no. 12, pp. 815-817, Dec. 2008.

[10] B. Ahmadi and A. Banai, "Substrateless Amplifier Module Realised by Ridge Gap Waveguide Technology for Millimeter-Wave Applications," in *IEEE Trans. Microw. Theory Techn*., vol. 64, no. 11, pp. 3623-3630, Nov. 2016.

[11] K. M. K. H. Leong, K. Hennig, Z. Chunbo, R. N. Elmadjian, Z. Zeyang, B. S. Gorospe, et al., "WR1.5 Silicon Micromachined Waveguide Components and Active Circuit Integration Methodology," IEEE Trans. *Microw. Theory Techn.*, vol. 60, pp. 998-1005, 2012

[12] B. Thomas et al., "A Broadband 835–900-GHz Fundamental Balanced Mixer Based on Monolithic GaAs Membrane Schottky Diodes," in IEEE *Trans. Microw. Theory Techn*., vol. 58, no. 7, pp. 1917-1924, July 2010.

[13] Y. S. Lin, J. F. Wu, W. F. Hsia, P. C. Wang and Y. H. Chung, "Design of electronically switchable single-to-balanced bandpass low-noise amplifier," *IET Microw. Antennas Propag.*, vol. 7, no. 7, pp. 510-517, May 15, 2013.

[14] S. F. Sabouri, "A GaAs MMIC active filter with low noise and high gain," 1998 *IEEE MTT-S Int. Microw. Symp. Digest* (Cat. No.98CH36192), Baltimore, MD, USA, 1998, pp. 1177-1180 vol.3.

[15] Young-Hoon Chun, Sang-Won Yun and Jin-Koo Rhee, "Active impedance inverter: analysis and its application to the bandpass filter design," *2002 IEEE MTT-S Int. Microw. Symp. Digest (Cat. No.02CH37278)*, Seattle, WA, USA, 2002, pp. 1911-1914 vol.3.

[16] L. Darcel, P. Dueme, R. Funck and G. Alquie, "New MMIC approach for low noise high order active filters," *IEEE MTT-S Int. Microw. Symp. Digest*, 2005., 2005, pp. 4 pp.-doi: 10.1109/MWSYM.2005.1516731.

[17] F. Bergeras, P. Duême, J. Plaze, L. Darcel, B. Jarry and M. Campovecchio, "Novel MMIC architectures for tunable microwave wideband active filters," 2010 *IEEE MTT-S Inter. Microw. Symp.*, Anaheim, CA, 2010, pp. 1-1.

[18] C. Y. Chang and T. Itoh, "Microwave active filters based on coupled negative resistance method," *IEEE Trans. Microw. Theory Techn.*, vol. 38, no. 12, pp. 1879-1884, Dec 1990.

[19] M. Ito, K. Maruhashi, S. Kishimoto and K. Ohata, "60-GHz-band coplanar MMIC active filters," *IEEE Trans. Microw. Theory Techn.*, vol. 52, no. 3, pp. 743-750, March 2004.

[20] Young-Hoon Chun, Jae-Ryong Lee, Sang-Won Yun and Jin-Koo Rhee, "Design of an RF low-noise bandpass filter using active capacitance circuit," *IEEE Trans. Microw. Theory Techn.*, vol. 53, no. 2, pp. 687-695, Feb. 2005

[21] K. Chen, J. Lee, W. J. Chappell and D. Peroulis, "Co-Design of Highly Efficient Power Amplifier and High-Q Output Bandpass Filter," *IEEE Trans., Microw. Theory Techn.*, vol. 61, no. 11, pp. 3940-3950, Nov. 2013.

[22] Y. C. Li, K. C. Wu and Q. Xue, "Power Amplifier Integrated with Bandpass Filter for Long Term Evolution Application," *IEEE Microw. Wirel. Compon. Lett.*, vol. 23, no. 8, pp. 424-426, Aug. 2013.

[23] K. Minot, B. Nelson and W. Jones, "A low noise, phase linear distributed coplanar waveguide amplifier," *IEEE Trans. Microw. Theory Techn.*, vol. 41, no. 9, pp. 1650-1653, Sep 1993.

[24] M. Abdolhamidi and M. Shahabadi, "X-Band Substrate Integrated Waveguide Amplifier," *IEEE Microw. Wirel. Compon. Lett.*, vol. 18, no. 12, pp. 815-817, Dec. 2008.

[25] B. Ahmadi and A. Banai, "Substrateless Amplifier Module Realised by Ridge Gap Waveguide Technology for Millimeter-Wave Applications," *IEEE Trans. Microw. Theory Techn.*, vol. 64, no. 11, pp. 3623-3630, Nov. 2016.

CHAPTER 2

MICROWAVE FILTERS AND THE AMPLIFIER CONCEPTS

This chapter introduces the theories of microwave filters and the microwave amplifier. A filter is usually a linear time-invariant (LTI) system. A particularly important and useful class of continuous-time LTI system are those for which the input and output satisfy a linear constant-coefficient differential equation of the form [1]

$$\sum_{k=0}^{N} a_k \frac{d^k y(t)}{dt^k} = \sum_{k=0}^{M} b_k \frac{d^k x(t)}{dt^k} \tag{2.1}$$

where $y(t)$ denotes the output signal versus time variable t and $x(t)$ is the input signal of the system; M and N are the order of the derivative of the input $x(t)$ and output $y(t)$; a_k and b_k are the constant coefficients. Thus, a two-port network filter can be characterised by the transfer function $H(j\omega)$ according to the Fourier transformation given in (2.1), where ω is the frequency variable in rad/s and j the imaginary factor with $j^2=-1$.

In this chapter, we look at some basic concepts related to the research in the rest of the thesis. Here, Section 2.1 starts from the two-port network model, and the polynomials of filter transfer function $H(j\omega)$ are synthesised. This is the mathematical foundation for the filter theory. Section 2.2 introduces a physical model, the lumped circuit prototype of the lowpass filter, and some

important lumped elements *J* and *K* inverters are detailed. The lowpass filter prototype obtains element impedance values of some commonly used filters instead of deriving the polynomials of transfer functions. A general synthesis dealing with filters, that is, the coupling matrix technology is addressed in Section 2.3. Finally, Section 2.4 discusses the transistors and the microwave amplifiers.

2.1 Filter Characteristics

2.1.1 Filter transfer function

The two-port network model (see Fig. 2.1) plays an important role in the filter theory because it builds the relationship between the lumped circuit components and wave variables. This enables us to analyse or synthesise the microwave circuits more effectively as dealing with the lumped circuit problems. For a two-port network, in the microwave frequency range, it is desirable to characterise it in terms of scattering (*S*) parameters, because the *S*-parameters are directly measurable and are able to describe the frequency characteristics of the two-port network completely. Besides, *S*-parameters give a visualised energy flowing intuitively, i.e. the amount of power reflected and the amount transmitted through the network.

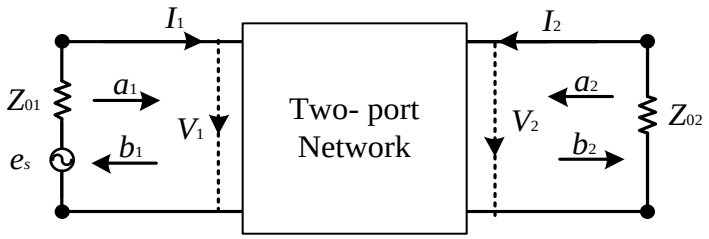

Fig. 2.1 Two port network: V_n and I_n are the voltages and currents (n=1,2).

In Fig. 2.1, Z_{01} and Z_{02} are the source and load impedance; *a* and *b* stand for the incident and

reflected waves, which are defined in terms of currents and voltages through the following equations [2], [3]

$$a_n = \frac{V_n + Z_{0n} I_n}{2\sqrt{\left|\mathrm{Re}\left(Z_{0n}\right)\right|}} \qquad n=1,\ 2$$
$$b_n = \frac{V_n - Z_{0n}^{*} I_n}{2\sqrt{\left|\mathrm{Re}\left(Z_{0n}\right)\right|}} \qquad (2.2)$$

The reflection coefficient S_{11}, S_{22}, and transmission coefficient S_{21}, S_{12} are thereby defined by [1]

$$S_{11} = \left.\frac{b_1}{a_1}\right|_{a_2=0} \qquad S_{12} = \left.\frac{b_1}{a_2}\right|_{a_1=0}$$
$$S_{21} = \left.\frac{b_2}{a_1}\right|_{a_2=0} \qquad S_{22} = \left.\frac{b_2}{a_2}\right|_{a_1=0} \qquad (2.3)$$

Note that the transfer coefficient S_{21}, which is a function of frequency $j\omega$, is also named as the transfer function of a system, that is

$$S_{21}\left(j\omega\right) = H\left(j\omega\right) \qquad (2.4)$$

For a lossless two-port network, *S*-parameters must satisfy the condition of power conservation given as

$$S_{11}S_{11}^{*} + S_{21}S_{21}^{*} = 1$$
$$S_{22}S_{22}^{*} + S_{12}S_{12}^{*} = 1 \qquad (2.5)$$

Here the asterisk in term of S_{11}^{*}, S_{12}^{*}, S_{21}^{*}, and S_{22}^{*} denote the conjugates of the *S*-parameters. Another two practical parameters are insertion loss (L_A) and return loss (L_R) which are related and given by [2]

$$L_A = -20\log_{10}\left(\left|S_{21}\right|\right)$$
$$L_R = -20\log_{10}\left(\left|S_{11}\right|\right) \qquad (2.6)$$

For an arbitrary two-port lossless filter network, the transfer function can be expressed as

$$\left|S_{21}(s)\right|^2 = \frac{1}{1+\varepsilon^2\left|D(s)\right|^2}, \tag{2.7}$$

where $s = \sigma + j\omega$ is a complex variable and ε is a real number known as the ripple constant. $D(s)$ is defined as the characteristic function and can be expressed as a ratio of two polynomials $P(s)$ and $F(s)$ [4]

$$D(s) = \frac{F(s)}{P(s)} \tag{2.8}$$

Together with polynomial $E(s)$, the filter's reflection coefficient S_{11} and transfer coefficient S_{21} can be mathematically expressed as [4]

$$S_{11}(s) = \frac{F(s)}{E(s)} \quad S_{21}(s) = \frac{P(s)}{\varepsilon E(s)} \tag{2.9}$$

The highest-power coefficients of these characteristic polynomials $E(s)$, P(s) and $F(s)$ are assumed to be unity. The degree of the $E(s)$ and $F(s)$ is N, where N is the order of the filter. The polynomial $P(s) = \prod_{n=1}^{N_z}(s - s_n)$ carries N_z transfer function finite position transmission zeros [4], where s_n is the root of $P(s)$. The properties of the characteristic polynomials $F(s)$, $P(s)$, and $E(s)$ are summarised as [4]:

- $F(s)$ is an N^{th} degree polynomial, where N is the order of the filter. Its coefficients are real, and its roots lie along the imaginary axis. A root of $F(s)$ may only be repeated at the origin.
- $P(s)$ is a polynomial of N_z^{th} degree. When N_z is zero, there are no finite position transmission zeros, and the response is known as all-pole. The zeros of $P(s)$ must be either on the imaginary axis of the s-plane or arranged in symmetrical pairs about the imaginary axis. Roots of $P(s)$ which do not lie on the imaginary axis are often incorporated to produce linear phase filters.
- $E(s)$ is an N^{th} degree polynomial with complex coefficients. It is a strictly Hurwitz

polynomial, that is, all roots lie strictly in the left half of the complex plane. These roots need not be symmetric about the real axis.

Here the ripple constant ε is involved in normalising $E(s)$ and $P(s)$ at a special frequency ($s=\pm j$), which can be computed by the prescribed return loss [7]

$$\varepsilon = \frac{1}{\sqrt{10^{L_R/10}-1}} \cdot \left.\frac{P(s)}{F(s)}\right|_{s=\pm j} \tag{2.10}$$

It can be observed from (2.9) that the roots of $F(s)$ correspond to the reflection zeros, where signals all get through from input to output; the roots of $P(s)$ correspond to transmission zeros, where no energy is transmitted; and the roots of $E(s)$ are referred to the transfer function's poles. According to (2.5) and (2.9), the relationship of $F(s)$, $E(s)$, and $P(s)$ is derived as

$$F \cdot F^* + \frac{1}{\varepsilon^2} P \cdot P^* = E \cdot E^* \tag{2.11}$$

As a result, if $F(s)$ and $P(s)$ are known, $E(s)$ can be found by an alternative pole method, which is detailed in [7].

2.1.2 All-pole Chebyshev filter

The prototype of the all-pole Chebyshev response gives an equal-ripple in the passband, where the band edges are $s = \pm j$. The polynomials of Chebyshev transfer function can be derived by the recursive procedure described in [7] and [8] and are given by

$$\begin{aligned} P(s) &= 1 \\ F(s) &= \cosh\left[\sum_{n=1}^{N} \cosh^{-1}(s)\right] \end{aligned} \tag{2.12}$$

As an example, a 6th order Chebyshev filter response is presented in Fig. 2.2(a) with the maximum reflection loss L_R of 20 dB over the passband $\omega = -1$ to 1. Note that in (2.12), $F(s)$ is

the Chebyshev polynomial of first kind [9], [10]. Chebyshev polynomial satisfies the recursion formulation and its coefficients can be calculated using the recursive method detailed in [11]. Once the coefficients $F(s)$ are identified, the poles and the coefficients of $E(s)$ can be found according to their relationship in (2.11) with the help of alternative pole method [4]. The location of the poles and zeros are shown in Fig. 2.2(b). Table 2.1 gives the coefficients of the polynomials.

TABLE 2.1
COEFFICIENTS OF THE POLYNOMIALS CORRESPOND TO THE 6TH ORDER ALL-POLE CHEBYSHEV FILTER.

ω^n , n	$P(\omega)$	$F(\omega)$	$E(\omega)$
0	**1**	**-0.0313**	**-0.3125**
1	**0**	**0**	**1.2988*j***
2	**0**	**0.5625**	**2.7553**
3	**0**	**0**	**-3.6108*j***
4	**0**	**-1.500**	**-3.5169**
5	**0**	**0**	**2.0084*j***
6	**0**	**1**	**1**

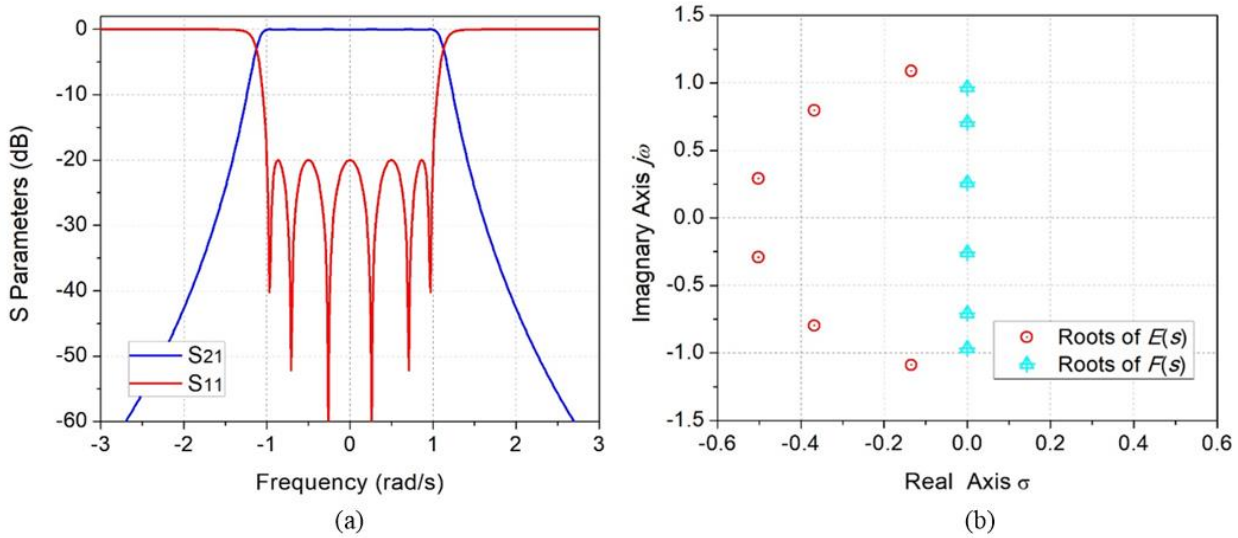

(a) (b)

Fig. 2.2 Six[th] order Chebyshev response and polynomials roots. (a) Scatting parameters S_{11} and S_{21}. (b) The roots of $E(s)$ and $F(s)$.

2.2 Microwave Filter Theory

2.2.1 Lumped circuit prototype

The filter response synthesised by polynomials can be physically realised using the lumped element circuits. Three basic lumped elements are resistors, capacitors and inductors [1], [2]. These elements can form periodic ladder topologies, producing different types of the filter response. The n^{th} order prototype all-pole lowpass filter response can be achieved by the lumped circuit ladder topologies in Fig. 2.3 [2].

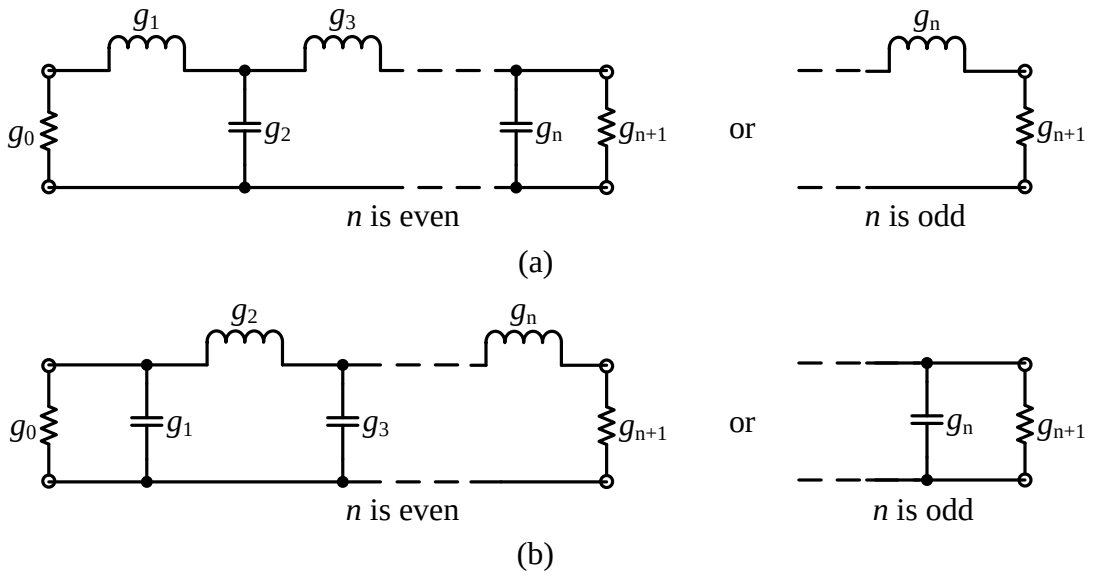

Fig. 2.3 Lumped element based low-pass filters with all poles responses in (a) a ladder topology and (b) its dual [2].

In Fig. 2.3, g_0 is the source conductance or resistance and g_{n+1} represents the conductance or resistance of the load. g_i (i=1 to n) is the capacitance of the parallel capacitors or the inductance of the series inductors. These two lumped circuit topologies serve as the prototype of many filters. Some practical filters can be constructed from this lumped circuit topology through frequency and element transformation [1]. The g values can be calculated for several types of the filter including

Butterworth, Chebyshev, and Gaussian responses which are summarised in [2].

2.2.2 *J* and *K* inverters

An idealised immittance inverter is a frequency invariant two-port network that can convert the input admittance or impedance as shown in Fig. 2.4. There are two types of immittance inverters, *J* inverter and *K* inverter. The transformed impedance Z_b and admittance Y_b are given by

$$Z_b = \frac{K^2}{Z_a}, \quad Y_b = \frac{J^2}{Y_a} \tag{2.13}$$

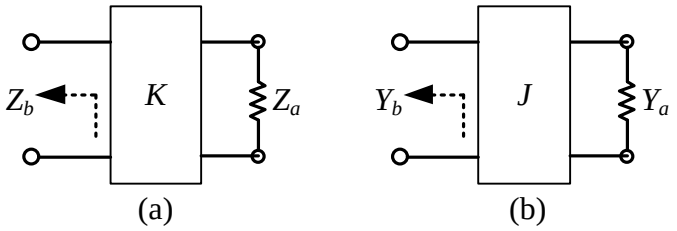

Fig. 2.4 Immittance impedance transformation: (a) *K* inverter. (b) *J* inverter.

K and *J* are real constants and defined as the characteristic impedance and admittance of the inverters if they are made of the quarter wavelength long transmission line. Based on the narrowband assumption, one type of *J* and *K* inverters can be constructed in the form of capacitors *C* and inductors *L*, as depicted in Fig. 2.5, and the value of the immittance *K* and *J* are evaluated [2].

The properties of the *J* and *K* inverters allow us to convert the lumped circuit prototype in Fig. 2.3 which comprise both capacitors and inductors to equivalent lumped circuit ladder that use only capacitors or only inductors. These equivalent circuits are shown in Fig. 2.6. This property is useful because it increases the feasibility of choosing the different circuit topologies, especially with

microwave structures.

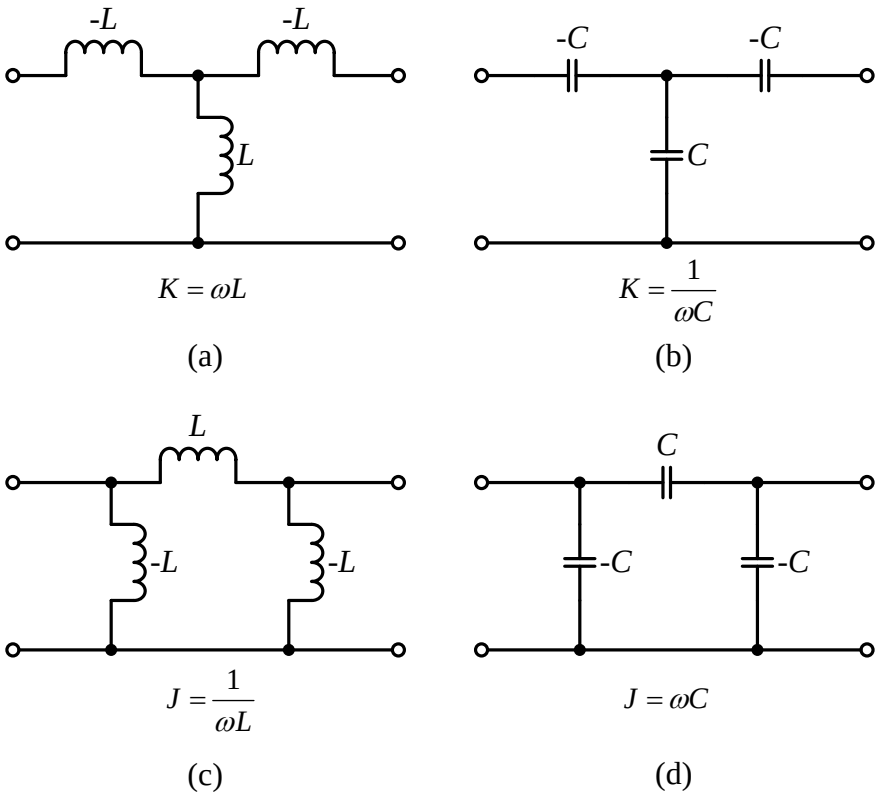

Fig. 2.5 Immittance inverters formed lumped elements [2].

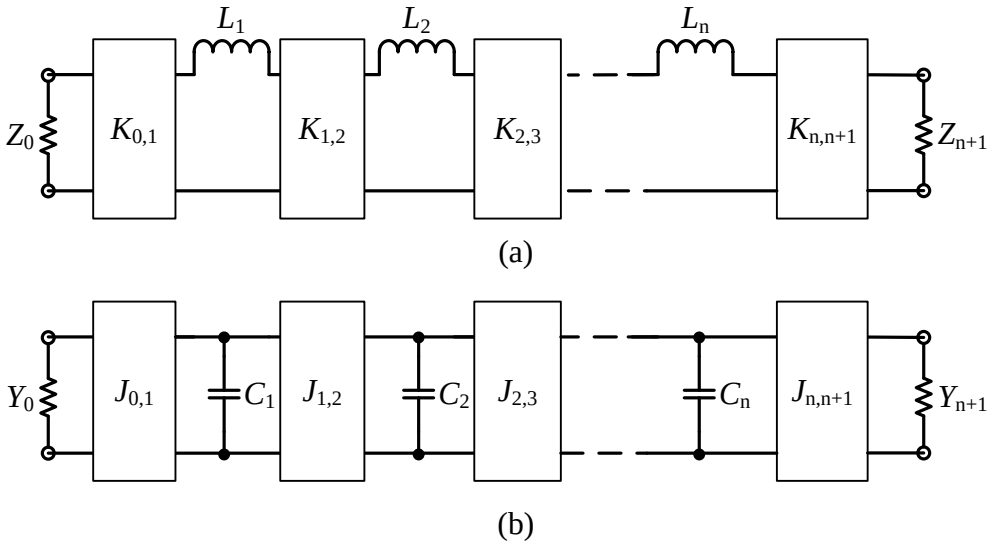

Fig. 2.6 Lumped circuit prototype of the lowpass filter with immittances [2].

The elements' values using the impedance inverters are given by [2]

$$K_{k,k+1} = \sqrt{\frac{L_k L_{k+1}}{g_k g_{k+1}}}, \quad k = 1 \text{ to } n-1$$
$$K_{0,1} = \sqrt{\frac{Z_0 L_1}{g_0 g_1}}, \quad K_{n,n+1} = \sqrt{\frac{Z_{n+1} L_n}{g_n g_{n+1}}} \tag{2.14}$$

The element's value using the admittance inverters are given by [2]

$$J_{k,k+1} = \sqrt{\frac{C_k C_{k+1}}{g_k g_{k+1}}}, \quad k = 1 \text{ to } n-1$$
$$J_{0,1} = \sqrt{\frac{Y_0 C_1}{g_0 g_1}}, \quad J_{n,n+1} = \sqrt{\frac{Y_{n+1} C_n}{g_n g_{n+1}}} \tag{2.15}$$

Note that there is flexibility for the lumped elements in the circuits in Fig. 2.6 as the values of the inductor, capacitors and the terminations are totally arbitrary.

2.2.3 Bandpass ladders

The lowpass lumped filter circuits with immittance inverters can be transformed into the bandpass lumped ladder. A prototype lowpass filter that transforms the frequency to a bandpass one with a passband $\omega_2 - \omega_1$ can be expressed as [2]

$$\omega \rightarrow \frac{\omega_c}{FBW}\left(\frac{\omega}{\omega_0} - \frac{\omega_0}{\omega}\right) \tag{2.16}$$

with

$$FBW = \frac{\omega_2 - \omega_1}{\omega_0}$$
$$\omega_0 = \sqrt{\omega_1 \cdot \omega_2} \tag{2.17}$$

where ω is the frequency variable; ω_1 and ω_2 are the angular frequencies of the passband edges; ω_c is the lowpass prototype cut-off frequency; ω_0 denotes the centre angular frequency, and *FBW*

is defined as the fractional bandwidth. Applying this frequency transformation to a parallel capacitor C and a series inductor L of the lowpass prototype filter, we have [2]

$$\begin{aligned} j\omega C &\rightarrow j\omega \frac{\omega_c C}{FBW\,\omega_0} + \frac{1}{j\omega \dfrac{FBW}{\omega_c \omega_0 C}} \\ j\omega L &\rightarrow j\omega \frac{\omega_c L}{FBW\,\omega_0} + \frac{1}{j\omega \dfrac{FBW}{\omega_c \omega_0 L}} \end{aligned} \tag{2.18}$$

The frequency transformation in (2.18) implies that a parallel capacitor C or a series inductor L in the lowpass prototype is transferred to a parallel or series LC resonant circuit as illustrated in Fig. 2.7.

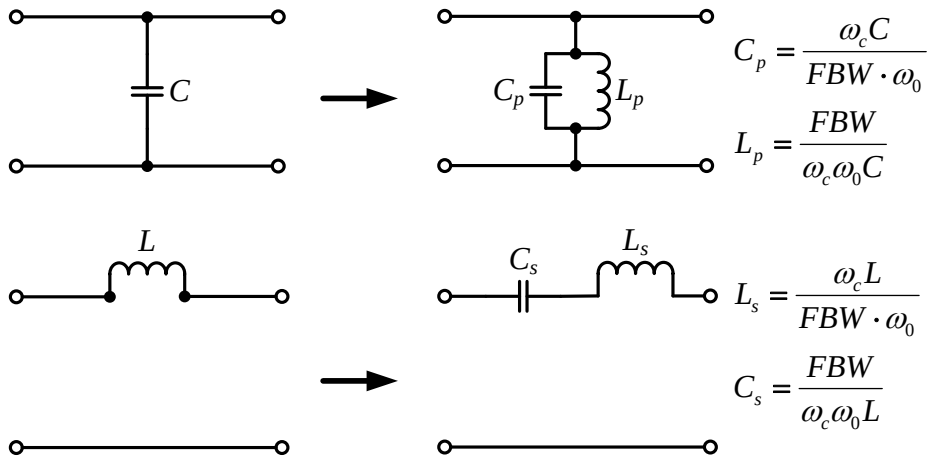

Fig. 2.7 Lowpass to bandpass element transformation [2].

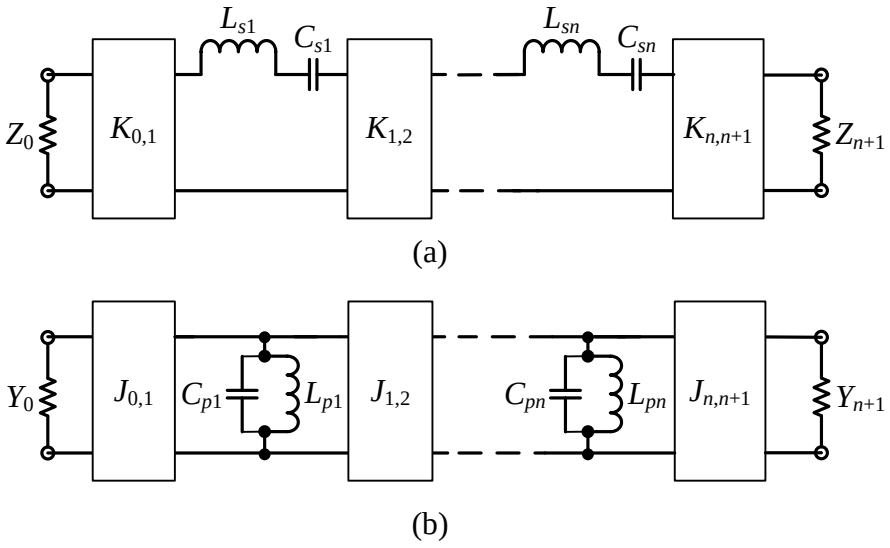

Fig. 2.8 Bandpass filters with immittance inverters [2].

The bandpass impedance or admittance inverter prototypes are shown in Fig. 2.8 and the circuits are formed of immittance inverters and *LC* resonators. The elements' values using the impedance inverters are given by [2]

$$K_{k,k+1} = FBW \cdot \omega_0 \sqrt{\frac{L_{sk} L_{sk+1}}{g_k g_{k+1}}}, \quad k = 1 \text{ to } n-1$$
$$K_{0,1} = \sqrt{\frac{FBW \cdot \omega_0 Z_0 L_{s1}}{g_0 g_1}}, \quad K_{n,n+1} = \sqrt{\frac{FBW \cdot \omega_0 Z_{n+1} L_{sn}}{g_n g_{n+1}}} \tag{2.19}$$

The elements' values using the admittance inverters are given by [2]

$$J_{k,k+1} = FBW \cdot \omega_0 \sqrt{\frac{C_{sk} C_{sk+1}}{g_k g_{k+1}}}, \quad k = 1 \text{ to } n-1$$
$$J_{0,1} = \sqrt{\frac{FBW \cdot \omega_0 Y_0 C_{s1}}{g_0 g_1}}, \quad J_{n,n+1} = \sqrt{\frac{FBW \cdot \omega_0 Y_{n+1} C_{sn}}{g_n g_{n+1}}} \tag{2.20}$$

With different techniques, such lumped circuits can be converted into different forms of distributed circuits including waveguides or microstrips [2].

2.3 Coupling Matrix

The concept of the coupling matrix was first introduced by A. Atia and A. Williams in the 1970's in the application of waveguide cavity filter design [13]-[15]. Initially, an $N\times N$ matrix design approach was developed based on lumped circuit elements, and ideal transformer coupling, following which later was extended to the N+2 coupling matrix with port impedances were extracted [4]. This section discusses the two types of coupling matrices for the filter.

2.3.1 $N\times N$ coupling matrix

Fig. 2.7 gives a bandpass filter prototype with N resonators coupled by transformers. In this figure, every resonator is in the form of a C=1 F capacitor and an L=1 H inductor, with ω_0=1 rad/s centre frequency.

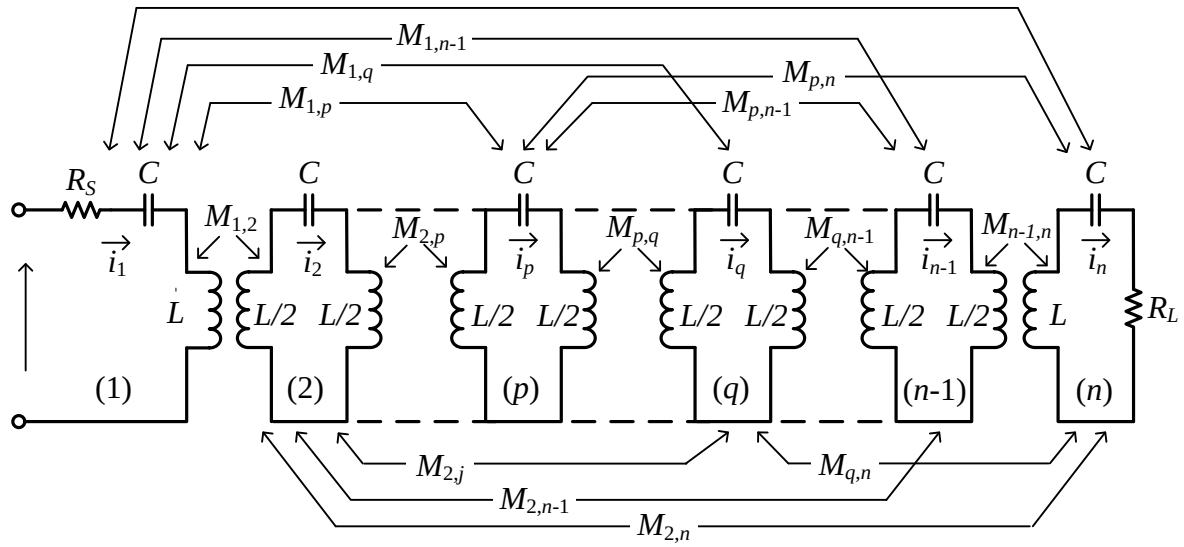

Fig. 2.7 Lumped circuit of resonators coupled by magnetic transformers [17].

R_S and R_L are the source resistor and the load resistor. $M_{p,q}$ is the coupling coefficient between the p^{th} resonator and q^{th} resonator. $M_{p,q}$ is determined by the ratio of the mutual inductance $L_{p,q}$ and the

self-inductance L, given by $M_{p,q}= L_{p,q}/L$ [2]. Note that the N loop voltage is denoted as v_1, v_2, …, e_n with the loop current i_1, i_2, …, i_n. Applying the Kirhhoff's voltage law, the complete set of loop equations can be written in a matrix form as [2]

$$\begin{bmatrix} j\omega L+\frac{1}{j\omega C}+R_S & -j\omega L_{1,2} & -j\omega L_{1,3} & \cdots & -j\omega L_{1,n-1} & -j\omega L_{1,n} \\ -j\omega L_{2,1} & j\omega L+\frac{1}{j\omega C} & -j\omega L_{2,3} & \cdots & -j\omega L_{2,n-1} & -j\omega L_{2,n} \\ -j\omega L_{3,1} & -j\omega L_{3,2} & j\omega L+\frac{1}{j\omega C} & \cdots & -j\omega L_{3,n-1} & -j\omega L_{3,n} \\ \vdots & \vdots & \vdots & \ddots & \vdots & \vdots \\ -j\omega L_{n-1,1} & -j\omega L_{n-1,2} & -j\omega L_{n-1,3} & \cdots & j\omega L+\frac{1}{j\omega C} & -j\omega L_{n-1,n} \\ -j\omega L_{n,1} & -j\omega L_{n,2} & -j\omega L_{n,3} & \cdots & -j\omega L_{n,n-1} & j\omega L+\frac{1}{j\omega C}+R_L \end{bmatrix} \begin{bmatrix} i_1 \\ i_2 \\ i_3 \\ \vdots \\ i_{n-1} \\ i_n \end{bmatrix} = \begin{bmatrix} e_s \\ 0 \\ 0 \\ \vdots \\ 0 \\ 0 \end{bmatrix} \quad (2.21)$$

or

$$[Z][i]=[e] \quad (2.22)$$

Now $[Z]$ is normalised as

$$[Z]=\omega_0 L\cdot FBW\cdot[\bar{Z}] \quad (2.23)$$

where FBW is the fractional bandwidth of the filter and is defined by the 3-dB bandwidth and Δf ratio of centre frequency f_0.

$$FBW=\frac{\Delta f}{f_0} \quad (2.24)$$

Then $[\bar{Z}]$ decomposes into three matrices

$$[\bar{Z}]=[q]+p[I]-j[m]=\begin{bmatrix} \frac{1}{q_{eS}} & 0 & \cdots & 0 \\ 0 & 0 & \cdots & 0 \\ \vdots & \vdots & \ddots & \vdots \\ 0 & 0 & \cdots & \frac{1}{q_{eL}} \end{bmatrix}+p\begin{bmatrix} 1 & 0 & \cdots & 0 \\ 0 & 1 & \cdots & 0 \\ \vdots & \vdots & \ddots & \vdots \\ 0 & 0 & \cdots & 1 \end{bmatrix}-j\begin{bmatrix} m_{1,1} & m_{1,2} & \cdots & m_{1,n} \\ m_{2,1} & m_{2,2} & \cdots & m_{2,n} \\ \vdots & \vdots & \ddots & \vdots \\ m_{n,1} & m_{n,2} & \cdots & m_{n,n} \end{bmatrix} \quad (2.25)$$

p is the complex frequency variable; q_{eS} and q_{eL} are the normalised external quality factor; $[I]$ is

the identity matrix; [m] is the normalised coupling matrix. They are,

$$p = j\frac{1}{FBW}\left(\frac{\omega}{\omega_0}-\frac{\omega_0}{\omega}\right) \tag{2.26}$$

$$m_{p,q} = \frac{M_{p,q}}{FBW} \tag{2.27}$$

$$q_{eS} = FBW\,\frac{\omega_0 L}{R_S}, \quad q_{eL} = FBW\,\frac{\omega_0 L}{R_L} \tag{2.28}$$

According to [2], the S-parameters can be obtained by

$$\begin{aligned} S_{21} &= \frac{2}{\sqrt{q_{eS}q_{eL}}}\left[\bar{Z}\right]^{-1}_{n1} \\ S_{11} &= 1-\frac{2}{\sqrt{q_{eS}}}\left[\bar{Z}\right]^{-1}_{11} \end{aligned} \tag{2.29}$$

The dual circuit model of Fig. 2.7 is resonators with electrical coupling. It is analysed in a similar way in [2], where S-parameters can be derived from the admittance (Y) matrix,

$$\begin{aligned} S_{21} &= \frac{2}{\sqrt{q_{eS}q_{eL}}}\left[\bar{Y}\right]^{-1}_{n1} \\ S_{11} &= -\left(1-\frac{2}{\sqrt{q_{eS}}}\left[\bar{Y}\right]^{-1}_{11}\right) \end{aligned} \tag{2.30}$$

The normalised impedance matrix [$\bar{Z}$] and normalised admittance matrix [$\bar{Y}$] are the same form. Thus, the general coupling matrix [A] can be formulated to calculate the S-parameters [2]

$$\begin{aligned} S_{21} &= \frac{2}{\sqrt{q_{eS}q_{eL}}}\left[A\right]^{-1}_{n1} \\ S_{11} &= \pm\left(1-\frac{2}{\sqrt{q_{eS}}}\left[A\right]^{-1}_{11}\right) \end{aligned} \tag{2.31}$$

where

$$\left[A\right] = \left[q\right] + p\left[U\right] - j\left[m\right] \tag{2.32}$$

2.3.2 *N*+2 coupling matrix

As shown in Fig. 2.8, the source resistance R_S and load resistance R_L can be normalised to unity through the impedance inverter K_{S1} and K_{nL} [4]. The values of the impedance inverter K_{S1} and K_{nL} are $\sqrt{R_S R_{P1}}$ and $\sqrt{R_L R_{P2}}$, respectively. Thus, the source R_S and load R_L can be extracted from the 1st and the, n^{th} resonators, replacing by R_{P1} and R_{P2}, of those values are normalised to one. The impedance matrix [*Z*] can be replaced by the dual network admittance matrix [*Y*], as depicted in Fig. 2.8. The corresponding coupling matrix now has extra rows at the top and bottom and at both sides surrounding the general *N*×*N* matrix, known as *N*+2 coupling matrix. The values of the main inter-resonator couplings and cross couplings of the new *N*+2 matrix will not change.

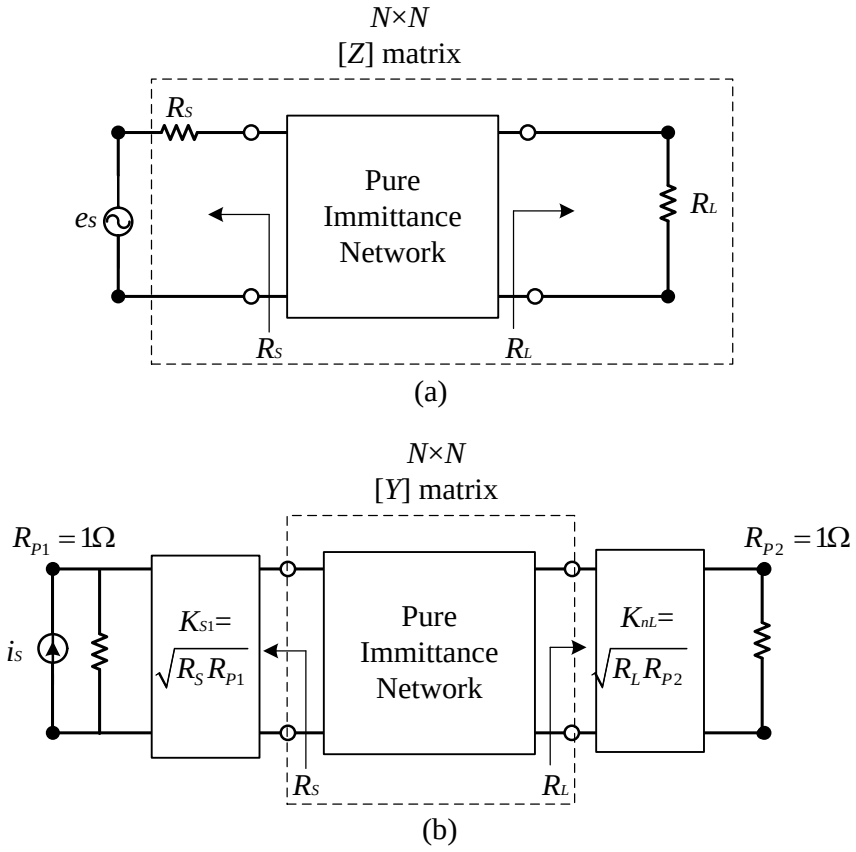

Fig. 2.8 Configuration of circuits' input and output in the representation of (a) *N*×*N* coupling matrix; (b) *N*+2 coupling matrix [4].

The multiple coupling circuit model including ports couplings is shown in Fig. 2.9. In Fig. 2.9,

$M_{p,q}$ is determined by the ratio of the mutual capacitance $C_{p,q}$ and the self- capacitance C, given by $M_{p,q}= C_{p,q}/C$ [2]. The process of analysing and derivations of the N+2 coupling matrix was introduced in [4]. The normalised N+2 coupling matrix form is presented in Fig. 2.10. The advantages of the N+2 coupling matrix are summarised by [16] as follows: first, it allows for ports to multiple resonators couplings; second, the coupling between source and load is possible to achieve a fully canonical filtering function. Furthermore, it fulfils the requirement of the scaling process when filters are incorporated with some other devices (e.g. transistors), making it possible to synthesise the coupling matrix for multiple devices, which will be introduced in Chapter 3.

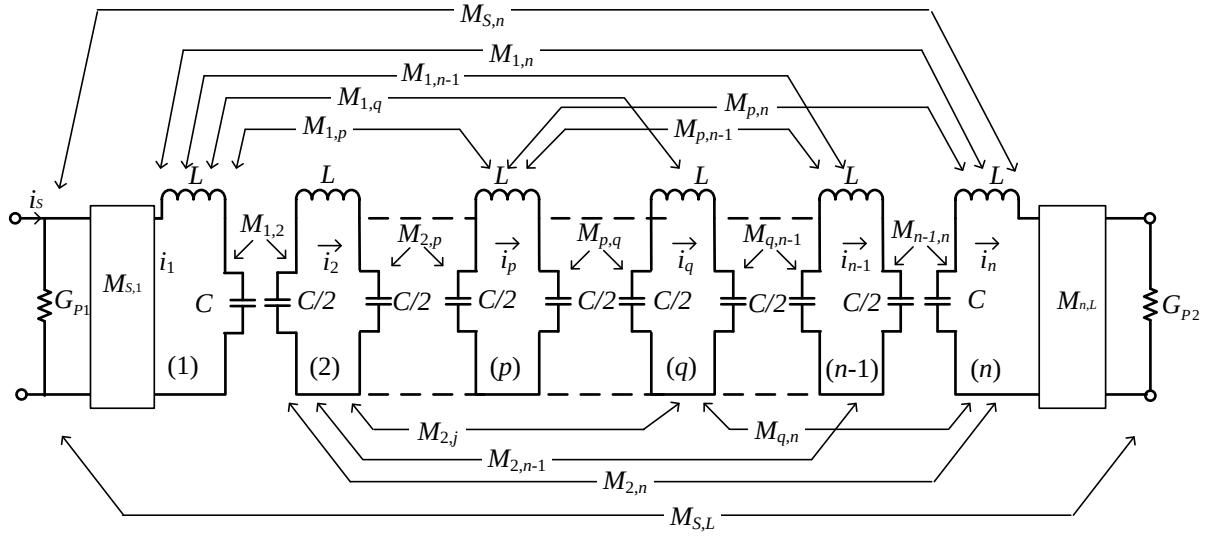

Fig. 2.9 Electrically coupled resonators model including input and output ports [4].

$$
\begin{array}{c}
\\ S \\ 1 \\ \\ n\text{-}1 \\ n \\ L
\end{array}
\begin{array}{c}
\begin{array}{ccccccc} S & 1 & & n\text{-}1 & n & L \end{array} \\
\begin{bmatrix}
m_{S,S} & m_{S,1} & \cdots & m_{S,n-1} & m_{S,n} & m_{S,L} \\
m_{1,S} & m_{1,1} & \cdots & m_{1,n-1} & m_{1,n} & m_{1,L} \\
\vdots & \vdots & \ddots & \vdots & \vdots & \vdots \\
m_{n-1,S} & m_{n-1,1} & \cdots & m_{n-1,n-1} & m_{n-1,n} & m_{n-1,L} \\
m_{n,S} & m & \cdots & m_{n,n-1} & m_{n,n} & m_{n,L} \\
m_{L,S} & m_{L,1} & \cdots & m_{L,n-1} & m_{L,n} & m_{L,L}
\end{bmatrix}
\end{array}
$$

$N \times N$ Coupling Matrix

Fig. 2.10 N+2 coupling matrix with all possible cross-couplings; the $N \times N$ coupling matrix is indicated within the dashed line [4].

2.3.2 Coupling matrix synthesis with Chebyshev response

The coupling matrix with Chebyshev response can be obtained directly from the *g* values, and *g* values with Chebyshev response are given in (2.33) [2]

$$
\begin{aligned}
g_0 &= 1 \\
g_1 &= \frac{2}{\gamma}\sin\left(\frac{\pi}{2n}\right) \\
g_i &= \frac{1}{g_{i-1}} \frac{4\sin\left(\frac{(2i-1)\pi}{2n}\right)\cdot\sin\left(\frac{(2i-3)\pi}{2n}\right)}{\gamma^2+\sin^2\left(\frac{(i-1)\pi}{n}\right)}, \quad (i = 2 \text{ to } n) \\
g_{n+1} &= \begin{cases} 1 & \text{for } n \text{ odd} \\ \coth^2\left(\frac{\beta}{4}\right) & \text{for } n \text{ even} \end{cases} \\
\beta &= \ln\left[\coth\left(\frac{L_{Ar}}{17.37}\right)\right] \\
\gamma &= \sinh\left(\frac{\beta}{2n}\right)
\end{aligned}
\tag{2.33}
$$

g values for other response, such as Butterworth and Elliptic, are available in [2]. In the $N\times N$ coupling matrix, the normalised coupling coefficients $m_{i,i+1}$, and the normalised external quality factors q_S and q_L to produce Chebyshev filter response are calculated by

$$
\begin{aligned}
q_{eS} &= Q_{eS}\cdot FBW = g_0 g_1, \;\; q_{eL} = Q_{eL}\cdot FBW = g_n g_{n+1} \\
m_{i,i+1} &= \frac{M_{i,i+1}}{FBW} = \frac{1}{\sqrt{g_i g_{i+1}}}, \qquad \text{for } i = 1 \text{ to } n-1
\end{aligned}
\tag{2.34}
$$

2.4 Microwave Transistor Amplifiers

Three-terminal transistors are widely employed in the solid microwave amplifiers [18]-[22]. The current at the output terminal of the transistor can be controlled in an efficient manner once the input terminal has a small voltage applied. By this way, the weak signal comes from the input

port is increased with the help of direct current (DC) power supply. There are various types of the transistor such as silicon bipolar junction transistors (BJTs), silicon germanium (SiGe) and gallium arsenide (GaAs) heterojunction bipolar transistors (HBTs), field effect transistors (MOSFETs), GaAs metal semiconductor field effect transistors (MESFETs), and pseudomorphic high electron mobility transistors (pHEMTs) [23]. The choice of the transistor depends on the category of the amplifier, application, required performance, or some other conditions. In this section, we choose the field effect transistors (FET) as our transistor example to introduce, which is also commonly employed in the microwave amplifier design [23]. The amplifier devices which are of concern in the following chapters primarily rely on the field effect transistors (FET). Based on two-port network analysis, some commonly used definitions in microwave amplifier design, such as two-port power gain, stability factor, and noise figure are discussed.

2.4.1 Two-port power gains

The most generally used gain definition of an amplifier is the transducer power gain G_T, and the definition is given by [23], i.e

$$G_T = \frac{P_L}{P_{avs}} \tag{2.35}$$

G_T is the ratio of the power delivered to the load P_L and the power available from the source P_{avs}. Transducer power gain depends on the source impedance Z_S and load impedance Z_L. It accounts for both source and load mismatch [23]. Consider an arbitrary two-port network model, characterised by *S*-parameters, as shown in Fig. 2.11. Z_S and Z_L are the source and load impedances [23].

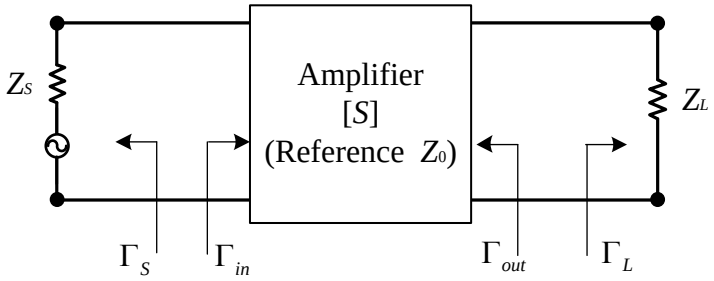

Fig. 2.11 An amplifier's two-port network with arbitrary source and load impedances [23].

Γ_S and Γ_L are the reflection coefficients seen from the source and the load, and they are calculated by

$$\Gamma_L = \frac{Z_L - Z_0}{Z_L + Z_0}$$
$$\Gamma_S = \frac{Z_S - Z_0}{Z_S + Z_0} \tag{2.36}$$

where Z_0 is the characteristic impedance. Γ_{in} and Γ_{out} are the reflection coefficients seen from the input and output of the amplifier, and they are calculated to give [23], [28], [29]

$$\Gamma_{in} = S_{11} + \frac{S_{12}S_{21}\Gamma_L}{1 - S_{22}\Gamma_L}$$
$$\Gamma_{out} = S_{22} + \frac{S_{12}S_{21}\Gamma_S}{1 - S_{11}\Gamma_S} \tag{2.37}$$

The transducer power gain can be calculated as [23]

$$G_T = \frac{|S_{21}|^2 \left(1 - |\Gamma_S|^2\right)\left(1 - |\Gamma_L|^2\right)}{|1 - \Gamma_S\Gamma_{in}|^2 |1 - S_{22}\Gamma_L|^2} \tag{2.38}$$

It can be seen from (2.38) that if the source and the load are perfectly matched, i.e. $\Gamma_S = \Gamma_L = 0$, and the transducer power gain equation collapse to

$$G_T = |S_{21}|^2 \tag{2.39}$$

Another important characteristic of the amplifier is the stability condition. Two types of stability

conditions are defined as [23]:

- *Unconditional stability*: The network is unconditional stable if $|\Gamma_{in}| < 1$ and $|\Gamma_{out}| < 1$ for all passive source and load impedances.
- *Conditional stability*: The network is conditional stable if $|\Gamma_{in}| < 1$ and $|\Gamma_{out}| < 1$ only for certain range of passive source and load impedances.

Because the input and output network of an amplifier is frequency-variant, the stability conditions depend on frequency. So, it may be possible for an amplifier to be stable in the desired band but oscillate at other frequencies.

The stability factor and stability circles are applied to check the stability conditions of the amplifier. The stability factor μ defines the minimum distance between the centre of the unit Smith chart and the unstable region in the load plane [23]. Having $\mu > 1$ examines the unconditional stability condition of the two-port network; μ is calculated as

$$\mu = \frac{1-|S_{11}|^2}{|S_{22}-S_{11}^*\Delta|+|S_{21}S_{12}|} > 1 \tag{2.40}$$

*S** is the complex conjugate of the corresponding *S*-parameters. Δ is the determinant of the two-port network *S*-parameters matrix.

$$\Delta = |S_{11}S_{22} - S_{12}S_{21}| \tag{2.41}$$

Having $\mu < 1$ means the potential unstable condition for the amplifier. Thus, stability circles are used to confine the range of values for Γ_S and Γ_L where amplifier will be stable. The detailed process for judging stability by stability circles were introduced in [23] and [28].

2.4.2 Large signal model of the transistor

Field effect transistors have many forms, such as MESFET (metal semiconductor FET),

MOSFET (metal oxide semiconductor), HEMT (high electron mobility transistor) and PHEMT (pseudomorphic HEMT) [23]. The maximum operating frequencies of the FETs are hundreds of GHz [24]-[26]. Not only do they have the broad operating frequency, but also other advantages including small size, low noise figure, broad bandwidth and low cost, which allow for a wide range of applications [26].

The structural model of an *n*-channel MOSFET is presented in Fig. 2.12, comprising three parts i.e. source, drain and gate.

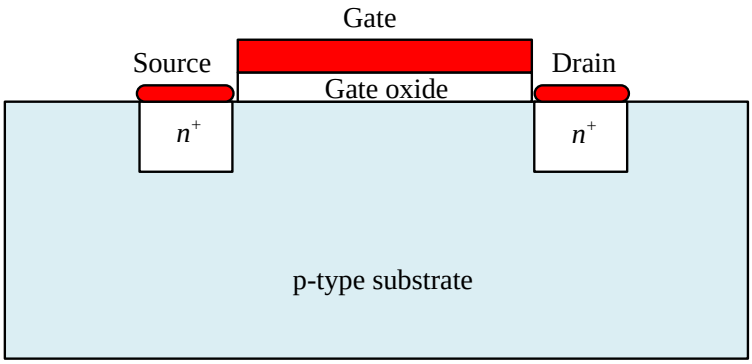

Fig. 2.12 A simplified cross-section view of an n-channel MOSFET [27].

The circuit behaviour of a MOSFET device is discussed below. Fig. 2.13 is the large signal circuit setup of the MOSFET with *G*, *S*, and *D* to represent the three terminals: gate, source and drain. Voltages between the gate, the drain and the source are denoted as v_{GS}, v_{DS} and the current through drain and source is i_{DS}.

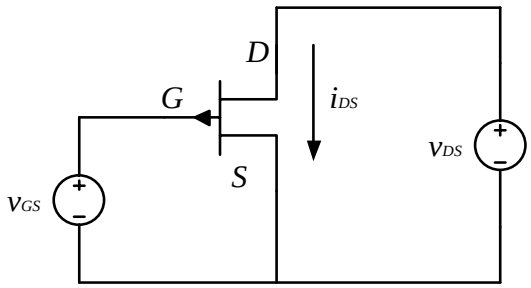

Fig. 2.13 Setup for observing the large signal behaviour of the MOSFET.

Setting different values of v_{GS}, and plotting the curves of i_{DS} versus v_{DS}, gives the illustration in Fig. 2.14. If $v_{GS}<V_T$, i_{DS} will be zero all the time, in other words, the MOSFET is in the OFF state. At this stage, MOSFET device is assumed working in a cut-off region. Here V_T is named by the threshold voltage of the MOSFET [27]. The device operates at ON state when the v_{GS} is beyond the voltage V_T.

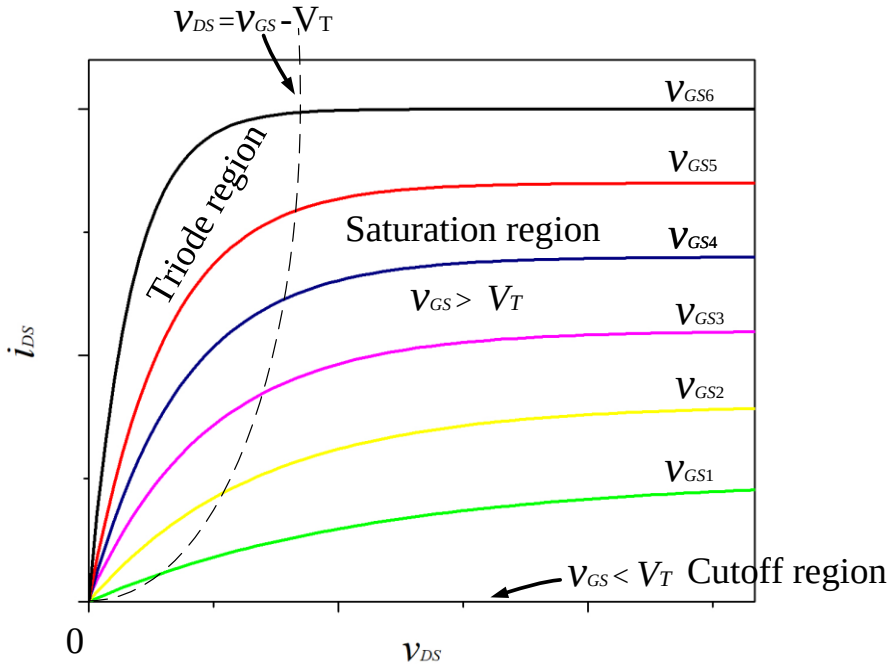

Fig. 2.14 Actual characteristics of MOSFET showing the triode, saturation, and cutoff-regions [27].

With the condition $v_{GS}>V_T$ satisfied, when the voltage v_{DS} is increased the current v_{DS} grows approximate linearly. When v_{DS} approach the value of $v_{GS}-V_T$, the curve bends and begin to flatten out. This property can be explained as the current i_{DS} saturates when v_{DS} exceeds $v_{GS}-V_T$. As i_{DS} saturates, the current strength i_{DS} will also depend on the value of v_{GS}. As shown in Fig. 2.14, we get several curves of i_{DS} versus v_{DS} for each set of v_{GS}, producing a family of i_{DS} versus v_{DS} curves. When the MOSFET is working at saturation region, the value of i_{DS} mainly depends on v_{GS}, the

mechanism of which behaves as a voltage-controlled current source. Generally, we will constrain amplifier designs to operate MOSFETs exclusively in their saturation region, thereby satisfying the saturation discipline [27], [28].

2.4.3 Narrowband amplifier design for maximum power gain

A narrow band amplifier usually has a bandwidth less than 10% [29]. The circuit diagram of the transistor with input and output matching network is shown in Fig. 2.15. In Fig. 2.15, matching networks are employed on both sides of the transistor to transform the input and output impedances Z_0 to the source and load impedances Z_S and Z_L. For the target of achieving maximum power gain, the reflection coefficient of the source impedance and the reflection coefficient of the load impedance should conjugately match the input and output of reflection coefficient of the transistor, that is

$$\Gamma_{in} = \Gamma_S^*, \Gamma_{out} = \Gamma_L^* \tag{2.42}$$

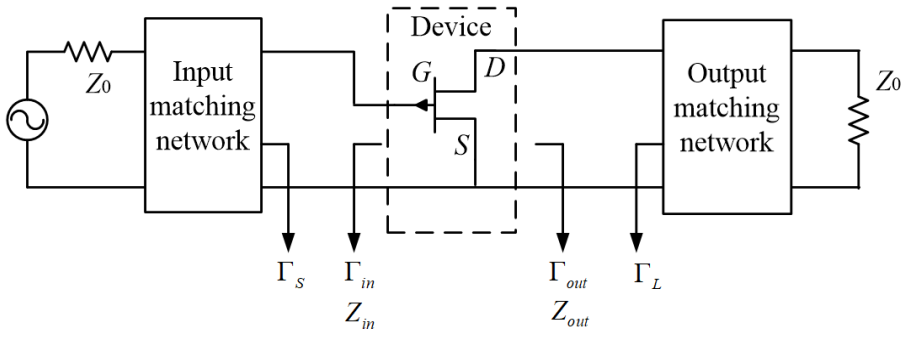

Fig. 2.15 The general transistor amplifier with input and output matching network [23].

The conditions of (2.42) will maximise the overall transducer gain. This maximum transducer gain will be given by [23], [29]

$$G_{T\max} = \frac{1}{1-|\Gamma_S|^2}|S_{21}|^2 \frac{1-|\Gamma_L|^2}{|1-S_{22}\Gamma_L|^2} \tag{2.43}$$

With this conjugate matching, the input and output of the amplifier are matched to characteristic impedance Z_0 [23].

As the transistor is usually a bilateral device ($S_{12}\neq 0$), Γ_{in} is affected by Γ_{out} and vice versa. If the input and output of the transistor are matched simultaneously, it should satisfy the conditions in (2.42). The reflection coefficients seen looking toward the input and the output of the transistor can be calculated by [23]

$$\begin{aligned} \Gamma_{in} &= S_{11} + \frac{S_{12}S_{21}\Gamma_L}{1-S_{22}\Gamma_L} \\ \Gamma_{out} &= S_{22} + \frac{S_{12}S_{21}\Gamma_S}{1-S_{11}\Gamma_S} \end{aligned} \tag{2.44}$$

Substitute (2.42) into (2.44) giving the necessary equations satisfying simultaneous matching conditions

$$\begin{aligned} \Gamma_S^* &= S_{11} + \frac{S_{12}S_{21}\Gamma_L}{1-S_{22}\Gamma_L} \\ \Gamma_L^* &= S_{22} + \frac{S_{12}S_{21}\Gamma_S}{1-S_{11}\Gamma_S} \end{aligned} \tag{2.45}$$

The solutions of (2.45) are given by

$$\begin{aligned} \Gamma_S &= \frac{B_1 \pm \sqrt{B_1^2 - 4|C_1|^2}}{2C_1} \\ \Gamma_L &= \frac{B_2 \pm \sqrt{B_2^2 - 4|C_2|^2}}{2C_2} \end{aligned} \tag{2.46}$$

The variables B_1, B_2, C_1, C_2 in (2.46) are defined as

$$
\begin{aligned}
B_1 &= 1 + |S_{11}|^2 - |S_{22}|^2 - |\Delta|^2 \\
B_2 &= 1 + |S_{22}|^2 - |S_{11}|^2 - |\Delta|^2 \\
C_1 &= S_{11} - \Delta S_{22}^* \\
C_2 &= S_{22} - \Delta S_{11}^*
\end{aligned}
\tag{2.47}
$$

The solutions in (2.46) are possible only if the value within the square root is positive and it can be shown that it is equivalent to the required stability factor $\mu > 1$ in (2.40). Therefore, the unconditional table device can be conjugately matched for maximum gain [23].

REFERENCES

[1] A. Oppenheim, S. Nawab and A. Willsky, *Signals and systems*. London: Prentice-Hall International, 1997.

[2] J. S. Hong and M. J. Lancaster, *Microstrip Filters for RF/Microwave Applications*. New York, NY, USA: Wiley, 2001.

[3] K. Kurokawa, "Power Waves and the Scattering Matrix," *IEEE Trans. Microw. Theory Techn.*, vol. 13, no. 2, pp. 194-202, Mar 1965.

[4] R. J. Cameron, R. Mansour and C. M Kudsia, *Microwave Filters for Communication Systems: Fundamentals, Design and Applications*. 1st. New York, NY, USA: Wiley, 2007.

[5] H. Baher, *Synthesis of electrical networks*. Chichester: Wiley, 1984.

[6] A.E. Atia, A.E. Williams, and R.W. Newcomb, "*Narrow-band multiple-coupled cavity synthesis*," *IEEE Trans Circ. Syst*, 1974, 21, (5), pp. 649-655.

[7] R. Cameron, "*General coupling matrix synthesis methods for Chebyshev filtering functions*,", *IEEE Trans Microw. Theory Techn.*, 47(4), pp.433-442.

[8] J. Mason and D. Handscomb, *Chebyshev polynomials*. Boca Raton: Chapman & Hall/CRC, 2003.

[9] P. L. Chebyshev (1854) "Théorie des mécanismes connus sous le nom de parallélogrammes," *Mémoires des Savants étrangers présentés à l'Académie de Saint-Pétersbourg*, vol. 7, pages 539–586.

[10] J. Rivlin, J. Theodore, *The Chebyshev polynomials*. Pure and Applied Mathematics. *Wiley-Interscience* [John Wiley & Sons], New York-London-Sydney, 1974.

[11] U. W. Hochstrasser, *Orthogonal Polynomials*, *Handbook of Mathematical Functions with Formulas, Graphs, and Mathematical Tables*. (M. Abramowitz and I. A. Stegun, eds.). New York: Dover, 1972.

[12] G. Matthaei, L. Young and, E. Jones, *Microwave filters, impedance-matching networks, and coupling structures*. [S.l.]: Mcgraw-Hill, 1964.

[13] A. E. Atia; and A. E. Williams, "New types of bandpass filters for satellite transponders," *COMSAT Tech. Rev.,* vol. 1, pp. 21-43, Fall 1971.

[14] A. E. Atia and A. E. Williams, "Narrow-Bandpass Waveguide Filters," *IEEE Trans. Microw. Theory and Techn.,* vol. 20, pp. 258-265, 1972.

[15] A. E. Atia, A. E. Williams, and R. W. Newcomb, "Narrow-band multiple-coupled cavity synthesis," *Circuits and Systems, IEEE Transactions on,* vol. 21, pp. 649-655, 1974.

[16] R. J. Cameron, "Advanced coupling matrix synthesis techniques for microwave filters," *IEEE Trans. Microw. Theory Techn.s*, vol. 51, pp. 1-10, 2003.

[17] A. E. Atia and A. E. Williams, "New types of bandpass filters for satellite transponders," *COMSAT Tech. Rev.,* vol. 1, pp. 21-43, Fall 1971.

[18] R. S. Engelbrecht and K. Kurokawa, "A wideband low noise L-band balanced transistor amplifier," *Proc. IEEE*, Vol. 53, pp. 237–247, March 1965.

[19] K. Kurokawa, Design theory of balanced transistor amplifiers, Bell Syst. Tech. J., Vol. 44, pp. 1675–1698, October 1965.

[20] H. F. Cooke, *Microwave transistors: theory and design*. Proc. IEEE, Vol. 59, pp. 1163–1181, August 1971.

[21] H. Krauss, C. Bostian, and F. Raab, *Solid-State Radio Engineering*. John Wiley & Sons, Hoboken, NJ, 1980.

[22] J. V. Dilorenzo and D. D. Khandelwal (Eds.), *GaAs FET Principles and Technology*. Artech House, Norwood, MA, 1982.

[23] D. Pozar, *Microwave engineering*. Hoboken, NJ: Wiley, 2012.

[24] K. Leong *et al*. "A 0.85 THz Low Noise Amplifier Using InP HEMT Transistors," *IEEE Microw. Wirel. Compon. Lett.*, 25(6), pp.397-399.

[25] H. Wang, R. Lai, S. Chen, and J. Berenz, "A monolithic 75-110 GHz balanced InP-based HEMT amplifier," *IEEE Microw. Guided Wave Lett.*, 1993, pp.381-383.

[26] M. Urteaga *et al*., "InP HBTs for THz frequency integrated circuits," *IPRM 2011 - 23rd Inter. Conf. Indium Phosphide Related Materials*, Berlin, 2011, pp. 1-4.

[27] A. Agarwal, and J. Lang, *Foundations of analog and digital electronic design*. San Francisco, Calif.: Morgan Kaufmann, 2005.

[28] I. Bahl, *Fundamentals of RF and microwave transistor amplifiers*. Hoboken, N.J.: Wiley, 2009.

[29] S. Liao, *Microwave circuit analysis and amplifier design*. Englewood Cliffs, N.J.: Prentice Hall, 1987.

CHAPTER 3

COUPLING MATRICES OF THE INTEGRATED COMPONENTS

The coupling matrix technique is widely utilised in the design and synthesis of a broad range of resonator-based structures such as filters, diplexers, and multiplexers [1], [2]. This chapter extends the conventional coupling matrix to the novel $N+X$ coupling matrices to describe multiple integrated components (e.g. amplifiers, cascaded filters). Here N is the number of the resonators. The overall performance of the integrated components can be predicted using matrix calculation and the initial parameters of the components' physical structure can also be extracted from the coupling matrix. The physical implementations of the integrated components will be discussed in Chapter 4 and Chapter 5. Both analytical and numerical methods are employed for the synthesis of the novel coupling matrices corresponding to the filter amplifier which is extensively investigated in the thesis.

Section 3.1 introduces the coupling matrix of cascaded filters, generalising the cascaded filters. An active $N+3$ coupling matrix representing a filter amplifier is synthesised in Section 3.2. This $N+3$ coupling matrix includes active elements of the transistor's parameters, resulting in a filter response with gain. In Section 3.3, resonators used for matching both the input and output of the

transistor is described by an N+4 coupling matrix. In this case, the transistor is located in the middle of the resonators, and the matrix optimisation based on a local algorithm is involved to achieve simultaneous filter matching, eliminating the influence of the parasitic parameters of the transistor. Appropriate initial parameters can be extracted for the physical device based on the coupling matrix, where EM optimisation always relies on accurate starting points to improve the design efficiency.

3.1 Coupling Matrix of the Cascade Filters

Filters are often cascaded in series to improve the performance by rejecting outside bands or some other functionalities [3], [4]. The half-wavelength transmission line is often employed in cascaded filters to realise non-resonance-nodes [3], [4]. Extra columns and rows are added to the conventional coupling matrix corresponding to the non-resonance nodes, producing a novel N+4 coupling matrix [4]. However, this coupling matrix can only be applied in the filters cascaded by a fixed length of transmission line, i.e. half-wavelength transmission line. In this section, based on the Y matrix of the transmission line, the coupling matrix of cascaded filters with any length of transmission line is synthesised. This discussion will help to develop the coupling matrix corresponding to a more general situation, as well as predict the cascaded filter response with any length of transmission line. The cascaded device is characterised as a whole entity in matrix form.

3.1.1 Y matrix of the transmission line

Fig. 3.1 shows the voltages and currents relationships at the two ports of the transmission line. V_i and I_i (i=1 to 2) are the voltages and currents at the two ports.

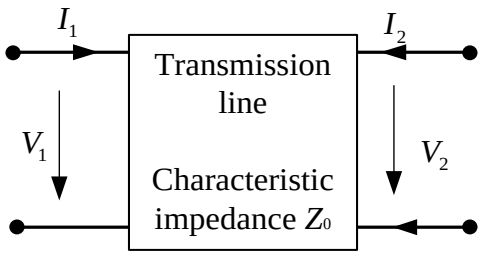

Fig. 3.1 The voltages and currents at the two ports of the transmission line.

The ABCD matrix for the transmission line is given by [1],

$$\begin{bmatrix} A & B \\ C & D \end{bmatrix} = \begin{bmatrix} \cosh \gamma l & Z_0 \sinh \gamma l \\ \dfrac{\sinh \gamma l}{Z_0} & \cosh \gamma l \end{bmatrix} \tag{3.1}$$

where l is denoted as the length of the transmission line. Here, we assume the transmission is lossless, thus $\gamma = jk$. k is known as the propagation constant and is defined by $k=\omega\sqrt{\mu\epsilon}$; its unit is 1/m. μ is the permeability and ϵ is the permittivity. Z_0 is the characteristic impedance and in our examples below, it is usually Z_0=50 Ω. The admittance (Y) matrix can be calculated using the ABCD matrix to Y matrix transformation formulas provided in [1] to give

$$Y_{TL} = \begin{bmatrix} \dfrac{\cosh \gamma l}{Z_0 \sinh \gamma l} & \dfrac{-1}{Z_0 \sinh \gamma l} \\ \dfrac{-1}{Z_0 \sinh \gamma l} & \dfrac{\cosh \gamma l}{Z_0 \sinh \gamma l} \end{bmatrix} \tag{3.2}$$

3.1.2 Coupling matrix of cascaded filters

Non-resonating-nodes (NRN) cascading two filters are schematically exhibited in Fig. 3.2(a), where the clear circles denote the source and load, and solid circles refer to the resonators and NRNs.Fig. 3.2(b) is the lumped circuit of the resonators coupled by J inverters and the transmission line. All the parallel capacitors and inductors representing the resonators are coupled by inverters.

Here $J_{i,j}$, $J_{k,in}$ and $J_{out,k+1}$ are the inverters coupling to the k^{th} and $(k+1)^{th}$ resonators to the transmission line; the input port admittance and output admittance are denoted by Y_{P1} and Y_{P2}. We use v_{P1}, v_{P2}, v_{in}, and v_{out} with the subscript to distinguish the node voltages for resonators and ports, respectively. The voltage at the i^{th} resonator is denoted as v_i (i=1 to n), whereas the v_{Pi} (i=1 to 2) is the voltage at input and output ports. v_{in} and v_{out} are the voltages at input and output ports of the transmission line. i_S is the current source at port 1.

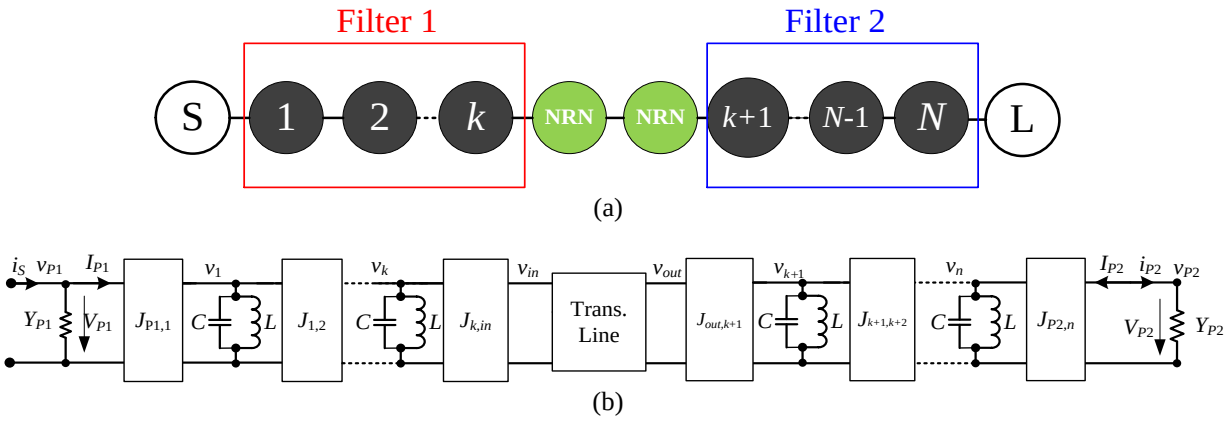

Fig. 3.2 Topology and circuit schematic of the cascaded filter. (a) Topology. (b) Lumped circuit representation.

Appling Kirchoff's current laws at each nodes of the circuit in Fig. 3.2(b), we can write down the equations as

$$
\begin{aligned}
Y_{P1}v_{P1} - jJ_{P1,1}v_1 &= i_s \\
-jJ_{1,P1}v_{P1} + j\left(\frac{1}{j\omega L} + j\omega C\right)v_1 - jJ_{1,2}v_2 &= 0 \\
&\vdots \\
-jJ_{in,k}v_k + \frac{\cosh\gamma l}{Z_0\sinh\gamma l}v_{in} + \frac{-1}{Z_0\sinh\gamma l}v_{out} &= 0 \\
\frac{-1}{Z_0\sinh\gamma l}v_{in} + \frac{\cosh\gamma l}{Z_0\sinh\gamma l}v_{out} - jJ_{out,k+1}v_{k+1} &= 0 \\
&\vdots \\
-jJ_{n,n-1}v_{n-1} + \left(\frac{1}{j\omega L} + j\omega C\right)v_n - jJ_{n,P2}v_{P2} &= 0 \\
-jJ_{P2,n}v_n + Y_{P2}v_{P2} &= 0
\end{aligned}
\tag{3.3}
$$

In matrix form,

$$
\begin{bmatrix}
Y_{P1} & -jJ_{P1,1} & 0 & \cdots \\
-jJ_{1,P1} & \left(\frac{1}{j\omega L}+j\omega C\right) & -jJ_{1,2} & \cdots \\
\vdots & \vdots & \vdots & \vdots \\
0 & 0 & \cdots & \left(\frac{1}{j\omega L}+j\omega C\right) \\
0 & 0 & \cdots & -jJ_{in,k} \\
0 & 0 & \cdots & \cdots \\
0 & 0 & \cdots & \cdots \\
\vdots & \vdots & \vdots & \vdots \\
0 & 0 & 0 & \cdots \\
0 & 0 & 0 & \cdots
\end{bmatrix}
$$

$$
\begin{bmatrix}
\cdots & \cdots & \cdots & \cdots & 0 & 0 \\
\cdots & \cdots & \cdots & \cdots & 0 & 0 \\
\vdots & \vdots & \vdots & \vdots & \vdots & \vdots \\
-jJ_{k,out} & 0 & \cdots & \cdots & 0 & 0 \\
\frac{\cosh\gamma l}{Z_0\sinh\gamma l} & \frac{-1}{Z_0\sinh\gamma l} & \cdots & \cdots & 0 & 0 \\
\frac{-1}{Z_0 j\sin\gamma l} & \frac{\cosh\gamma l}{Z_0\sinh\gamma l} & -jJ_{out,k+1} & \cdots & 0 & 0 \\
0 & -jJ_{k+1,out} & \left(\frac{1}{j\omega L}+j\omega C\right) & \cdots & \cdots & 0 \\
\vdots & \vdots & \vdots & \vdots & \vdots & \vdots \\
\cdots & \cdots & \cdots & \cdots & \left(\frac{1}{j\omega L}+j\omega C\right) & -jJ_{n,P2} \\
\cdots & \cdots & \cdots & \cdots & -jJ_{P2,2} & Y_{P2}
\end{bmatrix}
\begin{bmatrix} v_{P1} \\ v_1 \\ v_2 \\ \vdots \\ v_{in} \\ v_{out} \\ \vdots \\ v_{P2} \end{bmatrix}
=
\begin{bmatrix} i_s \\ 0 \\ 0 \\ \vdots \\ 0 \\ 0 \\ \vdots \\ 0 \end{bmatrix}
\qquad (3.4)
$$

Or

$$[Y]\cdot[v]=[i] \qquad (3.5)$$

The next step is to find the relationships between the admittance matrix [*Y*] and the scattering parameters. The wave variables a_k and b_k are defined by [5]

$$a_k = \frac{1}{2}\left(\frac{V_{Pk}\cdot Y_{Pk} + I_{Pk}}{2\sqrt{\left|\mathrm{Re}\left(Y_{Pk}\right)\right|}}\right) \qquad \left(k = 1 \text{ to } 2\right) \tag{3.6}$$
$$b_k = \frac{1}{2}\left(\frac{V_{Pk}\cdot Y_{Pk}^{*} - I_{Pk}}{2\sqrt{\left|\mathrm{Re}\left(Y_{Pk}\right)\right|}}\right)$$

V_{Pk} and I_{Pk} are the voltage and current at the ports of the network and Y_{Pk} is the admittance of the port k (k=1 to 2), and this two ports network is illustrated in Fig. 2.1. The relationships between the scattering parameters and the wave variables a_k and b_k are given by [1],

$$S_{11} = \left.\frac{b_1}{a_1}\right|_{a_2=0} \qquad S_{12} = \left.\frac{b_1}{a_2}\right|_{a_1=0}$$
$$S_{21} = \left.\frac{b_2}{a_1}\right|_{a_2=0} \qquad S_{22} = \left.\frac{b_2}{a_2}\right|_{a_1=0} \tag{3.7}$$

By inspecting the lumped element circuit in Fig. 3.2, it can be recognised that V_{Pk}=v_{Pk} (k=1, 2), I_{P2}=-i_{P2}, I_{P1}=i_S-$V_{P1}\cdot Y_{P1}$. Considering (3.6), we have

$$a_1 = \frac{i_s}{2\sqrt{\left|\mathrm{Re}\,Y_{P1}\right|}} \qquad b_1 = \frac{v_{P1}\left(Y_{P1} + Y_{P1}^{*}\right) - i_s}{2\sqrt{\left|\mathrm{Re}\,Y_{P1}\right|}} = \frac{2v_{P1}\left(\left|\mathrm{Re}\,Y_{P1}\right|\right) - i_s}{2\sqrt{\left|\mathrm{Re}\,Y_{P1}\right|}}$$
$$a_2 = 0 \qquad\qquad b_2 = \frac{v_{P2}\left(Y_{P2} + Y_{P2}^{*}\right)}{2\sqrt{\left|\mathrm{Re}\,Y_{P2}\right|}} = v_{P2}\sqrt{\left|\mathrm{Re}\,Y_{P2}\right|} \tag{3.8}$$

And therefore the relationship between the S-parameters and the wave variables can be formulated by substituting (3.8) into (3.7), given by

$$S_{11} = \left.\frac{b_1}{a_1}\right|_{a2=0} = \frac{2v_{P1}\sqrt{\left|\mathrm{Re}\,Y_{P1}\right|}}{i_s} - 1$$
$$S_{21} = \left.\frac{b_2}{a_1}\right|_{a2=0} = \frac{2v_{P2}\cdot\sqrt{\left|\mathrm{Re}\,Y_{P1}\right|\cdot\left|\mathrm{Re}\,Y_{P2}\right|}}{i_s} \tag{3.9}$$

v_{Pk} (k=1,2) are found from (3.4) as

$$v_{Pk} = i_s \cdot [Y]^{-1}_{Pk,P1} \tag{3.10}$$

where $[Y]^{-1}_{Pk,P1}$ is denoted as the entry in row P_k and column P_1 of $[Y]^{-1}$. Replacing the node voltages in (3.9) with those in (3.10) results in

$$\begin{aligned} S_{11} &= 2\left|\mathrm{Re}\, Y_{P1}\right|[Y]^{-1}_{P1,P1} - 1 \\ S_{21} &= 2\sqrt{\left|\mathrm{Re}\, Y_{P1}\right| \cdot \left|\mathrm{Re}\, Y_{P2}\right|}[Y]^{-1}_{P2,P1} \end{aligned} \tag{3.11}$$

In order to get the coupling matrix, the next step is to scale the $[Y]$ matrix in (3.4). Here each row i and column j (i, j=1 to n) of the matrix $[Y]$ is divided by $\sqrt{\omega_0 C \cdot FBW}$, where $\omega_0 = 1/\sqrt{LC}$ is the centre frequency of parallel capacitors (C) and inductors (L) circuit. FBW is the fractional bandwidth of the network. Except for row i and column j, the rows and columns P_1, P_2, P_{in}, and P_{out} (in Fig. 3.3) are divided by $\sqrt{Y_0}$, which Y_0=0.02 S is the referred characteristic admittance. Rows and columns P_1 and P_2 indicate the input port and output port of the filter; P_{in}, and P_{out} represent the input port and output port of the transmission line. The matrix scaling process is illustrated in Fig. 3.3 and the same matrix scaling technique is described in [2].

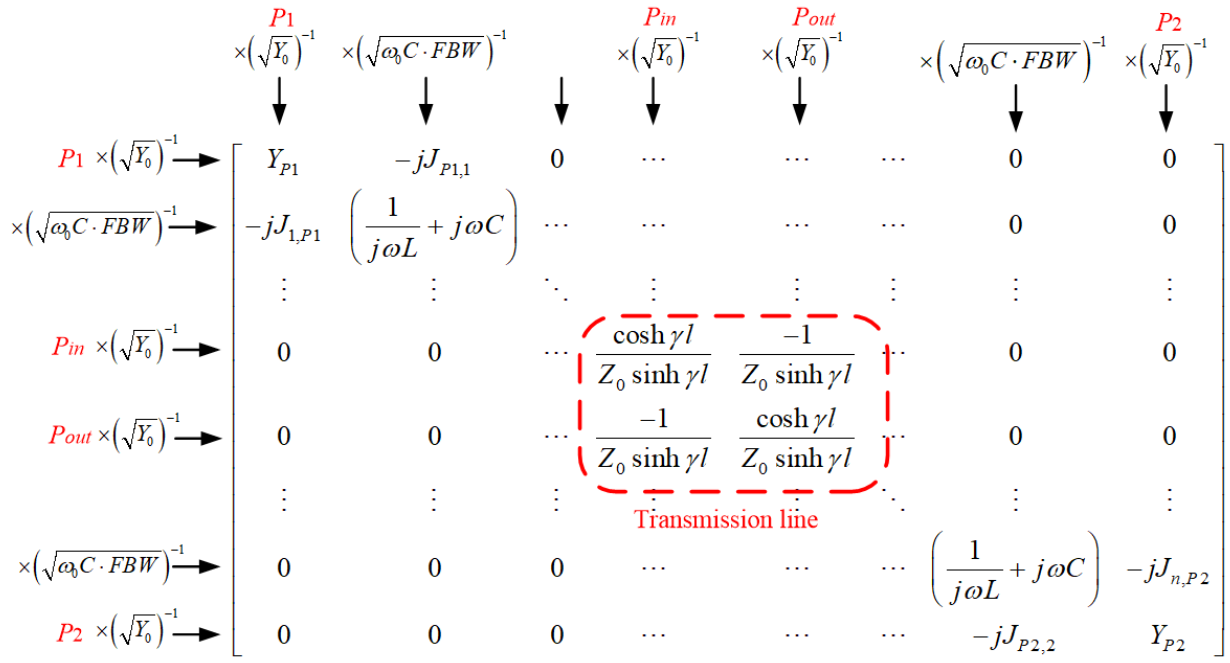

Fig. 3.3 Matrix operation from the $[Y]$ to $[\bar{Y}]$.

The resultant scaled matrix $[\bar{Y}]$ is

$$
\left[\bar{Y}\right]=\begin{bmatrix}
\bar{Y}_{P1} & -j\frac{J_{P1,1}}{\sqrt{\omega_0 C\cdot FBW\cdot Y_0}} & \cdots & & & & \\
-j\frac{J_{1,P1}}{\sqrt{\omega_0 C\cdot FBW\cdot Y_0}} & p & \cdots & & & & \\
\vdots & \vdots & \vdots & & & & \\
0 & 0 & \cdots & & & & \\
0 & 0 & \cdots & & & & \\
0 & 0 & \cdots & & & & \\
0 & 0 & \cdots & & & & \\
\vdots & \vdots & \vdots & & & & \\
\vdots & \vdots & \vdots & \vdots & \vdots & & \\
p & -j\frac{J_{k,in}}{\sqrt{\omega_0 C\cdot FBW\cdot Y_0}} & 0 & \cdots & \cdots & & \\
-j\frac{J_{in,k}}{\sqrt{\omega_0 C\cdot FBW\cdot Y_0}} & \frac{\cosh\gamma l}{\sinh\gamma l} & \frac{-1}{\sinh\gamma l} & \cdots & \cdots & & \\
0 & \frac{-1}{\sinh\gamma l} & \frac{\cosh\gamma l}{\sinh\gamma l} & -j\frac{J_{L2,out}}{\sqrt{\omega_0 C\cdot FBW\cdot Y_0}} & \cdots & & \\
\cdots & 0 & -j\frac{J_{k+1,out}}{\sqrt{\omega_0 C\cdot FBW\cdot Y_0}} & p & \cdots & & \\
\vdots & \vdots & \vdots & \vdots & \vdots & & \\
\cdots & \cdots & \cdots & \cdots & \cdots & & \\
\cdots & \cdots & \cdots & \cdots & \cdots & & \\
 & & \vdots & \vdots & \vdots & & \\
 & & \cdots & 0 & 0 & & \\
 & & \cdots & 0 & 0 & & \\
 & & \cdots & 0 & 0 & & \\
 & & \cdots & \cdots & 0 & & \\
 & & \vdots & \vdots & \vdots & & \\
 & & \cdots & p & -j\frac{J_{n,P2}}{\sqrt{\omega_0 C\cdot FBW\cdot Y_0}} & & \\
 & & \cdots & -j\frac{J_{P2,n}}{\sqrt{\omega_0 C\cdot FBW\cdot Y_0}} & \bar{Y}_{P2} & &
\end{bmatrix}
$$

(3.12)

p is the complex frequency variable, i.e.

$$p = \frac{j\omega C + \dfrac{1}{j\omega C}}{\omega_0 C \cdot FBW} = j\frac{1}{FBW}\left(\frac{\omega}{\omega_0} - \frac{\omega_0}{\omega}\right) \tag{3.13}$$

It should be noted that the scaled matrix $[\bar{Y}]$ in (3.12) is not equivalent to the matrix $[Y]$ in (3.4), because the different scaling factors are operated on the rows and columns of $[Y]$. However, the S-parameters response calculated by $[\bar{Y}]$ yields same results of as calculated using $[Y]$. This will be proven as follows.

The inverses of $[\bar{Y}]$ and $[Y]$ can be expressed by the ratios of their co-factors and determinants [6]

$$\begin{aligned} [Y]^{-1}_{Pi,Pj} &= \frac{cof\left(Y_{Pi,Pj}\right)}{|Y|}, \left(|Y| \neq 0\right) \\ [\bar{Y}]^{-1}_{Pi,Pj} &= \frac{cof\left(\bar{Y}_{Pi,Pj}\right)}{|\bar{Y}|}, \left(|\bar{Y}| \neq 0\right) \end{aligned} \qquad i, j = 1 \text{ to } n \tag{3.14}$$

where $|Y|$and $|\bar{Y}|$ are the determinant of $[Y]$ and $[\bar{Y}]$. $cof\left(Y_{Pi,Pj}\right)$ and $cof\left(\bar{Y}_{Pi,Pj}\right)$ are the entries in column P_i and row P_j of the cofactor matrices of $[Y]$ and $[\bar{Y}]$. Recalling matrix $[Y]$ in (3.4) and $[\bar{Y}]$ in (3.12), we obtain the relationships of their determinants and cofactors as

$$\begin{aligned} |Y| &= \left(\sqrt{\omega_0 C \cdot FBW}\right)^{2n} \cdot \left(\sqrt{Y_0}\right)^{8} |\bar{Y}| \\ cof\left(Y_{Pi,Pj}\right) &= \left(\sqrt{\omega_0 C \cdot FBW}\right)^{2n} \cdot \left(\sqrt{Y_0}\right)^{6} cof\left(\bar{Y}_{Pi,Pj}\right) \quad \left(i, j = 1 \text{ to } 2,\ i \neq j\right) \end{aligned} \tag{3.15}$$

Note that in Fig. 3.3, the rows and columns P_1, P_2, P_{in} and P_{out} of $[Y]$ are divided by $\sqrt{Y_0}$ up to eight times; the row i and column j (i, j=1 to n) are scaled by $\sqrt{\omega C \cdot FBW}$ up to 2n times. Thus, the exponents of $\sqrt{Y_0}$ and $\sqrt{\omega C \cdot FBW}$ in (3.15) are 8 and 2n, respectively.

Substituting (3.15) into (3.14) yields

$$[Y]^{-1}_{Pi,Pj} = \frac{[\bar{Y}]^{-1}_{Pi,Pj}}{Y_0} \tag{3.16}$$

Thus, the *S*-parameters can be calculated by substituting (3.16) into (3.11), given by

$$\begin{aligned} S_{11} &= 2\left|\mathrm{Re}\,\bar{Y}_{P1}\right|[\bar{Y}]^{-1}_{P1,P1} - 1 \\ S_{21} &= 2\sqrt{\left|\mathrm{Re}\,\bar{Y}_{P1}\right| \cdot \left|\mathrm{Re}\,\bar{Y}_{P2}\right|}[\bar{Y}]^{-1}_{P2,P1} \end{aligned} \tag{3.17}$$

We add a bar on the top of Y_{Pk} to denote the normalised port admittance $\bar{Y}_{Pk}$.

Let's continue to simplify the normalised matrix $[\bar{Y}]$. Referring to [1] the *J* inverters between resonators are formulated by

$$J_{i,j} = J_{i,j} = \omega C_{i,j} = \omega C_{j.i} \tag{3.18}$$

where $C_{i,j} = C_{j,i}$ represents the mutual capacitance between resonator *i* and *j*. The *J* inverters coupling the ports and transmission line to the resonators (see Fig. 3.2) $J_{P1,1}$, $J_{n,P2,}$ $J_{k,in}$, and $J_{out,k+1}$ are defined as

$$\begin{aligned} J_{P1,1} = J_{1,P1} &= \sqrt{\frac{\omega_0 C \cdot Y_0}{Q_{e1}}}, J_{P2,n} = J_{n,P2} = \sqrt{\frac{\omega_0 C \cdot Y_0}{Q_{en}}} \\ J_{in,k} = J_{k,in} &= \sqrt{\frac{\omega_0 C \cdot Y_0}{Q_{ek}}}, J_{k+1,out} = J_{out,k+1} = \sqrt{\frac{\omega_0 C \cdot Y_0}{Q_{ek+1}}} \end{aligned} \tag{3.19}$$

where Q_{ei} (*i*=1 to *n*) is the external quality factor of the i^{th} resonator defined in [1]. In (3.19), Q_{ek} and Q_{ek+1} are the external quality factors of the k^{th} and $(k+1)^{\text{th}}$ resonators.

Substitute (3.18) and (3.19) into (3.12), we have

$$
\left[\overline{Y}\right]=\begin{bmatrix}
\overline{Y}_{P1} & -j\sqrt{\frac{1}{FBW\cdot Q_{e1}}} & \cdots & & & \\
-j\sqrt{\frac{1}{FBW\cdot Q_{e1}}} & p & \cdots & & & \\
\vdots & \vdots & \vdots & & & \\
0 & 0 & \cdots & & & \\
0 & 0 & \cdots & & & \\
0 & 0 & \cdots & & & \\
0 & 0 & \cdots & & & \\
\vdots & \vdots & \vdots & & & \\
\vdots & \vdots & \vdots & \vdots & \vdots & \\
p & -j\sqrt{\frac{1}{FBW\cdot Q_{ek}}} & 0 & \cdots & \cdots & \\
-j\sqrt{\frac{1}{FBW\cdot Q_{ek}}} & \frac{\cosh\gamma l}{\sinh\gamma l} & \frac{-1}{\sinh\gamma l} & \cdots & \cdots & \\
0 & \frac{-1}{\sinh\gamma l} & \frac{\cosh\gamma l}{\sinh\gamma l} & -j\sqrt{\frac{1}{FBW\cdot Q_{ek+1}}} & \cdots & \\
\cdots & 0 & -j\sqrt{\frac{1}{FBW\cdot Q_{ek+1}}} & p & \cdots & \\
\vdots & \vdots & \vdots & \vdots & \vdots & \\
\cdots & \cdots & \cdots & \cdots & \cdots & \\
\cdots & \cdots & \cdots & \cdots & \cdots & \\
 & & \vdots & \vdots & \vdots & \\
 & & \cdots & 0 & 0 & \\
 & & \cdots & 0 & 0 & \\
 & & \cdots & 0 & 0 & \\
 & & \cdots & \cdots & 0 & \\
 & & \vdots & \vdots & \vdots & \\
 & & \cdots & p & -j\sqrt{\frac{1}{FBW\cdot Q_{en}}} & \\
 & & \cdots & -j\sqrt{\frac{1}{FBW\cdot Q_{en}}} & \overline{Y}_{P2} &
\end{bmatrix} \tag{3.20}
$$

Note that the normalised external quality factor can be expressed as

$$q_{ei} = FWB \cdot Q_{ei} \quad (i = 1 \text{ to } n) \tag{3.21}$$

and the inter-resonator coupling coefficient $M_{i,j}$ is given by

$$M_{i,j} = \frac{C_{i,j}}{C} = FBW \cdot m_{i,j} \quad (i, j = 1 \text{ to } n,\ i \neq j) \tag{3.22}$$

Define the coupling coefficients between two ports of the transmission line as

$$m_{in,out} = m_{out,in} = \frac{-j}{\sinh \gamma l} \tag{3.23}$$

The normalised external coupling coefficients between two ports and the resonators can be defined as

$$\begin{aligned} m_{k,in} &= m_{in,k} = \sqrt{\frac{1}{q_{ek}}} \\ m_{out,k+1} &= m_{k+1,out} = \sqrt{\frac{1}{q_{ek+1}}}, \end{aligned} \tag{3.24}$$

where q_{ek} and q_{ek+1} are the normalised external quality factors of the k^{th} and $(k+1)^{\text{th}}$ resonators. The coupling coefficients between the transmission line and the resonators can be defined as

$$\begin{aligned} m_{P1,1} &= m_{1,P1} = \sqrt{\frac{1}{q_{e1}}} \\ m_{P2,n} &= m_{n,P2} = \sqrt{\frac{1}{q_{en}}} \end{aligned} \tag{3.25}$$

In order to simplify the circuit, the normalised port admittance $\bar{Y}_{P1}$ and $\bar{Y}_{P2}$ are assumed to be one, i.e

$$\bar{Y}_{P1} = \bar{Y}_{P2} = 1 \tag{3.26}$$

Substitute (3.21)-(3.26) into (3.20) yielding

$$\left[\bar{Y}\right]=\begin{bmatrix} 1 & -jm_{P1,1} & 0 & \cdots & \cdots & \cdots & \cdots & \cdots & 0 & 0 \\ -jm_{1,P1} & p & -j\dfrac{\omega\cdot m_{1,2}}{\omega_0} & \cdots & \cdots & \cdots & \cdots & \cdots & 0 & 0 \\ \vdots & \vdots & \vdots & \vdots & \vdots & \vdots & \vdots & \vdots & \vdots & \vdots \\ 0 & 0 & \cdots & p & -jm_{k,in} & 0 & \cdots & \cdots & 0 & 0 \\ 0 & 0 & \cdots & -jm_{in,k} & \dfrac{\cosh\gamma l}{\sinh\gamma l} & m_{in,out} & \cdots & \cdots & 0 & 0 \\ 0 & 0 & \cdots & 0 & m_{out,in} & \dfrac{\cosh\gamma l}{\sinh\gamma l} & -jm_{out,k+1} & \cdots & 0 & 0 \\ 0 & 0 & \cdots & \cdots & 0 & -jm_{k+1,out} & p & \cdots & \cdots & 0 \\ \vdots & \vdots & \vdots & \vdots & \vdots & \vdots & \vdots & \vdots & \vdots & \vdots \\ 0 & 0 & 0 & \cdots & \cdots & \cdots & \cdots & \cdots & p & -jm_{n,P2} \\ 0 & 0 & 0 & \cdots & \cdots & \cdots & \cdots & \cdots & -jm_{P2,n} & 1 \end{bmatrix} \tag{3.27}$$

Applying narrowband approximation $\omega_0 = \omega$, $[\bar{Y}]$ can be simplified to the matrix $[A]$ as

$$[A]=\begin{bmatrix} 1 & -jm_{P1,1} & 0 & \cdots & \cdots & \cdots & \cdots & \cdots & 0 & 0 \\ -jm_{1,P1} & p & -jm_{1,2} & \cdots & \cdots & \cdots & \cdots & \cdots & 0 & 0 \\ 0 & -jm_{2,1} & p & -jm_{2,3} & \cdots & \cdots & \cdots & \cdots & 0 & 0 \\ \vdots & \vdots & \vdots & \vdots & \vdots & \vdots & \vdots & \vdots & \vdots & \vdots \\ 0 & 0 & \cdots & p & -jm_{k,in} & 0 & \cdots & \cdots & 0 & 0 \\ 0 & 0 & \cdots & -jm_{in,k} & \dfrac{\cosh\gamma l}{\sinh\gamma l} & -jm_{in,out} & \cdots & \cdots & 0 & 0 \\ 0 & 0 & \cdots & 0 & -jm_{out,in} & \dfrac{\cosh\gamma l}{\sinh\gamma l} & -jm_{out,k+1} & \cdots & 0 & 0 \\ 0 & 0 & \cdots & \cdots & 0 & -jm_{k+1,out} & p & \cdots & \cdots & \cdots \\ \vdots & \vdots & \vdots & \vdots & \vdots & \vdots & \vdots & \vdots & \vdots & \vdots \\ 0 & 0 & 0 & \cdots & \cdots & \cdots & \cdots & \cdots & p & -jm_{n,P2} \\ 0 & 0 & 0 & \cdots & \cdots & \cdots & \cdots & \cdots & -jm_{P2,n} & 1 \end{bmatrix} \tag{3.28}$$

Then, the *S*-parameters can be calculated by

$$\begin{aligned} S_{11} &= 2[A]^{-1}_{P1,P1} - 1 \\ S_{21} &= 2[A]^{-1}_{P2,P1} \end{aligned} \tag{3.29}$$

Matrix $[A]$ can be further decomposed into three matrices [1], given by

$$[A] = [T] + p \cdot [U] - j \cdot [m] \tag{3.30}$$

where the [*T*] matrix includes the filter's port admittance and the NRNs, given by

$$[T] = \begin{bmatrix} 1 & 0 & 0 & \cdots & \cdots & \cdots & \cdots & \cdots & 0 & 0 \\ 0 & 0 & 0 & \cdots & \cdots & \cdots & \cdots & \cdots & 0 & 0 \\ 0 & 0 & 0 & 0 & \cdots & \cdots & \cdots & \cdots & 0 & 0 \\ \vdots & \vdots & \vdots & \vdots & \vdots & \vdots & \vdots & \vdots & \vdots & \vdots \\ 0 & 0 & \cdots & 0 & 0 & 0 & \cdots & \cdots & 0 & 0 \\ 0 & 0 & \cdots & 0 & \dfrac{\cosh \gamma l}{\sinh \gamma l} & 0 & \cdots & \cdots & 0 & 0 \\ 0 & 0 & \cdots & 0 & 0 & \dfrac{\cosh \gamma l}{\sinh \gamma l} & 0 & \cdots & 0 & 0 \\ 0 & 0 & \cdots & \cdots & 0 & 0 & 0 & 0 & \cdots & 0 \\ \vdots & \vdots & \vdots & \vdots & \vdots & \vdots & \vdots & \vdots & \vdots & \vdots \\ 0 & 0 & 0 & \cdots & \cdots & \cdots & \cdots & \cdots & 0 & 0 \\ 0 & 0 & 0 & \cdots & \cdots & \cdots & \cdots & \cdots & 0 & 1 \end{bmatrix} \tag{3.31}$$

In (3.30), [*U*] is a matrix with diagonal entries are identity except for $U_{P1,P1}$, $U_{in,in}$, $U_{out,out}$ and $U_{P2,P2}$, which are zero.

$$[U] = \begin{bmatrix} 0 & 0 & 0 & \cdots & \cdots & \cdots & \cdots & \cdots & 0 & 0 \\ 0 & 1 & 0 & \cdots & \cdots & \cdots & \cdots & \cdots & 0 & 0 \\ 0 & 0 & 1 & 0 & \cdots & \cdots & \cdots & \cdots & 0 & 0 \\ \vdots & \vdots & \vdots & \vdots & \vdots & \vdots & \vdots & \vdots & \vdots & \vdots \\ 0 & 0 & \cdots & 1 & 0 & 0 & \cdots & \cdots & 0 & 0 \\ 0 & 0 & \cdots & 0 & 0 & 0 & \cdots & \cdots & 0 & 0 \\ 0 & 0 & \cdots & 0 & 0 & 0 & 0 & \cdots & 0 & 0 \\ 0 & 0 & \cdots & \cdots & 0 & 0 & 1 & 0 & \cdots & 0 \\ \vdots & \vdots & \vdots & \vdots & \vdots & \vdots & \vdots & \vdots & \vdots & \vdots \\ 0 & 0 & 0 & \cdots & \cdots & \cdots & \cdots & \cdots & 1 & 0 \\ 0 & 0 & 0 & \cdots & \cdots & \cdots & \cdots & \cdots & 0 & 0 \end{bmatrix} \tag{3.32}$$

The normalised coupling matrix [*m*] is given by

$$[m]=\begin{bmatrix} 0 & m_{P1,1} & 0 & \cdots & \cdots & \cdots & \cdots & \cdots & 0 & 0 \\ m_{1,P1} & 0 & m_{1,2} & \cdots & \cdots & \cdots & \cdots & \cdots & 0 & 0 \\ 0 & m_{2,1} & 0 & m_{2,3} & \cdots & \cdots & \cdots & \cdots & 0 & 0 \\ \vdots & \vdots & \vdots & \vdots & \vdots & \vdots & \vdots & \vdots & \vdots & \vdots \\ 0 & 0 & \cdots & 0 & m_{k,in} & 0 & \cdots & \cdots & 0 & 0 \\ 0 & 0 & \cdots & m_{in,k} & 0 & m_{in,out} & \cdots & \cdots & 0 & 0 \\ 0 & 0 & \cdots & 0 & m_{out,in} & 0 & m_{out,k+1} & \cdots & 0 & 0 \\ 0 & 0 & \cdots & \cdots & 0 & m_{k+1,out} & 0 & \cdots & \cdots & \cdots \\ \vdots & \vdots & \vdots & \vdots & \vdots & \vdots & \vdots & \vdots & \vdots & \vdots \\ 0 & 0 & 0 & \cdots & \cdots & \cdots & \cdots & \cdots & 0 & m_{n,P2} \\ 0 & 0 & 0 & \cdots & \cdots & \cdots & \cdots & \cdots & m_{P2,n} & 0 \end{bmatrix} \tag{3.33}$$

3.1.3 Example: A transmission line cascaded filter

An example of two 2nd order filters cascaded using the transmission line is presented in the section. The filter is specified with 10 GHz centre frequency, 500 MHz bandwidth (*FBW*=0.05), and 20 dB return loss. These two filters are cascaded by a section of the idealised transmission line (i.e. α=0) with Y_0=0.02 S characteristic admittance.

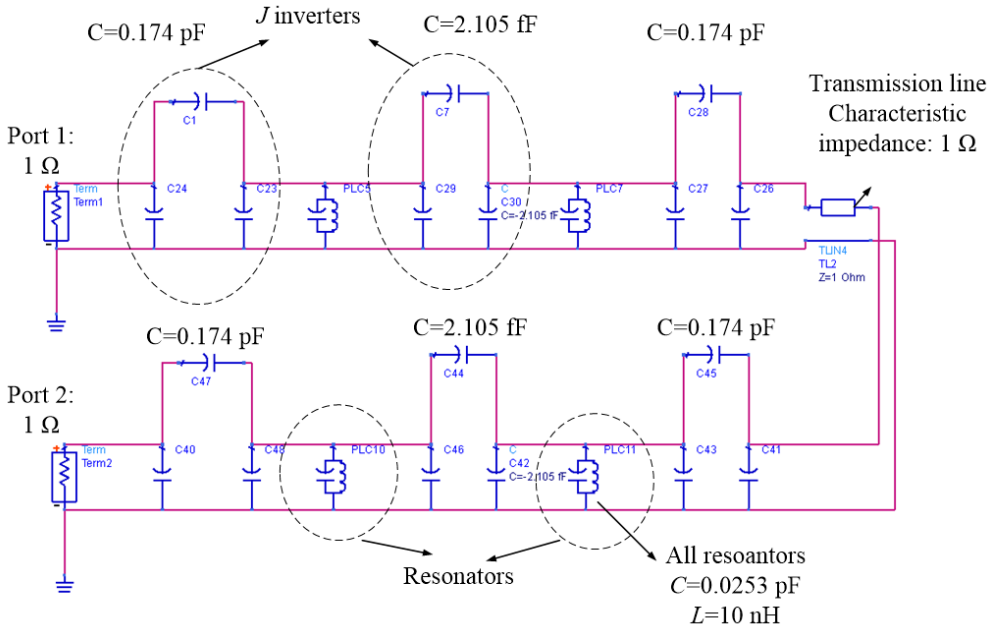

Fig. 3.4 Lumped circuit of the cascaded filter simulated in ADS.

A lump circuit example of the cascaded filter is constructed in ADS, as depicted in Fig. 3.4. The resonators are in the form of parallel inductors and capacitors which are coupled via *J* inverters to formulate the filters. Two identified filters are cascaded through the idealised transmission line as shown in Fig. 3.4. The values of the lumped elements including the capacitors, inductors and the *J* inverters can be calculated using (2.15) in Chapter 2. The simulated circuit response with different lengths of the transmission line is presented in Fig. 3.5.

Referring to (3.24) and (3.33), the coupling matrix is given by

$$[m] = \begin{bmatrix} 0 & 1.2264 & 0 & 0 & 0 & 0 & 0 & 0 \\ 1.2264 & 0 & 1.6621 & 0 & 0 & 0 & 0 & 0 \\ 0 & 1.6621 & 0 & 1.2264 & 0 & 0 & 0 & 0 \\ 0 & 0 & 1.2264 & 0 & \frac{-j}{\sinh \gamma l} & 0 & 0 & 0 \\ 0 & 0 & 0 & \frac{-j}{\sinh \gamma l} & 0 & 1.2264 & 0 & 0 \\ 0 & 0 & 0 & 0 & 1.2264 & 0 & 1.6621 & 0 \\ 0 & 0 & 0 & 0 & 0 & 1.6621 & 0 & 1.2264 \\ 0 & 0 & 0 & 0 & 0 & 0 & 1.2264 & 0 \end{bmatrix} \tag{3.34}$$

In (3.34), the couplings of the transmission line are expressed as a function of γl. The unity of γl is radians representing the phase of the transmission line. Note that the matrix in (3.34), two identical sub-matrices indicate the filters are cascaded by the transmission line. The couplings between two port of the transmission line are determined by its own properties. In [3] and [4], the couplings between the two non-resonance nodes are 1, but in our example in (3.34) they are variables related to the length of the transmission line. The *S*-parameters response calculated using the coupling matrix versus different lengths of the transmission line is illustrated in Fig. 3.5, compared with the circuit response simulated in ADS.

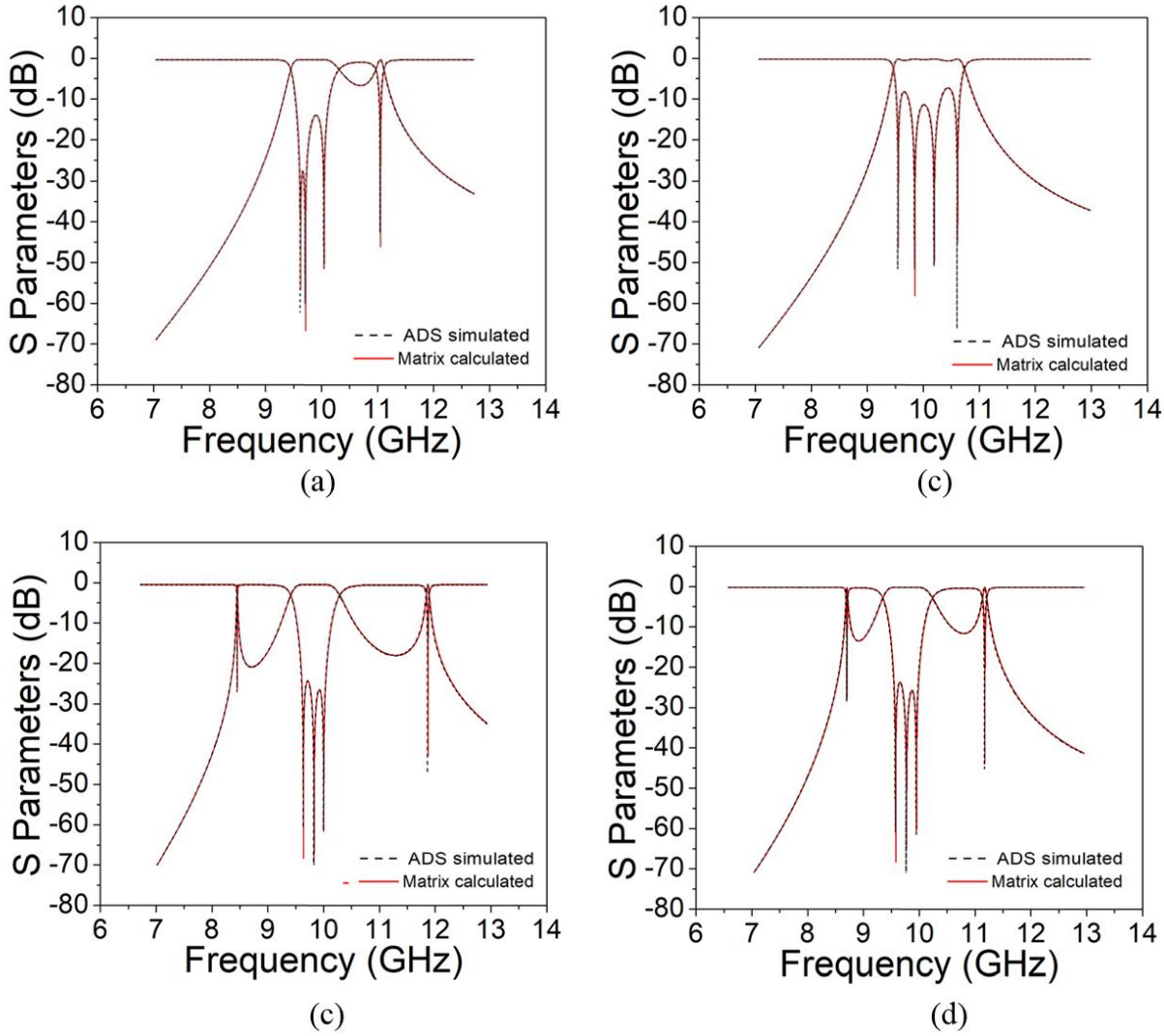

Fig. 3.5 *S*-parameters response using matrix formulation and circuit simulation. (a) $\gamma l = 1/4\pi j$. (b) $\gamma l = 1/2\pi j$. (c) $\gamma l = \pi j$. (b) $\gamma l = 2\pi j$. The transmission line works at 10 GHz centre frequency.

It can be seen from Fig. 3.5 that the responses of circuit simulation fit precisely to the *S*-parameters response calculated using the matrix calculation which validates the *N*+4 coupling matrix representation of the cascaded filters. Compared with [3] and [4], this newly synthesised *N*+4 coupling matrix can describe arbitrary lengths of the transmission line cascaded filters.

3.2 *N*+3 Coupling Matrix

The conventional coupling matrix can be extended to an active *N*+3 matrix describing the filter amplifiers. The device 'filter amplifier' is an integrated filter with the active component, which has both filtering and amplification functionalities. Extra elements indicating the transistor's parameters are included to synthesise the *N*+3 coupling matrix. In the *N*+3 coupling matrix, the self-coupling of the N^{th} resonator of the filter (adjacent to the transistor) and the coupling to the transistor are calculated to achieve a Chebyshev (or other) filter response with gain. Three practical examples in the form of waveguide filter amplifiers and a microstrip filter amplifier are presented in Chapter 4 and Chapter 5. In this section, the novel *N*+3 active coupling matrix is synthesised.

3.2.1 Y matrix of the transistor small signal model

Before discussing the active *N*+3 coupling matrix, an admittance network used to represent the simplified small signal model of the transistor is introduced. As shown in Fig. 3.6, Y_{gs}, Y_{ds}, and Y_{gd} are the admittance between the transistor's gate source and drain [7]. The transconductance g_m represents the voltage controlled current source.

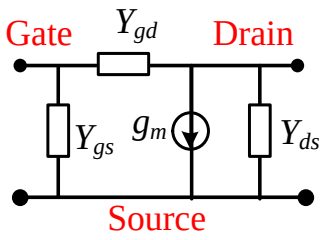

Fig. 3.6 Simplified small signal lumped circuit model for the transistor.

The parameters of the transistor small signal model can be calculated from measured *S*-parameters, which are usually provided in the transistor datasheet [9]. The Y parameters of the transistor can be calculated using *S*-parameters to *Y*-parameters formulas by [1]

$$\begin{bmatrix} Y_{11} & Y_{12} \\ Y_{11} & Y_{22} \end{bmatrix} = \begin{bmatrix} Y_0 \dfrac{(1-S_{11})(1+S_{22})+S_{12}S_{21}}{(1+S_{11})(1+S_{22})-S_{12}S_{21}} & Y_0 \dfrac{-2S_{12}}{(1+S_{11})(1+S_{22})-S_{12}S_{21}} \\ Y_0 \dfrac{-2S_{21}}{(1+S_{11})(1+S_{22})-S_{12}S_{21}} & Y_0 \dfrac{(1+S_{11})(1-S_{22})+S_{12}S_{21}}{(1+S_{11})(1+S_{22})-S_{12}S_{21}} \end{bmatrix} \tag{3.35}$$

Here Y_0 is the characteristic admittance. Referring to [7], the simplified Y matrix representation of the transistor is given by

$$[Y_T] = \begin{bmatrix} Y_{11} & Y_{12} \\ Y_{21} & Y_{22} \end{bmatrix} = \begin{bmatrix} Y_{ds}+Y_{gd} & -Y_{gd} \\ g_m - Y_{gd} & Y_{ds}+Y_{gd} \end{bmatrix} \tag{3.36}$$

The normalised admittance matrix of the transistor can be calculated by dividing the characteristic admittance Y_0, given by

$$\left[\overline{Y}_T\right] = \frac{[Y_T]}{Y_0} = \begin{bmatrix} \overline{Y}_{ds}+\overline{Y}_{gd} & -\overline{Y}_{gd} \\ \overline{g}_m - \overline{Y}_{gd} & \overline{Y}_{ds}+\overline{Y}_{gd} \end{bmatrix} \tag{3.37}$$

3.2.2 *N*+3 coupling matrix of the filter amplifier

The topology of filter amplifier is developed by replacing the load of the last resonator in the filter by the transistor. Fig. 3.7(a) introduces the lumped circuit representation of the N^{th} order resonator based filter amplifier: resonators in the form of parallel capacitors (C) and inductors (L) are coupled by the J inverters. The transistor is coupled to the N^{th} resonator by inverter J_Y, and the N^{th} resonator is in the form of capacitor C_Y and L. The lumped circuit is schematically represented in Fig. 3.7(b), with clear circles denoting the source and load and solid circles indicating the resonators. The input port admittance of the filter is denoted by Y_{P1}. A matching network is employed at the output to convert the load Y_L to Y_{ds}^*, conjugately matched to drain to source admittance Y_{ds}. The load admittance Y_L represents the measurement port at the output which is usually 50 Ω.

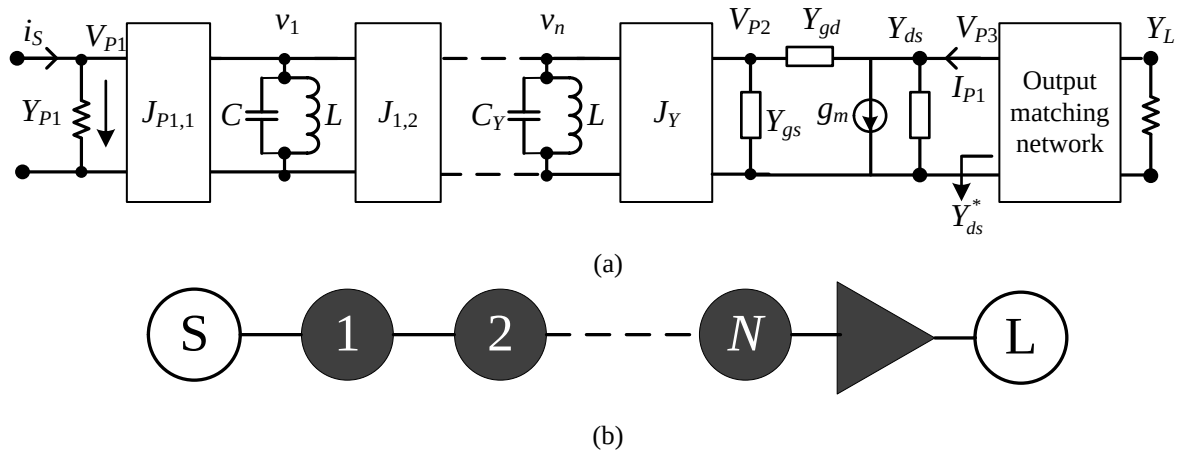

Fig. 3.7 Topology and equivalent lumped circuit for coupled resonators filter amplifier circuit. (a) Lumped circuit model. (b) Schematic representation of the circuit.

The voltage at the i^{th} resonator is denoted as v_i (i=1 to n), whereas V_{P1} is the voltage at the input of the filter; V_{P2} is the voltage at the gate of the transistor; V_{P3} indicates the voltage at the drain of the transistor. i_S is the current source at input port 1. Note that the N^{th} resonator, C_Y is set to a value different from C to achieve centre frequency shift allowing Chebyshev (or other) filter response.

Now Kirchoff's current laws can be applied to the circuit in Fig. 3.7(a) giving

$$\begin{aligned}
Y_{P1}v_{P1} - jJ_{P1,1}v_1 &= i_s \\
-jJ_{1,P1}v_{P1} + \left(\frac{1}{j\omega L_1} + j\omega C_1\right)v_1 - jJ_{1,2}v_2 &= 0 \\
-jJ_{2,1}v_1 + \left(\frac{1}{j\omega L_2} + j\omega C_2\right)v_2 - jJ_{2,3}v_3 &= 0 \\
&\vdots \\
-jJ_{n-1,n}v_{n-1}\cdots + \left(\frac{1}{j\omega L_n} + j\omega C_n\right)v_n - jJ_Y v_{P2} &= 0 \\
-jJ_{P2,n}v_n - \left(Y_{gs} + Y_{gd}\right)v_{P2} - Y_{gd}v_{P3} &= 0 \\
\left(g_m - Y_{gd}\right)v_{P2} + \left(Y_{gs} + Y_{gd} + Y_{ds}^*\right)v_{P3} &= 0
\end{aligned} \tag{3.38}$$

In matrix form,

$$\begin{bmatrix} Y_{P1} & -jJ_{P1,1} & 0 & \cdots & 0 & 0 & 0 \\ -jJ_{1,P1} & \left(\frac{1}{j\omega L}+j\omega C\right) & -jJ_{1,2} & \cdots & 0 & 0 & 0 \\ 0 & -jJ_{2,1} & \left(\frac{1}{j\omega L_2}+j\omega C_2\right) & \cdots & 0 & 0 & 0 \\ \vdots & \vdots & \vdots & \ddots & \vdots & \vdots & \vdots \\ 0 & 0 & 0 & \cdots & \left(\frac{1}{j\omega L}+j\omega C_Y\right) & -jJ_Y & 0 \\ 0 & 0 & 0 & \cdots & -jJ_Y & Y_{gs}+Y_{gd} & -Y_{gd} \\ 0 & 0 & 0 & \cdots & 0 & g_m-Y_{gd} & Y_{ds}+Y_{gd}+Y_{ds}^* \end{bmatrix} \begin{bmatrix} v_{P1} \\ v_1 \\ v_2 \\ \vdots \\ v_n \\ v_{P2} \\ v_{P3} \end{bmatrix} = \begin{bmatrix} i_s \\ 0 \\ 0 \\ \vdots \\ 0 \\ 0 \\ 0 \end{bmatrix}$$

(3.39)

Or

$$[Y]\cdot[v]=[i] \tag{3.40}$$

The admittance matrix [*Y*] can be expressed as

$$[Y]=\begin{bmatrix} Y_{P1} & -jJ_{P1,1} & 0 & \cdots & 0 & 0 & 0 \\ -jJ_{1,P1} & \left(\frac{1}{j\omega L}+j\omega C\right) & -jJ_{1,2} & \cdots & 0 & 0 & 0 \\ 0 & -jJ_{2,1} & \left(\frac{1}{j\omega L}+j\omega C\right) & \cdots & 0 & 0 & 0 \\ \vdots & \vdots & \vdots & \ddots & \vdots & \vdots & \vdots \\ 0 & 0 & 0 & \cdots & \left(\frac{1}{j\omega L}+j\omega C_Y\right) & -jJ_Y & 0 \\ 0 & 0 & 0 & \cdots & -jJ_Y & Y_{gs}+Y_{gd} & -Y_{gd} \\ 0 & 0 & 0 & \cdots & 0 & g_m-Y_{gd} & Y_{ds}+Y_{ds}^*+Y_{gd} \end{bmatrix}$$

(3.41)

The next step is to find the relationship between the admittance matrix [*Y*] and the scattering parameters. By inspecting the lumped circuit in Fig. 3.7(a), it can be recognised that $V_{Pk}=v_{Pk}$ (*k*=1 to 3), $I_{P3}=-i_{P2}$, $I_{P1}=i_S-V_{P1}\cdot Y_{P1}$. Considering (3.6), we have

$$a_1 = \frac{i_s}{2\sqrt{\left|\mathrm{Re}\,Y_{P1}\right|}} \qquad b_1 = \frac{v_{P1}\left(Y_{P1}+Y_{P1}^*\right)-i_s}{2\sqrt{\left|\mathrm{Re}\,Y_{P1}\right|}} = \frac{2v_{P1}\left(\left|\mathrm{Re}\,Y_{P1}\right|\right)-i_s}{2\sqrt{\left|\mathrm{Re}\,Y_{P1}\right|}}$$
$$a_2 = 0 \qquad\qquad b_2 = \frac{v_{P3}\left(Y_{ds}+Y_{ds}^*\right)}{2\sqrt{\left|\mathrm{Re}\,Y_{ds}^*\right|}} = v_{P3}\sqrt{\left|\mathrm{Re}\,Y_{ds}^*\right|} \tag{3.42}$$

The relationships between the scattering parameters and the wave variables a_k and b_k are given by [1]

$$S_{11} = \left.\frac{b_1}{a_1}\right|_{a2=0}$$
$$S_{21} = \left.\frac{b_2}{a_1}\right|_{a2=0} \tag{3.43}$$

Substitute (3.42) into (3.43) yielding

$$S_{11} = \left.\frac{b_1}{a_1}\right|_{a2=a3=0} = \frac{2v_{P1}\left|\mathrm{Re}\,Y_{P1}\right|}{i_s} - 1$$
$$S_{21} = \left.\frac{b_3}{a_1}\right|_{a2=a3=0} = \frac{2v_{P2}\cdot\sqrt{\left|\mathrm{Re}\,Y_{P1}\right|\cdot\left|\mathrm{Re}\,Y_{ds}^*\right|}}{i_s} \tag{3.44}$$

v_{Pk} (k=1 to 3) is found from (3.38) as

$$v_{Pk} = i_s \cdot [Y]^{-1}_{Pk,P1} \tag{3.45}$$

where $[Y]^{-1}_{Pk,P1}$ is denoted as the entry in row P_k and column P_1 of $[Y]^{-1}$. Replacing the node voltages in (3.45) with those in (3.44) results in

$$S_{11} = 2\left|\mathrm{Re}\,Y_{P1}\right|[Y]^{-1}_{P1,P1} - 1$$
$$S_{21} = 2\sqrt{\left|\mathrm{Re}\,Y_{P1}\right|\cdot\left|\mathrm{Re}\,Y_{ds}^*\right|}[Y]^{-1}_{P3,P1} \tag{3.46}$$

In order to get the coupling matrix, the next step is to scale the $[Y]$ matrix in (3.41), and this is similar to the matrix scaling process in Fig. 3.3. Here each row i and column j (i, j=1 to n) of the matrix $[Y]$ is divided by $\sqrt{\omega_0 C \cdot FBW}$, where $\omega_0 = 1/\sqrt{LC}$ is the centre frequency of parallel

capacitors (C) and inductors (L) circuit. FBW is the fractional bandwidth of the network. The rows and columns P_1, P_2 and P_3 are divided by $\sqrt{Y_0}$, which Y_0=0.02 S is the characteristic admittance. Rows and columns P_1 indicate the input port and output port of the filter; P_2 indicates input of the transistor and P_3 indicates the load with matching. The matrix scaling process is illustrated in Fig. 3.8 and the same matrix scaling technique is described in [2].

$$\left[\bar{Y}\right]=\begin{bmatrix} \frac{Y_{P1}}{Y_0} & -j\frac{J_{P1,1}}{\sqrt{\omega_0 C\cdot FBW\cdot Y_0}} & \cdots & 0 & 0 & 0 \\ -j\frac{J_{1,P1}}{\sqrt{\omega_0 C\cdot FBW\cdot Y_0}} & p & \cdots & 0 & 0 & 0 \\ \vdots & \vdots & \ddots & \vdots & \vdots & \vdots \\ 0 & 0 & \cdots & \left(\frac{j\omega C_Y+\frac{1}{j\omega L}}{\sqrt{\omega_0 C\cdot FBW}}\right) & -j\frac{J_Y}{\sqrt{\omega_0 C\cdot FBW\cdot Y_0}} & 0 \\ 0 & 0 & \cdots & -j\frac{J_Y}{\sqrt{\omega_0 C\cdot FBW\cdot Y_0}} & \frac{Y_{gs}+Y_{gd}}{Y_0} & \frac{-Y_{gd}}{Y_0} \\ 0 & 0 & \cdots & 0 & \frac{g_m-Y_{gd}}{Y_0} & \frac{Y_{gd}+Y_{ds}+Y_{ds}^*}{Y_0} \end{bmatrix} \tag{3.47}$$

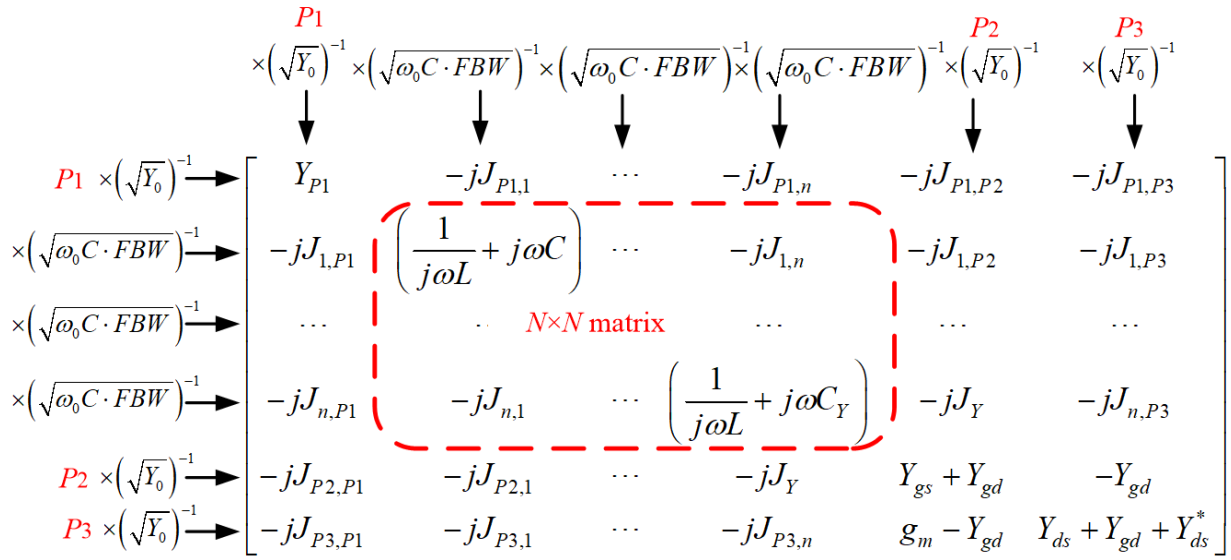

Fig. 3.8 Matrix operation from $[Y]$ to $[\bar{Y}]$.

It is necessary to claim here that the scaled matrix $[\bar{Y}]$ in (3.12) is not equivalent to the matrix $[Y]$ in (3.4), because the different scaling factors are operated on the rows and columns of $[Y]$. However, the *S*-parameters response calculated by $[\bar{Y}]$ yields same results of as calculated using $[Y]$. The matrix manipulation is discussed as follows.

The inverses of $[\bar{Y}]$ and $[Y]$ can be expressed by the ratios of their co-factors and determinants [6]

$$\begin{aligned} [Y]^{-1}_{Pi,Pj} &= \frac{cof\,(Y_{Pi,Pj})}{|Y|}, (|Y| \neq 0) \\ \left[\bar{Y}\right]^{-1}_{Pi,Pj} &= \frac{cof\,(\bar{Y}_{Pi,Pj})}{|\bar{Y}|}, (|\bar{Y}| \neq 0) \end{aligned} \tag{3.48}$$

The relationships of their determinants and cofactors are obtained

$$\begin{aligned} |Y| &= \left(\sqrt{\omega_0 C \cdot FBW}\right)^{2n} \cdot \sqrt{Y_0}^{6} \cdot |\bar{Y}| \\ cof\left(Y_{Pi,Pj}\right) &= \left(\sqrt{\omega_0 C \cdot FBW}\right)^{2n} \cdot \sqrt{Y_0}^{4} \cdot cof\left(\bar{Y}_{Pi,Pj}\right), (i, j = 1 \text{to } n, i \neq j) \end{aligned} \tag{3.49}$$

Note that in Fig. 3.8, the rows and columns P_1, P_2 and P_3 of $[Y]$ are divided by $\sqrt{Y_0}$ up to six times; the row *i* and column *j* (*i*, *j*=1 to *n*) are scaled by $\sqrt{\omega C \cdot FBW}$ up to 2*n* times. Thus, the exponents of $\sqrt{Y_0}$ and $\sqrt{\omega C \cdot FBW}$ in (3.49) are 6 and 2*n*, respectively.

Substitute (3.49) into (3.48) yielding

$$[Y]^{-1}_{Pi,Pj} = \frac{1}{Y_0}\left[\bar{Y}\right]^{-1}_{Pi,Pj} \tag{3.50}$$

According to (3.46) and (3.50), the *S*-parameters can be calculated by

$$\begin{aligned} S_{11} &= 2\left|\mathrm{Re}\,\bar{Y}_{P1}\right|[\bar{Y}]^{-1}_{P1,P1} - 1 \\ S_{21} &= 2\sqrt{\left|\mathrm{Re}\,\bar{Y}_{P1}\right| \cdot \left|\mathrm{Re}\,\bar{Y}^{*}_{ds}\right|}[\bar{Y}]^{-1}_{P3,P1} \end{aligned} \tag{3.51}$$

Now we continue to simply the normalised matrix [$\bar{Y}$]. Recalling the lumped circuit illustrated in Fig. 3.7(a), The capacitor C_Y and the J inverter J_Y are given by

$$C_Y = C\left(1 + \frac{b}{a \cdot q_{en}}\right) \tag{3.52}$$

$$J_Y = \sqrt{\frac{\left(a^2 + b^2\right)\omega_0 C \cdot Y_0}{a \cdot Q_{en}}} \tag{3.53}$$

a and b are the normalised real and the imaginary part of the transistor's input admittance $\bar{Y}_{in}$

$$\bar{Y}_{in} = a + j \cdot b \tag{3.54}$$

Fig. 3.9 illustrates the equivalent lumped circuit of the transistor with output matched. V_{in} and I_{in} are the voltage and current at the gate of the transistor; V_{out} is the voltage at the drain of the transistor.

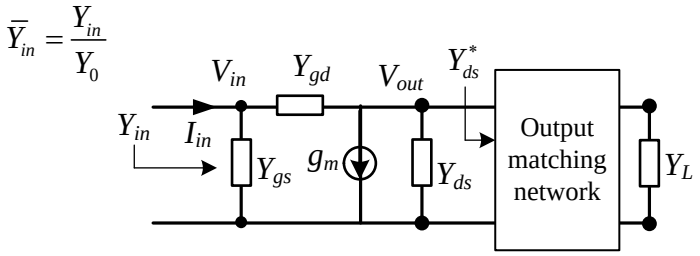

Fig 3.9 Lumped circuit of the transistor with output matched.

Apply the Kirchoff's current laws at the drain of the transistor, giving

$$\left(V_{out} - V_{in}\right)Y_{gd} + \left(Y_{ds} + Y_{ds}^*\right)V_{out} + V_{in} \cdot g_m = 0 \tag{3.55}$$

Solving (3.55) to give

$$V_{out} = \frac{\left(Y_{gd} - g_m\right)V_{in}}{Y_{gd} + Y_{ds} + Y_{ds}^*} \tag{3.56}$$

Then, I_{in} can be calculated by

$$I_{in} = \left(V_{in} - \frac{\left(Y_{gd} - g_m\right)V_{in}}{Y_{gd} + Y_{ds} + Y_{ds}^*} \right) \cdot Y_{gd} + V_{in} \cdot Y_{gs} \tag{3.57}$$

The input admittance of the transistor can be calculated by

$$Y_{in} = \frac{Y_{gd}\left(Y_{ds} + Y_{ds}^* + g_m\right)}{Y_{gd} + Y_{ds} + Y_{ds}^*} + Y_{gs} \tag{3.58}$$

Thus, *a* and *b* can be calculated from the normalised transistor's Y matrix parameters and load admittance as

$$\begin{aligned} a &= \mathrm{Re}\left\{ \frac{\overline{Y}_{gd}\left[\overline{g}_m + \overline{Y}_{ds} + \overline{Y}_{ds}^*\right]}{\overline{Y}_{gd} + \overline{Y}_{ds} + \overline{Y}_{ds}^*} + \overline{Y}_{gs} \right\} \\ b &= \mathrm{Im}\left\{ \frac{\overline{Y}_{gd}\left[\overline{g}_m + \overline{Y}_{ds} + \overline{Y}_{ds}^*\right]}{\overline{Y}_{gd} + \overline{Y}_{ds} + \overline{Y}_{ds}^*} + \overline{Y}_{gs} \right\} \end{aligned} \tag{3.59}$$

The *J* inverters coupling port 1 to the resonator and the *J* inverters between resonators are

$$J_{P1,1} = J_{1,P1} = \sqrt{\frac{\omega_0 C \cdot Y_0}{Q_{e1}}} \tag{3.60}$$

$$J_{i,j} = \omega C_{i,j} \qquad i \neq j \tag{3.61}$$

where $C_{i,j}$=$C_{j,i}$ represents the mutual capacitance between resonator *i* and *j*.

Substitute (3.52)-(3.61) into (3.47), the $[\bar{Y}]$ matrix can be simplified as

$$\left[\bar{Y}\right]=\begin{bmatrix} \bar{Y}_{P1} & -j\sqrt{\frac{1}{FBW\cdot Q_{e1}}} & 0 & \cdots & 0 & 0 & 0 \\ -j\sqrt{\frac{1}{FBW\cdot Q_{e1}}} & p & -j\frac{\omega C_{1,2}}{FBW\omega_0 C} & \cdots & 0 & 0 & 0 \\ 0 & -j\frac{\omega C_{2,1}}{FBW\omega_0 C} & p & \cdots & 0 & 0 & \\ \vdots & \vdots & \vdots & \ddots & \vdots & \vdots & \vdots \\ 0 & 0 & 0 & \cdots & \left(p+j\frac{b}{a\cdot FBW\cdot Q_{e1}}\right) & -j\sqrt{\frac{a^2+b^2}{a\cdot FBW\cdot Q_{e1}}} & 0 \\ 0 & 0 & 0 & \cdots & -j\sqrt{\frac{a^2+b^2}{a\cdot FBW\cdot Q_{e1}}} & \bar{Y}_{gs}+\bar{Y}_{gd} & -\bar{Y}_{gd} \\ 0 & 0 & 0 & \cdots & 0 & \bar{g}_m-\bar{Y}_{gd} & \bar{Y}_{gd}+\bar{Y}_{ds}+\bar{Y}_{ds}^* \end{bmatrix} \tag{3.62}$$

Note that

$$q_{ei}=FWB\cdot Q_{ei}\quad (i=1\quad \text{to}\quad n) \tag{3.63}$$

Coupling coefficients $M_{i,j}$ between two resonators is given by

$$M_{i,j}=\frac{C_{i,j}}{C}=FBW\cdot m_{i,j}\quad (i,j=1 \text{ to } n,\ i\neq j) \tag{3.64}$$

Define $m_{P1,1}=m_{1,P1}$ as the couplings from the 1st resonator to the input filter as

$$m_{P1,1}=m_{1,P1}=\sqrt{\frac{1}{q_{e1}}} \tag{3.65}$$

and the couplings from the N^{th} resonator to the transistor $m_{P2,n}=m_{n,P2}$ as

$$m_{n,P2}=m_{P2,n}=\sqrt{\frac{a^2+b^2}{a\cdot q_{en}}} \tag{3.66}$$

The normalised coupling coefficients between the input and output of the transistor are defined by

$$m_{P3,P2}=\frac{\bar{Y}_{gd}}{j},m_{P2,P3}=\frac{\bar{Y}_{gd}-\bar{g}_m}{j} \tag{3.67}$$

$m_{n,n}$, namely self-coupling, indicating the centre frequency shift, is given by

$$m_{n,n} = -\frac{b}{a \cdot q_{en}} \tag{3.68}$$

For simplification, the normalised port admittance of the filter is defined by

$$\overline{Y}_{P1} = 1 \tag{3.69}$$

Substitute (3.65)-(3.69) into (3.62), yielding

$$[\overline{Y}] = \begin{bmatrix} 1 & -jm_{P1,1} & 0 & \cdots & 0 & 0 & 0 \\ -jm_{1,P1} & p & -j\frac{\omega}{\omega_0}m_{1,2} & \cdots & 0 & 0 & 0 \\ 0 & -j\frac{\omega}{\omega_0}m_{2,1} & p & \cdots & 0 & 0 & 0 \\ \cdots & \cdots & \cdots & \ddots & \cdots & \cdots & \cdots \\ 0 & 0 & 0 & \cdots & p - jm_{n,n} & -jm_{n,P2} & 0 \\ 0 & 0 & 0 & \cdots & -jm_{P2,n} & \overline{Y}_{gs} + \overline{Y}_{gd} & -jm_{P2,P3} \\ 0 & 0 & 0 & \cdots & 0 & -jm_{P3,P2} & \overline{Y}_{gd} + \overline{Y}_{ds} + \overline{Y}_{ds}^{*} \end{bmatrix} \tag{3.70}$$

Assuming $\omega_0 = \omega$ for narrow band approximation, $[\overline{Y}]$ can be simplified to the matrix $[A]$

$$[A] = \begin{bmatrix} 1 & -jm_{P1,1} & 0 & \cdots & 0 & 0 & 0 \\ -jm_{1,P1} & p & -jm_{1,2} & \cdots & 0 & 0 & 0 \\ 0 & -jm_{2,1} & p & \cdots & 0 & 0 & 0 \\ \cdots & \cdots & \cdots & \ddots & \cdots & \cdots & \cdots \\ 0 & 0 & 0 & \cdots & p - jm_{n,n} & -jm_{n,P2} & 0 \\ 0 & 0 & 0 & \cdots & -jm_{P2,n} & \overline{Y}_{gs} + \overline{Y}_{gd} & -jm_{P2,P3} \\ 0 & 0 & 0 & \cdots & 0 & -jm_{P3,P2} & \overline{Y}_{gd} + \overline{Y}_{ds} + \overline{Y}_{ds}^{*} \end{bmatrix} \tag{3.71}$$

Therefore, the *S*-parameters response of the filter amplifier can be calculated by

$$\begin{aligned} S_{11} &= 2[A]^{-1}_{P1,P1} - 1 \\ S_{21} &= 2\sqrt{\left|\mathrm{Re}\,\overline{Y}_{ds}^{*}\right|}[A]^{-1}_{P3,P1} \end{aligned} \tag{3.72}$$

Matrix $[A]$ can be further decomposed into three matrices, given by

$$[A]=[T]+p[U]-j[m] \tag{3.73}$$

[*T*] indicates the matrix including normalised filter input port admittance and the transistor's input and output admittance.

$$T=\begin{bmatrix} 1 & 0 & 0 & 0 & 0 \\ 0 & 0 & 0 & 0 & 0 \\ 0 & 0 & 0 & 0 & 0 \\ 0 & 0 & 0 & \overline{Y}_{gs}+\overline{Y}_{gd} & 0 \\ 0 & 0 & 0 & 0 & \overline{Y}_{gd}+\overline{Y}_{ds}+\overline{Y}_{ds}^{*} \end{bmatrix} \tag{3.74}$$

[*U*] is a matrix with diagonal entries are identity except for the position at the ports and transistor input.

$$[U]=\begin{bmatrix} 0 & 0 & \cdots & 0 & 0 & 0 \\ 0 & 1 & \cdots & 0 & 0 & 0 \\ \vdots & \vdots & \ddots & \vdots & \vdots & \vdots \\ 0 & 0 & \cdots & 1 & 0 & 0 \\ 0 & 0 & \cdots & 0 & 0 & 0 \\ 0 & 0 & \vdots & 0 & 0 & 0 \end{bmatrix} \tag{3.75}$$

The normalised coupling matrix [*m*] can be expressed as

$$[m]=\begin{bmatrix} 0 & m_{P1,1} & \cdots & 0 & 0 & 0 \\ m_{1,P1} & 0 & \cdots & 0 & 0 & 0 \\ \vdots & \vdots & \ddots & \vdots & \vdots & \vdots \\ 0 & 0 & \cdots & m_{n,n} & m_{n,P2} & 0 \\ 0 & 0 & \cdots & m_{P2,n} & 0 & m_{P2,P3} \\ 0 & 0 & \cdots & 0 & m_{P3,P2} & 0 \end{bmatrix} \tag{3.76}$$

3.3 *N*+4 Coupling Matrix

In this section, we propose the topology of the filter amplifier with resonators matching at the input and output of the transistor. This filter amplifier can be expressed using an *N*+4 coupling

matrix. Complex values of the input and output impedances/admittances of the transistor can be matched simultaneously, achieving Chebyshev filter response with S_{11} and S_{22} and the S_{21} response with a gain over the passband. The N+4 active coupling matrix, which includes the parameters of the transistor, describes the performance of the integrated filter amplifier.

3.3.1 N+4 coupling matrix of the input and output resonator matching filter amplifier

The discussion follows closely the N+3 derivations but is included in full here. Fig. 3.10(a) shows the small signal lumped circuit of the transistor coupled by J inverters to the resonators based filters. This can be translated into the filter amplifier schematic topology with clear circles representing the source and the load, and solid circles denoting the resonators, as shown in Fig. 3.10(b).

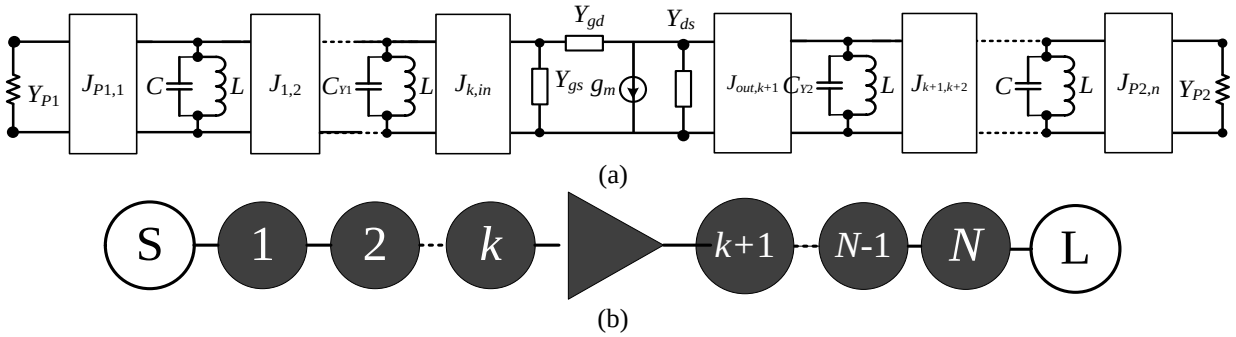

Fig. 3.10 Lumped circuit and topology of the transistor with input and output resonators matching. (a) Lumped circuit model. (b) Schematic representation of the circuit.

The input and output matching resonators are formed by parallel capacitors (C) and inductors (L) and are coupled by the J inverters. The input of transistor is coupled to the k^{th} resonator through the inverter $J_{k,in}$, and the $(k+1)^{th}$ resonator is coupled by the inverter $J_{out,k+1}$. The resonator

adjacent to the transistor's input has capacitor C_{Y1} and the $(k+1)^{th}$ resonator adjacent to the output of the transistor has capacitor C_{Y2}.

As the derivation of admittance matrix is exactly same as the example of the transmission line coupled between resonators in Section 3.1, we directly write down the admittance matrix [Y] of the circuit in Fig. 3.10(a), i.e.

$$[Y]=\begin{bmatrix} Y_{P1} & -jJ_{P1,1} & \cdots & 0 & 0 & 0 & 0 & 0 & 0 & 0 \\ -jJ_{1,P1} & \frac{1}{j\omega L}+j\omega C & \cdots & 0 & 0 & 0 & 0 & 0 & 0 & 0 \\ \vdots & \vdots & \ddots & \vdots & \vdots & 0 & 0 & 0 & 0 & 0 \\ 0 & 0 & \cdots & \frac{1}{j\omega L}+j\omega C_{Y1} & -jJ_{k,in} & 0 & 0 & 0 & 0 & 0 \\ 0 & 0 & \cdots & -jJ_{in,k} & Y_{gs}+Y_{gd} & -Y_{gd} & 0 & 0 & 0 & 0 \\ 0 & 0 & 0 & 0 & g_m-Y_{gd} & Y_{ds}+Y_{gd} & -jJ_{out,k+1} & \cdots & 0 & 0 \\ 0 & 0 & 0 & 0 & 0 & -jJ_{k+1,out} & \frac{1}{j\omega L}+j\omega C_{Y2} & \cdots & 0 & 0 \\ 0 & 0 & 0 & 0 & 0 & \vdots & \vdots & \ddots & \vdots & \vdots \\ 0 & 0 & 0 & 0 & 0 & 0 & 0 & \cdots & \frac{1}{j\omega L}+j\omega C & -jJ_{n,P2} \\ 0 & 0 & 0 & 0 & 0 & 0 & 0 & \cdots & -jJ_{P2,n} & Y_{P2} \end{bmatrix} \tag{3.77}$$

The next step is to scale the [Y] matrix in (3.77). The scaling process is exactly same as the scaling process in Fig.3.3 in Section 3.1. Here each row i and column j of the matrix [Y] are divided by $\sqrt{\omega_0 C \cdot FBW}$, where $\omega_0 = 1/\sqrt{LC}$ is the centre frequency of parallel capacitors (C) and inductors (L) circuit. FBW is the fractional bandwidth of the network. The rows and columns P_1, P_2, P_{in}, and P_{out} are divided by $\sqrt{Y_0}$, which Y_0=0.02 S is the characteristic admittance. Rows and columns P_1 and P_2 indicate the input port and output port of the filter; P_{in}, and P_{out} represent the input port and output port of the transistor.

$$
[\bar{Y}] = \begin{bmatrix}
\bar{Y}_{P1} & -j\frac{J_{P1,1}}{\sqrt{\omega_0 C \cdot FBW \cdot Y_0}} 0 & \cdots & & & & \\
-j\frac{J_{1,P1}}{\sqrt{\omega_0 C \cdot FBW \cdot Y_0}} & \cdots & \cdots & & & & \\
\vdots & \ddots & \cdots & & & & \\
0 & \cdots & \cdots & & & & \\
0 & \cdots & \cdots & & & & \\
0 & 0 & \cdots & & & & \\
0 & 0 & \cdots & & & & \\
0 & 0 & \ddots & & & & \\
0 & 0 & \cdots & & & & \\
0 & 0 & \cdots & & & & \\
0 & 0 & 0 & 0 & 0 & 0 \\
0 & 0 & 0 & 0 & 0 & 0 \\
\vdots & \vdots & 0 & 0 & 0 & 0 \\
\left(\frac{j\omega C_Y + \frac{1}{j\omega L}}{\sqrt{\omega_0 C \cdot FBW}}\right) & -j\frac{J_{k,in}}{\sqrt{\omega_0 C \cdot FBW \cdot Y_0}} & 0 & 0 & 0 & 0 \\
-j\frac{J_{in,k}}{\sqrt{\omega_0 C \cdot FBW \cdot Y_0}} & \bar{Y}_{gs} + \bar{Y}_{gd} & -\bar{Y}_{gd} & 0 & 0 & 0 \\
0 & \bar{g}_m - \bar{Y}_{gd} & \bar{Y}_{ds} + \bar{Y}_{gd} & -j\frac{J_{out,k+1}}{\sqrt{\omega_0 C \cdot FBW \cdot Y_0}} & \cdots & 0 \\
0 & 0 & -j\frac{J_{k+1,out}}{\sqrt{\omega_0 C \cdot FBW \cdot Y_0}} & \left(\frac{j\omega C_Y + \frac{1}{j\omega L}}{\sqrt{\omega_0 C \cdot FBW}}\right) & \cdots & 0 \\
0 & 0 & \vdots & \vdots & \ddots & \vdots \\
0 & 0 & 0 & 0 & \cdots & -j\frac{J_{n,P2}}{\sqrt{\omega_0 C \cdot FBW \cdot Y_0}} \\
0 & 0 & 0 & 0 & \cdots & \bar{Y}_{P2}
\end{bmatrix}
$$

(3.78)

The derivations of the *S*-parameters are exactly same as these describe in Section 3.1, and the *S*-parameters response can be calculated by

$$
\begin{aligned}
S_{11} &= 2\left|\mathrm{Re}\,\overline{Y}_{P1}\right|[\overline{Y}]^{-1}_{P1,P1} - 1 \\
S_{21} &= 2\sqrt{\left|\mathrm{Re}\,\overline{Y}_{P1}\right| \cdot \left|\mathrm{Re}\,\overline{Y}_{P2}\right|}[\overline{Y}]^{-1}_{P2,P1} \\
S_{22} &= 2\left|\mathrm{Re}\,\overline{Y}_{P2}\right|[\overline{Y}]^{-1}_{P2,P2} - 1 \\
S_{21} &= 2\sqrt{\left|\mathrm{Re}\,\overline{Y}_{P2}\right| \cdot \left|\mathrm{Re}\,\overline{Y}_{P1}\right|}[\overline{Y}]^{-1}_{P1,P2}
\end{aligned}
\tag{3.79}
$$

Let's continue to simplify the normalised matrix $[\overline{Y}]$. *J* inverters which couple the resonators to the transistor's input and output are given by

$$
\begin{aligned}
J_{k,in} = J_{in,k} &= \sqrt{\frac{\left(\mathrm{Re}^2(\overline{Y}_{gs}) + \mathrm{Im}^2(\overline{Y}_{gs})\right)\omega_0 C \cdot Y_0}{\mathrm{Re}(\overline{Y}_{gs}) \cdot Q_{ek}}} \\
J_{out,k+1} = J_{k+1,out} &= \sqrt{\frac{\left(\mathrm{Re}^2(\overline{Y}_{ds}) + \mathrm{Im}^2(\overline{Y}_{ds})\right)\omega_0 C \cdot Y_0}{\mathrm{Re}(\overline{Y}_{ds}) \cdot Q_{ek+1}}}
\end{aligned}
\tag{3.80}
$$

The capacitor C_{Y1} and C_{Y2} are given by

$$
\begin{aligned}
C_{Y1} &= \sqrt{\frac{\left(\mathrm{Re}^2(\overline{Y}_{gs}) + \mathrm{Im}^2(\overline{Y}_{gs})\right)\omega_0 C \cdot Y_0}{\mathrm{Re}(\overline{Y}_{gs}) \cdot Q_{ek}}} \\
C_{Y2} &= \sqrt{\frac{\left(\mathrm{Re}^2(\overline{Y}_{ds}) + \mathrm{Im}^2(\overline{Y}_{ds})\right)\omega_0 C \cdot Y_0}{\mathrm{Re}(\overline{Y}_{ds}) \cdot Q_{ek+1}}}
\end{aligned}
\tag{3.81}
$$

Substitute (3.19) (3.22) (3.80) and (3.81) into (3.78) yielding

$$
[\bar{Y}] = \begin{bmatrix}
\bar{Y}_{P1} & \cdots & 0 & 0 \\
-j\sqrt{\dfrac{1}{FBW \cdot Q_{e1}}} & \cdots & 0 & 0 \\
\vdots & \ddots & \vdots & \vdots \\
0 & \cdots & p + j\dfrac{b}{a \cdot FBW \cdot Q_{e1}} & -j\sqrt{\dfrac{\mathrm{Re}^2(\bar{Y}_{gs}) + \mathrm{Im}^2(\bar{Y}_{gs})}{\mathrm{Re}(\bar{Y}_{gs}) \cdot FBW \cdot Q_{ek}}} \\
0 & \cdots & -j\sqrt{\dfrac{\mathrm{Re}^2(\bar{Y}_{gs}) + \mathrm{Im}^2(\bar{Y}_{gs})}{\mathrm{Re}(\bar{Y}_{gs}) \cdot FBW \cdot Q_{ek}}} & \bar{Y}_{gs} + \bar{Y}_{gd} \\
0 & 0 & 0 & \bar{g}_m - \bar{Y}_{gd} \\
0 & 0 & 0 & 0 \\
0 & 0 & 0 & 0 \\
0 & 0 & 0 & 0 \\
0 & 0 & 0 & 0
\end{bmatrix}
\begin{bmatrix}
0 & 0 & 0 & 0 \\
0 & 0 & 0 & 0 \\
0 & 0 & 0 & 0 \\
0 & 0 & 0 & 0 \\
-\bar{Y}_{gd} & 0 & 0 & 0 \\
\bar{Y}_{ds} + \bar{Y}_{gd} & -j\sqrt{\dfrac{\mathrm{Re}^2(\bar{Y}_{gs}) + \mathrm{Im}^2(\bar{Y}_{gs})}{\mathrm{Re}(\bar{Y}_{gs}) \cdot FBW \cdot Q_{ek+1}}} & \cdots & 0 \\
-j\sqrt{\dfrac{\mathrm{Re}^2(\bar{Y}_{ds}) + \mathrm{Im}^2(\bar{Y}_{ds})}{\mathrm{Re}(\bar{Y}_{ds}) \cdot FBW \cdot Q_{ek+1}}} & p + j\dfrac{b}{a \cdot FBW \cdot Q_{e1}} & \cdots & 0 \\
\vdots & \vdots & \ddots & \vdots \\
0 & 0 & \cdots & -j\sqrt{\dfrac{1}{FBW \cdot Q_{en}}} \\
0 & 0 & \cdots & \bar{Y}_{P2}
\end{bmatrix} \tag{3.82}
$$

The couplings between the resonators to the transistor $m_{k,in} = m_{in,k}$ and $m_{k+1,out} = m_{out,k+1}$ are defined by

$$
\begin{aligned}
m_{k,in} = m_{in,k} &= \sqrt{\frac{\mathrm{Re}^2(\bar{Y}_{gs}) + \mathrm{Im}^2(\bar{Y}_{gs})}{\mathrm{Re}(\bar{Y}_{gs}) \cdot q_{ek}}} \\
m_{k+1,out} = m_{out,k+1} &= \sqrt{\frac{\mathrm{Re}^2(\bar{Y}_{ds}) + \mathrm{Im}^2(\bar{Y}_{ds})}{\mathrm{Re}(\bar{Y}_{ds}) \cdot q_{ek+1}}}
\end{aligned} \tag{3.83}
$$

The normalised coupling coefficients between the input and output of the transistor are defined by

$$m_{in,out} = \frac{\overline{Y}_{gd}}{j}, m_{out,in} = \frac{\overline{Y}_{gd} - \overline{g}_m}{j} \tag{3.84}$$

$m_{k,k}$ and $m_{k+1,k+1}$ namely self-coupling, indicating the centre frequency shift, are given by

$$m_{n,n} = -\frac{\mathrm{Im}(\overline{Y}_{gs})}{\mathrm{Re}(\overline{Y}_{gs}) \cdot q_{ek}}, \quad m_{k+1,k+1} = -\frac{\mathrm{Im}(\overline{Y}_{ds})}{\mathrm{Re}(\overline{Y}_{ds}) \cdot q_{ek+1}} \tag{3.85}$$

Substitute (3.26) (3.63) (3.64) (3.83) (3.84) and (3.85) into (3.82) yielding

$$\left[\overline{Y}\right] = \begin{bmatrix}
1 & -jm_{P1,1} & 0 & \vdots & 0 & 0 & 0 & 0 & \vdots & 0 & 0 \\
-jm_{1,P1} & p & -j\frac{\omega}{\omega_0}m_{1,2} & \vdots & 0 & 0 & 0 & 0 & \vdots & 0 & 0 \\
0 & -j\frac{\omega}{\omega_0}m_{2,1} & p & \vdots & 0 & 0 & 0 & 0 & \vdots & 0 & 0 \\
\cdots & \cdots & \cdots & \ddots & \cdots & \cdots & \cdots & \cdots & \ddots & \cdots & \cdots \\
0 & 0 & 0 & \vdots & p - m_{k,k} & -jm_{k,in} & 0 & 0 & \vdots & 0 & 0 \\
0 & 0 & 0 & \vdots & -jm_{in,k} & Y_{gs} + Y_{gd} & -jm_{in,out} & 0 & \vdots & 0 & 0 \\
0 & 0 & 0 & \vdots & 0 & -jm_{out,in} & Y_{ds} + Y_{gs} & -jm_{out,k+1} & \vdots & 0 & 0 \\
0 & 0 & 0 & \vdots & 0 & 0 & -jm_{k+1,out} & p - m_{k+1,k+1} & \vdots & 0 & 0 \\
\cdots & \cdots & \cdots & \ddots & \cdots & \cdots & \cdots & \cdots & \ddots & \cdots & \cdots \\
0 & 0 & 0 & \vdots & 0 & 0 & 0 & 0 & \vdots & p & -jm_{n,P2} \\
0 & 0 & 0 & \vdots & 0 & 0 & 0 & 0 & \vdots & -jm_{P2,n} & 1
\end{bmatrix} \tag{3.86}$$

Assuming $\omega_0 = \omega$ for narrow band approximation, $[\bar{Y}]$ can be simplified to $[A]$

$$[A]=\begin{bmatrix} 1 & -jm_{P1,1} & 0 & \vdots & 0 & 0 & 0 & 0 & \vdots & 0 & 0 \\ -jm_{1,P1} & p & -jm_{1,2} & \vdots & 0 & 0 & 0 & 0 & \vdots & 0 & 0 \\ 0 & -jm_{2,1} & p & \vdots & 0 & 0 & 0 & 0 & \vdots & 0 & 0 \\ \cdots & \cdots & \cdots & \ddots & \cdots & \cdots & \cdots & \cdots & \ddots & \cdots & \cdots \\ 0 & 0 & 0 & \vdots & p-m_{k,k} & -jm_{k,in} & 0 & 0 & \vdots & 0 & 0 \\ 0 & 0 & 0 & \vdots & -jm_{in,k} & Y_{gs}+Y_{gd} & -jm_{in,out} & 0 & \vdots & 0 & 0 \\ 0 & 0 & 0 & \vdots & 0 & -jm_{out,in} & Y_{ds}+Y_{gs} & -jm_{out,k+1} & \vdots & 0 & 0 \\ 0 & 0 & 0 & \vdots & 0 & 0 & -jm_{k+1,out} & p-m_{k+1,k+1} & \vdots & 0 & 0 \\ \cdots & \cdots & \cdots & \ddots & \cdots & \cdots & \cdots & \cdots & \ddots & \cdots & \cdots \\ 0 & 0 & 0 & \vdots & 0 & 0 & 0 & 0 & \vdots & p & -jm_{n,P2} \\ 0 & 0 & 0 & \vdots & 0 & 0 & 0 & 0 & \vdots & -jm_{P2,n} & 1 \end{bmatrix} \tag{3.87}$$

Therefore, the *S*-parameters response of the filter amplifier can be calculated by

$$\begin{aligned} S_{11} &= 2[A]^{-1}_{P1,P1}-1 \quad S_{12} = 2[A]^{-1}_{P1,P2} \\ S_{21} &= 2[A]^{-1}_{P2,P1} \qquad S_{22} = 2[A]^{-1}_{P2,P2}-1 \end{aligned} \tag{3.88}$$

Matrix [*A*] can be further decomposed into three matrices, given by

$$[A]=[T]+p[U]-j[m] \tag{3.89}$$

[*T*] represents the matrix including the normalised filter's input port, the normalised transistor's input and output, and the normalised filter's output port.

$$[T]=\begin{bmatrix} 1 & 0 & 0 & \vdots & 0 & 0 & 0 & 0 & \vdots & 0 & 0 \\ 0 & 0 & 0 & \vdots & 0 & 0 & 0 & 0 & \vdots & 0 & 0 \\ 0 & 0 & 0 & \vdots & 0 & 0 & 0 & 0 & \vdots & 0 & 0 \\ \cdots & \cdots & \cdots & \ddots & \cdots & \cdots & \cdots & \cdots & \ddots & \cdots & \cdots \\ 0 & 0 & 0 & \vdots & 0 & 0 & 0 & 0 & \vdots & 0 & 0 \\ 0 & 0 & 0 & \vdots & 0 & \overline{Y}_{gs}+\overline{Y}_{gd} & 0 & 0 & \vdots & 0 & 0 \\ 0 & 0 & 0 & \vdots & 0 & 0 & \overline{Y}_{ds}+\overline{Y}_{gs} & 0 & \vdots & 0 & 0 \\ 0 & 0 & 0 & \vdots & 0 & 0 & 0 & 0 & \vdots & 0 & 0 \\ \cdots & \cdots & \cdots & \ddots & \cdots & \cdots & \cdots & \cdots & \ddots & \cdots & \cdots \\ 0 & 0 & 0 & \vdots & 0 & 0 & 0 & 0 & \vdots & 0 & 0 \\ 0 & 0 & 0 & \vdots & 0 & 0 & 0 & 0 & \vdots & 0 & 1 \end{bmatrix} \tag{3.90}$$

[*U*] is a matrix with diagonal entries identity except for the position at the ports and transistor's input and output.

$$[U]=\begin{bmatrix} 0 & 0 & 0 & \vdots & 0 & 0 & 0 & 0 & \vdots & 0 & 0 \\ 0 & 1 & 0 & \vdots & 0 & 0 & 0 & 0 & \vdots & 0 & 0 \\ 0 & 0 & 1 & \vdots & 0 & 0 & 0 & 0 & \vdots & 0 & 0 \\ \cdots & \cdots & \cdots & \ddots & \cdots & \cdots & \cdots & \cdots & \ddots & \cdots & \cdots \\ 0 & 0 & 0 & \vdots & 1 & 0 & 0 & 0 & \vdots & 0 & 0 \\ 0 & 0 & 0 & \vdots & 0 & 0 & 0 & 0 & \vdots & 0 & 0 \\ 0 & 0 & 0 & \vdots & 0 & 0 & 0 & 0 & \vdots & 0 & 0 \\ 0 & 0 & 0 & \vdots & 0 & 0 & 0 & 1 & \vdots & 0 & 0 \\ \cdots & \cdots & \cdots & \ddots & \cdots & \cdots & \cdots & \cdots & \ddots & \cdots & \cdots \\ 0 & 0 & 0 & \vdots & 0 & 0 & 0 & 0 & \vdots & 1 & 0 \\ 0 & 0 & 0 & \vdots & 0 & 0 & 0 & 0 & \vdots & 0 & 0 \end{bmatrix} \tag{3.91}$$

The general normalised coupling matrix can be expressed as

$$[m]=\begin{bmatrix} 0 & m_{P1,1} & 0 & \vdots & 0 & 0 & 0 & 0 & \vdots & 0 & 0 \\ m_{1,P1} & 0 & m_{1,2} & \vdots & 0 & 0 & 0 & 0 & \vdots & 0 & 0 \\ 0 & m_{2,1} & 0 & \vdots & 0 & 0 & 0 & 0 & \vdots & 0 & 0 \\ \cdots & \cdots & \cdots & \ddots & \cdots & \cdots & \cdots & \cdots & \ddots & \cdots & \cdots \\ 0 & 0 & 0 & \vdots & 0 & m_{k,in} & 0 & 0 & \vdots & 0 & 0 \\ 0 & 0 & 0 & \vdots & m_{in,k} & 0 & m_{in,out} & 0 & \vdots & 0 & 0 \\ 0 & 0 & 0 & \vdots & 0 & m_{out,in} & 0 & m_{out,k+1} & \vdots & 0 & 0 \\ 0 & 0 & 0 & \vdots & 0 & 0 & m_{k+1,out} & 0 & \vdots & 0 & 0 \\ \cdots & \cdots & \cdots & \ddots & \cdots & \cdots & \cdots & \cdots & \ddots & \cdots & \cdots \\ 0 & 0 & 0 & \vdots & 0 & 0 & 0 & 0 & \vdots & 0 & m_{n,P2} \\ 0 & 0 & 0 & \vdots & 0 & 0 & 0 & 0 & \vdots & m_{P2,n} & 0 \end{bmatrix} \tag{3.92}$$

3.3.2 *N*+4 coupling matrix optimisation

Section 3.3.1 introduces the circuit model of the transistor integrated with filters and an *N*+4 active coupling matrix which is proposed to characterise the topology and calculate the response.

Resonator based bandpass filters act as matching network both at the input and the output of the transistor, which are expected to achieve filtering response simultaneously. However, the parasitic parameter Y_{gd} provides feedback between gate and drain of the transistor [7], [8]. This presents a difficulty because the input impedance/admittance of the transistor is also influenced by the output matching network. The synthesised N+4 matrix produces standard Chebyshev responses at the input and output of the amplifier without Y_{gd}, whereas mismatching can be caused if there exists feedback. The difference of the S-parameters responses with or without feedback will be discussed later in an example.

In order to make a filter amplifier with Chebyshev response of return loss looking into both input and output of the transistor. A local optimisation based on the gradient algorithm can be applied to find a more accurate matrix [m] in order to produce the target response. The goal of the optimisation is to minimise a scalar Cost Function (*CF*), by modifying the values of $\boldsymbol{x}$, a set of independent parameters known as control variables. The cost function is formulated to quantify the difference between the optimised results and the desired response. Some critical characteristic points are chosen to form the cost function, including the Reflection Zeros (*RZ*), the Reflection Poles within the pass-band *(RP)*, and the equal-ripple pass-Band Edges (*BE)*. The cost function is formulated by

$$\begin{aligned} CF = &\sum_{i=1}^{k} a_i \left|S_{11}(\Omega_{RZi})\right| + \sum_{i=1}^{2} b_i \left|\left|S_{11}(\Omega_{BEi})\right| - \varepsilon\right| + \sum_{i=1}^{k-2} c_i \left|\left|S_{11}(\Omega_{RPi})\right| - \varepsilon\right| \\ &+ \sum_{i=1}^{N-k} d_i \left|S_{22}(\Omega_{RZi})\right| + \sum_{i=1}^{2} e_i \left|\left|S_{22}(\Omega_{BEi})\right| - \varepsilon\right| + \sum_{i=1}^{N-k-2} f_i \left|\left|S_{22}(\Omega_{RPi})\right| - \varepsilon\right| \end{aligned} \tag{3.93}$$

where a_i, b_i, c_i, d_i and e_i are the weights of each term, ε represents the maximum value of return loss in the passband. The critical points are illustrated using a 2nd order filter with Chebyshev

response in Fig. 3.11. The cost-function in (3.93) is a general case, that is, a k^{th} order filter is matched at the transistor's input and an $(N\text{-}k)^{th}$ order filter is coupled at the transistor's output.

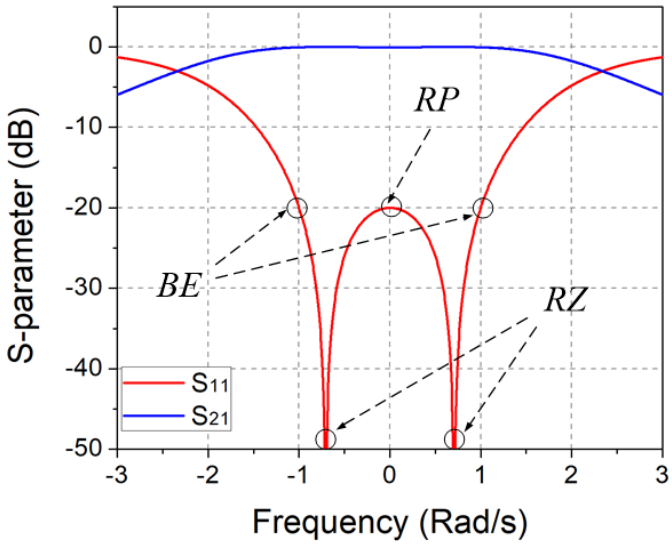

Fig. 3.11 The critical points of a filter having Chebyshev response.

The gradient algorithm is based on a local optimisation, which can be fast and effective for finding a solution given an initial point sufficiently close to a local minimum. Local methods will seek the minimum points within the local neighbourhood of points; however, this minimum is not guaranteed to have the lowest value of all points within the feasible region. This local optimisation algorithm succeeds to generate a vector $\boldsymbol{x}$ producing Chebyshev filter response S_{11} and S_{22} simultaneously and also gain in S_{21}.

The flowchart of the optimisation algorithm is illustrated in Fig. 3.12. First, a vector is given as an input. The positions of the reflection zeros, transmission zeros, and bandwidth edges are generated according to the prescribed specification of the filter. Then, the *S*-parameters are calculated using the input vector, following by the evaluation of the cost-function. Then, a local optimisation algorithm based on the gradient method is applied, which similar matrix optimisation

approaches can be found in [10] and [11]. Appropriate vector ***x*** can be returned once the cost-function constrains.

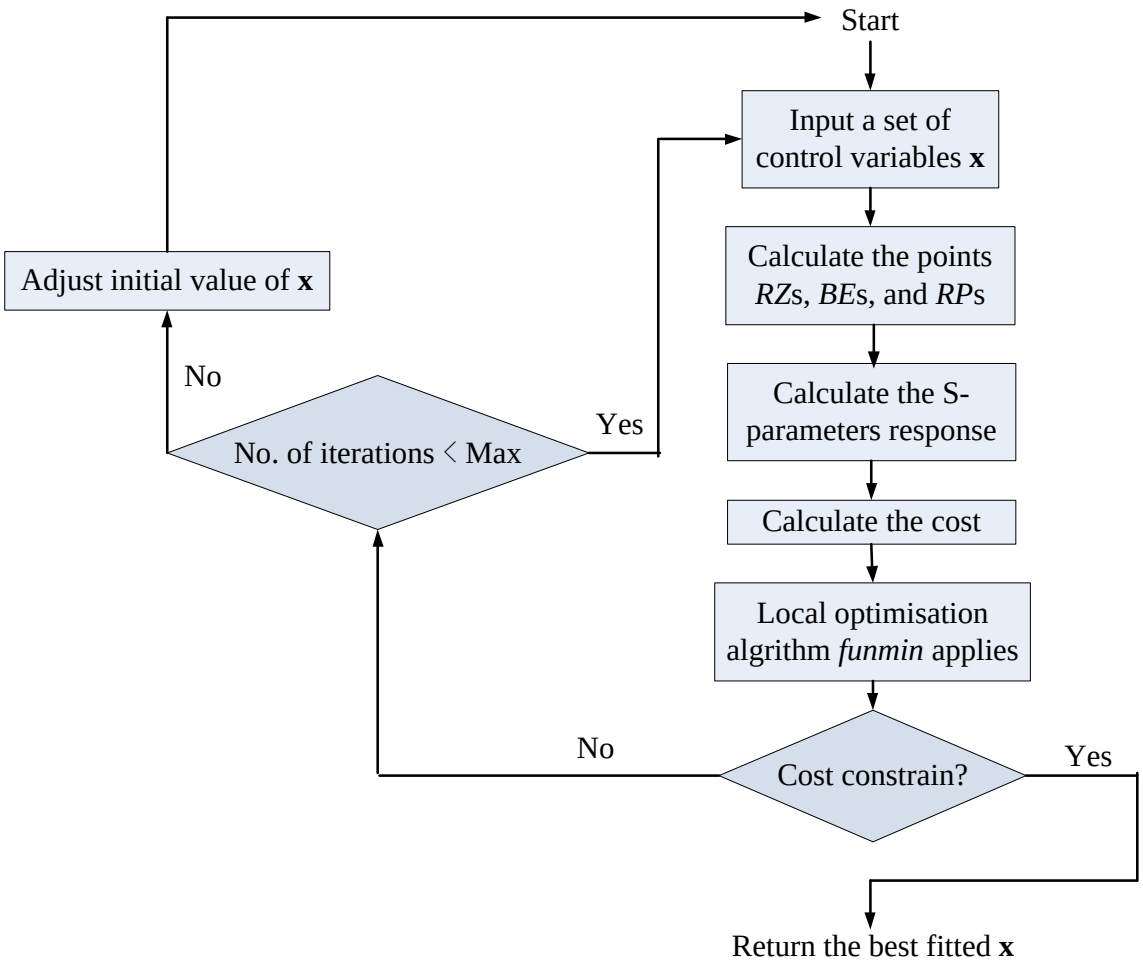

Fig. 3.12 Flowchart of the local optimisation algorithm.

3.3.3 Example: A filter amplifier using matrix optimisation

An example of N=4, k=2 matching filter amplifier is discussed. Two 2nd order bandpass filters are implemented both at input and output of the transistor, with a centre frequency f_0 of 10 GHz, a bandwidth of 500 MHz (fractional bandwidth FBW=0.05) and a passband return loss of 20 dB.

The transistor used is the NE310S01 with Y matrix parameters summarised in Table 3.1 [9]. It should be noted that the Y matrix parameters employed here are calculated, assuming the transistor operates at 10 GHz centre frequency. The corresponding normalised parameters of the transistor are presented in Table 3.1.

TABLE 3.1
VALUES OF TRANSISTOR'S Y MATRIX PARAMETERS

***Y* parameters**	**Value**	**Normalised $\bar{Y}$ parameters**	**Value**
g_m	**0.0696- 0.1350*j***	$\bar{g}_m$	**3.4812-6.7500*j***
Y_{gd}	**0.0003+ 0.0033*j***	$\bar{Y}_{gd}$	**0.0164+ 0.16298*j***
Y_{ds}	**0.0055+ 0.0127*j***	$\bar{Y}_{ds}$	**0.2752+ 0.6367*j***
Y_{gs}	**0.0051+ 0.0276*j***	$\bar{Y}_{gs}$	**0.2528+ 1.3799*j***
a	**2.4093**	b	**1.7238**

All parameters are calculated from the datasheet as the transistor operating at 10 GHz.

The normalised coupling coefficient $[m]$ can be calculated using (2.34) and (3.92), given by

$$[m]=\begin{bmatrix} 0 & 1.2264 & 0 & 0 & 0 & 0 & 0 & 0 \\ 1.2264 & 0 & 1.6621 & 0 & 0 & 0 & 0 & 0 \\ 0 & 1.6621 & -8.2104 & 3.4219 & 0 & 0 & 0 & 0 \\ 0 & 0 & 3.4219 & 0 & 0.1629-0.0164\,j & 0 & 0 & 0 \\ 0 & 0 & 0 & 6.75+3.4812j & 0 & 1.6216 & 0 & 0 \\ 0 & 0 & 0 & 0 & 1.6216 & -3.4800 & 1.6621 & 0 \\ 0 & 0 & 0 & 0 & 0 & 1.6621 & 0 & 1.2264 \\ 0 & 0 & 0 & 0 & 0 & 0 & 1.2264 & 0 \end{bmatrix} \tag{3.94}$$

According to the normalised Y parameters of the transistor in Table 3.1, matrix $[T]$ is given by

$$[T]=\begin{bmatrix} 1 & 0 & 0 & 0 & 0 & 0 & 0 & 0 \\ 0 & 0 & 0 & 0 & 0 & 0 & 0 & 0 \\ 0 & 0 & 0 & 0 & 0 & 0 & 0 & 0 \\ 0 & 0 & 0 & 0.2692+1.5428j & 0 & 0 & 0 & 0 \\ 0 & 0 & 0 & 0 & 0.2917+0.7997j & 0 & 0 & 0 \\ 0 & 0 & 0 & 0 & 0 & 0 & 0 & 0 \\ 0 & 0 & 0 & 0 & 0 & 0 & 0 & 0 \\ 0 & 0 & 0 & 0 & 0 & 0 & 0 & 1 \end{bmatrix} \tag{3.95}$$

The *S*-parameters response calculated using (3.88) is presented in Fig. 3.13.

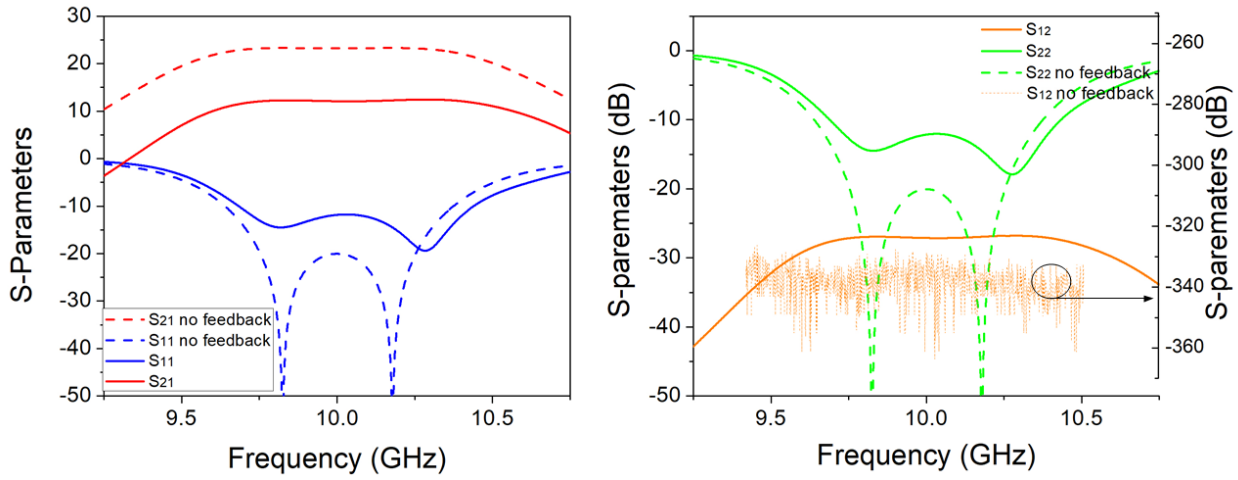

Fig. 3.13 Calculated filter amplifier *S*-parameters response using *N*+4 coupling matrix formulas. (a) Scattering parameters S_{11} and S_{21}. (b) Scattering parameters S_{22} and S_{12}.

It can be seen from Fig. 3.13 that the return loss S_{11} and S_{22} (solid line) are not a standard Chebyshev filter response because the transistor is usually a bilateral component and the input impedance is influent by the output matching network. The dashed line in Fig. 3.13 represents the *S*-parameters response with Y_{gd}=0. It is readily seen that S_{11} and S_{22} show Chebyshev response, and this is the idealised situation of a unilateral device. It can also be observed that the gain shown in S_{21} is larger and S_{12}=0. In practice, an amplifier can be assumed no feedback and designed separately [8]. The *N*+4 coupling matrix can predict the *S*-parameters of these two situations.

The *S*-parameters response with feedback in Fig. 3.13 resembles the desired filter response. Thus, the coupling coefficients in matrix [*m*] can be optimised to obtain the desired *S*-parameters response, where the coupling matrix [*m*] in (3.94) can be regarded as the initial value. The control variable ***x*** is given by

$$\begin{aligned} x &= \begin{bmatrix} m_{P1,1} & m_{1,2} & m_{2,in} & m_{out,3} & m_{3,4} & m_{2,2} & m_{3,3} \end{bmatrix} \\ &= \begin{bmatrix} 1.2264 & 1.6621 & 3.4219 & 1.6216 & 1.6621 & -8.2104 & -3.4800 \end{bmatrix} \end{aligned} \tag{3.96}$$

Note that the couplings between the transistor's gate and drain ($m_{in,out}$ $m_{out,in}$) which calculated from the transistor's parameters is taken as a fixed constant.

The optimisation is performed according to the methedology discussed above. The optimised ***x*** are shown in Table 3.2.

TABLE 3.2
INITIAL AND OPTIMISED VALUES OF PARAMETERS IN THE COUPLING MATRIX

	$m_{P1,\ 1}$ $m_{1,\ P1}$	$m_{1,2}$ $m_{2,1}$	$m_{in,2}$ $m_{2,in}$	$m_{3,out}$ $m_{out,3}$	$m_{3,4}$ $m_{4,3}$	$m_{4,P2}$ $m_{P2,4}$	$m_{2,2}$	$m_{3,3}$
Initial	**1.2264**	**1.6621**	**3.4219**	**1.6216**	**1.6621**	**1.2264**	**-8.2104**	**-3.4800**
Optimised	**1.1632**	**1.5260**	**3.2642**	**3.3534**	**2.9880**	**1.7030**	**-4.1620**	**-5.8360**

Substitute ***x*** into (3.92), the corresponding coupling matrix [m_{opt}] is given by

$$[m_{opt}] = \begin{bmatrix} 0 & 1.1632 & 0 & 0 & 0 & 0 & 0 & 0 \\ 1.1632 & 0 & 1.5260 & 0 & 0 & 0 & 0 & 0 \\ 0 & 1.5260 & -4.1620 & 3.2642 & 0 & 0 & 0 & 0 \\ 0 & 0 & 3.2642 & 0 & 0.1629 - 0.0164\,j & 0 & 0 & 0 \\ 0 & 0 & 0 & 6.9129 + 3.4658\,j & 0 & 3.3534 & 0 & 0 \\ 0 & 0 & 0 & 0 & 3.3534 & -5.8360 & 2.9880 & 0 \\ 0 & 0 & 0 & 0 & 0 & 2.9880 & 0 & 1.7030 \\ 0 & 0 & 0 & 0 & 0 & 0 & 1.7030 & 0 \end{bmatrix} \tag{3.97}$$

The calculated *S*-parameters response is presented in Fig. 3.14, compared with the unoptimised *S*-parameters response calculated using (3.94). The *S*-parameters response using optimised matrix is shown in solid line; the *S*-parameters response produced by the unoptimised matrix is represented by dashed line. It can be observed from Fig. 3.14 that the scattering parameters S_{11} and S_{22} display Chebyshev filtering response simultaneously, and about 15 dB gain in S_{21} indicating amplification. The maximum insertion losses seen from the input and the output of the transistor are below -20 dB over the passband. Not only the insertion losses are optimised, but the gain has also increased about 3.8 dB in the passband.

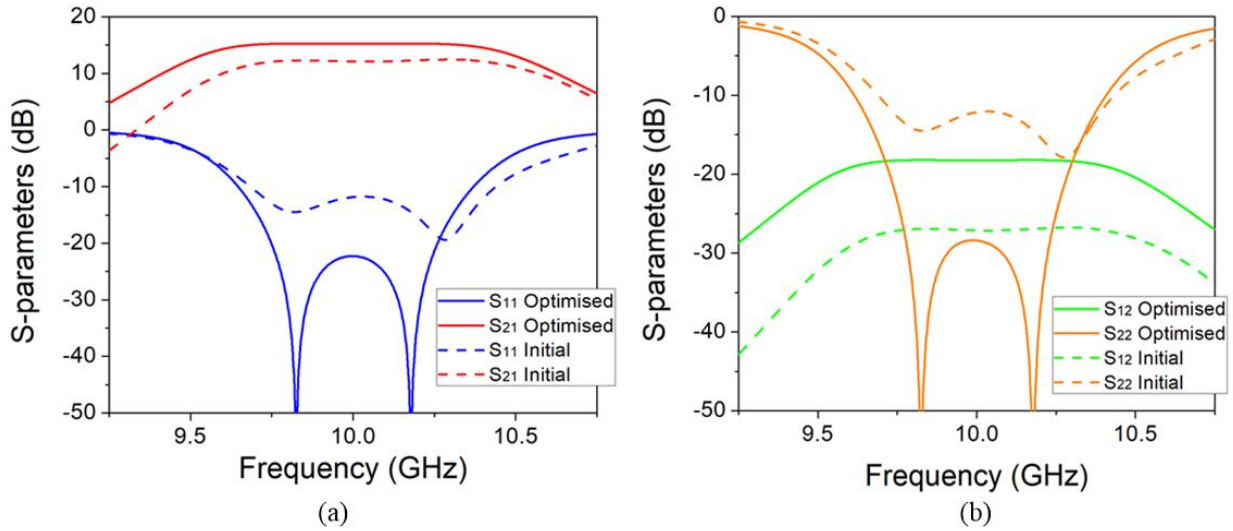

Fig. 3.14 Calculated *S*-parameters response using initial coupling matrix [*m*] and optimised coupling matrix [m_{opt}]. (a) Scattering parameters S_{11} and S_{21}. (b) Scattering parameters S_{12} and S_{22}.

3.4 Summary

In Chapter 3, three novel *N+X* matrices have been developed based on conventional coupling matrix synthesis and the simplified small signal transistor model. With the extra elements

introduced, the *S*-parameters response of the integrated topologies can be produced, enabling the prediction of the performance of multiple integrated components.

The coupling matrix of the cascaded filters is generalised to an arbitrary length of the transmission line to describe cascaded filters with any phase shift of the transmission line. The N+3 coupling matrix is synthesised in Section 3.2 to describe the filter amplifier, which has both filtering and amplification functionalities. Coupling strength between the transistor and the N^{th} resonator, and $m_{n,n}$ indicating the centre frequency shift are modified to achieve standard filtering response, is Chebyshev response in our case. This approach can be generalised to match other components with the complex input impedance, e.g. mixers, triplers and antennas. The resonator matching approach is applied simultaneously at both input and output of the transistor as discussed in Section 3.3 with the synthesised N+4 coupling matrix. As the transistor is a bilateral device, a numerical optimisation approach is used to compensate the error caused by the feedback of the transistor. The matrix optimisation based on the local gradient algorithm is involved to work out the coupling matrix generating the desired filtering response including a gain.

The coupling matrices providing initial values in the design of integrated devices will be introduced in Chapter 4 and Chapter 5 where a microstrip filter amplifier and two waveguide filter amplifiers are implemented as the demonstration.

REFERENCES

[1] J. S. Hong and M. J. Lancaster, *Microstrip Filters for RF/Microwave Applications*. New York, NY, USA: Wiley, 2001.

[2] R. J. Cameron, R. Mansour and C. M Kudsia, *Microwave Filters for Communication Systems: Fundamentals, Design and Applications*. 1st. New York, NY, USA: Wiley, 2007. pp. 283-288.

[3] S. Saeedi, J. Lee and H. H. Sigmarsson, "Tunable, High-Q, Substrate-Integrated, Evanescent-Mode Cavity Bandpass-Bandstop Filter Cascade," *IEEE Microw. Wirel. Compon. Lett.*, vol. 26, no. 4, pp. 240-242, April 2016.

[4] E. J. Naglich, J. Lee, D. Peroulis and W. J. Chappell, "Bandpass–Bandstop Filter Cascade Performance Over Wide Frequency Tuning Ranges," *IEEE Trans. Microw. Theory Techn.*, vol. 58, no. 12, pp. 3945-3953, Dec. 2010.

[5] Kurokawa, "Power Waves and the Scattering Matrix," *IEEE Trans. Microw. Theory Techn.*, vol. 13, no. 2, pp. 194-202, Mar 1965.

[6] G. Strang, *Introduction to linear algebra*. Wellesley [Massachusetts]: Wellesley-Cambridge Press, 2016.

[7] I. Bahl, *Fundamentals of RF and Microwave Transistor Amplifiers*. Hoboken, N.J.: Wiley, 2009.

[8] D. Pozar, *Microwave engineering*. Hoboken, NJ: Wiley, 2012.

[9] California Eastern Laboratories (2004, July). CEL Corp., CA. [Online]. Available: http://www.cel.com/pdf/datasheets/ne3210s1.pdf

[10] S. Amari, "Synthesis of cross-coupled resonator filters using an analytical gradient-based optimization technique," *IEEE Trans. Microw. Theory Techn.*, vol. 48, no. 9, pp. 1559-1564, Sep 2000.

[11] S. Amari, U. Rosenberg and J. Bornemann, "Adaptive synthesis and design of resonator filters with source/load-multiresonator coupling," *IEEE Trans. Microw. Theory Techn.*, vol. 50, no. 8, pp. 1969-1978, Aug 2002.

CHAPTER 4

N+3 COUPLING MATRIX BASED FILTER AMPLIFIERS

Amplifiers are commonly employed in communication systems to increase the incoming signal strength. There is always a demand of various design approaches for the amplifiers in the sense that it has to meet the electrical, thermal, physical, and cost requirements [1]-[3]. Several design examples have been reported for various fabrication processes and design technologies depending on the categories of the amplifier and their applications [4], [5]. MMIC with impedance matching technology applied in designing X-band power amplifiers is investigated in [4] and [5]. In waveguide amplifier design, connection to planar circuits often uses waveguide to planar circuit transitions. A Ku-band low noise waveguide amplifier is presented in [6], where step ridges act as the transition interconnecting the waveguide with the on-chip amplifier. In [7], the antipodal finline arrays have been combined with a coaxial waveguide for the design of a GaAs MMIC amplifier. CPW lines act as single stubs to match the transistor's input and output in [8]. The matching networks in [6]-[8] give the bandpass filter characteristics, allowing the transistor to operate at certain frequencies. However, the independent design of the transitions and the matching networks leads to additional losses and circuit complexity.

Some filters and the transistor are combined via impedance/admittance transformation referring to a common terminal impedance, usually 50 Ω; examples are in [9]-[11]. Compared with the waveguide co-design approach described here, the additional planar matching structure adds losses as well as circuit complexity and also the cost is more expense on size and weight. In this chapter, we propose combining the matching network and transition into the (low loss) waveguide resonators of the adjoining filter thereby minimising losses. This approach also leads to a reduction in the overall size of the combined component.

Based on the *N*+3 active coupling matrix synthesis, this chapter introduces the filter amplifiers, which transfer the matching network into resonators achieving filter functionality as well as amplification. By eliminating the intermediate planar matching network, the filter and the transistor can be combined in a compact manner, where the lowest loss is required. This is especially essential when frequencies rise to THz frequencies. The co-design approach proposed in this chapter is demonstrated by the examples of a microstrip amplifier and a waveguide amplifier. Although the physical constructions are different, the coupling matrix used is exactly the same.

4.1 Coupling Matrix applied in Design of Filter Amplifiers

The *N*+3 coupling matrix introduced in Chapter 3 is based on normalised admittance (impedance) parameters, and the provided the normalised admittance stays consistent from the input to output, this works well and is able to predict of the circuit response. However, when we have waveguide and microstrip combined, with a transition, and a transistor is matched to a 50 Ω output impedance, we no longer have a consistent normalising impedance/admittance throughout. The matrix [*A*], scaled from the admittance matrix [*Y*], enables us to ignore the matching and

impedance conditions and to concern ourselves only with the coupling coefficients in coupling matrix [m].

$$[m]=\begin{bmatrix} 0 & m_{P1,1} & \cdots & 0 & 0 & 0 \\ m_{1,P1} & 0 & \cdots & 0 & 0 & 0 \\ \vdots & \vdots & \ddots & \vdots & \vdots & \vdots \\ 0 & 0 & \cdots & m_{n,n} & m_{n,P2} & 0 \\ 0 & 0 & \cdots & m_{P2,n} & 0 & m_{P2,P3} \\ 0 & 0 & \cdots & 0 & m_{P3,P2} & 0 \end{bmatrix} \tag{4.1}$$

In practice, the geometries of the filter and the coupling structure of the N^{th} resonator to the input of the transistor can be determined from the coupling matrix [m] in (4.1). The process and equations follow closely from those of simple filters [12], but with differences associated with the new N+3 matrix. This process is discussed below.

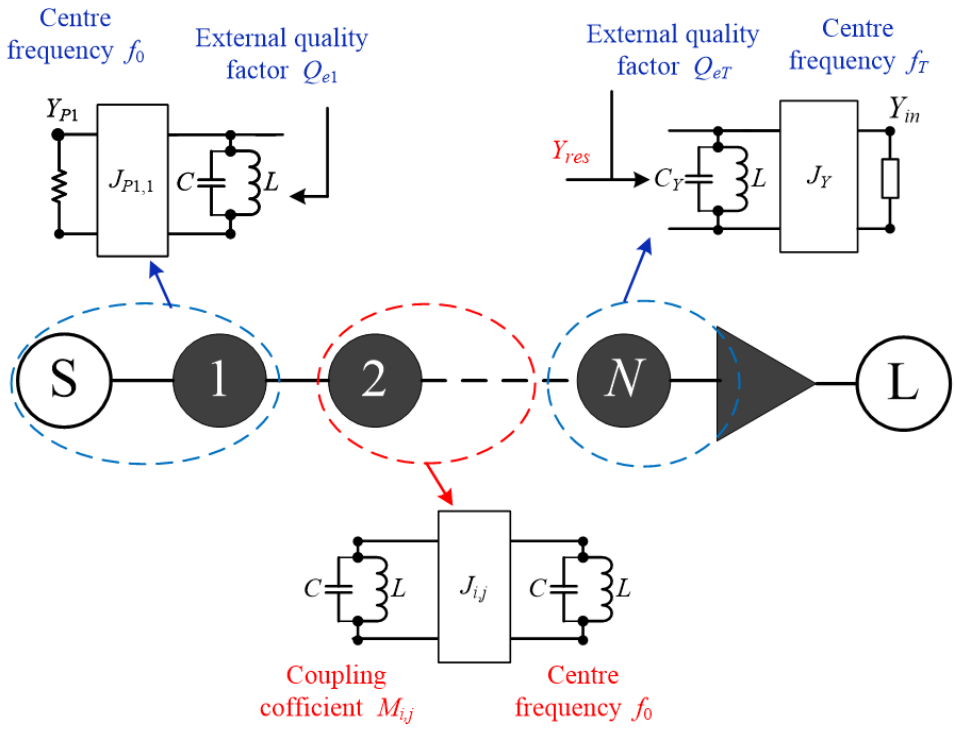

Fig. 4.1 Topology of the resonator based filter amplifier and the equivalent lumped circuit.

Fig. 4.1 presents the topology of the filter amplifier and some equivalent lumped circuits: the 1st resonator coupling to the source, the i^{th} and j^{th} resonators coupled by the J inverter; the N^{th} resonator coupling to transistor's input.

The first step is to determine the inter-resonator coupling coefficient. As with just a conventional filter, the coupling coefficient $M_{i,j}=M_{j,i}$ between the two resonators can be calculated by scaling with the fractional bandwidth (FBW)

$$M_{i,j} = FBW \cdot m_{i,j} \quad i, j = 1 \quad \text{to} \quad n \tag{4.2}$$

The next step is to determinate the external coupling from port 1 to the 1st resonator. This can be done by extracting the external quality factor of the 1st resonator (Q_{e1}) as illustrated in Fig. 4.1. In the N+3 coupling matrix, Q_{e1} is related to the external couplings $m_{P1,1}= m_{P1,1}$.

$$Q_{e1} = \frac{1}{FBW \cdot m_{1,P1}^2} = \frac{1}{FBW \cdot m_{P1,1}^2} \tag{4.3}$$

From (4.3) the required external quality factor Q_{e1} can be found.

Then, we need to consider the $m_{P2,n}=m_{n,P2}$ corresponding to the coupling strength between the resonator and the transistor as well as the self-coupling $m_{n,n}$ representing resonator centre frequency. In practical design, the external coupling $m_{P2,n}=m_{n,P2}$ and self-coupling $m_{n,n}$ can be determined by extracting the external quality factor (Q_{eT}) and frequency (f_T) of the N^{th} resonator incorporating the input of the transistor. The whole structure includes the resonator itself and the complex input admittance of the transistor. The equivalent circuit of the N^{th} resonator coupled to the complex admittance Y_{in} is illustrated in Fig. 4.1, where Y_{in} is the input admittance of the transistor and calculated by

$$Y_{in} = \left(a + jb\right)Y_0 \tag{4.4}$$

Referring (3.52) and (3.53), the capacitor C_Y and the inverter J_Y can be expressed in terms of self-

coupling $m_{n,n}$ and external coupling $m_{P2,n}$=$m_{n,P2}$ by

$$C_Y = C\left(1 - FBW \cdot m_{n,n}\right) \tag{4.5}$$

$$J_Y = \sqrt{FBW\,\omega_0 C \cdot Y_0} \cdot m_{n,P2} = \sqrt{FBW\,\omega_0 C \cdot Y_0} \cdot m_{P2,n} \tag{4.6}$$

where C is the capacitance of the 1st to the (N-1)th resonators and Y_0 is the characteristic admittance. The input admittance (Y_{res}) of the corresponding circuit in Fig. 4.1 can now be calculated and compared with the standard equation for the admittance of a loaded resonant circuit. This enables the extraction of the frequency (f_T) and quality factor (Q_{eT}). The centre frequency f_T and the external quality factor Q_{eT} are calculated as follows.

As the equivalent lumped circuit shown in Fig. 4.1, the N^{th} resonator is coupled to Y_{in} via inverter J_Y. The input admittance (Y_{res}) of the N^{th} resonator incorporating Y_{in} can be expressed as

$$Y_{res} = j\omega C_Y + \frac{1}{j\omega L} + \frac{J_Y^2}{Y_0\left(a + b \cdot j\right)} \tag{4.7}$$

Substitute (4.5) and (4.6) into (4.7), we have

$$Y_{res} = j\omega C\left(1 - FBW \cdot m_{n,n} - \frac{b \cdot FBW\,\omega_0 \cdot m_{P2,n}^2}{\left(a^2 + b^2\right)\cdot \omega}\right) + \frac{1}{j\omega L} + \frac{a \cdot FBW\,\omega_0 C \cdot m_{P2,n}^2}{\left(a^2 + b^2\right)} \tag{4.8}$$

At the centre frequency ($\omega_T = 2\pi f_T$), where for the narrowband approximation ($\omega = \omega_T$), Y_{res} satisfies

$$\mathrm{Im}\left(Y_{res}\right)\Big|_{\omega=\omega_T} = 0 \tag{4.9}$$

Substitute (4.8) into (4.9), yielding

$$\left(\frac{\omega_0}{\omega_T}\right)^2 + \frac{b \cdot FBW \cdot m_{P2,n}^2}{\left(a^2 + b^2\right)}\left(\frac{\omega_0}{\omega_T}\right) - \left(1 - FBW \cdot m_{n,n}\right) = 0 \tag{4.10}$$

Then, (4.10) can be solved to give

$$\left(\frac{\omega_0}{\omega_T}\right)=\frac{-\frac{b\cdot FBW\cdot m_{P2,n}^2}{\left(a^2+b^2\right)}\pm\sqrt{\left(\frac{b\cdot FBW\cdot m_{P2,n}^2}{\left(a^2+b^2\right)}\right)^2+4\left(1-FBW\cdot m_{n,n}\right)}}{2} \tag{4.11}$$

Because the ratio of ω_T and ω_0 should be positive, only the positive root is used. Substitute $\omega_T = 2\pi f_T$ and $\omega_0 = 2\pi f_0$ into (4.11), the centre frequency f_T can be calculated as

$$f_T=\frac{2\left(a^2+b^2\right)\cdot f_0}{b\cdot FBW\cdot m_{n,P2}^2\left(\sqrt{1+\frac{4\left(1-m_{n,n}\cdot FBW\right)\left(a^2+b^2\right)^2}{b^2\cdot m_{n,P2}^4\cdot FBW^2}}-1\right)} \tag{4.12}$$

As the admittance Y_{res} is given in (4.8), the external quality factor Q_{eT} can be calculated by [12]

$$Q_{eT}=\frac{\omega_T C\left(1-FBW\cdot m_{n,n}-\frac{b\cdot FBW\omega_0\cdot m_{P2,n}^2}{\left(a^2+b^2\right)\cdot\omega}\right)}{\frac{a\cdot FBW\omega_0 C\cdot m_{P2,n}^2}{\left(a^2+b^2\right)}} \tag{4.13}$$

(4.13) can be simplified to give

$$Q_{eT}=\frac{\omega_T}{\omega_0}\left(\frac{\left(a^2+b^2\right)}{a\cdot FBWm_{P2,n}^2}-\frac{m_{n,n}\cdot\left(a^2+b^2\right)}{a\cdot m_{P2,n}^2}\right)-\frac{b}{a} \tag{4.14}$$

or

$$Q_{eT}=\frac{f_T}{f_0}\left(\frac{\left(a^2+b^2\right)}{a\cdot FBWm_{P2,n}^2}-\frac{m_{n,n}\cdot\left(a^2+b^2\right)}{a\cdot m_{P2,n}^2}\right)-\frac{b}{a} \tag{4.15}$$

Using (4.12) and (4.15), the external Q of the Resonator N coupled with Y_{in} can be calculated at its resonant frequency f_T.

Recall $m_{P2,n}$=$m_{n,P2}$ and $m_{n,n}$ are defined in (3.66) and (3.68). The final step is to substitute (3.66) and (3.68) into (4.15) and (4.12) to give the simple solutions

$$f_T = f_0 \tag{4.16}$$

$$Q_{eT} = \frac{q_{en}}{FBW} \tag{4.17}$$

It can be seen from (4.16) and (4.17) that the external Q and centre frequency of the resonator coupling with the active component are exactly the same as for conventional filter synthesis [12] with Q_{eT}=Q_{e1}. This fact allows the method of designing the filter amplifier to much more closely resembling the design of a standard filter [12].

4.2 Coupling Matrix Example of a Filter Amplifier

The elements of the N+3 coupling matrix [m] are calculated from the standard expressions for the desired filter response. In our demonstration, we will use an example of a 2-pole Chebyshev filter, N=2, with a centre frequency f_0 of 10 GHz, a bandwidth of 500 MHz (fractional bandwidth FBW=0.05) and a passband return loss of 20 dB. The g values for its lowpass prototype Chebyshev filter are given in Table 4.1.

TABLE 4.1
g VALUES FOR THE PROTOTYPE OF LOWPASS CHEBYSHEV FILTER

g_0	g_1	g_2	g_3
1	**0.6648**	**0.5445**	**1.2210**

Filter specification: 2-pole Chebyshev filter response with 20 dB return loss

The transistor used is the NE310S01 with normalised and unnormalised Y matrix parameters summarised in Table 4.2 [14]. It should be noted that the Y matrix parameters employed here are calculated, assuming the transistor operates at 10 GHz centre frequency.

TABLE 4.2
VALUES OF TRANSISTOR'S Y MATRIX PARAMETERS

***Y* parameters**	**Value**	**Normalised $\bar{Y}$ parameters**	**Value**
g_m	**0.0696- 0.1350*j***	$\bar{g}_m$	**3.4812-6.7500*j***
Y_{gd}	**0.0003+ 0.0033*j***	$\bar{Y}_{gd}$	**0.0164+ 0.16298*j***
Y_{ds}	**0.0055+ 0.0127*j***	$\bar{Y}_{ds}$	**0.2752+ 0.6367*j***
Y_{gs}	**0.0051+ 0.0276*j***	$\bar{Y}_{gs}$	**0.2528+ 1.3799*j***

All parameters are calculated from the datasheet as the transistor operating at 10 GHz.

The filter and transistor specifications can be translated into elements of the coupling matrix using the (2.34) and (4.1). The active coupling matrix [*m*] is

$$[m]=\begin{bmatrix} 0 & 1.2264 & 0 & 0 & 0 \\ 1.2264 & 0 & 1.6621 & 0 & 0 \\ 0 & 1.6621 & -1.0762 & 2.3407 & 0 \\ 0 & 0 & 2.3407 & 0 & 0.1629-0.0164\,j \\ 0 & 0 & 0 & 6.9129+3.46578\,j & 0 \end{bmatrix} \tag{4.18}$$

Note that $m_{2,P2}$ and $m_{P2,2}$ in representing the couplings between the resonator and the transistor's input. The $m_{2,2}$ in (4.18) indicates the self-coupling of the 2nd resonator. According to (3.74), the [*T*] matrix which represents the filter input admittance, the transistor's input admittance and the output admittance with matching, is given by

$$[T]=\begin{bmatrix} 1 & 0 & 0 & 0 & 0 \\ 0 & 0 & 0 & 0 & 0 \\ 0 & 0 & 0 & 0 & 0 \\ 0 & 0 & 0 & 0.2692+1.5428\,j & 0 \\ 0 & 0 & 0 & 0 & 0.5668+0.1630\,j \end{bmatrix} \tag{4.19}$$

Matrix [*U*] is

$$[U]=\begin{bmatrix}0&0&0&0&0\\0&1&0&0&0\\0&0&1&0&0\\0&0&0&0&0\\0&0&0&0&0\end{bmatrix} \tag{4.20}$$

Using (3.72) and (3.73), the resultant scattering parameters can be calculated from the asymmetrical active matrix [*A*] and are presented in Fig. 4.2. The novel active coupling matrix produces a standard Chebyshev filter response (*FBW*=0.05) with amplification.

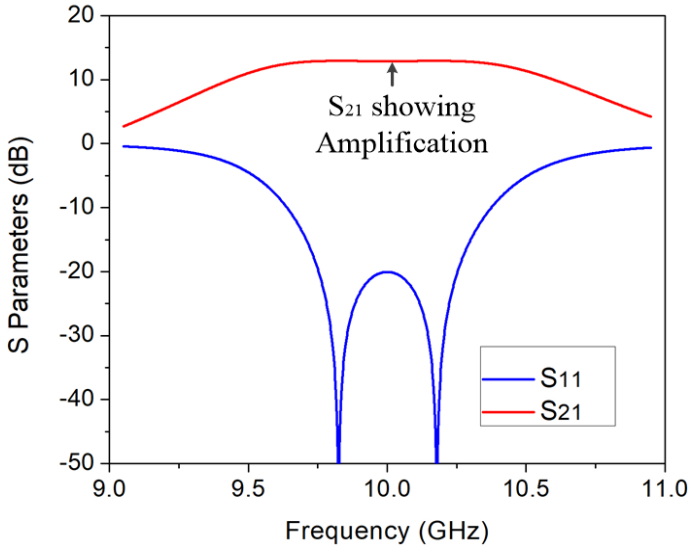

Fig. 4.2 Calculated *S*-parameters response of filter amplifier using matrix formulations.

The coupling matrix in (4.18) can be applied to the design of filter amplifiers. The fractional bandwidth *FBW*=0.05. Referring (4.3) and (4.18), the external Q of the 1st resonator can be calculated to give Q_{e1}=13.297. The coupling coefficient between Resonator 1 and Resonator 2 ($M_{1,2}$) can be computed using (4.2) and (4.18) to give $M_{1,2}$=0.0831. The external Q of the 2nd resonator incorporating the transistor's input (Q_{eT}) and its centre frequency (f_T) can be calculated using (4.16) (4.17) and (4.18). The results are Q_{eT}=13.297 and f_T=10 GHz.

4.3 Example A: A Microstrip Filter Amplifier Design

Based on the coupling matrix in (4.18), a hairpin resonator based microstrip filter amplifier design is introduced in this section. The layout of the hairpin resonator filter amplifier is illustrated in Fig. 4.3.

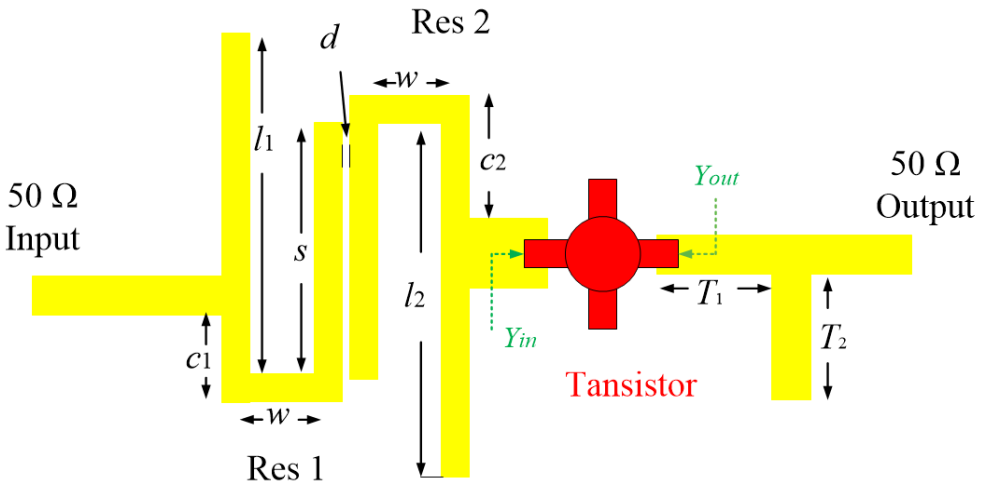

Fig 4.3 Layout illustration of the microstrip filter amplifier.

In practice, geometries of the coupling gaps and the transition from the resonator to the transistor's gate can be determined by the external quality factor Q_e and the coupling coefficients $M_{i,j}$. For a single hairpin microstrip resonator, the resonant frequency is mainly determined by the dimensions of s, w, l_1 and l_2. The external quality factor of the Resonator 1 (Q_{e1}) is primarily controlled by the tapped position c_1 of the transmission line. At the transistor input, the external quality factor of the Resonator 2 (Q_{eT}) is determinate by the tapped position t_2 and the length of the transition d_2 and the width w_3. In the bandpass microstrip filter design, the extraction of the external quality factor Q_{e1} and coupling coefficient $M_{1,2}$ are same as the conventional filter design approach [12], while the extraction of the external quality factor (Q_{eT}) is different because it includes the transistor. The detailed design procedure is discussed in the following sections.

4.3.1 Extraction of the external quality factor Q_{e1}

The first step is to determine the size of c_1 to fulfil the required Q_{e1}. The configuration of the extraction structure is shown in Fig. 4.4(a), where a single hairpin resonator is simulated in ADS [17] resulting in the response of a single resonance curve. Q_{e1} can be extracted by observing the curve shown in Fig. 4.4(b) and calculated by the ratio of the centre frequency and the 3 dB bandwidth.

$$Q_e = \frac{f_0}{\Delta f} \tag{4.21}$$

In the setup of the hairpin resonator, there is weak coupling from the narrow gap at port 1. The lengths of s and w are kept constant, and the required external quality factor Q_{e1} can be found by altering the length of c_1. Fig. 4.5 shows the relationship of the tapped position c_1 and external quality factor Q_e, thus the length of c_1 that decides the external quality factor can be read off as indicated in the figure. Note that the centre frequency of the resonator shifts as the length of c_1 alters. Thus, l_1 can be adjusted to keep the resonance at 10 GHz centre frequency.

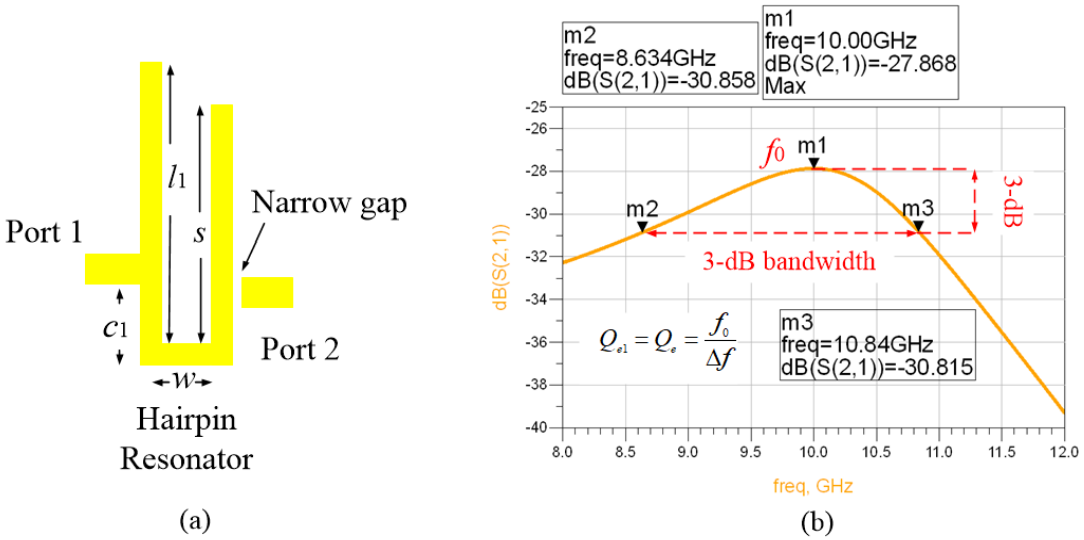

Fig. 4.4 (a) Single microstrip hairpin resonator to extract the external quality factor Q_{e1}. (b) EM simulation result of the hairpin resonator.

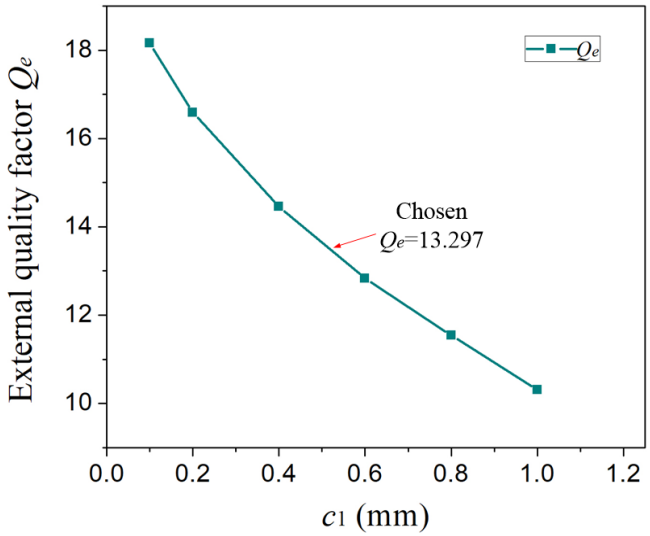

Fig. 4.5 External quality factor Q_e versus c_1. All points are at 10 GHz.

4.3.2 Extraction of the coupling coefficient

The configuration for the extraction of the coupling coefficient $M_{1,2}$ is shown in Fig. 4.6: a pair of hairpin resonators are coupled through gap d, and weak coupling is stimulated from port 1 and port 2 via the narrow gap.

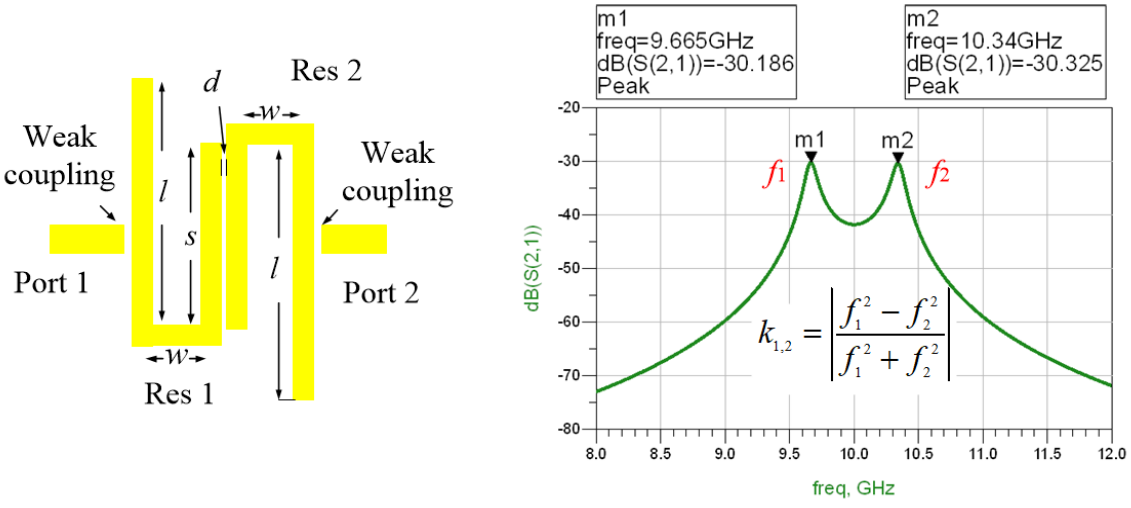

Fig. 4.6 (a) A pair of microstrip hairpin resonators to extract the coupling coefficient. (b) EM simulation result of the coupled hairpin resonators.

Two identical resonators have the same centre frequency 10 GHz. The coupled resonators structure is simulated in ADS [17], and the *S*-parameter response is given in Fig. 4.6(b) showing the resonance with two peaks. The coupling strength between the two resonators is determined by the size of *d*, and the length of the hairpin arm *l* influences the centre frequency. The coupling coefficient $M_{i,j}$ can be extracted from the *S*-parameters response and is calculated by

$$M_{i,j} = \left| \frac{f_i^2 - f_j^2}{f_i^2 + f_j^2} \right| \tag{4.22}$$

where f_i and f_j are the frequencies of the peaks in S_{21}. The coupling coefficient $M_{i,j}$ can be altered by varying *d* and a graph of the coupling coefficient $M_{1,2}$ versus dimension *d* is plotted in Fig. 4.7. The requited $M_{1,2}$ can be located according to the relationship of *d* and $M_{1,2}$ in Fig. 4.7 and hence a *d* can be found as shown.

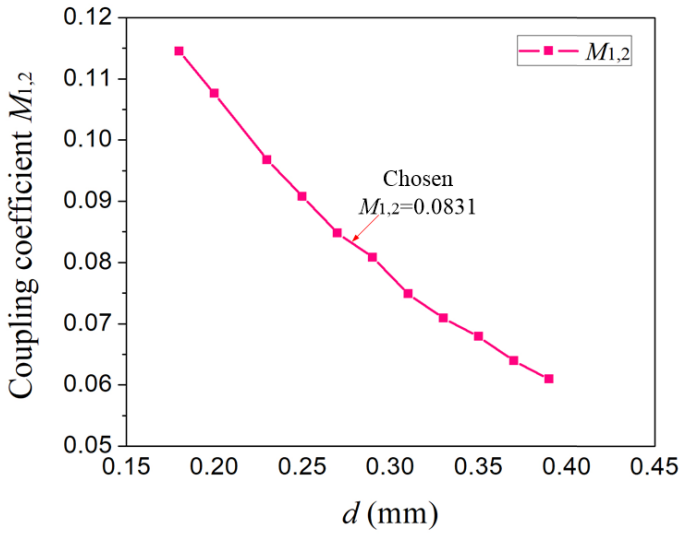

Fig. 4.7 Coupling coefficient $k_{1,2}$ versus *d*. All points are at 10 GHz.

4.3.3 Extraction of the external quality factor Q_{eT}

The next step is to extract the external quality factor (Q_{eT}) of the Resonator 2 incorporating the input of the transistor. Because the resonator is connected to the transistor which has a complex input impedance (admittance), the process of extracting Q_{eT} is different. The whole structure includes the parameters of the transistor. The circuit configuration is schematically illustrated in Fig. 4.8(a): a single resonator is coupled with port 1 via a narrow gap and is connected to the complex impedance port 2 (the complex value Z_{in} is the input impedance of the transistor). The circuit simulation is performed in ADS [17] and a resonance frequency *S*-parameters response curve is shown in Fig. 4.8(c).

For the structure in Fig. 4.8(b), the resonance of the centre frequency is mainly determinate by the length of the hairpin arms (l_2 and s). In the simulation, the hairpin width (w) is kept constant. The tapped position distance c_2 is changed. l_2 is adjusted to maintain the resonant frequency at 10 GHz. The simulation result of Q_e versus c_2 is shown in Fig. 4.9, where the appropriate size of c_2 can be read off.

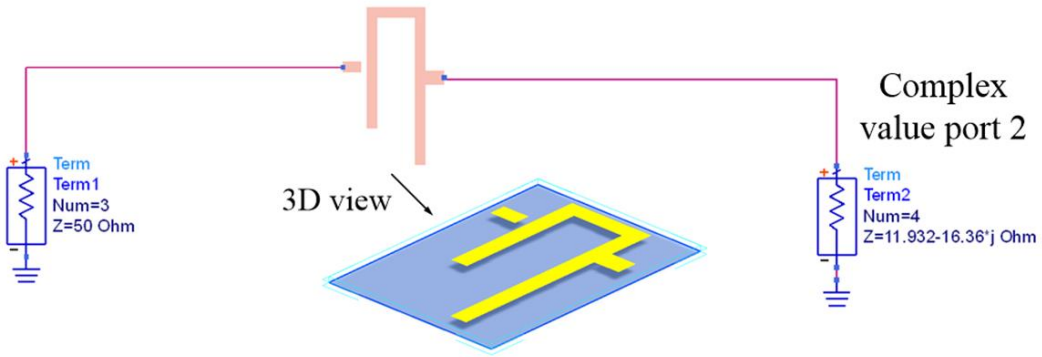

(a)

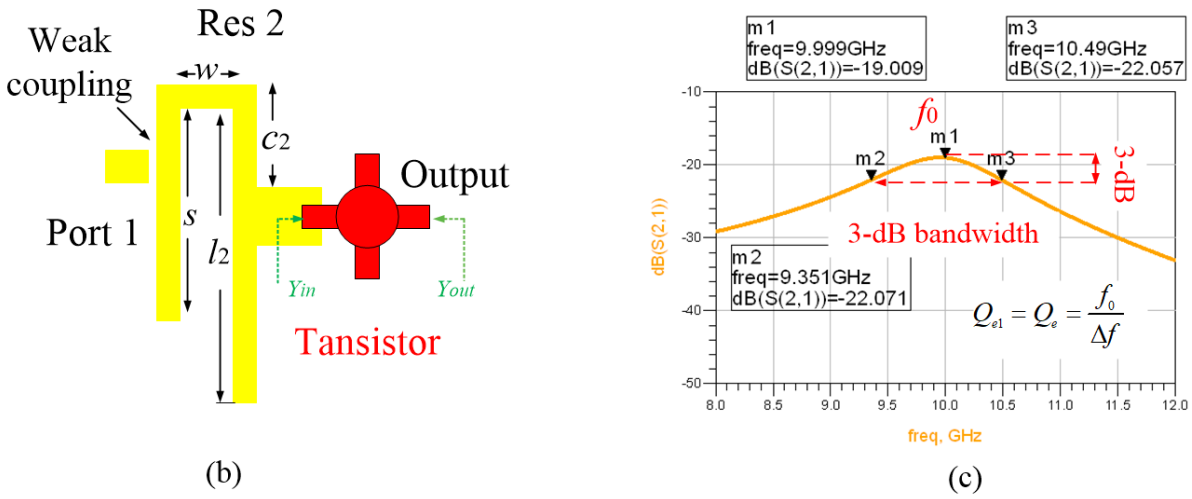

Fig. 4.8 Configuration to extract the external quality factor. (a) The circuit of the hairpin resonator with the transistor's input impedance simulated in ADS. (b) Layout of the hairpin resonator integrated with the transistor. (c) *S*-parameters response of single resonator incorporating the input impedance of the transistor.

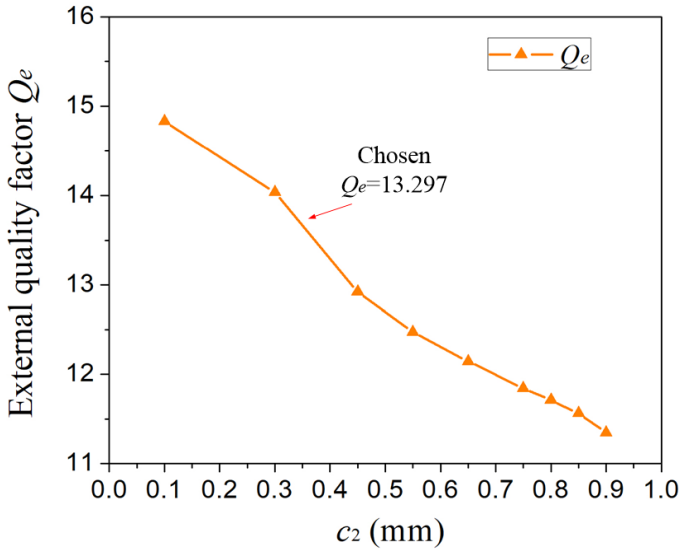

Fig. 4.9 External quality factor Q_e versus tapping position c_2. All points are at 10 GHz.

4.3.4 Output matching using single stub

We assumed that the output of the transistor is conjugately matched to the drain to source admittance Y_{ds}, as in the lumped circuit shown in Fig. 3.7(a). The single stub is employed to match the drain to source complex admittance Y_{ds} to 50 Ω transmission line. According to Table 4.2, the

normalised admittance Y_{ds} is 0.2752+0.6367j, and thus the normalised impedance is Z_{ds} is given by 0.5720-1.3234j.

As the Smith chart shows in Fig 4.10, the normalised impedance Z_{ds}=0.5720-1.3234j. The SWR circle, which intersects the 1+jx circle at two points, denoted as Z_1 and Z_2 as shown. The shortest distance from Z_{ds} to the stub T_1 is 0.321λ. Thus, the normalised impedance at the point Z_1 is 1+1.7λ. This requires a stub with the reactance of -j1.7. The length of the stub that offers this reactance can be found on the Smith chart by moving from the z=∞ point towards the generator -j1.7. This gives the stub length of 0.331λ.

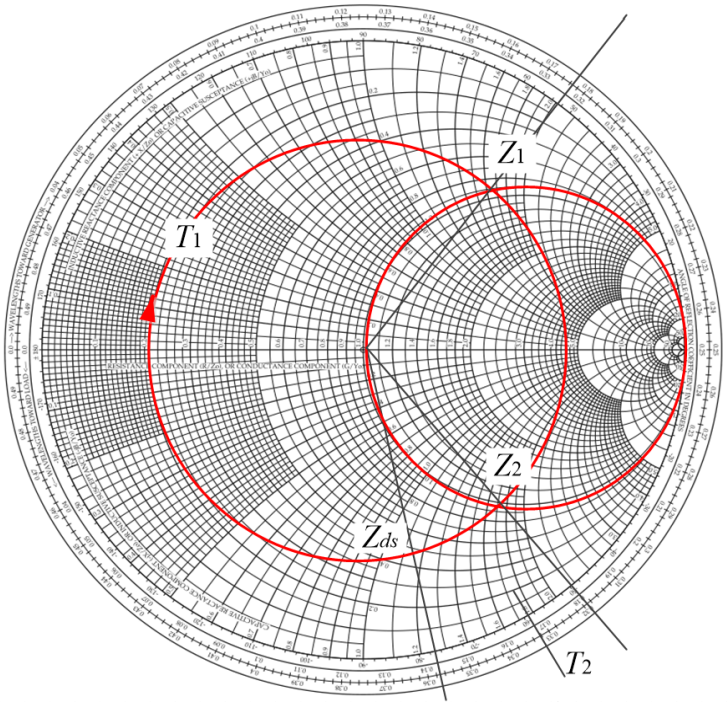

Fig. 4.10 Smith chart for the series-stub tuner.

The next step is to simulate the theoretically calculated stub dimensions in the ADS [17] to check and optimise the matching circuit. The corresponding lengths are given by T_1=9.63mm, T_2=9.93 mm. As shown in Fig. 10.11(a), the single stub is employed at the output of the transistor,

with the transistor in the form of an S2P file dataset. The dataset is provided by the transistor manufacture in [14]. We use the microstrip line with open-end, and ADS offers an accurate model for the single microstrip stub. As shown in Fig. 4.11(b), the matched centre frequency simulated using the theoretically calculated dimensions is around 12.8 GHz. We apply the tuning tool in the ADS simulator and adjust the length of T_1 and T_1, thereby finding the more accurate dimensions, i.e. T_1=3.8 mm, T_2=3.1 mm.

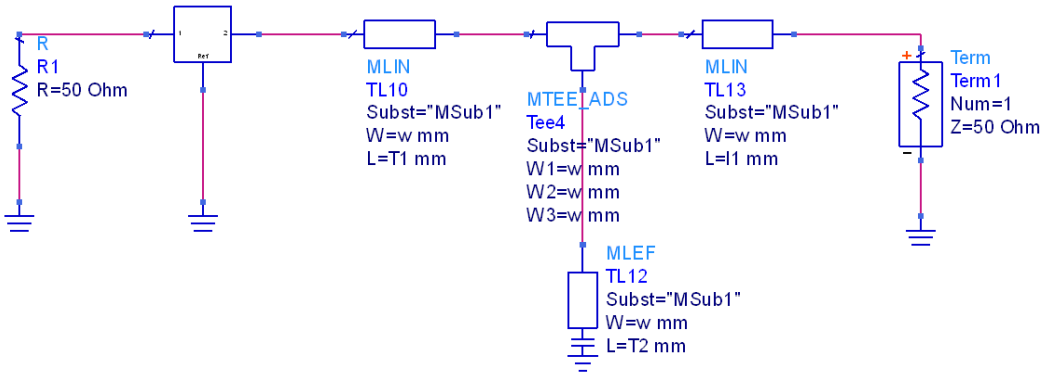

(a)

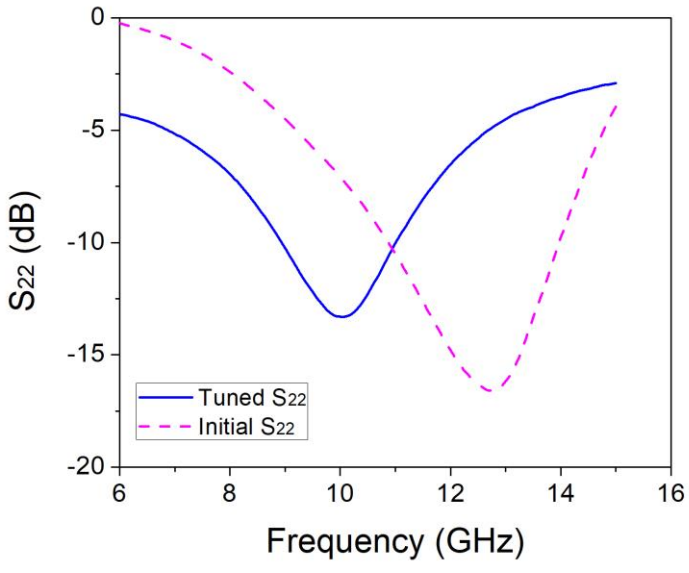

(b)

Fig. 4.11 Single stub to match the output of the transistor. (a) Schematic of the matching circuit in ADS. (b) Scattering parameter S_{22}.

4.3.5 Full EM simulation and optimisation

After the all the parameters are determined, full wave EM simulation is implemented for the entire filter amplifier. As illustrated in Fig. 4.12(a), the resonator based filter amplifier is simulated in ADS [17]. Note that bias connection is not included. The *S*-parameters response simulated using initial values is presented in Fig. 4.12(b). The *S*-parameters response shows a filter response with gain, which proves that the extraction procedures can provide good initial values for further optimisation.

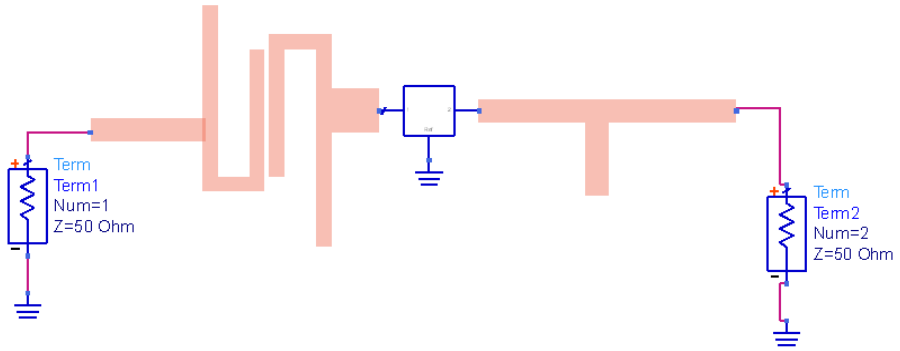

(a)

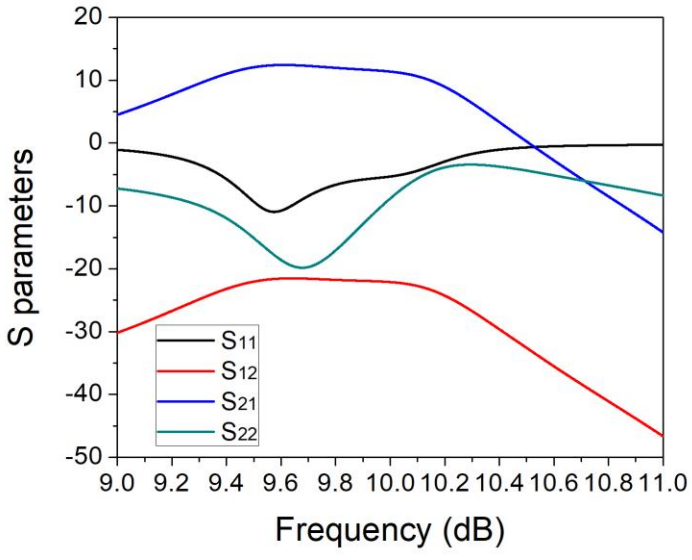

(b)

Fig. 4.12 EM simulation and *S*-parameters response. (a) Layout of the microstrip filter amplifier. (b) *S*-parameters response of EM simulation using initial values.

Before further optimisation, we have to consider the bias. The complete layout of the filter amplifier is presented in Fig. 4.13(a), and Fig. 4.13(b) showing a three-dimensional view. b_1 and b_3 are quarter-wavelength long bias tees at 10 GHz centre frequency. Quarter-wavelength long sectors are designed at the end of the bias arms providing short circuit conditions. Soldering pads are connected through b_2 and b_4, offering DC voltages. Two pins of the transistor are grounded via through-holes. The substrate used is Rogers RT/5870 with 0.254 mm thick and the dielectric constant of 2.33.

Now optimisation is performed for the whole structure. Optimisation goals, in this case, are set to be: from 9.75 GHz to 10.25 GHz, S_{11} under is -20 dB; from 9.75 GHz to 10.25 GHz S_{22} is under -10 dB; critical points 9.725 GHz and 10.178 GHz are under -40 dB.

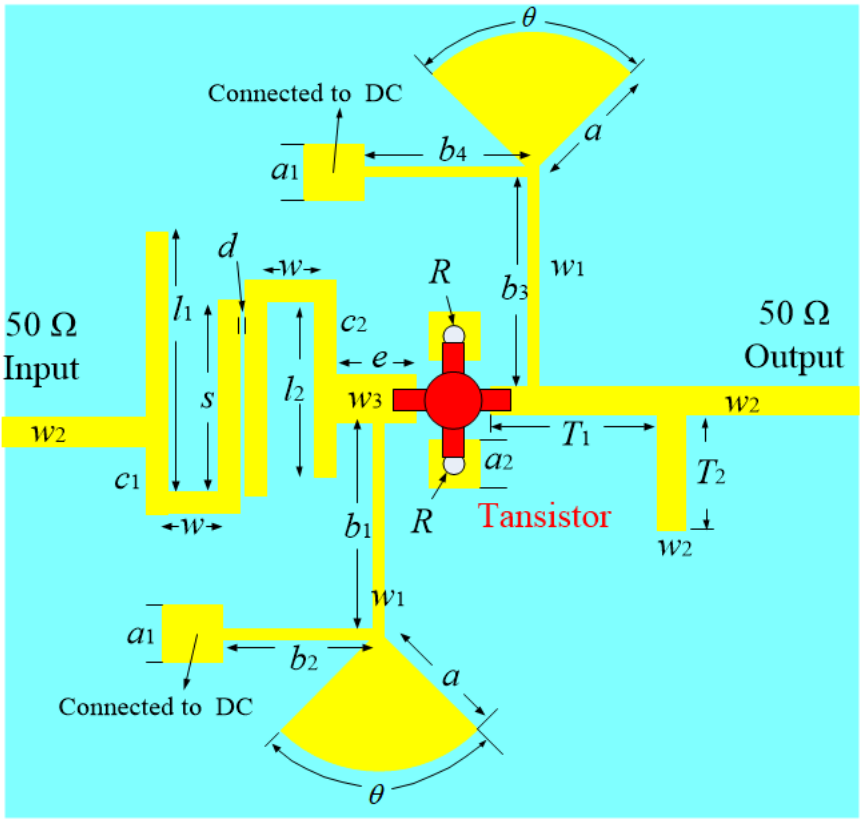

(a)

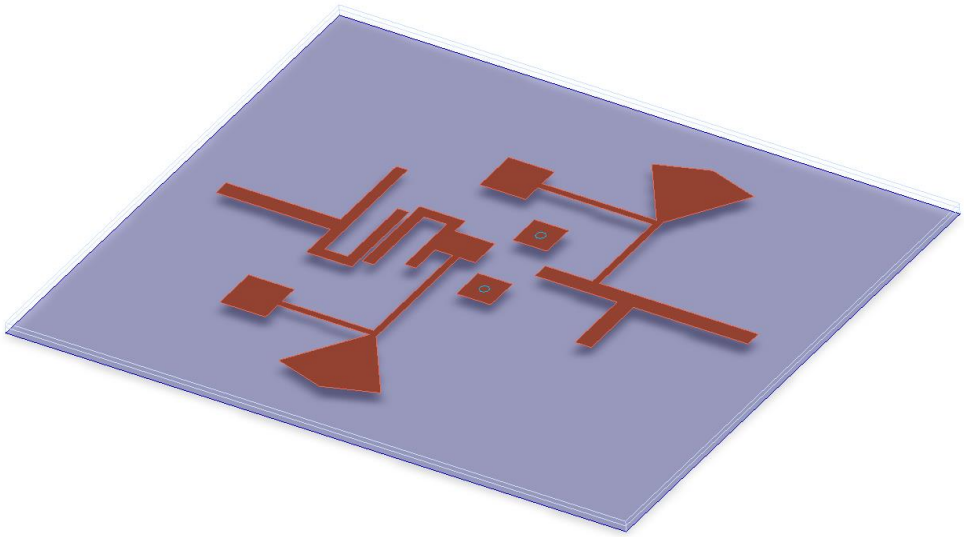

(b)

Fig. 4.13 Layout of the microstrip filter amplifier. (a) Layout Diagram. (b) Three-dimensional view.

TABLE 4.3
VALUES OF INITIAL AND NORMALISED MICROSTRIP FILTER AMPLIFIER PARAMETERS

	Initial (mm)	Optimised (mm)		Initial (mm)	Optimised (mm)
l_1	**4.10**	**4.14**	θ	**70(deg)**	**70(deg)**
l_2	**3.88**	**3.71**	b_1	**6.50**	**6.32**
c_1	**0.43**	**0.81**	b_2	**2.20**	**2.20**
c_2	**0.38**	**1.30**	b_3	**5.50**	**4.95**
s	**3.15**	**3.07**	b_4	**2.20**	**2.20**
d	**0.25**	**0.15**	a_1	**1.20**	**1.20**
R	**0.50**	**0.50**	T_1	**3.80**	**3.66**
a	**3.32**	**3.32**	T_2	**3.10**	**2.25**
e	**1.10**	**1.16**			
w_1	**0.30**	**0.30**			
w_2	**0.78**	**0.78**			
w_3	**1.20**	**1.67**			

The initial and optimised parameters are given in Table 4.3. Fig. 4.14 shows the optimised *S*-parameters response corresponding to the optimised values in Table 4.3. It can be observed from Fig. 4.14(a) that the two-pole Chebyshev response is achieved in S_{11} and S_{21} shows a filtering response with gain over the passband.

The noise figure and stability factor are also simulated and are shown in Fig. 4.14(b) and (c). The stability factor is above 1 from 0 GHz to 22 GHz indicating the transistor is stable. The noise figure is about 1.02 dB to 2 dB over the passband with a minimum value of 1.02 dB at 9.88 GHz.

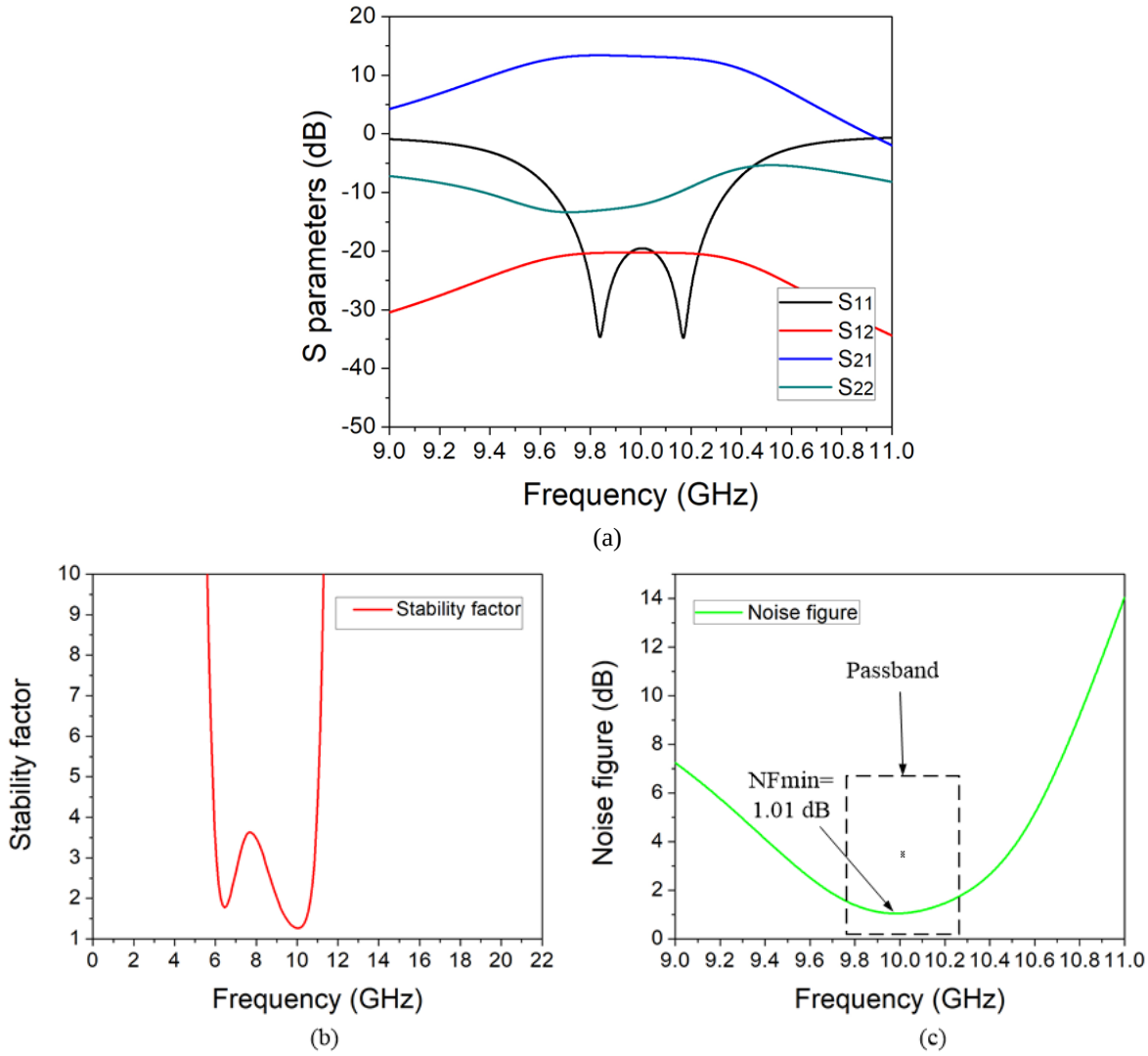

Fig. 4.14 EM simulation response with optimised values. (a) Scattering parameters. (b) Stability factor. (c) Noise figure.

4.3.6 Microstrip filter amplifier measurement

The circuit is fabricated using a standard printed circuit board fabrication process. DC wires and the transistor are mounted manually. The material used with 0.25 oz. copper cladding. Fig. 4.15 gives a photo of the fabricated microstrip filter amplifier. The measurement is performed on the Agilent VNA E8362B vector network analyser where input and output are referred to 50 Ω port impedance.

The measured *S*-parameters response is displayed by solid line in Fig. 4.16 and the dotted line is the simulated response as a comparison. Two reflection poles of the S_{11} and the gain of S_{21} over the passband show that both filtering and amplification functionalities have been achieved, indicating the validity of the design approach.

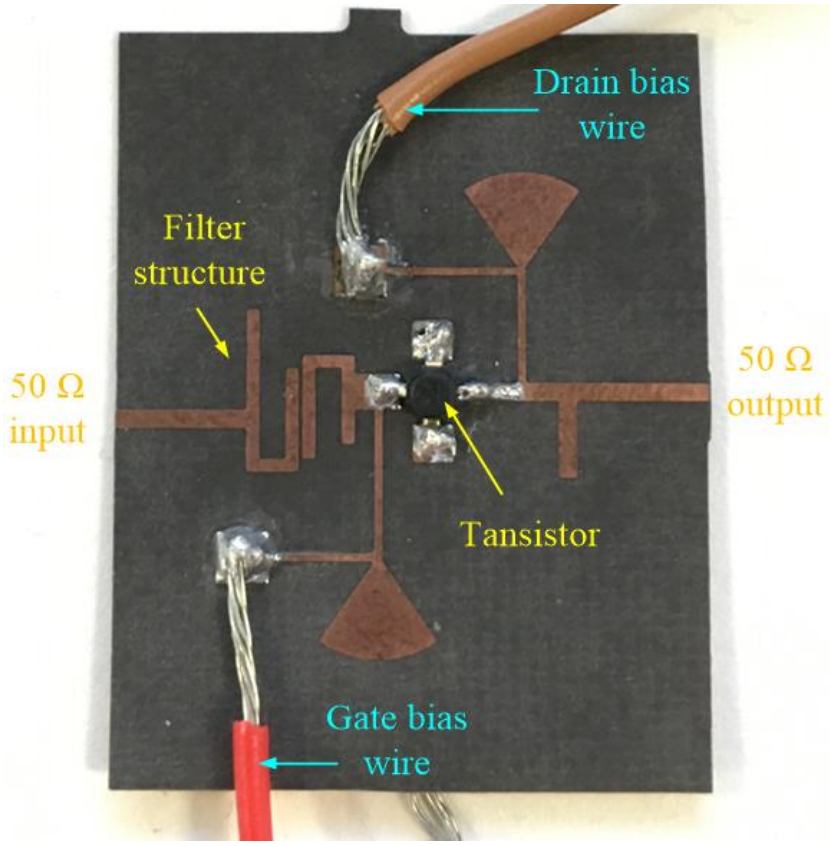

Fig. 4.15 Photograph of the fabricated microstrip filter amplifier device.

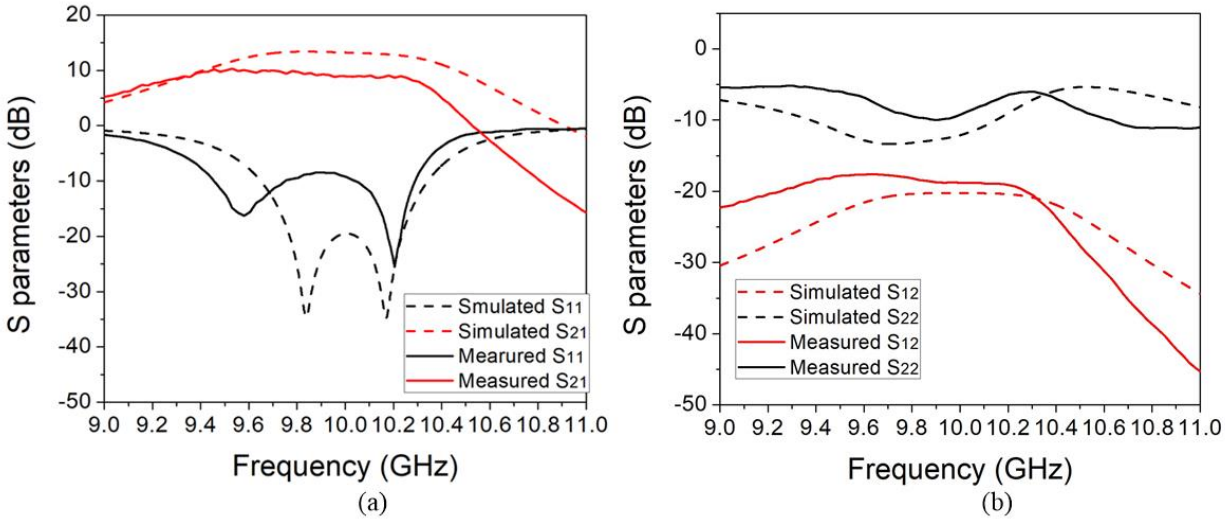

Fig. 4.16 Circuit simulation and measurement results. (a) Scattering parameters S_{11} and S_{21}. (b) Scattering parameters S_{22} and S_{12}.

As shown in Fig. 4.16, the disagreement between the measured results and simulated ones may be caused by the fabrication tolerance. The error of the dielectric constant that provided by the datasheet could lead to the electric length of the resonator, resulting in a shift of the centre frequency and the bandwidth [12]. Additionally, the DC wires assembly can influence the performance of the amplifier, and the circuit soldering could introduce losses [15].

4.4 Example B: An X-band Waveguide Filter Amplifier Design

Based on the N+3 coupling matrix discussed in Section 4.2, physical design of an X-band rectangular waveguide filter amplifier is introduced here. Fig. 4.17 illustrates the physical structure of the waveguide filter amplifier. Port 1 is assigned to the waveguide port, and Port 2 refers to the 50 Ω microstrip connecting to the SMA port. The 2-pole waveguide filter is made of Resonator 1 and Resonator 2, which are waveguide TE101 cavities coupled via asymmetrical capacitive irises. Resonator 2 is comprised of a waveguide cavity and the transistor coupling probe, interconnecting transmission line and the transistor. A section of waveguide is formed by a platform on which the

microstrip substrate sites. The substrate has the probe and transmission lines, and also the transistor with bias connection placed on it. It can be seen from Fig 4.17 that the dimension of the iris d_2 determines the external quality factor of Resonator 1 (Q_{e1}). The iris size d_1 which coupling Resonator 1 and Resonator 2 decides the coupling coefficient of the two resonators $k_{1,2}$. The length of the transition interconnection s and the probe l influence the coupling strength from the Resonator 2 to the input of the transistor. Resonator lengths L_1 and L_2 determinate the centre frequency of the resonators.

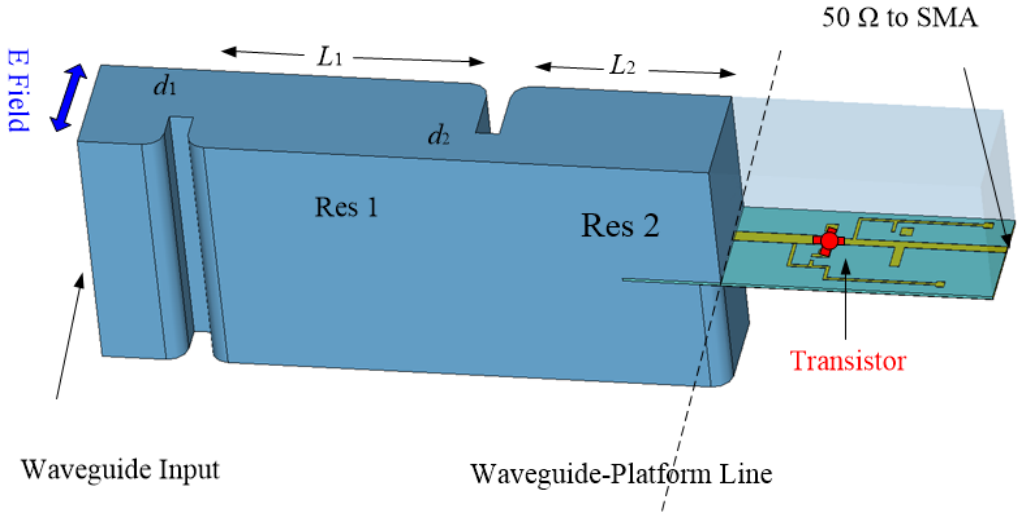

(a)

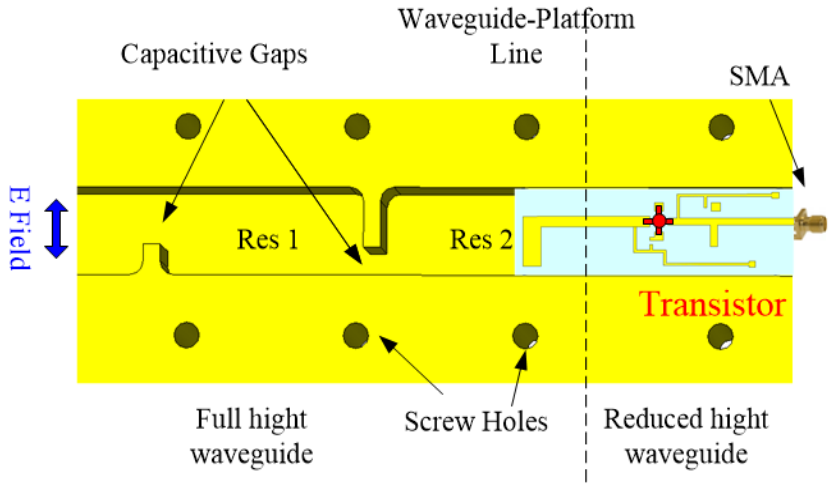

(b)

Fig. 4.17 The layout of waveguide filter amplifier. (a) Three-dimensional view of the internal waveguide and the transistor microstrip circuit. (b) Sectional view of the filter and platform for the transistor circuit.

4.4.1 Extraction of the external quality factor Q_{e1}

The external quality factor of the Resonator 1 (Q_{e1}) can be extracted from the simulation of the single waveguide cavity. As illustrated in Fig. 4.18(a), with narrow coupling gap set up at port 1, capacitive iris with the length of d_1 is at port 2, and the length of the waveguide resonator cavity is L_1. A resonance curve is simulated in CST as shown in Fig. 4.18(b), where external quality factor Q_{e1} can be extracted from the ratio of centre frequency and the 3 dB bandwidth by (4.21) [12].

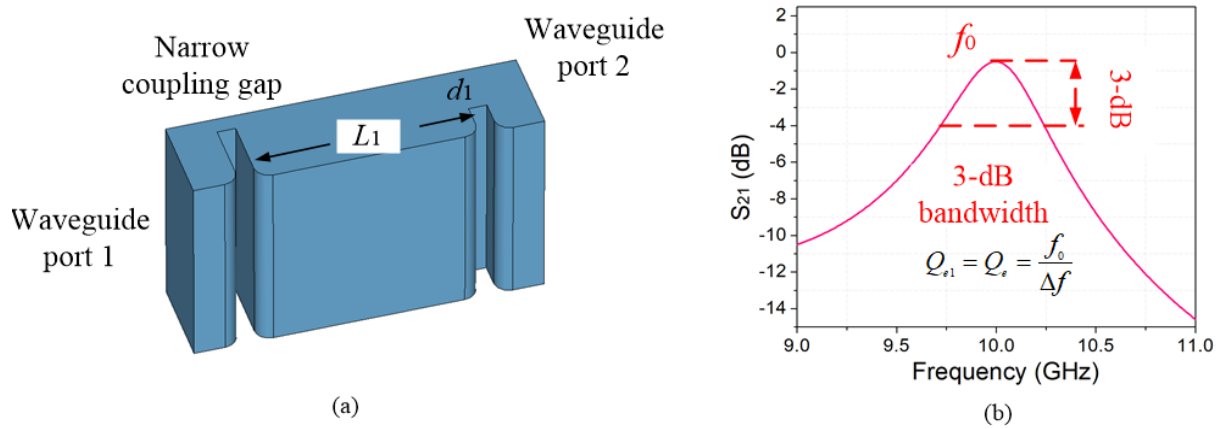

Fig. 4.18 Extraction of the external quality factor of Resonator 1. (a) Structure of single waveguide cavity. (b) *S*-parameter response of an individual waveguide resonator.

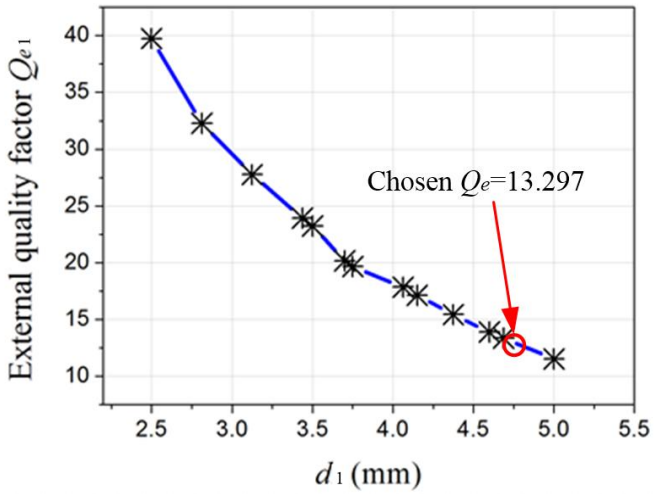

Fig. 4.19 External quality factors Q_e versus dimension d_1. All points are at 10 GHz.

As discussed in Section 4.2, the required Q_{e1} is13.297. The size of the coupling iris d_1 is altered resulting in various external quality factor Q_e. During the extraction process, the length of the resonator L_1 is adjusted to keep the resonance at 10 GHz centre frequency. The value of the Q_e is plotted corresponding to different d_1 in Fig. 4.19 and from this graph we can find the d_1 for the input iris of the waveguide filter.

4.4.2 Extraction of the coupling coefficient

As discussed in Section 4.2, $k_{1,2}$=$M_{1,2}$=0.0831. The construction to extract the coupling coefficient between Resonator 1 and Resonator 2 is shown in Fig. 4.20(a): a pair of the waveguide cavities coupled via the capacitive gaps (d_2). There is weak coupling at the two ports through the narrow gaps. The simulation result with two resonance peaks is presented in Fig. 4.20(b), which coupling coefficient $k_{1,2}$ can be extracted using (4.22).

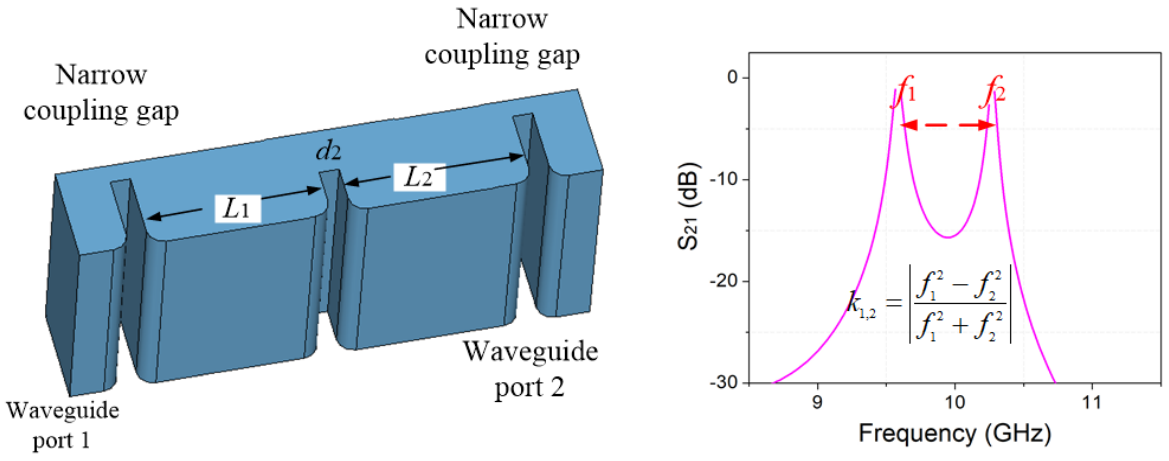

Fig. 4.20 Extraction of the coupling coefficient. (a) Structure of coupled waveguide cavities. (b) S-parameter response of the coupled waveguide resonators.

Changing the size of the iris d_2 can give different coupling coefficients between the two resonators. The relationship between d_2 and the corresponding coupling coefficient $M_{1,2}$ is presented in Fig. 4.21, where the required size of d_2 can be found to fulfil the required $M_{1,2.}$ During the extraction process, the lengths of the resonators L_1 and L_2 are adjusted to keep the centre frequency at 10 GHz frequency.

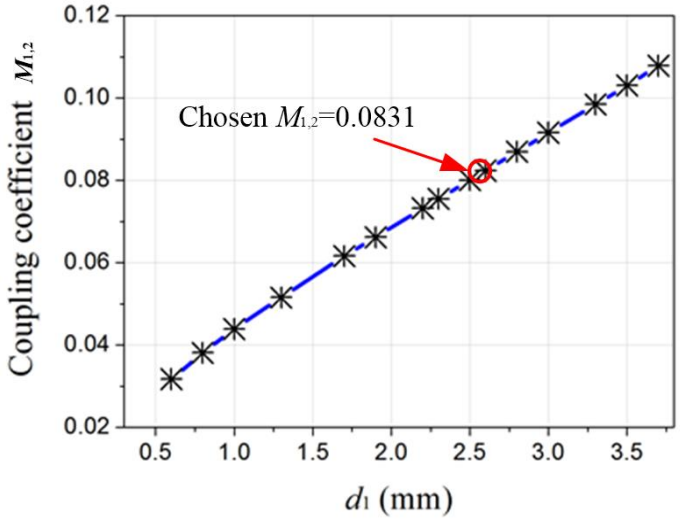

Fig. 4.21 Coupling coefficient $M_{1,2}$ versus dimension d_2. All points are at 10 GHz.

4.4.3 Extraction of the external quality factor Q_{eT}

Now let's consider the structure of the Resonator 2 which includes the waveguide cavity and part of the microstrip element. As depicted in Fig. 4.22(a), Resonator 2 is directly coupled to the input of the transistor via the E-field probe and the interconnecting transmission line. The combination of the waveguide and microstrip structure is treated as a whole resonance entity and the external Q_{eT}=13.297 and centre frequency f_T=10 GHz are required. This mixed resonator-microstrip construction can be simulated in CST [16] and the appropriate dimensions found to fulfil this requirement.

The geometries of the mixed structure, mainly including the length of the resonator L_2 and the dimensions of the probe l and interconnection transmission line length s, will determine the external quality factor Q_{eT}. Of course, Q_{eT} is also influenced by other parameters, but these three parameters are found to be the most convenient to adjust. Note that the input impedance of the transistor also affects the external quality factor Q_{eT}. Thus the transistor's parameters are incorporated during the extraction rather than a single physical structure. In the setup depicted in Fig. 4.22(b), the microstrip port is connected the port 2 in CST [16], with port 2 set to be the input admittance of the transistor Y_{in}. Y_{in} can be calculated using (4.4) and the parameters of the transistor. Port 1 is set to be the waveguide impedance, and then the whole structure is simulated.

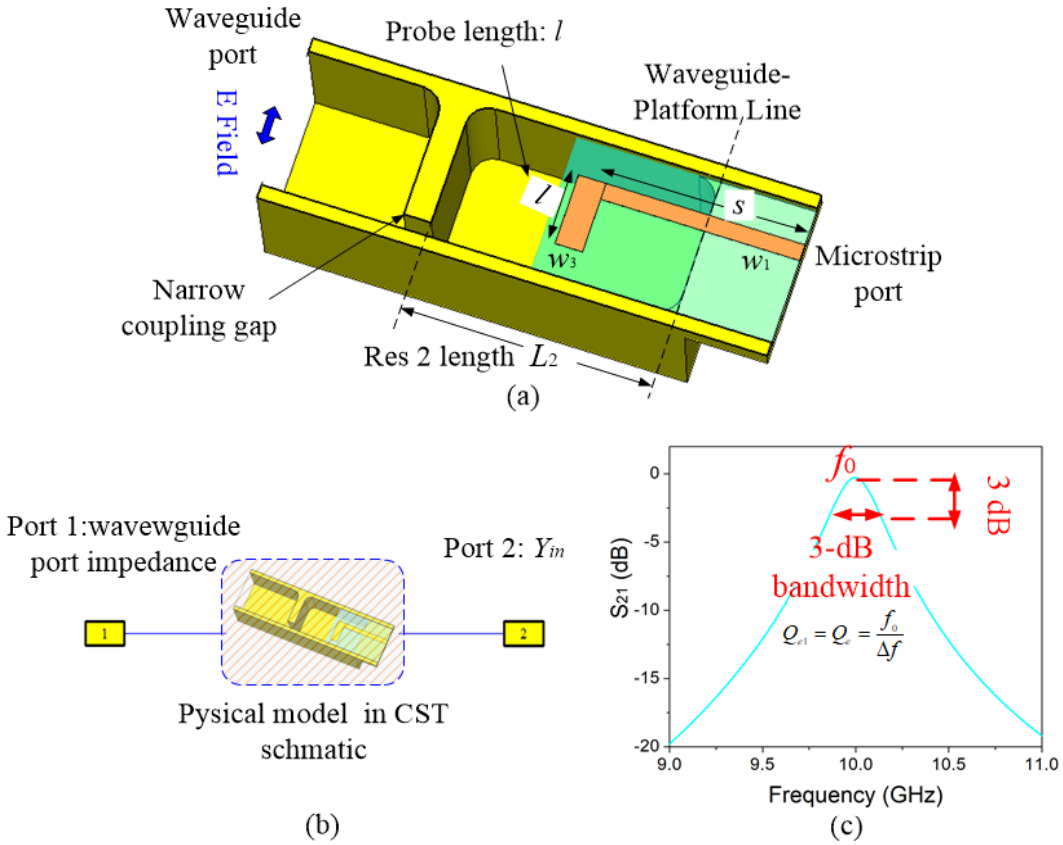

Fig. 4.22 Setup to extract external quality factor for resonator 2 incorporating the transistor's input. (a) Structure for extracting external quality factor of resonator 2 interconnecting the input of the transistor. (b) Q_{eT} extraction setup in CST. (c) *S*-parameter response of the waveguide resonator connected to a complex load.

The EM simulation of one single waveguide cavity with one port coupling to the transistor's input is performed in CST [16] as shown in Fig. 4.22(a) with a resonance plot displayed in Fig. 4.22(c), and hence the external quality factor Q_{eT} can be determined. As discussed above, the centre frequency and resonance curve are mainly influenced by the lengths of the resonator L_2, the length of the probe l and interconnection transmission line length s. Other parameters such as the width of the probe and transmission line w_3 and w_1 are kept constant during the simulations. The interconnection transmission line s and probe length l are tuned, and external Q is recorded for different values of s and l. To help with simulation process, L_2 is adjusted to keep the resonance at 10 GHz centre frequency. The external quality factor Q_{eT} versus interconnection transmission line s and probe length l are shown in Fig. 4.23 and the target Q_{eT}=13.297 can be achieved with dimensions of l.

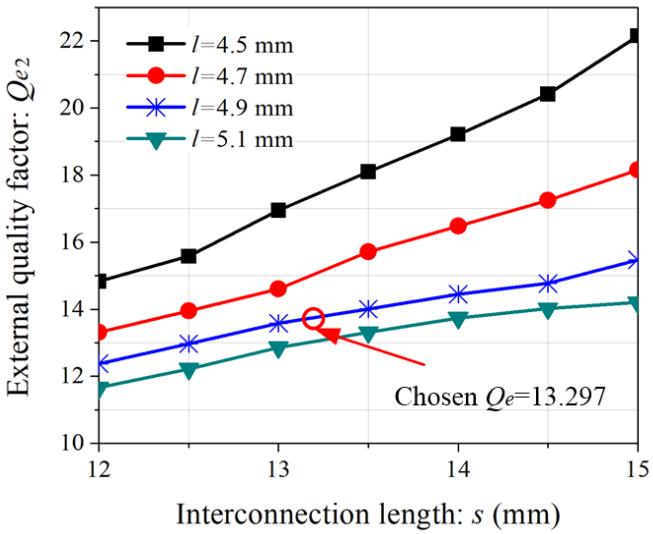

Fig. 4.23 External quality factor Q_{eT} versus interconnection length s. All points are at 10 GHz.

4.4.4 Microstrip part design

The microstrip part of the waveguide filter amplifier comprises the probe, feed transmission line, transistor, bias circuits and output matching stub. The layout of the microstrip circuit is

illustrated in Fig. 4.24: b_1+b_2 and b_3+b_4 are quarter-wavelength long bias tees at 10 GHz centre frequency. 100 pf capacitors are mounted on the end of the quarter-wavelength long bias arms, providing short circuit condition. The ground footprints of the transistor are connected to the ground via holes R_1 and R_2. Two square pads shown in Fig. 4.24(a) are soldered with DC wires, offering DC voltages at the gate and the drain.

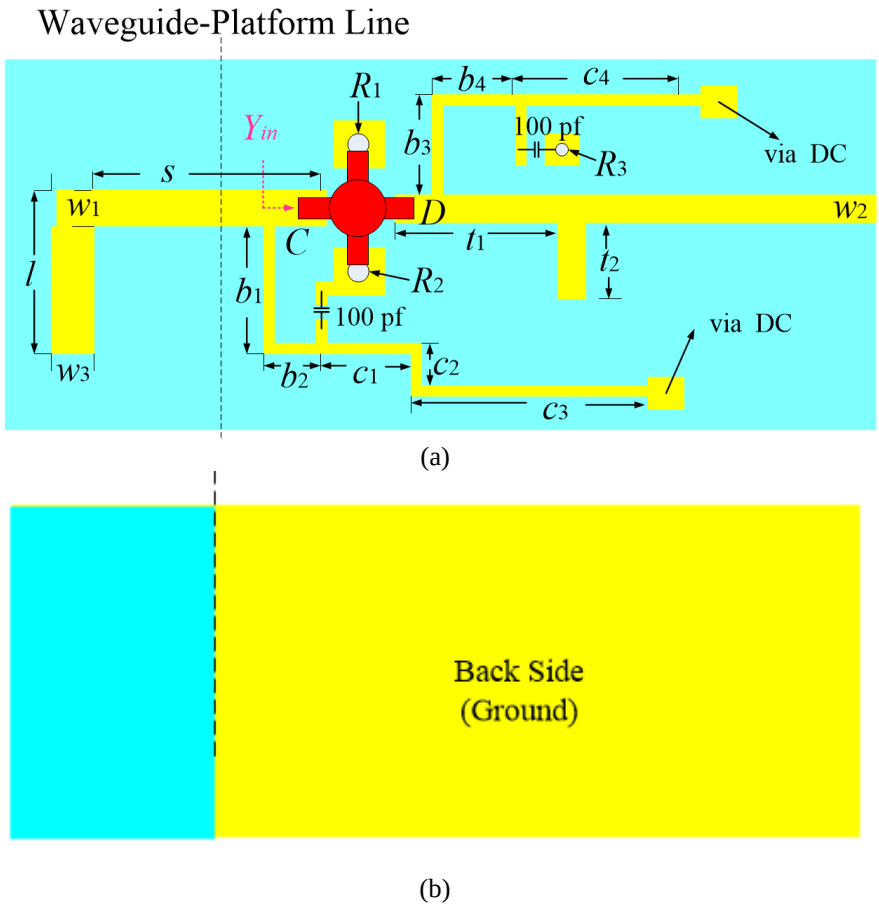

Fig. 4.24 Microstrip part of the filter amplifier. (a) Layout of microstrip with the transistor. (b) Backside.

Length t_2 is the length of a single stub matching the transistor to 50 Ω transmission line. The design of the single stub is exactly the same as the design in Section 4.3.4. The dimensions of the microstrip are given later in Table 4.4.

4.4.5 Full EM simulation and optimisation

After all the necessary parameters to form the waveguide filter amplifier have been determined above, the whole construction of the device can be simulated. The on-chip transistor and the waveguide filter are assembled as depicted in Fig. 4.25. The on-chip transistor with bias connection is located on the platform of the waveguide and sandwiched between two half-cut waveguide blocks.

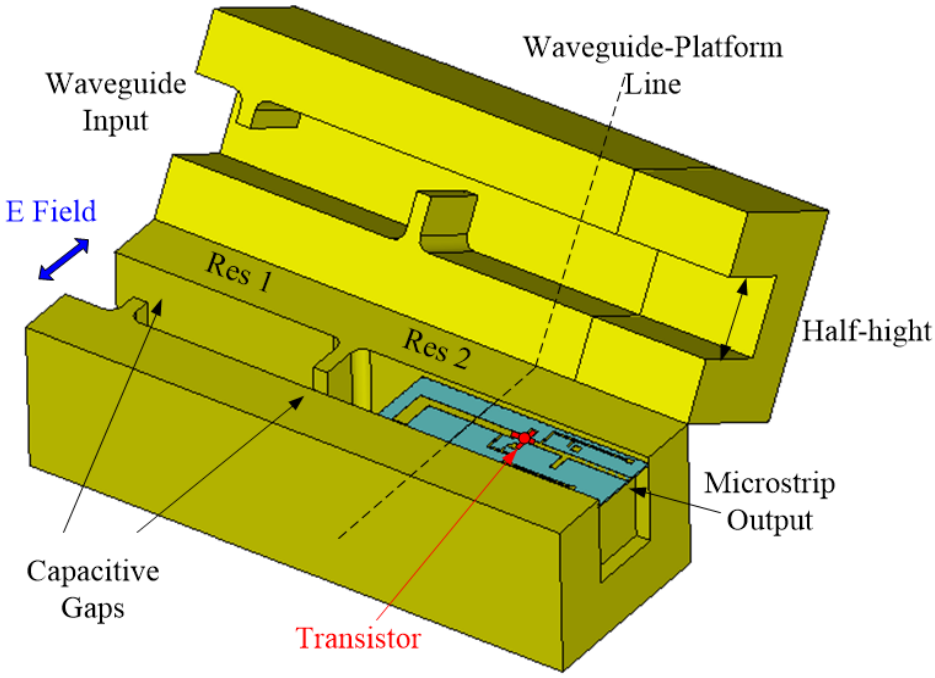

Fig. 4.25 Complete construction of the waveguide filter amplifier.

This simulation is combined in CST with the waveguide model and microstrip part of the transistor. As illustrated in Fig. 4.26, the microstrip part in the form of an S2P touchstone file is combined with 3D waveguide structure and simulated in CST. This S2P file is generated by EM simulation in ADS. Note that in the simulation setup depicted in Fig. 4.26, the embedded port

model is applied at the input of the transistor: the embedded section of the transmission line is excluded in CST because this section belongs to the microstrip part and has been simulated producing the S2P touchstone file.

The parameters used for the simulation are given in Table 4.4. The simulated *S*-parameters using initial values are presented in Fig. 4.27. It shows about 13 dB gain in S_{21} and 2 poles in S_{11} around -10 dB. The simulated operating conditions of the transistor are drain to source voltage of V_{ds}=2 V and drain to source current of I_{ds}=10 mA.

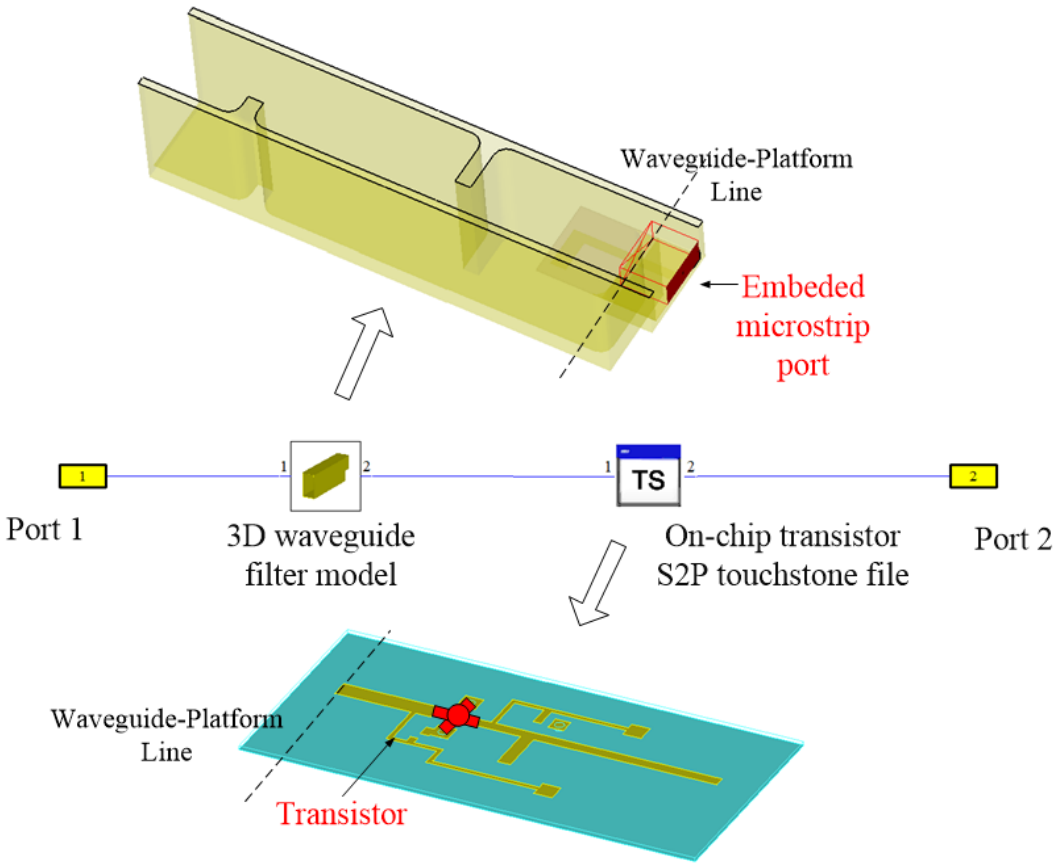

Fig. 4.26 Co-simulation of waveguide filter amplifier.

TABLE 4.4
VALUES OF INITIAL AND OPTIMISED WAVEGUIDE FILTER AMPLIFIER PARAMETERS

	Initial (mm)	Optimised (mm)		Initial (mm)	Optimised (mm)
L_1	**23.00**	**23.76**	w	**1.2**	**1.2**
L_2	**17.80**	**18.71**	b_1	**2.96**	**2.96**
d_1	**4.85**	**6.39**	b_2	**1.33**	**1.33**
d_2	**2.65**	**3.22**	b_3	**2.50**	**2.50**
l	**4.9**	**4.83**	b_4	**2.00**	**2.00**
s	**13.30**	**12.99**	c_1	**1.50**	**1.50**
R_1	**0.30**	**0.30**	c_2	**1.10**	**1.10**
R_2	**0.30**	**0.30**	c_3	**5.00**	**5.00**
R_3	**0.30**	**0.30**	c_4	**5.00**	**5.00**
w_1	**1.20**	**1.20**	t_1	**3.22**	**3.22**
w_2	**0.72**	**0.72**	t_2	**3.18**	**3.18**
w_3	**2.00**	**2.00**			

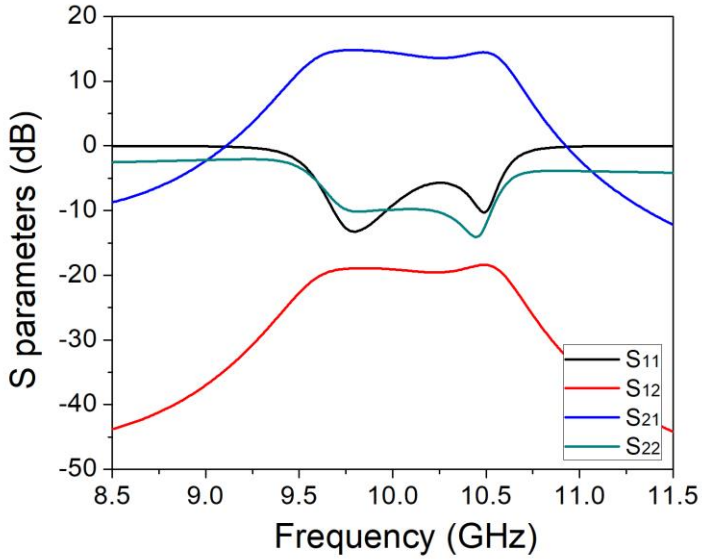

Fig. 4.27 *S*-parameters of EM simulation using initial values.

The optimisation is carried out by employing the optimiser tool in the CST [16]. The microstrip part is simulated in ADS [17] and the result is loaded in the CST in the form of a touchstone. The dimensions of the microstrip part are kept fixed. In this filter amplifier example, we set the optimised goals as: from 9.75 GHz to 10.25 GHz, S_{11} is under -20 dB; from 9.75 GHz to 10.25 GHz S_{22} is under -10 dB; critical points 9.725 GHz and 10.178 GHz are under -40 dB.

The optimised dimensions of the component are also presented in Table 4.4. The optimised *S*-parameters response is presented in Fig. 4.28(a) and (b) and is compared with initial response using dotted lines. The optimised result in Fig. 4.28(a) and (b) shows that over the passband S_{11} is below -20 dB, S_{21} is around 13 dB; and S_{22} is below -10 dB. The generally good agreement of the initial and optimised responses demonstrates the validity of the coupling matrix technique in providing starting values for the filter amplifier design process. The amplifier circuit is unconditionally stable as the stability factor is larger than 1 from 0 GHz to 22 GHz as shown in Fig. 4.28(c). For completeness, Fig. 4.28(d) shows noise figure is about 1.10 dB over the passband and the NFmin (minimum noise figure) for the device is 1.02 dB at 9.85 GHz.

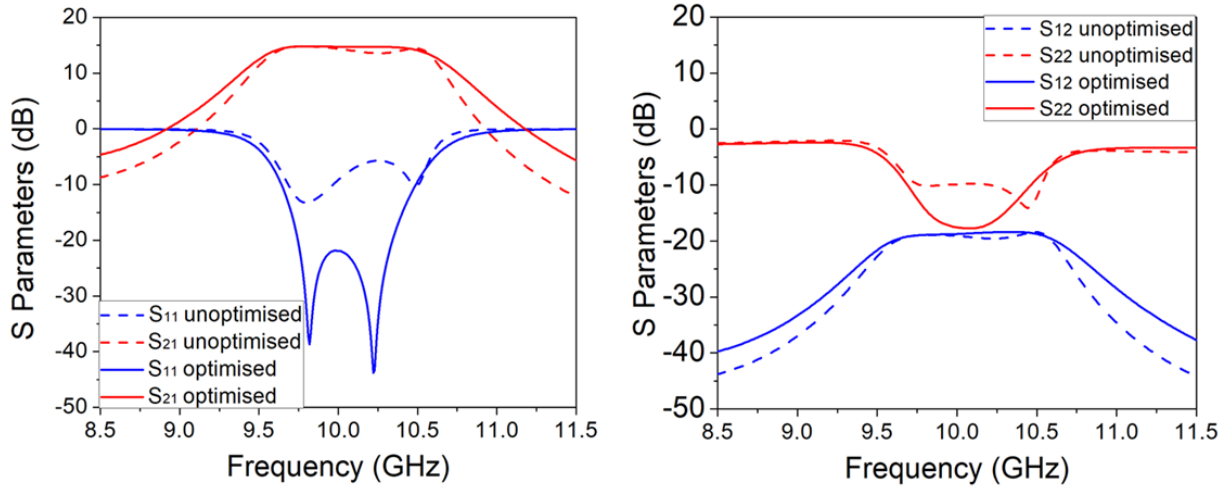

(a) (b)

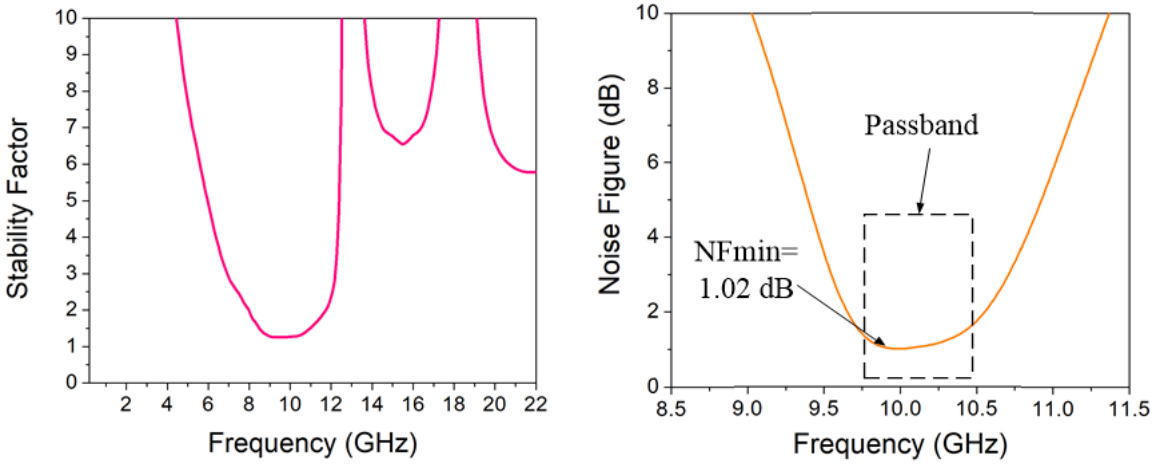

(c) (d)

Fig. 4.28 Co-simulation results of waveguide filter integrated with the transistor. (a) Scattering parameters S_{11} and S_{21}. (b) Scattering parameters S_{22} and S_{12}. (c) Stability factor. (d) Noise figure.

4.4.6 Waveguide filter amplifier measurement

The waveguide structure is fabricated from aluminium (AL5083) on a CNC machine. It is cut in two halves cut along the E-plane. The microstrip circuit is made of RT5870 substrate having the 0.254 mm thick and the dielectric constant of 2.33. The connection wires are mounted on the pads providing DC voltages at the gate and the drain of the transistor. The output of the microstrip is connected to the 50 Ω measurement port through the SMA adapter. Fig. 4.29 shows two photographs of the device.

The measurement is carried out employing the Agilent vector network analyser PNA E8362B with two measurement ports. A WR-90 coaxial to waveguide adapter is used at port 1, calibrated to the waveguide flange.

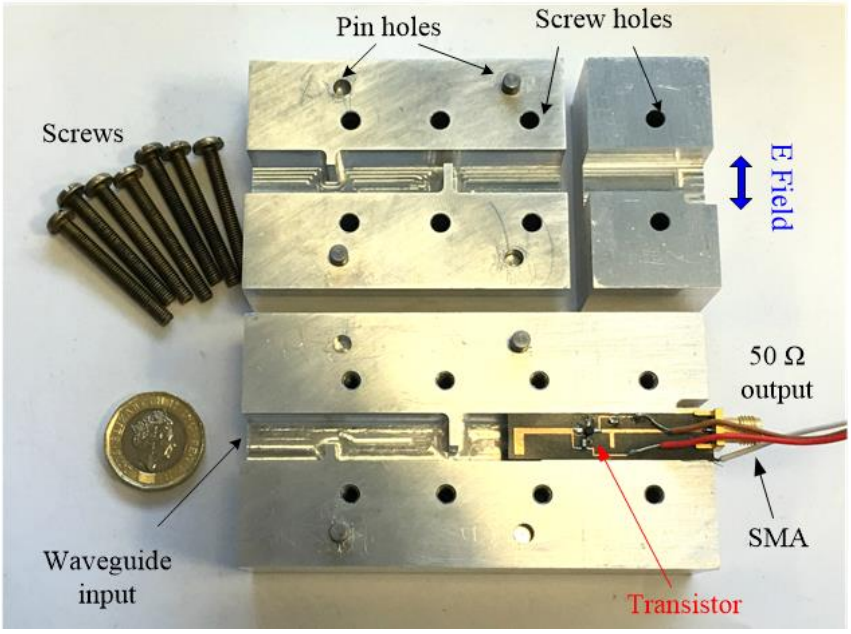

(a)

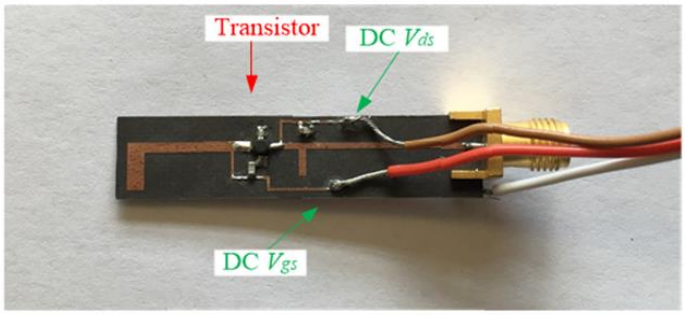

(b)

Fig. 4.29 Photographs of the fabricated device. (a) Sectional view of cut along E-plane. (b) Microstrip with DC wires connection.

The measurement result is displayed in Fig. 4.30 in solid lines, compared with the optimised simulation response using dotted lines. Bias condition of the transistor is provided by a gate to source voltage of V_{gs}=-0.52 V and a drain to source voltage of V_{ds}=2.2 V. The two poles in S_{11} shown in Fig. 4.30(a) provide evidence of resonator-based filter operating well. The S_{21} shows around 11 dB gain indicating the amplification function of the transistor. The S_{22} showing around -10 dB over the passband indicating a good output match of the transistor. The generally good

agreement between the measurement and the simulation validates the methodology of this integrated waveguide filter amplifier design.

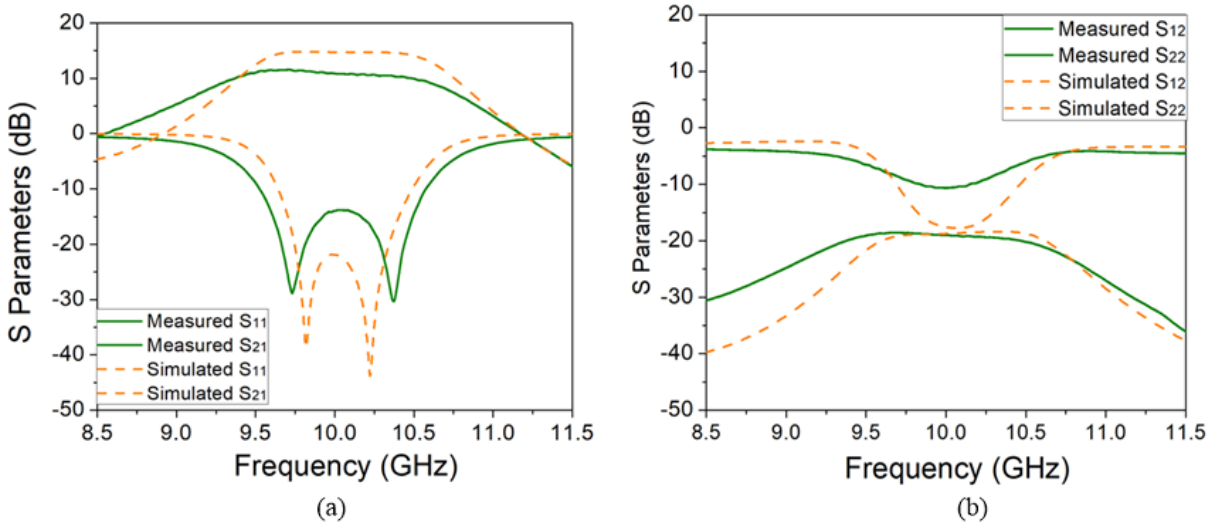

Fig. 4.30 Circuit simulation and measurement results. (a) Scattering parameters S_{11} and S_{21}. (b) Scattering parameters S_{22} and S_{12}.

The disagreement between the measured results and simulated ones is reasonable. The roughness of the waveguide cavity surface and the poor contact of two half-cut waveguides can lead to additional insertion loss in the measurement [18]. As the microstrip board is placed on the platform of the waveguide by pressure, the contact between them could also influence the results. The circuits soldering including the transistor and the surface mount components would also have an effect on the *S*-parameters response. It also can be observed in Fig. 4.30(a) that there exists a slop of S_{21} within the passband. In the filter amplifier design, we assume the transistor operating at 10 GHz centre frequency, but the impedance of the transistor changes to some extent within the bandwidth. In addition, the bias circuit may also influence the transistor performance. It is believed that with precisely fabricated waveguide and micsrostrip circuit, the measured results would agree better with the EM simulation results in terms of insertion loss and gain.

4.5 Summary

In this chapter, the *N*+3 coupling matrix is applied in the co-design of filter amplifiers. We introduced two examples: the microstrip amplifier and the waveguide amplifier. Both of them are designed using a resonator-based filter, achieving both filtering and amplification functionalities. With the specification of the filter and the transistor's parameters, the coupling matrix is synthesised and then is employed to extract the physical geometries of the device. The design process of the filter part is based on the general extraction procedures of the external quality factor and coupling coefficient [12]. In the simulated *S*-parameters response, illustrated in Fig. 4.14 and Fig. 4.28, initial values can be found for the geometries through the extraction processes, which can be used for further optimisation.

Although the two amplifiers introduced in this chapter are different in physical construction, they are designed based on the same circuit topology and same coupling matrix. The design processes are similar, which combine the conventional filter design synthesis with the transistor. The microstrip amplifier is a planner circuit and designed in the ADS, whereas the waveguide amplifier is constructed and co-simulated with the help of ADS and CST. Although the structure of the waveguide amplifier is more complicated than the microstrip one, the technique is more likely to be applied in higher frequencies where waveguide components are more commonplace.

The good measured results shown in Fig. 4.16 and Fig. 4.30, validate the integrated design of filter amplifiers using the *N*+3 coupling matrix synthesis. The topology proposed in this chapter makes it possible to extend this methodology to amplifier circuits which resonators matched at both the input and the output ports, and this will be described in Chapter 5.

REFERENCES

[1] P. Jarry; J. N. Bennett, Microwave Amplifier Fundamentals, *Microwave Amplifier and Active Circuit Design Using the Real Frequency Technique*, Wiley-IEEE Press, 2016.

[2] J. F. White, "Transistor Amplifier Design," *High Frequency Techniques:An Introduction to RF and Microwave Engineering*, 1, Wiley-IEEE Press, 2004.

[3] T. M. Braun, "Low-Noise Amplifier and Frequency Converter," *Satellite Communications Payload and System*, 1, Wiley-IEEE Press, 2012.

[4] J. B. Vincent and D. G. Van der Merwe, "A 16 w solid state mic x-band amplifier for twt replacement," AFRICON, 1996., IEEE AFRICON 4th, volume 2, pages 749–752 vol.2.

[5] E. M. Suijker, M. Sudow, M. Fagerlind, N. Rorsman, A. P. De Hoek, and F. E. van Vliet. Gan, "mimic power amplifiers for s-band and x-band," Microw. Conf., 2008. EuMC 2008. 38th European pages 297–300.

[6] Z. Y. Malik, A. Mueed and M. I. Nawaz, "Narrow band ridge waveguide-to-microstrip transition for low noise amplifier at Ku-band," *6th Inter. Bhurban Conf Applied Sci.s & Techn.*, Islamabad, 2009, pp. 140-143.

[7] P. G. Courtney, J. Zeng, T. Tran, H. Trinh and S. Behan, "120W Ka-Band Power Amplifier Utilizing GaN MMICs and Coaxial Waveguide Spatial Power Combining," 2015 IEEE Comp. Semi. Integ. Circ. Sympo. (CSICS), New Orleans, LA, 2015, pp. 1-4.

[8] T. B. Kumar, K. Ma and K. S. Yeo, "A 60-GHz Coplanar Waveguide-Based Bidirectional LNA in SiGe BiCMOS," *IEEE Microw. Wirel. Compon. Lett.*, vol. 27, no. 8, pp. 742-744, Aug. 2017.

[9] Y. C. Li, K. C. Wu and Q. Xue, "Power Amplifier Integrated with Bandpass Filter for Long Term Evolution Application," *IEEE Microw. Wirel. Compon. Lett.*, vol. 23, no. 8, pp. 424-426, Aug. 2013.

[10] Y. S. Lin, J. F. Wu, W. F. Hsia, P. C. Wang and Y. H. Chung, "Design of electronically switchable single-to-balanced bandpass low-noise amplifier," *IET Microw. Antenn. Propag.*, vol. 7, no. 7, pp. 510-517, May 15, 2013.

[11] J. Chen, S. Chang, C. Liu, and H. Kuo. "Design of a 20-to-40 GHz bandpass mmic amplifier," Microw. Sympo. Digest, 2003 IEEE MTT-S Inter., volume 2, pages 1275–1278. IEEE.

[12] J. S. Hong and M. J. Lancaster, *Microstrip Filters for RF/Microwave Applications*. New York, NY, USA: Wiley, 2001.

[13] W. Xia. "Diplexers and multiplexers design by using coupling matrix optimisation." PhD dissertation. Elect. Eng, Birmingham Univ., Birmingham, 2015

[14] California Eastern Laboratories (2004, July). CEL Corp., CA. [Online]. Available: http://www.cel.com/pdf/datasheets/ne3210s1.pdf

[15] P. H. Ladbrooke, *MMIC Design: GaAs FETs and HEMTs*. USA: Artech House, 1989.

[16] Computer Simulation Technology, CST company, Germany.

[17] Advanced Design System, Agilent Technologies, USA.

[18] W. Xia, X. Shang and M. J. Lancaster, "All-resonator-based waveguide diplexer with cross-couplings," *Electronics Lett.*, vol. 50, no. 25, pp. 1948-1950, 2014.

CHAPTER 5

N+4 COUPLING MATRIX BASED FILTER AMPLIFIERS

The waveguide filter amplifier with the resonator matching the transistor's input has been introduced in Chapter 4. Based on the *N*+3 coupling matrix, filter response (in our case, Chebyshev) is achieved, and the gain of the amplifier can also be predicted using the matrix calculation. The coupling matrix based design methodology offers a co-design approach in designing amplifiers for X-band or higher frequencies.

However, the design examples in Chapter 4 can be categorised as input filter matching amplifiers, and the output is conventionally matched to a traditional 50 Ω transmission line. The *N*+3 coupling matrix is able to describe the topology of the transistor coupling to the end of the filter. As the rectangular waveguide is used throughout the systems and the assembled ports of devices are made with waveguide end to end, particularly in THz applications [1]-[3], the waveguide amplifiers with input and output waveguide are necessary for the sub-millimetre components. In this chapter, all waveguide resonator structure is implemented in designing waveguide amplifiers.

Here, we apply the *N*+4 coupling matrix with the transistor coupling in the middle of the resonators as deduced in Chapter 3. Filter matching can be achieved simultaneously, i.e. both the

return loss seen from the input S_{11} and the output S_{22} behave Chebyshev filter response. In this chapter, an X-band waveguide amplifier is introduced with two filters coupled at the drain and the gate of the transistor. This waveguide filter amplifier can be regarded as the physical implementation of the N+4 coupling matrix, and it also serves as the low frequency demonstrator for THz waveguide amplifiers.

In this chapter, circuit representation of the filter amplifier and the N+4 coupling matrix are reviewed at the beginning. Then, the physical design procedure including the waveguide part and on-chip transistor microstrip part is discussed in Section 5.3, followed by the co-simulation and the optimisation in Section 5.4. Finally, the fabrication of the device and its measurement are presented with further discussions and suggestions summarised in Section 5.5.

5.1 Coupling Matrix applied in Design of Filter Amplifiers

The active N+4 coupling matrix representing the filter amplifier has been synthesised in Chapter 3.

$$[m]=\begin{bmatrix} 0 & m_{P1,1} & 0 & \vdots & 0 & 0 & 0 & 0 & \vdots & 0 & 0 \\ m_{1,P1} & 0 & m_{1,2} & \vdots & 0 & 0 & 0 & 0 & \vdots & 0 & 0 \\ 0 & m_{2,1} & 0 & \vdots & 0 & 0 & 0 & 0 & \vdots & 0 & 0 \\ \cdots & \cdots & \cdots & \ddots & \cdots & \cdots & \cdots & \cdots & \ddots & \cdots & \cdots \\ 0 & 0 & 0 & \vdots & 0 & m_{k,in} & 0 & 0 & \vdots & 0 & 0 \\ 0 & 0 & 0 & \vdots & m_{in,k} & 0 & m_{in,out} & 0 & \vdots & 0 & 0 \\ 0 & 0 & 0 & \vdots & 0 & m_{out,in} & 0 & m_{out,k+1} & \vdots & 0 & 0 \\ 0 & 0 & 0 & \vdots & 0 & 0 & m_{k+1,out} & 0 & \vdots & 0 & 0 \\ \cdots & \cdots & \cdots & \ddots & \cdots & \cdots & \cdots & \cdots & \ddots & \cdots & \cdots \\ 0 & 0 & 0 & \vdots & 0 & 0 & 0 & 0 & \vdots & 0 & m_{n,P2} \\ 0 & 0 & 0 & \vdots & 0 & 0 & 0 & 0 & \vdots & m_{P2,n} & 0 \end{bmatrix} \quad (5.1)$$

In practice, the geometries of the resonators and the transition from the resonators to the transistor can be determined by the coupling matrix [m] in (5.1). The physical construction resembles the input waveguide filter design in Section 4.1.

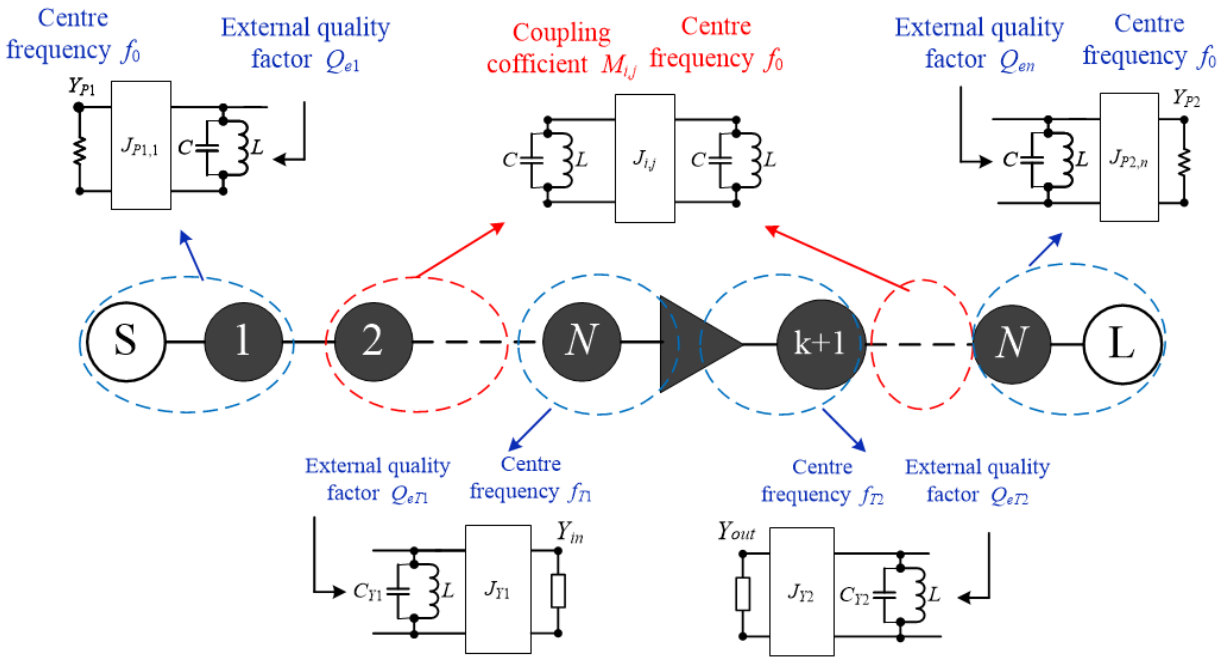

Fig. 5.1 Topology of the resonator based filter amplifier and the equivalent lumped circuit.

Fig. 5.1 presents the topology of the filter amplifier and the equivalent lumped circuits: (i) the 1st resonator coupling to the source; (ii) the k^{th} resonator coupling to the transistor's input; (iii) the $(k+1)^{th}$ resonator coupling to the transistor's output; (iv) the N^{th} resonator coupling to the load; (v) the i^{th} and the j^{th} resonators coupled by the J inverter. The centre frequency of the 1st to the n^{th} resonator is f_0.

As with just a conventional simple filter [4] the coupling coefficient $M_{i,j}=M_{j,i}$ between the two resonators are scaled by the fractional bandwidth from the coupling matrix [m]

$$M_{i,j} = FBW \cdot m_{i,j} \quad i, j = 1 \quad \text{to} \quad n \tag{5.2}$$

According to (5.2) the coupling coefficient between Resonator *i* and Resonator *j* can be calculated using the normalised coupling matrix [*m*].

The next step is to determinate the coupling from port 1 to the Resonator 1 and the coupling from the port 2 to the Resonator *n.* This can be done by extracting the external quality factor of Resonator 1 (Q_{e1}) and the external quality factor of Resonator *N* (Q_{en}) as illustrated in Fig. 5.1. In the *N*+4 coupling matrix, Q_{e1} is related to the external couplings $m_{P1,1}= m_{P1,1}$, and Q_{en} is related to the external couplings $m_{P2,n}=m_{P2,n}$.

$$Q_{e1} = \frac{1}{FBW \cdot m_{1,P1}^2} = \frac{1}{FBW \cdot m_{P1,1}^2}$$
$$Q_{en} = \frac{1}{FBW \cdot m_{n,P2}^2} = \frac{1}{FBW \cdot m_{Pn,2}^2} \tag{5.3}$$

From (5.3) the required external quality factor Q_{e1} and Q_{en} can be found.

The external couplings $m_{in,k}=m_{k,in}$ and self-coupling $m_{k,k}$ can be determined by extracting the external quality factor (Q_{eT1}) of the Resonator *k* incorporating the input of the transistor. The external couplings $m_{out,k+1}=m_{k+1,out}$ and self-coupling $m_{k+1,k+1}$ can be determined by extracting the external quality factor (Q_{eT2}) of the Resonator k+1 incorporating the output of the transistor. The centre frequency of the k^{th} resonator incorporating the transistor input admittance Y_{in} is f_{T1}; the centre frequency of the $(k+1)^{\text{th}}$ resonator incorporating the transistor output admittance Y_{out} is f_{T2}. Y_{in} and Y_{out} can be complex value. We regard one filter is coupled at the gate of the transistor, and another filter is coupled at the drain of the transistor. The reflection coefficients seen from the input and output are expected to produce filter response, in our case, are Chebyshev response. The derivations of Q_{eT1}, f_{T1}, Q_{eT2}, f_{T2} are exactly same as the for Q_{eT} and f_T in Section 4.1. Here we directly write down resultant equations

$$Q_{eT1} = \frac{q_{ek}}{FBW}, \quad Q_{eT2} = \frac{q_{ek+1}}{FBW} \tag{5.4}$$

$$f_{T1} = f_0, \quad f_{T2} = f_0 \tag{5.5}$$

5.2 Coupling Matrix Example of a Filter Amplifier

In our filter amplifier example, we use two 2nd Chebyshev filters at the input and output of the transistor. The filter has a centre frequency f_0 of 10 GHz, a bandwidth of 500 MHz (fractional bandwidth FBW=0.05) and a passband return loss of 20 dB. The filter specification is the same as the filter in Chapter 4, and the g values for its lowpass prototype Chebyshev filter are given in Table 4.1

TABLE 5.1
VALUES OF TRANSISTOR'S Y MATRIX PARAMETERS

***Y* parameters**	**Value**	**Normalised $\bar{Y}$ parameters**	**Value**
g_m	**0.0696- 0.1350*j***	$\bar{g}_m$	**3.4812-6.7500*j***
Y_{gd}	**0**	$\bar{Y}_{gd}$	**0**
Y_{ds}	**0.0055+ 0.0127*j***	$\bar{Y}_{ds}$	**0.2752+ 0.6367*j***
Y_{gs}	**0.0051+ 0.0276*j***	$\bar{Y}_{gs}$	**0.2528+ 1.3799*j***

All parameters are calculated from the datasheet as the transistor operating at 10 GHz.

The transistor used is the NE310S01 with Y matrix parameters summarised in Table 5.1. Note that we use the same transistor (NE310S01) as in Chapter 4. But in Table 5.1, the admittance between the gate and the drain of the transistor (Y_{gd}) is assumed to be zero in order to simplify the design procedure. In the practical design, the feedback between the transistor's gate and drain are often ignored [5]-[10], because its value is usually relatively small [11]. The advantage of the regardless of the feedback is that the filter amplifier can be constructed separately which make it easier in practical design. Also, if Y_{gd}=0 the N+4 coupling matrix that produces standard Chebyshev filter responses can be directly synthesised as described in Section 3.3.3. The effect of

the feedback can be cancelled by further optimisation. Therefore, the corresponding coupling from the drain to gate $m_{in,out}$ is zero but taken into account in the final optimisation.

The filter and transistor specifications can be translated into elements of the coupling matrix using the (2.34) and (5.1). The active coupling matrix [m] is

$$[m]=\begin{bmatrix} 0 & 1.2264 & 0 & 0 & 0 & 0 & 0 & 0 \\ 1.2264 & 0 & 1.6621 & 0 & 0 & 0 & 0 & 0 \\ 0 & 1.6621 & -8.2104 & 3.4219 & 0 & 0 & 0 & 0 \\ 0 & 0 & 3.4219 & 0 & 0 & 0 & 0 & 0 \\ 0 & 0 & 0 & 6.75+3.4812j & 0 & 1.6216 & 0 & 0 \\ 0 & 0 & 0 & 0 & 1.6216 & -3.4800 & 1.6621 & 0 \\ 0 & 0 & 0 & 0 & 0 & 1.6621 & 0 & 1.2264 \\ 0 & 0 & 0 & 0 & 0 & 0 & 1.2264 & 0 \end{bmatrix} \quad (5.6)$$

According to the (3.90), the [T] matrix representing the normalised port admittances is calculated to give

$$[T]=\begin{bmatrix} 1 & 0 & 0 & 0 & 0 & 0 & 0 & 0 \\ 0 & 0 & 0 & 0 & 0 & 0 & 0 & 0 \\ 0 & 0 & 0 & 0 & 0 & 0 & 0 & 0 \\ 0 & 0 & 0 & 0.2528+1.3799j & 0 & 0 & 0 & 0 \\ 0 & 0 & 0 & 0 & 0.2752+0.6367j & 0 & 0 & 0 \\ 0 & 0 & 0 & 0 & 0 & 0 & 0 & 0 \\ 0 & 0 & 0 & 0 & 0 & 0 & 0 & 0 \\ 0 & 0 & 0 & 0 & 0 & 0 & 0 & 1 \end{bmatrix} \quad (5.7)$$

Matrix [U] is

$$[U]=\begin{bmatrix} 0 & 0 & 0 & 0 & 0 & 0 & 0 & 0 \\ 0 & 1 & 0 & 0 & 0 & 0 & 0 & 0 \\ 0 & 0 & 1 & 0 & 0 & 0 & 0 & 0 \\ 0 & 0 & 0 & 0 & 0 & 0 & 0 & 0 \\ 0 & 0 & 0 & 0 & 0 & 0 & 0 & 0 \\ 0 & 0 & 0 & 0 & 0 & 1 & 0 & 0 \\ 0 & 0 & 0 & 0 & 0 & 0 & 1 & 0 \\ 0 & 0 & 0 & 0 & 0 & 0 & 0 & 0 \end{bmatrix} \tag{5.8}$$

The *S*-parameters response can be calculated using (3.88) and (3.89), and is presented in Fig. 5.2. This newly introduced *N*+4 coupling matrix produces the standard Chebyshev filter response in return loss S_{11} and S_{22}, and also gain about 22 dB across the passband. Recalling the *S*-parameters calculated for the same filter in Fig. 3.14, the gain (S_{21}) in Fig. 5.2 is larger than the optimised one in Fig. 3.14 by about 7.3 dB. This is because the transistor is approximately assumed as a unilateral device (S_{12}=0).

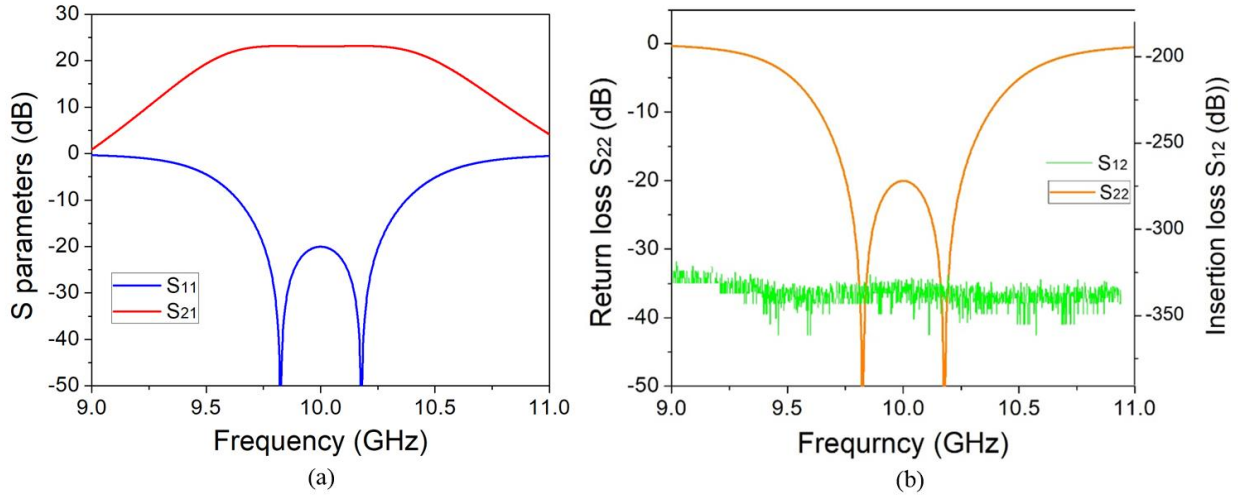

Fig. 5.2 Calculated filter amplifier responses using the coupling matrix formulation. (a) Scattering parameters S_{11} and S_{21}. (b) Scattering parameters S_{22} and S_{12}.

This coupling matrix can be used in the design of the filter amplifier. Referring to (5.3) and (5.6), the external Q of the 1st resonator and external Q of the *N*st resonator can be calculated, given

by Q_{e1}=Q_{en}=13.297. The coupling coefficient between Resonator 1 and Resonator 2 ($M_{1,2}$) can be calculated using (5.2) and (5.6) to give $M_{1,2}$=0.0831. The coupling coefficient between Resonator 3 and Resonator 3 ($M_{3,4}$) can be calculated using (5.2) and (5.6) to give $M_{3,4}$=0.0831. The external Q of the 2nd resonator incorporating the transistor's input (Q_{eT1}) and the external Q of the 3ed resonator incorporating the transistor's output (Q_{eT2}) can be calculated using (5.4) (5.5) and (5.6) to give Q_{eT1}=Q_{eT2}=13.297 at the resonator frequencies are f_{T1}= f_{T2}=10 GHz.

5.3 Example: A Waveguide Filter Amplifier Design

Based on the N+4 coupling matrix in (5.7), two 2nd Chebyshev filters are implemented to match the input and the output of the transistor. The physical design process of an X-band waveguide filter amplifier is discussed below.

The physical structure is comprised of the waveguide resonators, and the transistor mounted on a printed circuit board (PCB) and is illustrated in Fig. 5.3. The transistor PCB is placed on the platform in the middle of the waveguide. The feeding structures on the PCB, coupling Resonator 2 and Resonator 3 to the transistors' gate and drain, are probes of length l_1 and l_2 on the end of feed lines of lengths s_1 and s_2. The waveguide filters are formed of four TE_{101} waveguide cavities. It can be seen from Fig 5.3 that the iris d_1 determines the external quality factor of Resonator 1, Q_{e1} and the iris d_4 determines the external quality factor of Resonator 4, $Q_{e4.}$ The iris size d_2 which couples Resonator 1 and Resonator 2 decides the coupling coefficient of the two resonators $M_{1,2}$. Similarly, the iris d_3 which couples Resonator 3 and Resonator 4 decides the coupling coefficient of the two resonators $M_{3,4}$. The length of the transition interconnection s_1 and the probe l_1 influence the coupling strength from the Resonator 2 to the input of the resonator, and the transition s_2 and

the probe l_2 influence the coupling strength from the Resonator 3 to the output of the resonator. Resonator lengths L_1, L_2, L_3 and L_4 determine the centre frequency of the resonators.

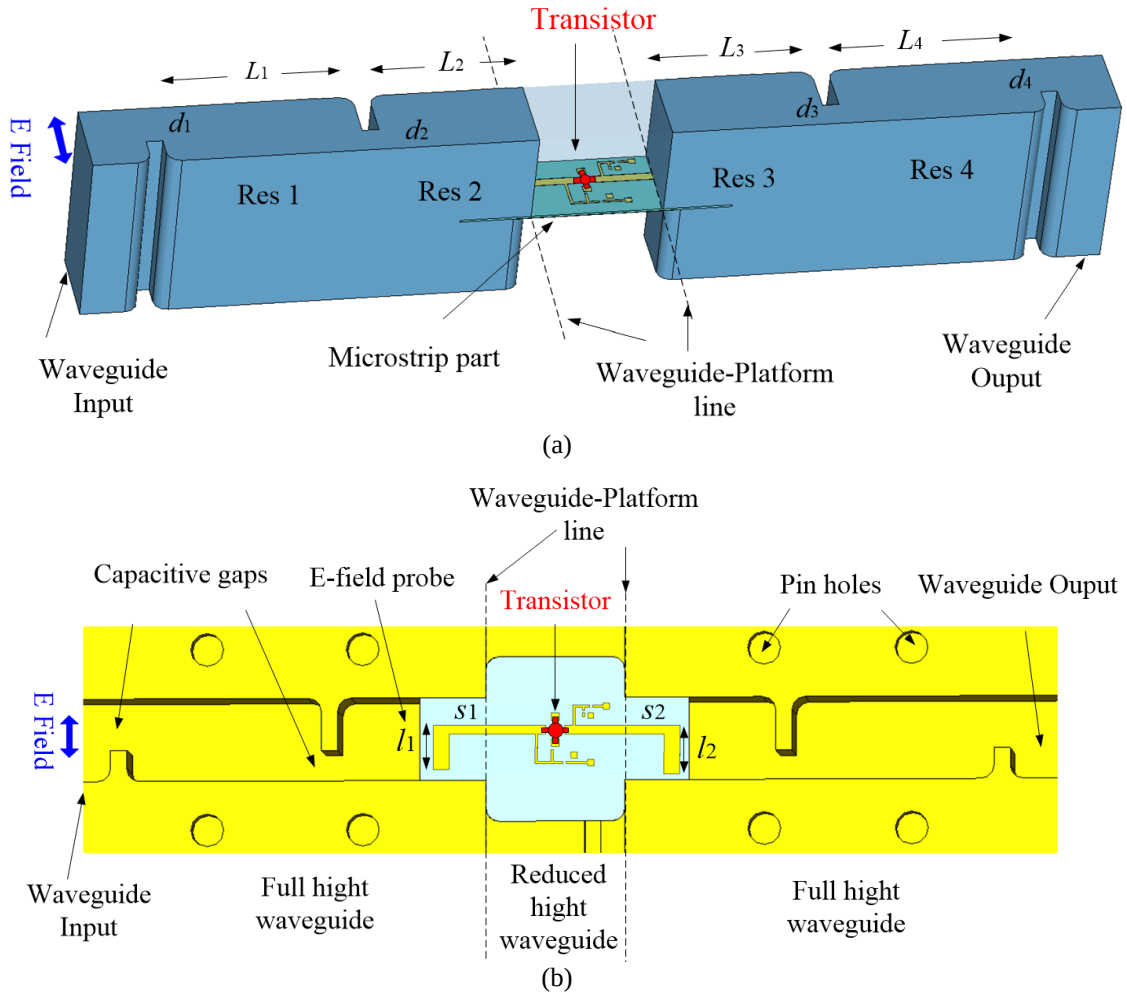

Fig. 5.3 Illustration diagrams of waveguide filter amplifier. (a) Three-dimensional view of the internal waveguide with the microstrip circuit. (b) Sectional view of the filter and platform for the transistor circuit.

5.3.1 Extraction of the external quality factors Q_{e1} and Q_{e4}

Q_{e1} and Q_{e4} can be extracted from the simulation of the single waveguide cavity. As illustrated in Fig. 5.4(a), there is a narrow coupling gap at port 1and capacitive iris with length of d_i is at port 2 and the length of the waveguide resonator cavity is L. A resonance response with centre frequency at 10 GHz is simulated using CST [4], where the external quality factor can be extracted with the help of the formula in Fig. 5.4(b).

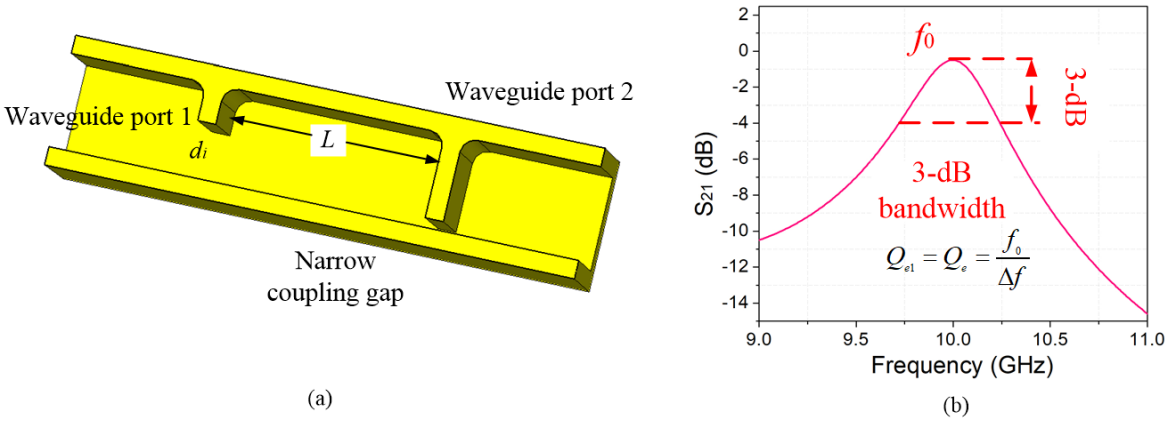

Fig. 5.4 Extraction of the external quality factor of the resonator. (a) Structure of single waveguide cavity. (b) *S*-parameter response of the waveguide resonator.

The length of the capacitive gap d_i is adjusted, corresponding different external quality factors Q_e. The Q_e versus the size of the gap d_i is plotted, which is the same curve in Fig. 4.19, where appreciate d_i can be found for the required Q_{e1}=13.297. As discussed above Q_{e1}=Q_{e4}=13.297, and thus d_i=d_1=d_2=4.85 mm. During the simulation process, the length of the resonator L is adjusted to keep the resonance at 10 GHz centre frequency.

5.3.2 Extraction of the coupling coefficients

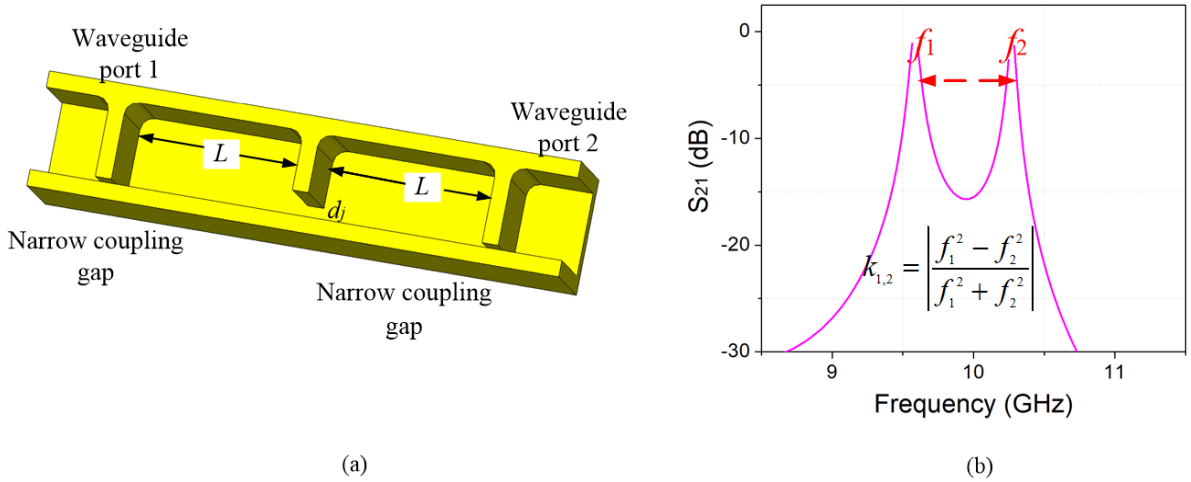

Fig. 5.5 Extraction of the coupling coefficient. (a) Structure of coupled waveguide cavities. (b) *S*-parameter response of the coupled waveguide resonators.

Fig. 5.5 illustrates the configuration of extract the coupling coefficient from the coupled resonators. Two the waveguide cavities are coupled via the capacitive gaps d_j (j=2 or 3). There is weak coupling at the two ports through the narrow gap. The simulated S-parameters response displays two peaks of S_{21} is present in Fig. 5.5(b), where coupling coefficients $M_{i,j}$ can be extracted according to

$$M_{i,j} = \left| \frac{f_i^2 - f_j^2}{f_i^2 + f_j^2} \right| \tag{5.9}$$

Adjust the size of the gap d_j and a series of corresponding coupling coefficients $M_{i,j}$ can be extracted. The relationship of coupling coefficient $M_{i,j}$ versus different d_j is the same as shown in Fig. 4.21, where the target $M_{1,2}$=$M_{3,4}$=0.0831 can be found with specified iris size d_j=d_2=d_3=2.65 mm. During the extraction process, the length of the resonator L is adjusted to keep the resonance at 10 GHz centre frequency.

5.3.3 Extraction of the external quality factors Q_{eT1} and Q_{eT2}

The next step is to determine the mixed structure around Resonator 2 and Resonator 3. It can be seen from Fig. 5.3(a) that the construction of Resonator 2 and Resonator 3 are similar, and the only difference is the dimensions. The extraction procedure is very close to that in Section 4.4.3.

The configuration of extracting the quality factors Q_{eT1} and Q_{eT2} is shown in Fig. 5.6(a) and (b). The microstrip port is connected the port 2 in CST (see Fig. 5.6(b)) [12], with the load of port 2 set to be the input (output) admittance of the transistor Y_{in}(Y_{out}). Y_{in} and Y_{out} are the input and output admittances of the transistor, respectively. It should be noted that, in this case, we assume Y_{gd}=0 and the transistor is a unilateral device. Thus, Y_{in} and Y_{out} can be easily got referring to the transistor' circuit in Fig. 3.6, i.e. Y_{in}=Y_{gs} and Y_{out}=Y_{ds}. In Fig. 5.6, port 1 is set to be the value of the waveguide

impedance. The whole structure is simulated in CST [12], and the S_{21} shows a resonance curve as presented in Fig. 5.6(c). The external quality factor can be extracted using the formulas in Fig. 5.6(c): the ratio of centre frequency and 3 dB bandwidth.

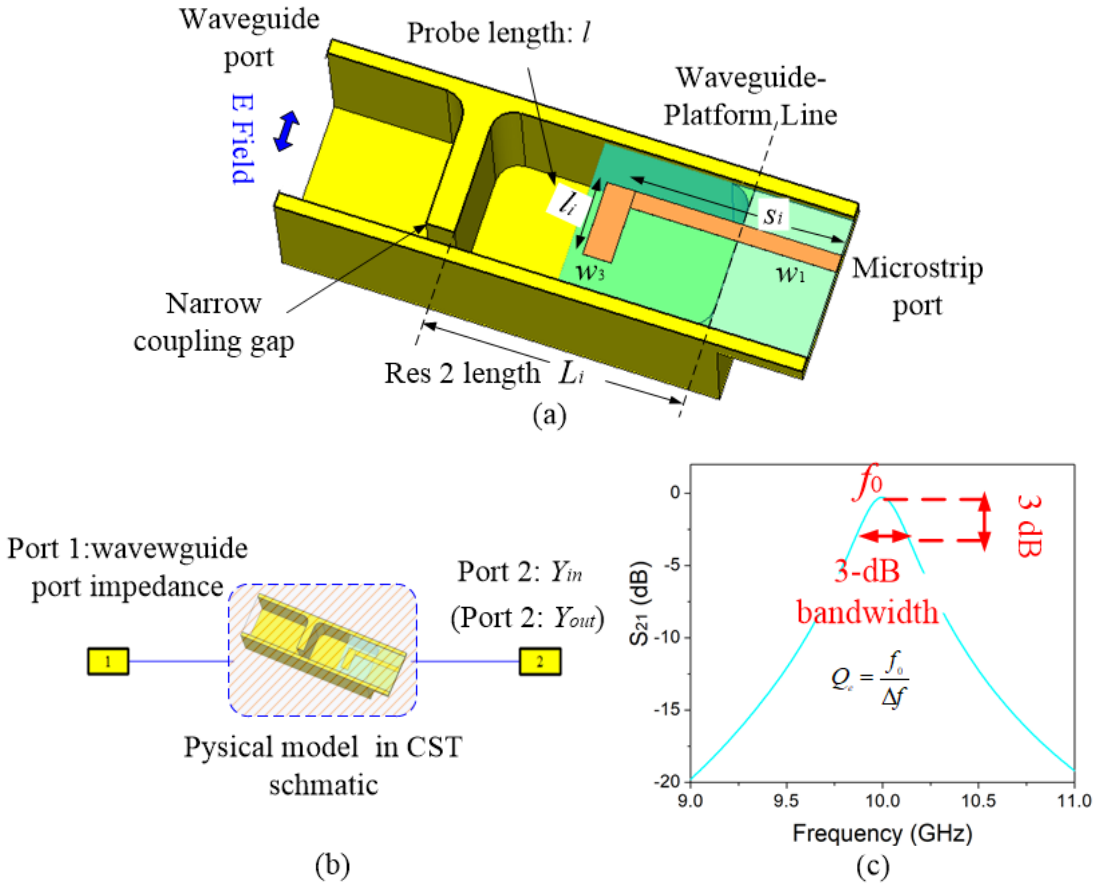

Fig. 5.6 Simulations to extract external quality factor of Resonator 1 and Resonator 3. (a) Structure for extracting eternal quality factor of the resonator with coupling structure. (b) Q_{eTi} extraction setup in CST. (c) *S*-parameter response of the waveguide resonator connected to a complex load.

We choose the length of the probe and transition line l_i, s_i as our variables. Although some other parameters also affect the external Q, these two dimensions are found to be more sensitive. Adjust the length of the transition line s_i and the probe l_i, and the corresponding quality factors are calculated. Here i=1, 2, which indicates external quality factors Q_{eT1} changes corresponding to s_1 and l_1; external quality factors Q_{eT2} changes corresponding to s_2 and l_2. The external Q versus

transition line s_i with various l_i is plotted in Fig. 5.7, where dimensions s_i, l_i can be found to achieve Q_{eT1}=13.297 and Q_{eT2}=13.297, respectively. During the process, L_i is adjusted to keep the resonance at 10 GHz centre frequency.

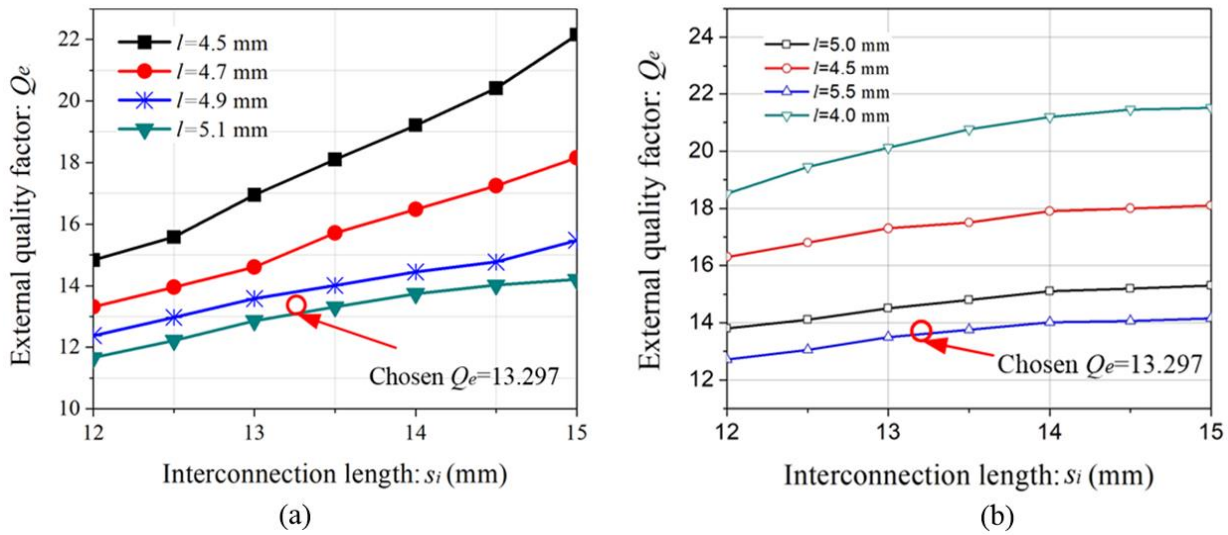

Fig. 5.7 (a) External quality factor Q_{eT1} versus interconnection length s_1. (b) External quality factor Q_{eT2} versus interconnection length s_2. All points are at 10 GHz.

5.3.4 Microstrip part design

The microstrip part of the waveguide filter amplifier is made of the probes, feed transmission lines, the transistor, and bias circuits. Fig. 5.8 illustrates the layout of the microstrip transistor. As shown in Fig. 5.8(a), b_1+b_2 and b_3+b_4 are quarter-wavelength long bias tees at 10 GHz centre frequency. 100 pF capacitors are mounted on the end of the quarter-wavelength long bias arms, providing open-end circuit condition. The ground pins of the transistor are connected to the ground via cut-through holes R_1 and R_2. Surface mount components such as resistors and capacitors are mounted on the bias tees ensuring transistor operating with unconditional stable. Two square pads

at the end of the bias are soldered with wires, offering DC voltages. Note that the middle part of the microstrip is designed to be wider to fix the PCB board on the platform.

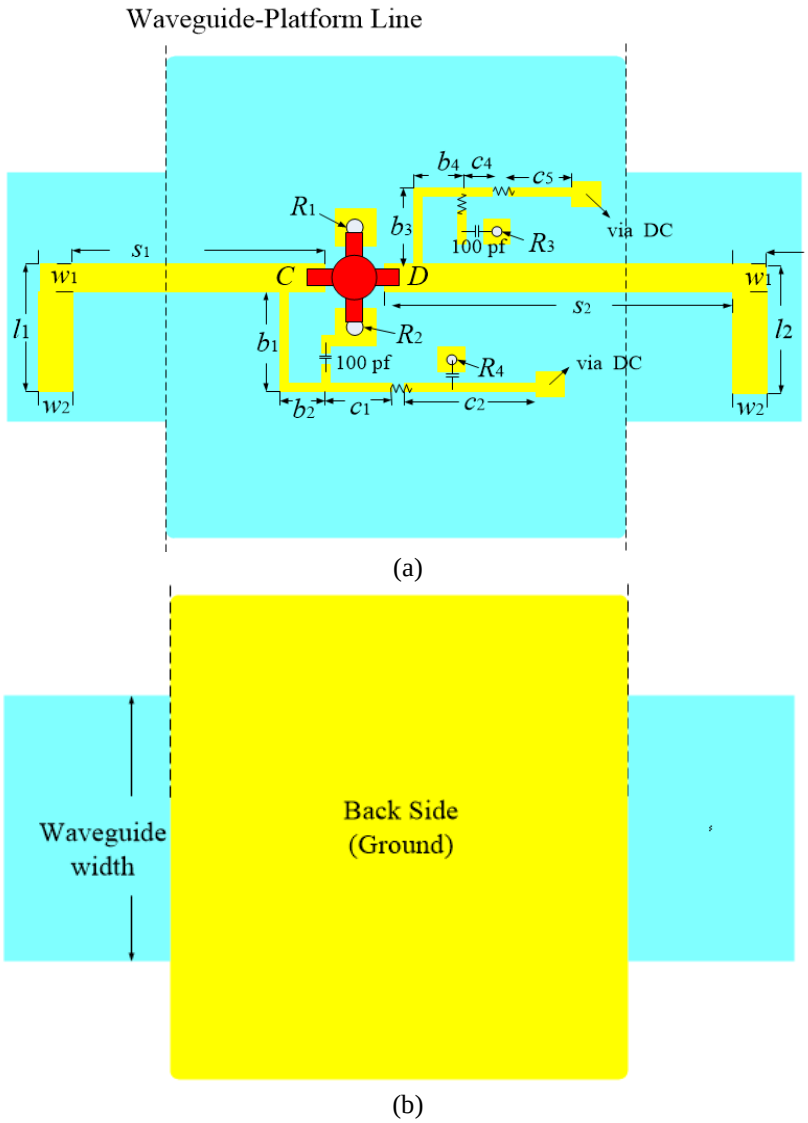

Fig. 5.8 Microstrip part of the filter amplifier. (a) Layout of microstrip with the transistor. (b) Back side.

5.3.5 Full EM simulation and optimisation

After all necessary dimensions of the waveguide filter amplifier have been determined above, the whole construction is co-simulated using the CST [12] and the ADS [13]. The assembled

model of waveguide filter amplifier is shown in Fig. 5.9. It can be seen from Fig. 5.9 that the waveguide part is cut along the E-plane of the waveguide flange. The microstrip transistor sits on the platform of the waveguide and sandwiched by two split waveguide blocks. The input and the output of the amplifier are the TE101 waveguide ports. The probes with part of the transition lines are suspended in the cavities, coupling the resonators to the transistor.

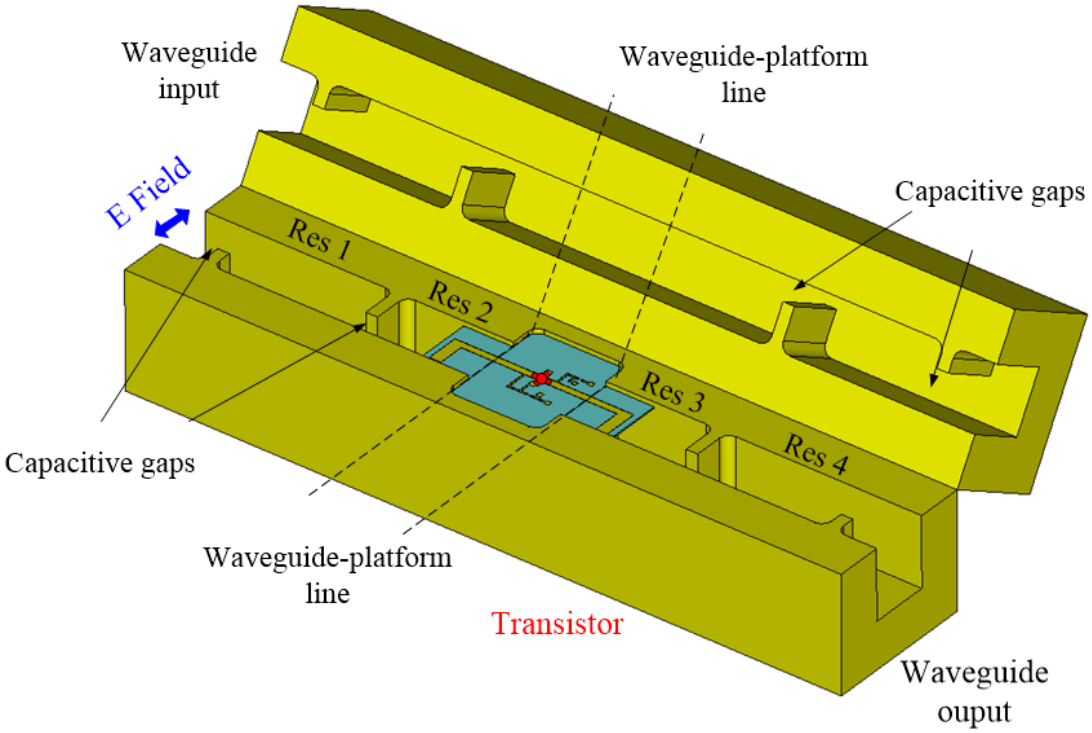

Fig. 5.9 Construction of the waveguide filter amplifier.

The setup of the simulation is schematically illustrated in Fig. 5.10. The waveguide and part of the microstrip (the probe and the transition line) are constructed in CST [12], combined with the S2P touchstone file of the microstrip transistor [11]. The S2P file is generated by simulating the microstrip part of the on-chip transistor in ADS, and the layout of the microstrip transistor is shown in Fig. 5.10. It is readily seen that the bias connection of the transistor is included in the ADS

simulation because the bias circuit also influences the performance of the transistor to some extent. Note that there are short sections of transition lines at the two ports of the transistor simulated in ADS, and during the simulation in CST, these section of transmission lines are removed by employing the embedded port mode in the CST [12]. As shown in Fig. 5.10, port 1 and port 2 are assigned to be waveguide port impedance. Port 3 and port 4 are connected to the gate and the drain of the transistor.

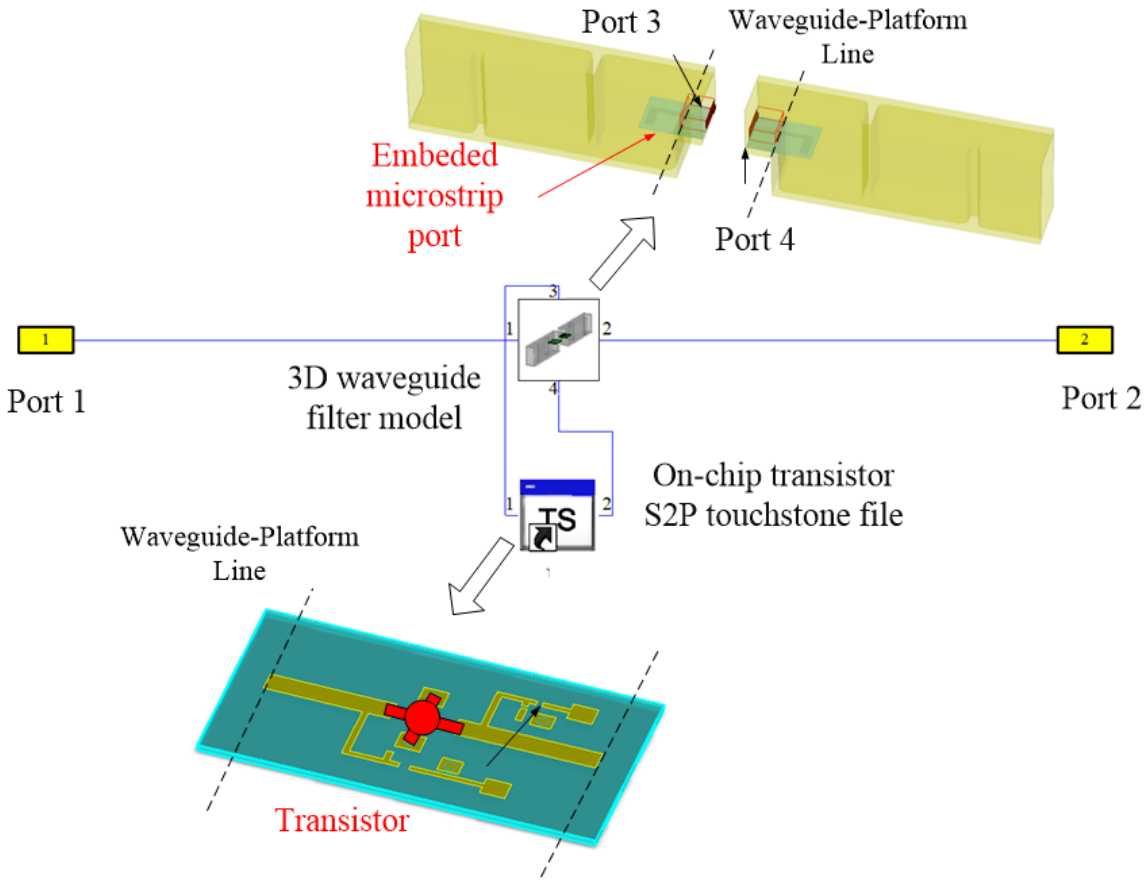

Fig. 5.10 Co-simulation of waveguide filter amplifier using CST and ADS.

The initial parameters used for the simulations are given in Table 5.2 and are the same as the values extracted from the design graphs in Fig. 4.19, Fig. 4.21 and Fig. 5.6. Table 5.2 also presents

the optimised values. Optimisation goals, in this case, are set to be: from 9.75 GHz to 10.25 GHz S_{11} is under -20 dB; from 9.75 GHz to 10.25 GHz S_{22} is under -20 dB; at critical points 9.725 GHz and 10.178 GHz, the S_{11} and S_{22} are under -40 dB.

Both the initial response and the optimised response, using the parameters in Table 5.2, are shown in Fig. 5.11. The optimised results in Fig. 5.11(a) and (b) show that over the passband S_{11} is below -20 dB; S_{21} is around 13 dB; and S_{22} is below -20 dB over the passband. The good correlation between the initial and optimised responses demonstrates the validity of the coupling matrix technique in providing starting parameters for the filter amplifier design. Note that the gain of S_{21} is different from that calculated using the coupling matrix in Fig. 5.2. This is because in the coupling matrix in (5.6), we regard the transistor as a unilateral component and there is no feedback. The gain is reduced once we use the physical model of the transistor. The stability factor illustrated in Fig. 5.11(c) is above 1 from 0 GHz to 22 GHz, indicating the transistor circuit is unconditional stable over these frequencies. Fig. 5.11(d) shows noise figure which is about 1.10 dB from 9.57 GHz to 10.25 GHz and NFmin (minimum noise figure) for the device is 1.12 dB at 9.85 GHz.

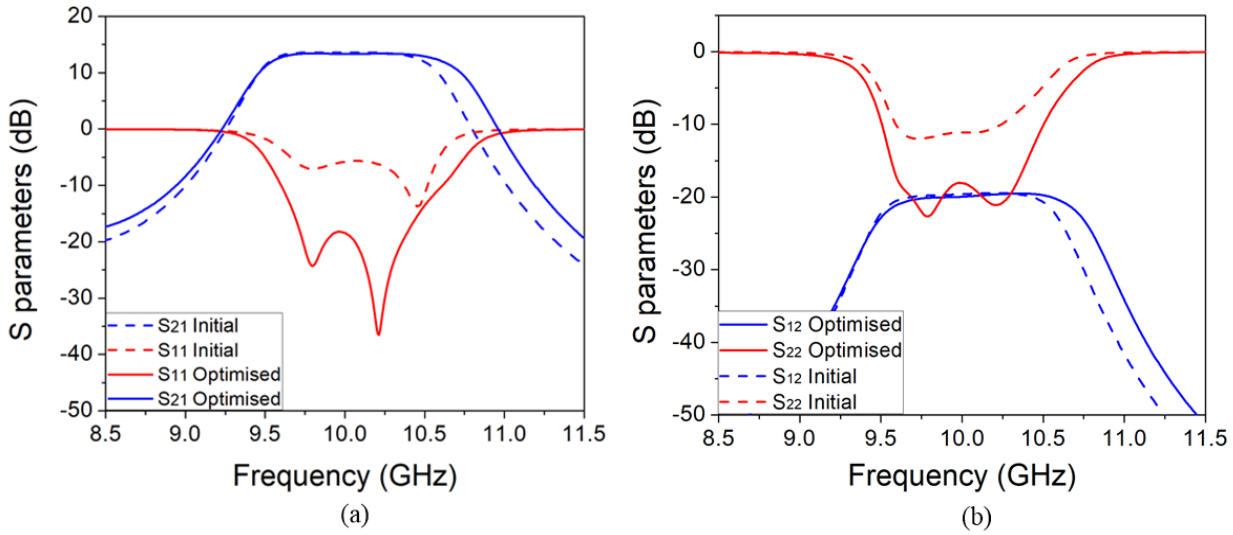

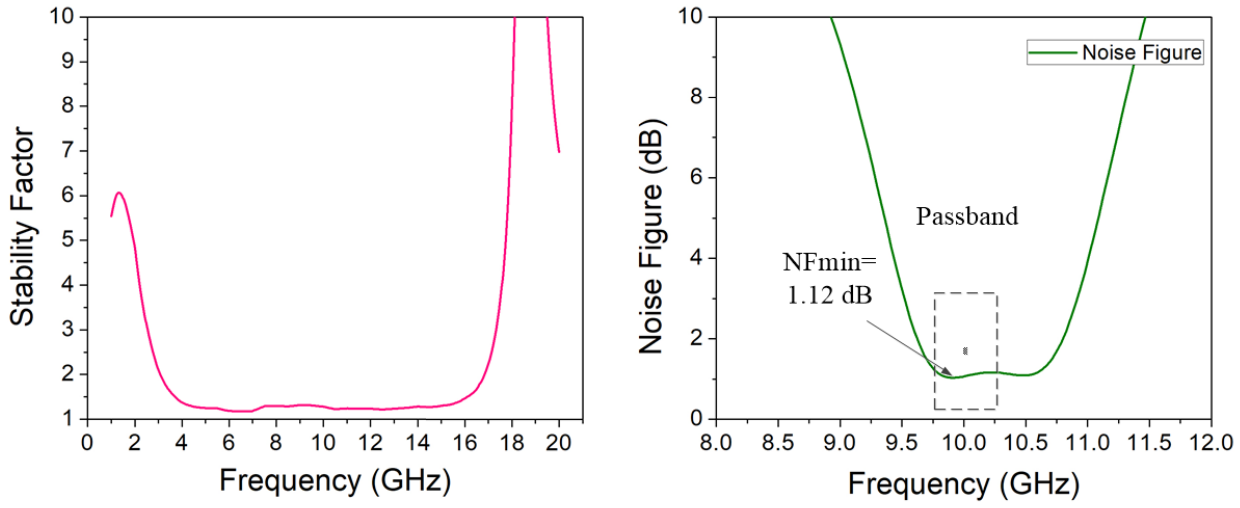

(c) (d)

Fig. 5.11 Co-simulation results of waveguide filter integrated amplifier. (a) Scattering parameters S_{11} and S_{21}. (b) Scattering parameters S_{22} and S_{12}. (c) Stability factor. (d) Noise figure.

TABLE 5.2
VALUES OF INITIAL AND NORMALISED WAVEGUIDE-AMPLIFIER PARAMETERS

	Initial (mm)	Optimised (mm)		Initial (mm)	Optimised (mm)
L_1	**23.00**	**23.76**	R_3	**1.2**	**1.2**
L_2	**17.80**	**18.71**	R_4	**2.96**	**2.96**
L_3	**4.85**	**6.39**	b_1	**1.33**	**1.33**
L_4	**2.65**	**3.22**	b_2	**2.50**	**2.50**
l_1	**4.9**	**4.83**	b_3	**2.00**	**2.00**
l_2	**13.30**	**12.99**	b_4	**1.50**	**1.50**
s_1	**0.30**	**0.30**	c_1	**1.10**	**1.10**
s_2	**0.30**	**0.30**	c_2	**5.00**	**5.00**
w_1	**0.30**	**0.30**	c_3	**5.00**	**5.00**
w_2	**1.20**	**1.20**	c_4	**3.22**	**3.22**
R_1	**0.72**	**0.72**	c_5	**3.18**	**3.18**
R_2	**2.00**	**2.00**			

5.4 Waveguide Filter Amplifier Measurement

The waveguide structure is fabricated from aluminium (AL5083) on a CNC machine. The microstrip circuit is made of RT5870 substrate having the 0.254 mm thickness and the dielectric constant of 2.33. The surface mount components are soldered on the PCB board manually. The

connection wires are mounted on the pads providing DC voltages at the gate and the drain of the transistor. Both input and output are connected to the 50 Ω measurement ports via two WR-90 waveguide adapters. Fig. 5.12 presents two photographs of the device. Several pinholes are drilled to help aline the building blocks, and the screws are used to fix the waveguide.

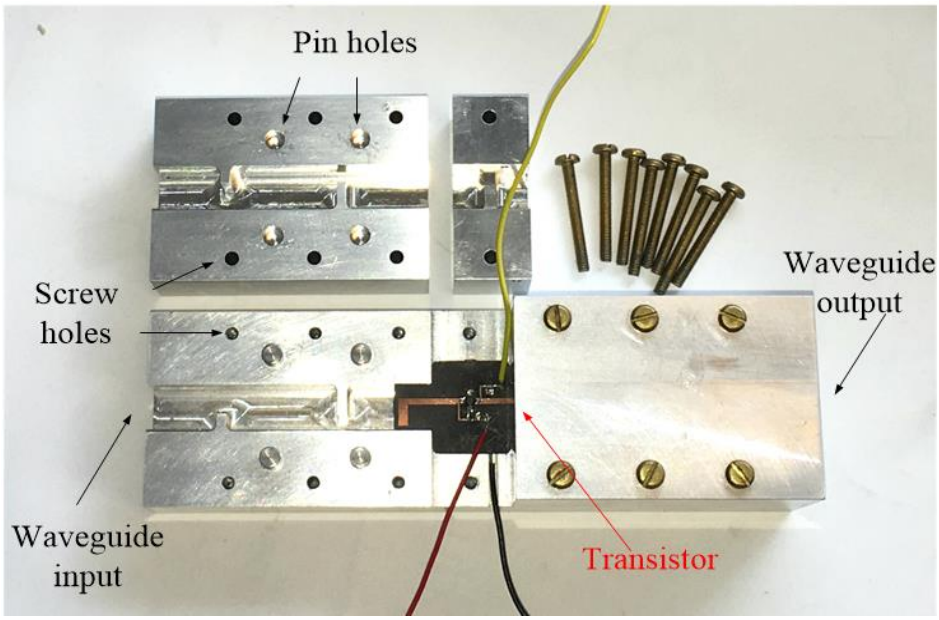

(a)

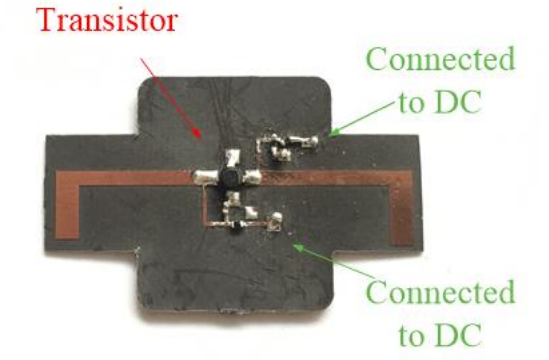

(b)

Fig. 5.12 Photographs of the fabricated device. (a) Waveguide filter amplifier device. (b) On-chip transistor PCB board.

The Agilent vector network analyser PNA E8362B is employed to in the *S*-parameters response measurement. The bias conditions of the amplifier are V_{ds}=2.3 V, V_{gs}=-0.56 V, provided by the DC power source.

The measurement results are shown in Fig 5.13 and are compared with the simulated responses. Two poles are displayed in both S_{11} and S_{22} of the response, indicating the resonators at input and output of the transistor works well. S_{21} shows about 11 dB gain over the passband. The measured input and output insertion are around 13.3 dB and 11.62 dB respectively, over the passband. The measurement results agree well to the simulated response validate the approach of co-design of waveguide filter amplifier.

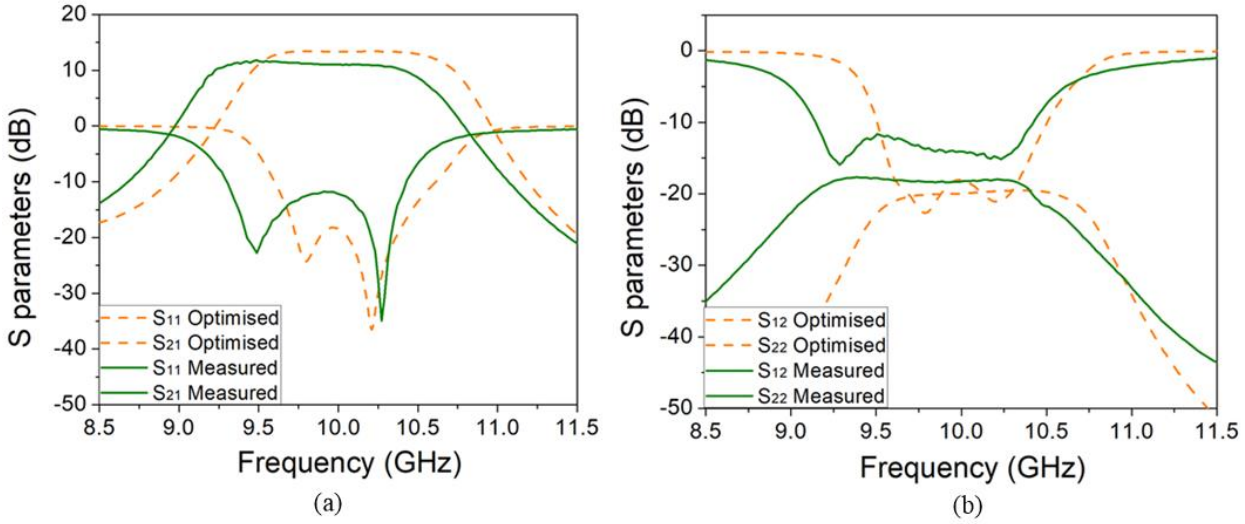

Fig. 5.13 Circuit simulation and measurement results. (a) Scattering parameters S_{11} and S_{21}. (b) Scattering parameters S_{22} and S_{12}

The disagreement between the measured results and simulated response may be caused by roughness of the waveguide cavity surface and the fabrication tolerance. The poor contacts between the splited waveguides and between the waveguide and microstrip board also have an effect on the measured results. Circuit soldering can add losses and degrade the gain of the transistor, and DC wires also have influence on the performance of the transistor. The components including the transistor and the surface mount capacitors and resistors can also be taken into account for the disagreement as they are soldered on the PCB board manually. It is suggested that

the pads which connect the DC wires should stay a certain distance from the transistor as the DC wires are found to affect the transistor's performance to some extent when they are nearby.

5.5 Summary

Following the input waveguide filter amplifier design in Chapter 4, this chapter has extended the design of resonator matching methodology to both the input and the output of the transistor. The hybrid structure is implemented to realise the easy impedance conversion from the rectangular waveguide to the on-chip active component. Compared to the waveguide amplifier with input resonator matching in Chapter 4, both the input and output are configurated standard waveguide port. The waveguide-microstrip-waveguide conversion is more complicated but with wider and more commonplace utilisation, especially at higher frequencies.

The novel N+4 active coupling matrix has been described in Chapter 3, but in the practical design, we assumed the feedback of the transistor is small and neglected [6] and designed the input and output matching filters separately. The whole structure simulation has accounted for all parameters of the transistor leading to an accurate simulation of the physical structure including the microstrip and waveguide. With the help of the N+4 coupling matrix, the dimension-extraction process results in good initial values for the filter amplifier as illustrated in Fig. 5.13. The general good measurement result validates the integration of waveguide filters with the active component. The X-band filter amplifier is implemented as an example, but the technique is general.

REFERENCES

[1] X. Phillips, *Terahertz technology*. Delhi: English Press, 2011.

[2] M. Horibe and R. Kishikawa, "Metrological Traceability in Waveguide S-parameter Measurements at 1.0 THz Band," *IEEE Trans. Instru. Measur.*, vol. 62, no. 6, pp. 1814-1820, June 2013.

[3] Guillermo Carpintero; Enrique Garcia-Munoz; Hans Hartnagel; Sascha Preu; Antti Raisanen, *THz Electronics*. Wiley-IEEE Press, 2015.

[4] J. S. Hong and M. J. Lancaster, *Microstrip Filters for RF/Microwave Applications*. New York, NY, USA: Wiley, 2001.

[5] I. Bahl, *Fundamentals of RF and Microwave Transistor Amplifiers*. Hoboken, N.J.: Wiley, 2009.

[6] D. Pozar, *Microwave engineering*. Hoboken, NJ: Wiley, 2012.

[7] J. Chen, J. Yang, S. Yang and X. Li, "A Coupled Circuit-Ambipolar Diffusion Equation Model and Its Solution Methodology for Insulated Gate Bipolar Transistors," *IEEE Trans. Magn.*, vol. 53, no. 6, pp. 1-4, June 2017.

[8] N. Lakhdar and B. Lakehal, "Modeling of submicron triple material GaAs MESFET including the effect of third region length for microwave frequency applications," *2017 Inter. Conf. Green Energy Conversion Syst. (GECS)*, Hammamet, 2017, pp. 1-5.

[9] D. Costa, W. U. Liu and J. S. Harris, "Direct extraction of the AlGaAs/GaAs heterojunction bipolar transistor small-signal equivalent circuit," *IEEE Trans. Electron Devices*, vol. 38, no. 9, pp. 2018-2024, Sep 1991.

[10] S. J. Spiegel, D. Ritter, R. A. Hamm, A. Feygenson and P. R. Smith, "Extraction of the InP/GaInAs heterojunction bipolar transistor small-signal equivalent circuit," *IEEE Trans. Electron Devices*, vol. 42, no. 6, pp. 1059-1064, Jun 1995.

[11] California Eastern Laboratories (2004, July). CEL Corp., CA. [Online]. Available: http://www.cel.com/pdf/datasheets/ne3210s1.pdf

[12] Computer Simulation Technology, CST company, Germany.

[13] Advanced Design System, Agilent Technologies, USA.

CHAPTER 6

CONCLUSION AND FUTURE WORK

6.1 Conclusions

The main subjects presented in this thesis can be classified into two categories: (a) The *N*+*X* coupling matrix synthesis. (b) The filter amplifier constructions based on these coupling matrices.

The first part of the thesis considers the coupling matrices in Chapter 3. Three novel coupling matrices are synthesised: (i) The *N*+4 coupling matrix of cascaded filters with a transmission line between filters; (ii) The *N*+3 coupling matrix of filter amplifiers, useful when the filter is only on the input to the transistor.; (iii) The *N*+4 coupling matrix of filter amplifiers representing transistor in the middle of the resonators providing filtering and matching on both input and output.

The *N*+4 coupling matrix of cascaded filters with transmission lines is developed based on the *Y* matrix of the transmission line and the lumped circuit of cascaded filters. Matrix manipulation and scaling process are applied to eliminate the admittance/impedance elements in the Y/Z matrix to synthesise the coupling matrix. This enable us to ignore the matching and impedance conditions and to concern ourselves only with the coupling coefficients in coupling matrix. The same matrix manipulating technique is also used in [1] and [2]. The newly introduced *N*+4 coupling matrix can

produce *S*-parameters response of cascaded filters with any length of the transmission line. Similar topologies and the cascaded coupling matrix are also presented in [3] and [4], but the length and the transmission line is fixed. The novel *N*+4 coupling matrix representation allows us to formulate the cascaded filters more flexible and predict the performance of a broader range. Significantly it provides an introduction to the concepts for the filter amplifier coupling matrices to follow.

The *N*+3 active coupling matrix introduced in Chapter 3 is formulated based on the lumped filter topology [5] and small signal lumped circuit of the transistor. With the matrix manipulation and a scaling process, the *N*+3 coupling matrix is synthesised. This *N*+3 coupling matrix allows us to describe the filters and transistor component in a single matrix and also make prediction of the overall performance showing filtering and gain.

The *N*+4 active coupling matrix is developed by generalising the filter amplifier with resonators coupled at both the input and output of the transistor. Using the *N*+4 coupling matrix, filter response can be produced to achieve filtering response both in S_{11} and S_{22}. However, feedback in the transistor affects the input and output impedance of the transistor and precludes a simple analytical formulation of the *N*+4 coupling matrix. A matrix optimisation algorithm is therefore introduced to modify an estimated *N*+4 coupling matrix taking the feedback into account. A cost-function is employed to estimate the difference between the responses to be optimised and the desired ones.

To summarise the *N*+3 and *N*+4 coupling matrices, additional elements (transistor' parameters) are included to the conventional coupling matrix for filters, and this leads to the overall circuit performance including return loss and amplification theoretically predicted. This thesis presents these new ideas for the first time.

The second part of the thesis is primarily concerned with the physical designs of the filter

amplifiers using the newly introduced coupling matrices. The filter amplifier design methodology is general and implemented using three examples, i.e. a microstrip amplifier and two waveguide amplifiers. The physical structures are specified using coupling coefficients and external quality factors, which are calculated using the coupling matrix, and then appropriate initial dimensions of the structure are found and used for further optimisation. This co-design approach much more closely resembles the design of a standard filter [5], and the coupling coefficients and the external Q calculated by the novel coupling matrices are exactly the same as these using conventional filter coupling matrix. The only difference is the extraction process of the quality factors of the resonators adjacent to the transistor. In extracting these resonators' external quality factors, the transistor's input or output admittances are included.

Compared to the conventional waveguide amplifiers [6]-[8] summarised in Table 1.1, the waveguide-microtrip transition is integrated into a resonator, achieving Chebyshev (or other) filtering response. The novel coupling matrix offers initial values of the waveguide and the coupling structures, which improves the dimensional design procedure in terms of accuracy, time and complexity. Compared to the microstrip amplifiers [9]-[17], high-Q waveguide resonator itself is a more appropriate choice at higher frequencies due to its low loss. Also, the conventional amplifier matching technologies for planner circuit cannot be applied in waveguide amplifiers design directly.

There are some limitations of the work in the thesis. As the coupling matrix is synthesised for narrow band approximation, it cannot be used to design wideband amplifiers. In our narrowband amplifier examples, the transistor is assumed a fixed input and output admittance. This design approach is validated when the transistor's input and output impedances/admittances do not change a lot near the centre frequency. As the wideband filter is synthesised in [18]-[20], they are

expected to combine with the amplifier operating at wider frequencies.

In chapter 5, the waveguide amplifier is designed according to the N+4 coupling matrix in (5.6). However, the S-parameters response produced by (5.6) is not accurate because the feedback is neglected. Recalling the optimised N+4 matrix in (3.97), this matrix could be applied in designing the waveguide amplifiers, which is expected to offer more accurate initial values.

As the measured results are shown in Fig. 4.16, Fig. 4.30 and Fig. 5.13, there is disagreement between the simulated and the measured responses. Following the possible reasons discussed in Chapter 4 and Chapter 5, the performance can be improved with more accurate fabrication and high-quality soldering. The transistor can also be pre-measured, of which the data can be applied in the design instead of the datasheet provided by the manufacture. Moreover, the bias circuits can be furtherly optimised to reduce the effects of the DC wires.

In general, this design methodology is particularly advantageous in waveguide amplifier designs because it is difficult to determine waveguide-microstrip structure using traditional planar circuit matching methods. Instead, the external quality factor of the resonator can be determined by EM simulation. Impedance/admittance conversion (waveguide to microstrip) can be easily realised by the waveguide and microstrip coupling structures. Moreover, conventional planar matching networks can be transferred to the high-Q waveguide resonators, reducing the size of the device and minimising losses. As waveguide technology is widely utilised in terahertz systems, where on-chip losses can be substantial, the technique is expected to be of advantage at these higher frequencies and is currently being exploited in the 300 GHz communication work at the University of Birmingham.

6.2 Future Work

Possible future developments based on the work in the thesis are given:

i. *Coupling Matrix Synthesis including Noise Figure.*

In the design examples, the noise performance is simulated after formulating the filters and is not further optimised. The aim of our work is to match the transistor to achieve Chebyshev filter response, demonstrating the synthesised coupling matrix. However, in practice, designers are more likely to be concerned with the noise figure rather than gain, particularly for low noise amplifiers. It is believed that the coupling matrix can be synthesised to achieve a better trade-off between noise performance and gain by choosing optimal transistor impedance.

ii. *Coupling Matrix for Communication or other Systems*

Conventional coupling matrix synthesis is mainly applied in the design of passive microwave components [1], [5]. The active coupling matrix synthesised in this thesis enables us to develop filter amplifiers indicating that transistors with complex port impedance/admittance can be matched with resonator based filters. Therefore, the coupling matrix technique can be generalised to deal with a wide range of components with complex ports, e.g. antennas, mixers and triplers. All these components can be assembled to form a communication system, and therefore the coupling matrix concept is expected to characterise the whole communication system.

iii. Terahertz Components

A circuit with microstrip port configurations is difficult to measure at higher frequencies, particularly over 100 GHz frequency and waveguide flanges are commonly employed for THz frequencies measurement [21]-[23]. As active components are widely utilised

at higher frequencies [24]-[26], THz waveguide amplifiers are expected to be more commonplace. A THz waveguide filter amplifier can be implemented following the amplifier layout presented in Chapter 5. The coupling matrix synthesised filter amplifier design approach is currently being used in the 300 GHz amplifier design.

REFERENCES

[1] R. J. Cameron, R. Mansour and C. M Kudsia, *Microwave Filters for Communication Systems: Fundamentals, Design and Applications*. 1st. New York, NY, USA: Wiley, 2007.

[2] W. Xia. "Diplexers and multiplexers design by using coupling matrix optimisation," PhD dissertation. Elect. Eng, Birmingham Univ., Birmingham, 2015.

[3] S. Saeedi, J. Lee and H. H. Sigmarsson, "Tunable, High-Q, Substrate-Integrated, Evanescent-Mode Cavity Bandpass-Bandstop Filter Cascade," *IEEE Microw. Wirel. Compon. Lett.*, vol. 26, no. 4, pp. 240-242, April 2016.

[4] E. J. Naglich, J. Lee, D. Peroulis and W. J. Chappell, "Bandpass–Bandstop Filter Cascade Performance Over Wide Frequency Tuning Ranges," *IEEE Trans. Microw. Theory Techn.*, vol. 58, no. 12, pp. 3945-3953, Dec. 2010.

[5] J. S. Hong and M. J. Lancaster, *Microstrip Filters for RF/Microwave Applications*. New York, NY, USA: Wiley, 2001.

[6] K. Minot, B. Nelson and W. Jones, "A low noise, phase linear distributed coplanar waveguide amplifier," *IEEE Trans. Microw. Theory Techn.*, vol. 41, no. 9, pp. 1650-1653, Sep 1993.

[7] M. Abdolhamidi and M. Shahabadi, "X-Band Substrate Integrated Waveguide Amplifier," *IEEE Microw. Wirel. Compon. Lett.*, vol. 18, no. 12, pp. 815-817, Dec. 2008.

[8] B. Ahmadi and A. Banai, "Substrateless Amplifier Module Realised by Ridge Gap Waveguide Technology for Millimeter-Wave Applications," *IEEE Trans. Microw. Theory Techn.*, vol. 64, no. 11, pp. 3623-3630, Nov. 2016.

[9] S. F. Sabouri, "A GaAs MMIC active filter with low noise and high gain," 1998 *IEEE MTT-S Int. Microw. Symp. Digest* (Cat. No.98CH36192), Baltimore, MD, USA, 1998, pp. 1177-1180 vol.3.

[10] Young-Hoon Chun, Sang-Won Yun and Jin-Koo Rhee, "Active impedance inverter: analysis and its application to the bandpass filter design," *2002 IEEE MTT-S Int. Microw. Symp. Digest (Cat. No.02CH37278)*, Seattle, WA, USA, 2002, pp. 1911-1914 vol.3.

[11] L. Darcel, P. Dueme, R. Funck and G. Alquie, "New MMIC approach for low noise high order active filters," *IEEE MTT-S Int. Microw. Symp. Digest*, 2005., 2005, pp. 4 pp.-doi: 10.1109/MWSYM.2005.1516731.

[12] F. Bergeras, P. Duême, J. Plaze, L. Darcel, B. Jarry and M. Campovecchio, "Novel MMIC architectures for tunable microwave wideband active filters," 2010 *IEEE MTT-S Inter. Microw. Symp.*, Anaheim, CA, 2010, pp. 1-1.

[13] C. Y. Chang and T. Itoh, "Microwave active filters based on coupled negative resistance method," *IEEE Trans. Microw. Theory Techn.*, vol. 38, no. 12, pp. 1879-1884, Dec 1990.

[14] M. Ito, K. Maruhashi, S. Kishimoto and K. Ohata, "60-GHz-band coplanar MMIC active filters," *IEEE Trans. Microw. Theory Techn.*, vol. 52, no. 3, pp. 743-750, March 2004.

[15] Young-Hoon Chun, Jae-Ryong Lee, Sang-Won Yun and Jin-Koo Rhee, "Design of an RF low-noise bandpass filter using active capacitance circuit," *IEEE Trans. Microw. Theory Techn.*, vol. 53, no. 2, pp. 687-695, Feb. 2005

[16] K. Chen, J. Lee, W. J. Chappell and D. Peroulis, "Co-Design of Highly Efficient Power Amplifier and High-Q Output Bandpass Filter," *IEEE Trans., Microw. Theory Techn.*, vol. 61, no. 11, pp. 3940-3950, Nov. 2013.

[17] Y. C. Li, K. C. Wu and Q. Xue, "Power Amplifier Integrated with Bandpass Filter for Long Term Evolution Application," *IEEE Microw. Wirel. Compon. Lett.,* vol. 23, no. 8, pp. 424-426, Aug. 2013.

[18] Z. Li and K. L. Wu, "Direct Synthesis and Design of Wideband Bandpass Filter With Composite Series and Shunt Resonators," *IEEE Trans. Microw. Theory Techn.*, vol. 65, no. 10, pp. 3789-3800, Oct. 2017.

[19] Z. Li and K. L. Wu, "Direct Synthesis and Design of a General Sequentially Coupled Wideband Bandpass Filter With N -Transmission Zeros," *IEEE Trans Microw. Theory Techn.*, vol. 64, no. 5, pp. 1484-1495, May 2016.

[20] R. Gomez-Garcia and J. I. Alonso, "Systematic Method for the Exact Synthesis of Ultra-Wideband Filtering Responses Using High-Pass and Low-Pass Sections," *IEEE Trans. Microw. Theory Techn.*, vol. 54, no. 10, pp. 3751-3764, Oct. 2006.

[21] X. Phillips, *Terahertz technology*. Delhi: English Press, 2011.

[22] M. Horibe and R. Kishikawa, "Metrological Traceability in Waveguide S-parameter Measurements at 1.0 THz Band," *IEEE Trans. Instrum. Measurem.,* vol. 62, no. 6, pp. 1814-1820, June 2013.

[23] Guillermo Carpintero; Enrique Garcia-Munoz; Hans Hartnagel; Sascha Preu; Antti Raisanen, *THz Electronics*. Wiley-IEEE Press, 2015.

[24] S. Moghadami, J. Isaac and S. Ardalan, "A 0.2–0.3 THz CMOS Amplifier with Tunable Neutralization Technique," in *IEEE Transactions on Terahertz Science and Technology*, vol. 5, no. 6, pp. 1088-1093, Nov. 2015.

[25] W. R. Deal *et al*., "Demonstration of a 0.48 THz Amplifier Module Using InP HEMT Transistors," *IEEE Microw. Wirel. Compon. Lett.*, vol. 20, no. 5, pp. 289-291, May 2010.

[26] C. R. Donaldson, L. Zhang, M. Beardsley, M. Harris, P. G. Huggard and W. He, "CNC Machined Helically Corrugated Interaction Region for a THz Gyrotron Traveling Wave Amplifier," *IEEE Trans. Terah. Sci. Techn.*, vol. 8, no. 1, pp. 85-89, Jan. 2018.

PUBLICATIONS

1. Y. Gao, J. Powell, X. Shang, M. J. Lancaster, “Coupling matrix based design of filter amplifiers,” *IEEE Transactions Microwave Theory and Technique.* (Revised and resubmitted)

2. Y. Gao, J. Powell, X. Shang, M. J. Lancaster, “Waveguide filter amplifier integration using coupling matrix technology,” *IEEE Microwave wireless and components letter*. (To be submit)

Coupling Matrix based Design of Waveguide Filter Amplifiers

Yang Gao, Jeff Powell, Xiaobang Shang, *IEEE Member*, Michael J. Lancaster, *IEEE, Senior Member*

***Abstract*—This paper extends the conventional coupling matrix theory for passive filters to the design of 'filter-amplifiers', which have both filtering and amplification functionality. For this approach, extra elements are added to the standard coupling matrix to represent the transistor. Based on the specification of the filter and small-signal parameters of the transistor, the active *N*+3 coupling matrix for the 'filter-amplifier' can be synthesized. Adopting the active coupling matrix, the last resonator of the filter (adjacent to the transistor) and the coupling between them are modified mathematically to provide a Chebyshev response with amplification. Although the transistor has a complex impedance, it can be matched to the filter input by the choice of coupling structure and resonator frequency. This is particularly useful as the filter resonators can be of a different construction (e.g. waveguide) to the amplifier (e.g. microstrip). Here an X-band filter-amplifier is implemented as an example, but the technique is general.**

***Index Terms*—active coupling matrix, amplifier, resonator, waveguide filter.**

I. Introduction

AMPLIFIERS are employed in, for example, communication systems to increase the incoming signal strength. The initial amplifier is ordinarily preceded by filtering to select desired bands of frequencies and reject others for channel selection and compliance. Combining the amplifier and filter in a compact manner can improve performance, through removing intermediate impedance matching, but also in terms of component size and weight. High Q-factor waveguide based components are of interest where the lowest loss is required and they are widely employed in submillimetre wave or terahertz applications. As active components become more commonplace at hundreds of GHz, where planar circuit losses are significant, the technology of choice for interconnects and filters are high-Q waveguides [1]-[3]. Waveguides components operating at more than 200 GHz have been demonstrated using such as precision milling [4], SU-8 [5], and DRIE process [6] techniques. In addition, silicon micromachining techniques [7] and MMIC membrane Schottky process [8] have been employed to realize millimeter wave components which offer the potential for lithographically defined feature precision typical for Monolithic Microwave Integrated Circuits.

In waveguide amplifier design, connection to planar circuits often uses waveguide to planar circuit transitions [9]-[13]. Various forms of structures including SIW [10], step ridges [11], antipodal finline arrays [12], and CPW lines [13] are employed as the interconnecting transition to the on-chip active components. However, the independent design of the transitions and the matching networks results in additional losses and circuit complexity. In this paper, we propose combining the matching network and transition into the (low loss) waveguide resonators of the adjoining filter thereby minimizing losses. This approach also leads to a reduction in the overall size of the combined component.

Several filter-amplifier examples have been reported previously, some of which filters and the transistor are combined via impedance/admittance transformation referring to a common terminal impedance, based on the conventional 50 Ω matching condition, examples are in [14] and [15]. An equivalent ¼λ impedance transformer is employed to transform the impedance of the transistor in [14] and coupled-lines are modeled according to the equivalent transmission line network to match the transistor in [15]. Compared with the waveguide co-design approach described here, the additional planar matching structure adds losses as well as circuit complexity. Another type of filter-amplifier design approach uses the concept of actively coupled resonators or active impedance/admittance inverters to design the filter-amplifier [16]-[19]. There are also some examples of active microwave filters implementing negative-resistance, which incorporates the active components into the resonators in [20]-[22]. However, these design approaches of the active filters usually need multiple active components to construct every active resonator or active inverter, and noise and nonlinear problems have to be investigated carefully. They are more likely applied in the planar amplifier circuits because it becomes difficult to construct the active resonators or active inverters with three-dimensional waveguide structures.

This paper develops the *N*+3 (*N* is the order of the filter) coupling matrix for the first time, which allows the prediction of the filter-amplifier response including gain since the transistor's parameters are included into the coupling matrix. A

This work was supported in part by the UK Engineering and Physical Science Research Council (EPSRC) under Contract EP/M016269/1. The authors are with the Department of Electronic, Electrical and Systems Engineering, University of Birmingham, Birmingham, B15 2TT, UK (Email: yxg311@student.bham.ac.uk).

complete method to synthesize the matrix is given. We consider the transistor and the filter as one entity, and the N+3 active coupling matrix predicts the overall performance of the component characterized by scattering parameters. The matrix is then used to facilitate the full component design with the example of an X band filter-amplifier.

This paper is organized as follows. In Section II the novel active N+3 coupling matrix, including a transistor, is introduced. Section III describes the design and construction of an X-band filter-amplifier circuit demonstrator. Experimental results for the circuit are given in Section IV, after which conclusions and suggestions for further developments are summarized in Section V.

II. The Active Coupling Matrix

A transistor is, in practice, a bilateral device where the output load influences the input port impedance. Before deriving the active N+3 coupling matrix below, a simplified admittance network, used to represent the transistor in small signal operation, is introduced in Fig. 1, [23].

The Y matrix describing the transistor is given by [23],

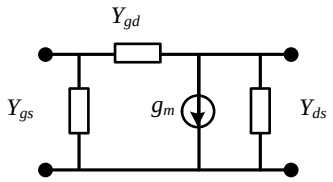

Fig. 1 Equivalent lumped circuit of small signal model for a transistor.

$$[Y_T] = \begin{bmatrix} Y_{gs}+Y_{gd} & -Y_{gd} \\ g_m - Y_{gd} & Y_{ds}+Y_{gd} \end{bmatrix} \tag{1}$$

Y_{gs}, Y_{gd}, and Y_{ds} are the admittances between the source, drain and gate; g_m is the voltage-controlled current source representing the transconductance.

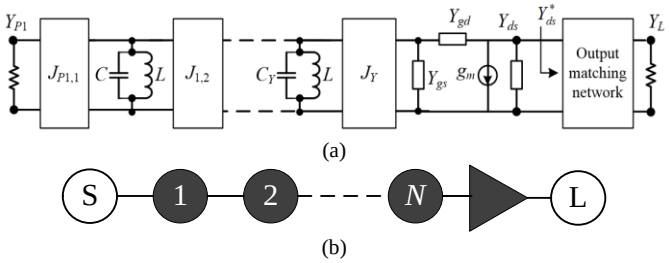

Fig. 2 Topology and equivalent lumped circuit for coupled resonators filter-amplifier circuit. (a) Lumped circuit model. (b) Schematic representation of the circuit.

Fig. 2(a) shows a circuit of an N^{th} order filter using lumped element representations of the resonators based on parallel capacitors and inductors coupled by J inverters. The load of the filter in this case is the transistor. The circuit shown in Fig. 2(a) is represented schematically in Fig. 2(b); where the resonators are represented by black filled circles, the clear circles denote the source and the load.

The input port admittance of the filter is denoted by Y_{P1}. The N^{th} resonator is directly coupled to the transistor by the inverter J_Y. A matching network is employed at the output to transfer

$$[A] = \begin{array}{c} \\ P_1 \\ \\ \\ \\ P_2 \\ P_3 \end{array} \begin{array}{c} \begin{array}{ccccccc} P_1 & & & & & P_2 & P_3 \end{array} \\ \begin{bmatrix} \overline{Y}_{P1} & -jm_{P1,1} & 0 & \cdots & 0 & 0 & 0 \\ -jm_{1,P1} & p & -jm_{1,2} & \cdots & 0 & 0 & 0 \\ 0 & -jm_{2,1} & p & \cdots & 0 & 0 & 0 \\ \cdots & \cdots & N\times N \text{ matrix} & & \cdots & \cdots & \cdots \\ 0 & 0 & 0 & \cdots & p-jm_{n,n} & -jm_{n,P2} & 0 \\ 0 & 0 & 0 & \cdots & -jm_{P2,n} & \overline{Y}_{gs}+\overline{Y}_{gd} & -jm_{P2,P3} \\ 0 & 0 & 0 & \cdots & 0 & -jm_{P3,P2} & \overline{Y}_{ds}+\overline{Y}_{ds}^*+\overline{Y}_{gd} \end{bmatrix} \end{array}$$

Fig. 3 Matrix [A] showing the general $N\times N$ coupling matrix surrounded by extra columns and rows.

$$[Y] = \begin{bmatrix} Y_{P1} & -jJ_{P1,1} & 0 & \cdots & 0 & 0 & 0 \\ -jJ_{1,P1} & \left(\frac{1}{j\omega L}+j\omega C\right) & -jJ_{1,2} & \cdots & 0 & 0 & 0 \\ 0 & -jJ_{2,1} & \left(\frac{1}{j\omega L}+j\omega C\right) & \cdots & 0 & 0 & 0 \\ \vdots & \vdots & \vdots & \ddots & \vdots & \vdots & \vdots \\ 0 & 0 & 0 & \cdots & \left(\frac{1}{j\omega L}+j\omega C_Y\right) & -jJ_Y & 0 \\ 0 & 0 & 0 & \cdots & -jJ_Y & Y_{gs}+Y_{gd} & -Y_{gd} \\ 0 & 0 & 0 & \cdots & 0 & g_m-Y_{gd} & Y_{ds}+Y_{ds}^*+Y_{gd} \end{bmatrix} \tag{2}$$

the load Y_L to Y_{ds}^*, conjugately matched to drain to source admittance Y_{ds}. The load admittance Y_L represents the measurement port at the output which is usually 50 Ω.

We recall that the aim of formulating this topology is to demonstrate a filter response with gain; and for our demonstrator a Chebyshev response will be synthesized. Kirchoff's laws can be applied to the circuit in Fig. 2(a) to write down the equations at each circuit node. The resulting Y matrix is given in (2). Following the matrix scaling process described in [24] and [25], this N+3 matrix [Y] in (2) can now be manipulated to derive matrix [A] shown in Fig. 3. This N+3 matrix has the rows and columns P_1, P_2, and P_3 for the filter's input, the transistor's input and the load with matching, surrounding the conventional $N \times N$ general coupling matrix. The diagonal entries, $A_{P1,P1}$, $A_{P2,P2}$, and $A_{P3,P3}$ indicate the input admittance of the filter, the input admittance of the transistor and the transistor's load admittance with matching network included.

Matrix [A], shown in Fig. 3, can be further decomposed into three matrices [26],

$$[A] = [T] + p \cdot [U] - j \cdot [m] \tag{3}$$

where the [T] matrix, expanded later in (14), includes the filter's port admittance, the input admittance of the transistor and the load admittance. In (3), [U] is the identity matrix except for entries $U_{P1,P1}$, $U_{P2,P2}$ and $U_{P3,P3}$, which are zero. p is the complex frequency variable defined in [26] as

$$p = j\frac{1}{FBW}\left(\frac{\omega}{\omega_0} - \frac{\omega_0}{\omega}\right) \tag{4}$$

Here FBW is the fractional bandwidth and ω_0 is the center frequency. The matrix [m] in (3) is the coupling matrix, of which $m_{i,j}$ denotes the inter-resonator coupling and $m_{Pk,i}$=$m_{i,Pk}$ are the coupling between ports and resonators (i =1 to N; k=1 to 3). The terms $m_{P2,P3}$ and $m_{P3,P2}$ are the couplings between the transistor's input and load. For the matrix [A], shown in Fig. 3, as the common factor -j is extracted as -j[m], the normalized coupling coefficients in the transistor become

$$m_{P2,P3} = \frac{\overline{Y}_{gd}}{j}, m_{P3,P2} = \frac{\overline{Y}_{gd} - \overline{g}_m}{j} \tag{5}$$

Compared with the general coupling matrix, three more entries of the [m] matrix are modified to achieve a Chebyshev input matching; namely the self-coupling $m_{n,n}$, and the external couplings from the N^{th} resonator to the transistor, $m_{n,P2}$ and $m_{P2,n}$. The value of $m_{n,n}$, $m_{P2,n}$, and $m_{n,P2}$ are given by

$$m_{n,n} = -\frac{b}{a \cdot g_n g_{n+1}} \tag{6}$$

$$m_{n,P2} = m_{P2,n} = \sqrt{\frac{a^2 + b^2}{a \cdot g_n g_{n+1}}} \tag{7}$$

g_n and g_{n+1} are the standard g values that are defined and calculated in [26]. a and b are the normalized real and the imaginary part of the transistor's input admittance $\overline{Y}_{in}$ and can be calculated from the transistor's Y matrix parameters

$$a = \mathrm{Re}\left\{\frac{\overline{Y}_{gd}\left[\overline{g}_m + \overline{Y}_{ds} + \overline{Y}_{ds}^*\right]}{\overline{Y}_{gd} + \overline{Y}_{ds} + \overline{Y}_{ds}^*} + \overline{Y}_{gs}\right\} \tag{8}$$

$$b = \mathrm{Im}\left\{\frac{\overline{Y}_{gd}\left[\overline{g}_m + \overline{Y}_{ds} + \overline{Y}_{ds}^*\right]}{\overline{Y}_{gd} + \overline{Y}_{ds} + \overline{Y}_{ds}^*} + \overline{Y}_{gs}\right\} \tag{9}$$

$$\overline{Y}_{in} = a + jb \tag{10}$$

Note the term $jm_{n,n}$ visible at the bottom right corner of the $N \times N$ matrix shown within the red dotted line in Fig. 3 represents a frequency shift of the last resonator in the filter. This has been observed before for the case of transistors, mixers and antennas, and is described in [27]. The shift in frequency is described by $m_{n,n}$ in (6), allowing the Chebyshev (or other) filtering response to be maintained independent of the nature of the complex input impedance of the transistor.

The following relationships can be used to calculate the S-parameters for the complete circuit [24], [26], [28].

$$S_{11} = 2[A]_{P1,P1}^{-1} - 1 \tag{11}$$

$$S_{21} = 2\sqrt{\mathrm{Re}\left(\overline{Y}_{ds}^*\right)}[A]_{P3,P1}^{-1} \tag{12}$$

III. Filter-Amplifier Design Using Coupling Matrix Approach

In this section the design procedure and simulation results for an X-band rectangular waveguide filter-amplifier are described. Before discussing the design procedure, it is informative to illustrate the completed filter-amplifier components, which are shown in the Fig. 4.

Port 1 is assigned to the waveguide port, and Port 2 refers to the 50 Ω microstrip output port. As shown in Fig. 4, the 2-pole waveguide filter is comprised of Resonator 1 and Resonator 2, which are waveguide TE101 cavities coupled via asymmetrical capacitive irises. Resonator 2 is formed by a waveguide cavity and the transistor coupling probe, interconnecting transmission line and the transistor. A reduced height section of waveguide forms a platform on which the microstrip substrate is located. The substrate has the probe and transmission line, and also the transistor with bias connections placed on it.

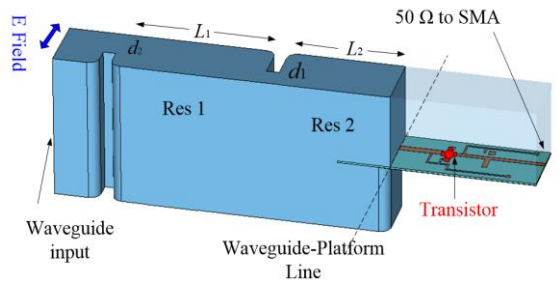

(a)

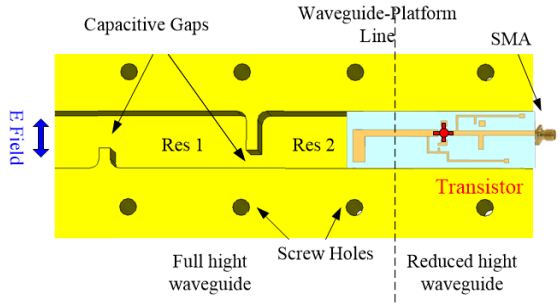

(b)

Fig. 4 The layout of waveguide filter-amplifier. (a) Three-dimensional view of the internal waveguide and the microstrip circuit. (b) Sectional view of the filter and platform for the transistor circuit.

A. *Circuit Response Calculation using the Coupling Matrix*

The values of the coupling coefficients are given by the standard expressions for the desired filter response except for the couplings $m_{n,n}$, $m_{P2,n}$, and $m_{n,P2}$,. The filter and transistor specifications can be translated into elements of the N+3 coupling matrix in Fig. 3 using standard tables or formulas [25], [26]. Here we will use an example of a 2-pole Chebyshev filter with a center frequency f_0 of 10 GHz, a bandwidth of 500 MHz (fractional bandwidth FBW=0.05) and a passband return loss of 20 dB. The transistor used is an NE310S01 with unnormalized parameters Y and normalized parameters $\bar{Y}$ (i.e. scaled by Y_0=0.02 S) summarized in Table 1 [23], [29]. It should be noted that the Y matrix parameters employed here are calculated, assuming the transistor operates at 10 GHz center frequency.

Based on the prototype Chebyshev lowpass filter and the normalized transistor's Y matrix parameters, the active coupling matrix [m] can be calculated according to (6), (8) and (9) to give

TABLE I
VALUES OF AMPLIFIER'S Y MATRIX PARAMETERS

Y parameters	Value	Normalized $\bar{Y}$ parameters	Value
g_m	**0.0696-0.1350*j***	$\bar{g}_m$	**3.4812-6.7500*j***
Y_{gd}	**0.0003+0.0033*j***	$\bar{Y}_{gd}$	**0.0164+0.16298*j***
Y_{ds}	**0.0055+0.0127*j***	$\bar{Y}_{ds}$	**0.2752+0.6367*j***
Y_{gs}	**0.0051+0.0276*j***	$\bar{Y}_{gs}$	**0.2528+1.3799*j***

All parameters are calculated from the data sheet as the transistor operating at 10 GHz.

$$[m]=\begin{bmatrix} 0 & 1.2264 & 0 & 0 & 0 \\ 1.2264 & 0 & 1.6621 & 0 & 0 \\ 0 & 1.6621 & -1.0762 & 2.3407 & 0 \\ 0 & 0 & 2.3407 & 0 & 0.1629-0.0164\,j \\ 0 & 0 & 0 & 6.9129+3.46578\,j & 0 \end{bmatrix} \quad (13)$$

This coupling matrix is asymmetric because of the active element. The matrix [T], used to describe the filter ports admittance as well as the transistor's input and output is given by

$$[T]=\begin{bmatrix} 1 & 0 & 0 & 0 & 0 \\ 0 & 0 & 0 & 0 & 0 \\ 0 & 0 & 0 & 0 & 0 \\ 0 & 0 & 0 & 0.2692+1.5428\,j & 0 \\ 0 & 0 & 0 & 0 & 0.5668+0.1630\,j \end{bmatrix} \quad (14)$$

Using (11) and (12), the resultant scattering parameters can be calculated from the active coupling matrix and are presented in Fig. 5. The novel active coupling matrix produces a standard Chebyshev response with amplification.

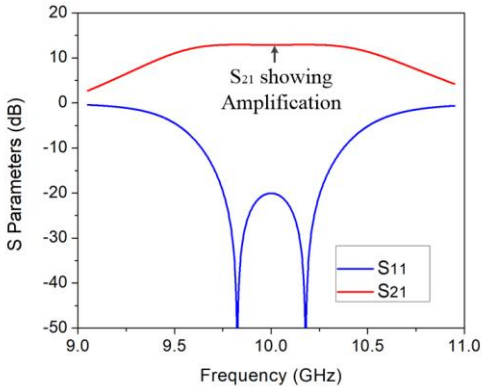

Fig. 5 Calculated filter-amplifier response using the coupling matrix formulation.

B. *Physical Design of the Waveguide Filter–Amplifier.*

The coupling matrix in the previous section was based on normalized admittance parameters, and assumed the normalized admittance stayed consistent from the input to output，this works well and results in good prediction of the circuit response as shown in Fig. 5. Matrix [A] scaled from admittance matrix [Y] enables us to ignore the matching and impedance conditions and to concern ourselves with the coupling coefficients in coupling matrix [m].

Hence, in practice the geometries of the coupling gaps in the input waveguide filter and the physical structure of the transition from the waveguide to the microstrip input of the transistor can be determined from the coupling matrix [m] in (13). The process and equations follow closely from just a simple filter [26], but with differences associated with new N+3 matrix. This process is discussed below.

The first step is to determine the inter-resonator coupling strength. As with just a conventional simple filter the coupling

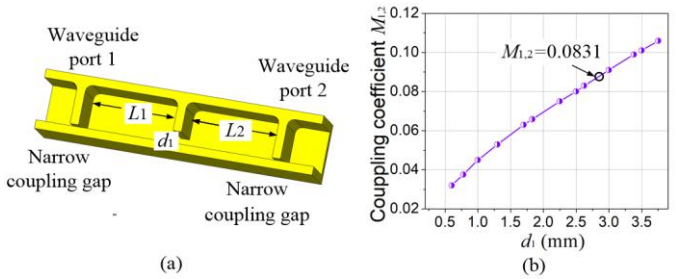

Fig. 6 Coupled waveguide cavities and the process to extract the coupling coefficients. (a) Structure to determine the physical dimension of the coupling aperture. (b) Coupling coefficients versus dimension d_1. All points are at 10 GHz.

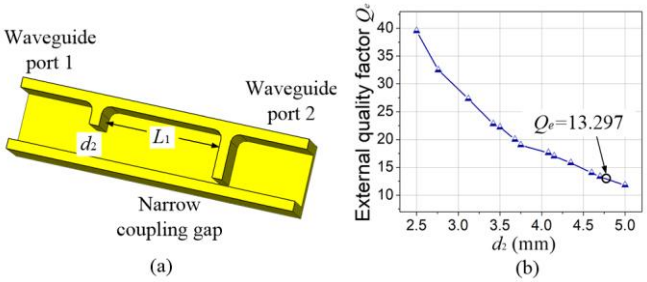

Fig. 7 Waveguide structure to extract quality factor for Resonator 1. (a) Structure to determine physical dimension for waveguide cavity with quality factor. (b) External quality factors Q_e versus dimension d_2. All points are at 10 GHz.

coefficient $m_{1,2}$=$m_{2,1}$ between the two resonators are scaled by the fractional bandwidth from the coupling matrix [m] in (13).

$$M_{1,2} = FBW \cdot m_{1,2} \quad M_{2,1} = FBW \cdot m_{2,1} \tag{15}$$

For this example, $M_{1,2}$=0.0831. The coupling coefficients can be realized by a suitable gap in the wall between waveguide resonators. A pair of waveguide coupled resonators, shown in Fig. 6(a), are simulated in a full wave simulator; CST [30] was used here. This is in order to find the target coupling coefficient $M_{1,2}$ [26]. There is weak coupling to the input and output via a narrow capacitive gap as shown in Fig. 6(a). The coupling coefficient $M_{1,2}$ between the two resonators can be altered by varying the iris gap d_1. A graph of the coupling coefficient $M_{1,2}$, as shown in Fig. 6(b), can be plotted [26]. The coupling coefficient given in (15) can now be located and is shown in Fig. 6(b) and hence a d_1 of 2.65 mm can be found.

The next step is to determine the iris size at port 1 of the waveguide filter. This can be done by extracting the external quality factor of Resonator 1 (Q_{e1}). In the N+3 coupling matrix, Q_{e1} is related to the external couplings $m_{P1,1}$= $m_{P1,1}$.

$$Q_{e1} = \frac{1}{FBW \cdot m_{1,P1}^2} = \frac{1}{FBW \cdot m_{P1,1}^2} \tag{16}$$

From (13) and (16) it is found that the external quality factor required is Q_{e1}=13.297. Fig. 7 shows the set up for determining Q_{e1} i.e. the quality factor at the input to the waveguide filter. The S-parameter response generated by simulating the single waveguide resonator in Fig. 7(a) is a single resonance curve and Q_{e1} is extracted by calculating its quality factor. Changing the iris length d_2 alters the values of Q_{e1}, and this is shown in Fig. 7(b). As shown in the graph, for the example, we can find a value of d_2=4.85 mm for the input iris to the filter. Note both the inter resonator coupling (Fig. 6(b)) and the external quality factor (Fig. 7(b)) are evaluated at 10 GHz, the centre frequency of the filter amplifier.

Now we need to consider the connection to the transistor via Resonator 2 as shown in Fig. 4. This comprises a combination of the waveguide cavity and planar circuit elements including the transistor itself. This is depicted in Fig. 8(a). Through an E-field probe, Resonator 2 is directly coupled to the transistor's input, which is a complex value impedance.

The coupling strength from the resonator to the transistor is related to $m_{P2,2}$=$m_{2,P2}$=2.3407, and the self-coupling $m_{2,2}$=-1.0762, and all these couplings can be achieved by constructing appropriate geometries of the structure shown in Fig. 8(a). The external coupling $m_{P2,2}$=$m_{2,P2}$ mainly depends on the coupling structure; that is the probe length l and the interconnecting transition length s. The self-coupling $m_{2,2}$ depends upon the resonant center frequency.

In the practical design, the external coupling $m_{P2,2}$=$m_{2,P2}$ and self-coupling $m_{2,2}$ can be determined by extracting the external quality factor (Q_{eT}) and the resonant frequency (f_T) of Resonator 2 incorporating the input of the transistor. The derivations of the frequency (f_T) and quality factor (Q_{eT}) are given in the Appendix and f_T and Q_{eT} can be calculated using the external coupling $m_{P2,n}$=$m_{n,P2}$ and self-coupling $m_{n,n}$. Significantly appendix also shows that f_T=f_0 and Q_{eT}=Q_{e1}, and this fact now allows the design procedure to continue in exactly the same way as for a conventional filter. That is the same as for the input port described above.

The whole structure includes the resonator itself and the complex input impedance of the transistor as well as the

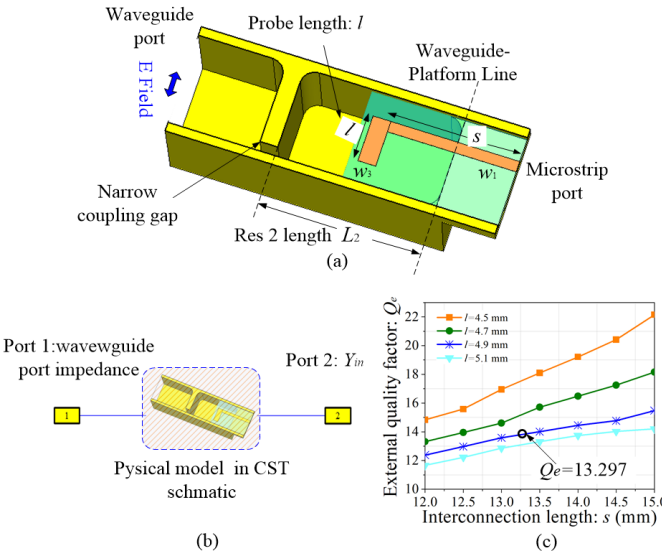

Fig. 8 Setup to extract external quality factor for resonator 2 incorporating the transistor's input. (a) Structure for extracting eternal quality factor of resonator 2 interconnecting the input of the transistor. (b) Q_{eT} extraction setup in CST. (c) External quality factor Q_e versus interconnection length s. All points are at 10 GHz.

transition from waveguide to microstrip. This mixed resonator-microstrip construction can be simulated in CST and the appropriate dimensions found to fulfil the requirement of, in this case, Q_{eT}=13.297 at the center frequency f_T=10 GHz.

The simulation of the single resonator, shown in Fig. 8(b), was performed in CST and a resonance frequency and external quality factor determined. As the setup schematically depicts in Fig. 8(b), the microstrip port is connected the port 2 in CST [30], with port 2 load set to be the input admittance of the transistor Y_{in}. Port 1 is set to be the value of waveguide impedance, then the whole structure is simulated. The center frequency is mainly determined by the length of the resonator (L_2), the length of the E-field probe (l) and the length of the feed transmission line (s). In the simulation, the width of the feed line and probe (w_1, w_3) are kept constant and only the dimensions of l and s are changed. During this tuning process, L_2 is adjusted to keep the center frequency at 10 GHz. The simulation results are shown in Fig. 8(c) from which the appropriate lengths of L_2, l and s, can be chosen to achieve the target Q_{eT}=13.297.

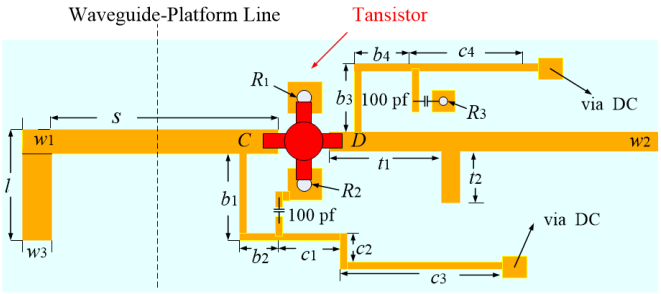

Fig. 9 Layout of microstrip transistor part. Length t_2 is a single stub matching for the output of the transistor to 50 Ω transmission line.

To complete the discussion, here we briefly consider the microstrip transistor circuit design. The microstrip part of the device consists of the probe, feed transmission line, transistor, bias circuits and output matching stub. The output matching network is assumed to conjugately match to Y_{ds} as shown in Fig. 2(a). The characteristic impedance of the output transmission line of width w_2 is 50 Ω. The lengths of t_1 and t_2 are found using the single stub matching method in [23]. The lengths b_1+b_2 and b_3+b_4 are quarter-wavelength long bias tees at 10 GHz center frequency, and are connected to the via-ground holes through 100 pf surface mount capacitors. Square pads are located at the end of the bias tees to connect the DC power. The ground of the PCB is connected to the base of the platform by pressure. The simulated operating conditions of the transistor are drain *to* source voltage V_{ds}=2 V and drain current I_{ds}=10 mA, [29]. The layout of the microstrip circuit is illustrated in Fig. 9.

The simulated noise performance for the matched amplifier is illustrated in Fig. 10. In the Smith chart (Fig. 10(b)), the impedance synthesized at the transistor input port is superimposed over the device noise and gain contours. The reflection coefficient looking into the source (see Fig. 10(a)) has been calculated [26] as Γ_S, as shown on the Smith chart (Fig. 10(b)), where 14.3 dB gain circle and 0.78 dB noise figure circle intersect. As the aim of our work is to demonstrate the filter-amplifier with Chebyshev response using the N+3

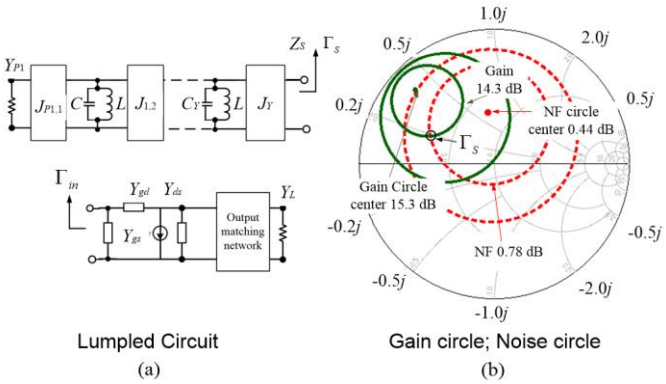

Fig. 10 Circuit design for the transistor amplifier. (a) Equivalent lumped circuit of the matching filter. (b) Constant-gain and constant–noise figure circles.

coupling matrix, this noise figure has not been optimized.

All the parameters necessary to form the filter-amplifier have been determined as discussed above, therefore the complete component can be simulated. The microstrip part including the transistor model is simulated in ADS to generate an S2P file [31]. Then, this co-simulation is combined in CST with the waveguide model and microstrip part for the complete filter-amplifier structure. The parameters used for the simulations are given in bold in Table II, and are the same as the values shown on the design graphs in Fig. 6(b), Fig. 7(b), and Fig. 8(c). Table II shows the initial values and optimized values. Optimization goals in this case are set to be: from 9.75 GHz to 10.25 GHz, S_{11} is under -20 dB; from 9.75 GHz to 10.25 GHz S_{22} is under -10 dB; critical points 9.725 GHz and 10.178 GHz are under -40 dB.

Both the initial response and an optimized response, using the sizes specified in Table II, are shown in Fig. 11. The optimized results in Fig. 11(a) and (b) show that over the passband S_{11} is below -20 dB, S_{21} shows gain around 13 dB, and S_{22} is below -10 dB. The good correlation of the initial and optimized responses demonstrates the validity of the coupling matrix technique in providing starting values for the waveguide filter-amplifier design process. Fig. 11(c) shows noise figure which is about 1.10 dB over the passband and the NFmin for the device is 1.02 dB at 9.85 GHz. The real and imaginary parts of the input impedance of the transistor are shown in Fig. 11(d).

TABLE II
VALUES OF INITIAL AND NORMALIZED FILTER-AMPLIFIER PARAMETERS

	Initial (mm)	Optimized (mm)		Initial (mm)	Optimized (mm)
L_1	**23.00**	**23.76**	w	**1.2**	**1.2**
L_2	**17.80**	**18.71**	b_1	**2.96**	**2.96**
d_1	**2.65**	**6.39**	b_2	**1.33**	**1.33**
d_2	**4.85**	**3.22**	b_3	**2.50**	**2.50**
l	**4.9**	**4.83**	b_4	**2.00**	**2.00**
s	**13.30**	**12.99**	c_1	**1.50**	**1.50**
R_1	**0.30**	**0.30**	c_2	**1.10**	**1.10**
R_2	**0.30**	**0.30**	c_3	**5.00**	**5.00**
R_3	**0.30**	**0.30**	c_4	**5.00**	**5.00**
w_1	**1.20**	**1.20**	t_1	**3.22**	**3.22**
w_2	**0.72**	**0.72**	t_2	**3.18**	**3.18**
w_3	**2.00**	**2.00**			

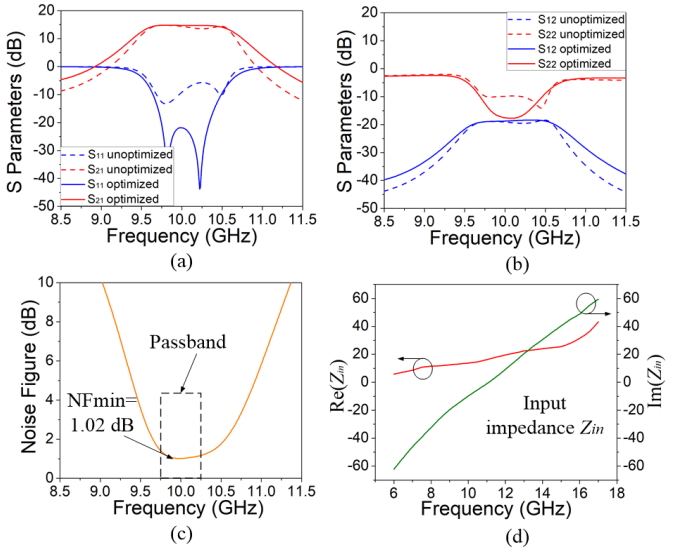

Fig. 11 Co-simulation results of waveguide filter integrated with amplifier. (a) Scattering parameters S_{11} and S_{21}. (b) Scattering parameters S_{22} and S_{12}. (c) Noise figure. (d) The input impedance of the transistor.

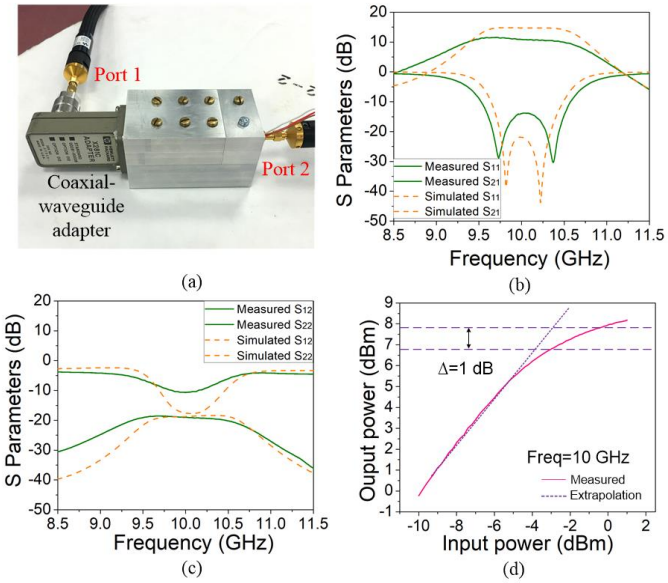

Fig. 13 Circuit simulation and measurement results. (a) Measurement setup. (b) Scattering parameters S_{11}, S_{21}. (c) Scattering parameters S_{22}, S_{12}. (d) P1dB measurement.

IV. Fabrication and Measurements

The waveguide structure is made in two halves cut along the E-plane and are machined from aluminum (AL5083) on a CNC machine. The microstrip circuit is fabricated on the 0.254 mm thick RT/5870 substrate. Fig. 12 shows a photograph of the device.

The measurement is performed using an Agilent PNA E8362B vector network analyzer referenced to the input and output ports. As the picture in Fig. 13(a) shows, a WR-90 coaxial to waveguide adapter is used at port 1, calibrated to the waveguide flange and the 50 Ω microstrip output is connected to the other port of the analyzer through an SMA connector. Bias condition of the transistor is provided by a gate to source voltage of V_{gs}=-0.52 V and drain to source voltage of V_{ds}=2.2 V. The measured *S*-parameters responses are compared with the simulation in Fig. 12(b) and (c) and display a good agreement with the 2-pole Chebyshev filtering characteristic and also a gain. The measured in-band small signal gain is within 11.0.7±0.46 dB from 9.75 GHz to 10.25 GHz. The measured input and output return loss are around 13.8 dB and 10.62 dB respectively, over the passband. The 1 dB compression point examined at 10 GHz is about -2.9 dBm as shown in Fig. 13(d).

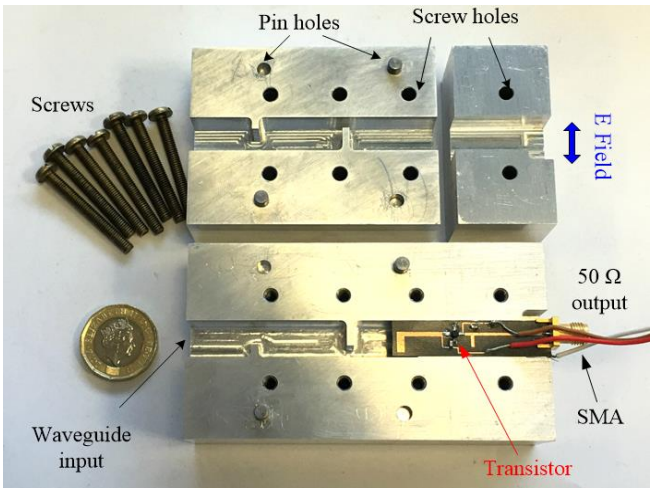

Fig. 12 Photograph for the fabricated device.

V. Conclusion

This paper described a novel active coupling matrix with transistor parameters included, it is used to synthesize a specified filter response including gain. The extended *N*+3 active coupling matrix builds on the general *N*+2 coupling matrix formulation. The resulting *N*+3 active coupling matrix can be used to generate the necessary matrix elements from which circuit optimization is performed. This allows the prediction of the response for the filter-amplifier and provides initial values of the waveguide filter structure. Semi empirical simulation trials can be used to realize the physical geometries corresponding to the matrix values for a given circuit technology. Further applications of matching a complex port through the resonator circuit can be generalized to other components e.g. mixers, antennas, etc.

The topology proposed here makes it possible to extend this methodology to amplifier circuits resonator matched both at the input and output ports. Although in this example only input resonators matching circuits are employed, this approach is currently being extended for matrix descriptions which incorporate both input, inter-stage and output resonators matching, for multistage amplifiers.

For this demonstrator, a microstrip circuit containing the transistor is combined with a WR-90 rectangular waveguide. Combining the filter design with the active element can allow for more compact components. Elements of the matching network have been transferred to waveguide resonators,

shrinking the overall size of the device and also increasing the port to port isolation. It is also noted that waveguide high-Q filter structures can be employed to offer lower loss impedance matching/filtering functions to the active devices. This latter effect will become more significant as the operating frequency, and therefore planar circuit losses, increase.

APPENDIX

Here we calculate the center frequency f_T and the external quality factor Q_{eT} of the last resonator in the filter when it is connected to the transistor input.

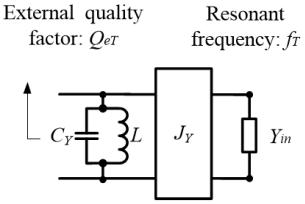

Fig. 14 Equivalent lumped circuit the N^{th} resonator coupled to the input admittance of the transistor.

The equivalent lumped circuit of the N^{th} resonator coupled to the input admittance of the transistor (Y_{in}) is illustrated in Fig. 14. The input admittance of the transistor Y_{in}, which is a complex value, is coupled through the inverter J_Y. Referring [24] and [25], the capacitor C_Y and the inverter J_Y can be expressed in terms of self-coupling $m_{n,n}$ and external couplings $m_{P2,n}$=$m_{n,P2}$ by

$$C_Y = C\left(1 - FBW \cdot m_{n,n}\right) \tag{17}$$

$$J_Y = \sqrt{FBW\,\omega_0 C \cdot Y_0}\cdot m_{n,P2} = \sqrt{FBW\,\omega_0 C \cdot Y_0}\cdot m_{P2,n} \tag{18}$$

where C is the capacitance of the 1st to the (N-1)th resonators in Fig. 2. The value of transistor's admittance Y_{in} is given by

$$Y_{in} = \left(a + jb\right)\cdot Y_0 \tag{19}$$

The input admittance of the circuit in Fig. 14 can now be calculated and compared with the standard equation for the admittance of a loaded resonant circuit. The input admittance (Y_{res}) of N^{th} the resonator incorporating Y_{in} can be expressed as

$$Y_{res} = j\omega C_Y + \frac{1}{j\omega L} + \frac{J_Y^2}{Y_{in}} \tag{20}$$

Substitute (17), (18) and (19) into (20), we have

$$Y_{res} = j\omega C\left(1 - FBW \cdot m_{n,n} - \frac{b \cdot FBW\,\omega_0 \cdot m_{P2,n}^2}{\left(a^2 + b^2\right)\cdot\omega}\right) + \frac{1}{j\omega L} + \frac{a \cdot FBW\,\omega_0 C \cdot m_{P2,n}^2}{\left(a^2 + b^2\right)} \tag{21}$$

At the center frequency, (ω_T), where for the narrowband approximation ($\omega = \omega_T$) as Y_{res} satisfies

$$\mathrm{Im}\left(Y_{res}\right)\Big|_{\omega=\omega_T} = 0 \tag{22}$$

Substitute (21) into (22), yielding

$$\left(\frac{\omega_0}{\omega_T}\right)^2 + \frac{b \cdot FBW \cdot m_{P2,n}^2}{\left(a^2 + b^2\right)}\left(\frac{\omega_0}{\omega_T}\right) - \left(1 - FBW \cdot m_{n,n}\right) = 0 \tag{23}$$

Then, (23) can be solved to give

$$\left(\frac{\omega_0}{\omega_T}\right) = \frac{-\frac{b \cdot FBW \cdot m_{P2,n}^2}{\left(a^2 + b^2\right)} \pm \sqrt{\left(\frac{b \cdot FBW \cdot m_{P2,n}^2}{\left(a^2 + b^2\right)}\right)^2 + 4\left(1 - FBW \cdot m_{n,n}\right)}}{2} \tag{24}$$

Because the ratio of ω_T and ω_0 should be positive, only the positive root is used. Substitute $\omega_T = 2\pi f_T$ and $\omega_0 = 2\pi f_0$ into (24), the center frequency f_T can be calculated as

$$f_T = \frac{2\left(a^2 + b^2\right)\cdot f_0}{b \cdot FBW \cdot m_{n,P2}^2\left(\sqrt{1 + \frac{4\left(1 - m_{n,n}\cdot FBW\right)\left(a^2 + b^2\right)^2}{b^2 \cdot m_{n,P2}^4 \cdot FBW^2}} - 1\right)} \tag{25}$$

As the admittance Y_{res} is given in (21), the external quality factor Q_{eT} can be calculated by [26],

$$Q_{eT} = \frac{f_T}{f_0}\left(\frac{\left(a^2 + b^2\right)}{a \cdot FBW m_{P2,n}^2} - \frac{m_{n,n}\cdot\left(a^2 + b^2\right)}{a \cdot m_{P2,n}^2}\right) - \frac{b}{a} \tag{26}$$

It is interesting to substitute $m_{P2,2}$=$m_{P2,2}$=2.3407 and $m_{2,2}$=− 1.0762 in the coupling matrix (13) into (25) and (26), the external Q of the Resonator 2 coupled with Y_{in} can be calculated to give Q_{eT}=13.297 and the resonant frequency is calculated as f_T=10 GHz.

Now, recalling $m_{P2,n}$=$m_{n,P2}$ and $m_{n,n}$ which are defined in (6) and (7). The final step is to substitute (6) and (7) into (25) and (26), respectively, to give the simple solutions

$$f_T = f_0 \tag{27}$$

$$Q_{eT} = \frac{g_n g_{n+1}}{FBW} = Q_{e1} \tag{28}$$

It can be seen from (27) and (28) that the external Q and center frequency of the resonator coupled with the active component are the same as the case for conventional filter [26]. That is

$Q_{eT}=Q_{e1}$ even though the load is complex. This fact allows the method of designing the filter amplifier to much more closely resemble the design of a standard filter [26].

ACKNOWLEDGMENTS

The authors would like thank to Prof. Peter Gardner and Dr. Timothy Jackson with the University of Birmingham for their assistance with the measurement and Mr Warren Hay for fabricating the waveguide.

REFERENCES

[1] W. Deal, X. B. Mei, K. M. K. H. Leong, V. Radisic, S. Sarkozy and R. Lai, "THz Monolithic Integrated Circuits Using InP High Electron Mobility Transistors," *IEEE Trans. THz Sci. Techn.*, vol. 1, no. 1, pp. 25-32, Sept. 2011.

[2] M. Abdolhamidi and M. Shahabadi, "X-Band Substrate Integrated Waveguide Amplifier," *IEEE Microw. Compon. Lett.*, vol. 18, no. 12, pp. 815-817, Dec. 2008.

[3] B. Ahmadi and A. Banai, "Substrateless Amplifier Module Realized by Ridge Gap Waveguide Technology for Millimeter-Wave Applications," *IEEE Trans. Microw. Theory Techn.*, vol. 64, no. 11, pp. 3623-3630, Nov. 2016.

[4] H. Yang *et al*., "WR-3 Waveguide Bandpass Filters Fabricated Using High Precision CNC Machining and SU-8 Photoresist Technology," *IEEE Trans. THz Sci. Techn.*, vol. 8, no. 1, pp. 100-107, Jan. 2018.

[5] X. Shang *et al*., "*W*-Band Waveguide Filters Fabricated by Laser Micromachining and 3-D Printing," *IEEE Trans. Microw. Theory Techn.*, vol. 64, no. 8, pp. 2572-2580, Aug. 2016.

[6] J. Q. Ding, S. C. Shi, K. Zhou, D. Liu and W. Wu, "Analysis of 220-GHz Low-Loss Quasi-Elliptic Waveguide Bandpass Filter," *IEEE Microw. Wirel. Compon. Lett.*, vol. 27, no. 7, pp. 648-650, July 2017.

[7] K. M. K. H. Leong, K. Hennig, Z. Chunbo, R. N. Elmadjian, Z. Zeyang, B. S. Gorospe, et al., "WR1.5 Silicon Micromachined Waveguide Components and Active Circuit Integration Methodology," *IEEE Trans. Microw. Theory Techn.*, vol. 60, pp. 998-1005, 2012

[8] B. Thomas *et al*., "A Broadband 835–900-GHz Fundamental Balanced Mixer Based on Monolithic GaAs Membrane Schottky Diodes," *IEEE Trans. Microw. Theory Techn.*, vol. 58, no. 7, pp. 1917-1924, July 2010.

[9] A. U. Zaman, V. Vassilev, P. S. Kildal and H. Zirath, "Millimeter Wave E-Plane Transition From Waveguide to Microstrip Line With Large Substrate Size Related to MMIC Integration," *IEEE Microw. Wirel. Compon. Lett.*, vol. 26, no. 7, pp. 481-483, July 2016.

[10] A. Aljarosha, A. U. Zaman and R. Maaskant, "A Wideband Contactless and Bondwire-Free MMIC to Waveguide Transition," *IEEE Microw. Wirel. Compon. Lett.*, vol. 27, no. 5, pp. 437-439, May 2017.

[11] Z. Y. Malik, A. Mueed and M. I. Nawaz, "Narrow band ridge waveguide-to-microstrip transition for low noise amplifier at Ku-band," *6th Inter. Bhurban Conf. on Appl. Sci. & Techn.*, Islamabad, 2009, pp. 140-143.

[12] P. G. Courtney, J. Zeng, T. Tran, H. Trinh and S. Behan, "120W Ka Band Power Amplifier Utilizing GaN MMICs and Coaxial Waveguide Spatial Power Combining," *2015 IEEE Comp. Semi. Integ. Circ. Symp. (CSICS)*, New Orleans, LA, 2015, pp. 1-4.

[13] T. B. Kumar, K. Ma and K. S. Yeo, "A 60-GHz Coplanar Waveguide-Based Bidirectional LNA in SiGe BiCMOS," *IEEE Microw. Wirel. Compon. Lett.*, vol. 27, no. 8, pp. 742-744, Aug. 2017.

[14] Y. C. Li, K. C. Wu and Q. Xue, "Power Amplifier Integrated With Bandpass Filter for Long Term Evolution Application," *IEEE Microw. Wirel. Compon. Lett.*, vol. 23, no. 8, pp. 424-426, Aug. 2013.

[15] Y. S. Lin, J. F. Wu, W. F. Hsia, P. C. Wang and Y. H. Chung, "Design of electronically switchable single-to-balanced bandpass low-noise amplifier," *IET Microw. Antennas Propag.*, vol. 7, no. 7, pp. 510-517, May 15 2013.

[16] S. F. Sabouri, "A GaAs MMIC active filter with low noise and high gain," 1998 *IEEE MTT-S Int. Microw. Symp. Digest* (Cat. No.98CH36192), Baltimore, MD, USA, 1998, pp. 1177-1180 vol.3.

[17] Young-Hoon Chun, Sang-Won Yun and Jin-Koo Rhee, "Active impedance inverter: analysis and its application to the bandpass filter design," *2002 IEEE MTT-S Int. Microw. Symp. Digest (Cat. No.02CH37278)*, Seattle, WA, USA, 2002, pp. 1911-1914 vol.3.

[18] L. Darcel, P. Dueme, R. Funck and G. Alquie, "New MMIC approach for low noise high order active filters," *IEEE MTT-S Int. Microw. Symp. Digest*, 2005., 2005, pp. 4 pp.-doi: 10.1109/MWSYM.2005.1516731.

[19] F. Bergeras, P. Duême, J. Plaze, L. Darcel, B. Jarry and M. Campovecchio, "Novel MMIC architectures for tunable microwave wideband active filters," 2010 *IEEE MTT-S Inter. Microw. Symp.*, Anaheim, CA, 2010, pp. 1-1.

[20] C. Y. Chang and T. Itoh, "Microwave active filters based on coupled negative resistance method," *IEEE Trans. Microw. Theory Techn.*, vol. 38, no. 12, pp. 1879-1884, Dec 1990.

[21] M. Ito, K. Maruhashi, S. Kishimoto and K. Ohata, "60-GHz-band coplanar MMIC active filters," *IEEE Trans. Microw. Theory Techn.*, vol. 52, no. 3, pp. 743-750, March 2004.

[22] Young-Hoon Chun, Jae-Ryong Lee, Sang-Won Yun and Jin-Koo Rhee, "Design of an RF low-noise bandpass filter using active capacitance circuit," *IEEE Trans. Microw. Theory Techn.*, vol. 53, no. 2, pp. 687-695, Feb. 2005.

[23] I. Bahl, *Fundamentals of RF and Microwave Transistor Amplifiers*. Hoboken, N.J.: Wiley, 2009. pp. 18-21.

[24] W. Xia. "Diplexers and multiplexers design by using coupling matrix optimization." Ph.D. dissertation. Elect. Eng, Birmingham Univ., Birmingham, 2015.

[25] R. J. Cameron, R. Mansour and C. M Kudsia, *Microwave Filters for Communication Systems: Fundamentals, Design and Applications*. 1st. New York, NY, USA: Wiley, 2007. pp. 283-288.

[26] J. S. Hong and M. J. Lancaster, *Microstrip Filters for RF/Microwave Applications*. New York, NY, USA: Wiley, 2001.

[27] H. Meng, P. Zhao, K. L. Wu and G. Macchiarella, "Direct Synthesis of Complex Loaded Chebyshev Filters in a Complex Filtering Network," *IEEE Trans. Microw. Theory Techn.*, vol. 64, no. 12, pp. 4455-4462, Dec. 2016.

[28] K. Kurokawa, "Power Waves and the Scattering Matrix," *IEEE Trans. Microw. Theory Techn.*, vol. 13, no. 2, pp. 194-202, Mar 1965

[29] California Eastern Labotatories (2004, July). CEL Corp., CA. [Online]. Available: http://www.cel.com/pdf/datasheets/ne3210s1.pdf

[30] Computer Simulation Technology, CST company, Germany.

[31] Advanced Design System, Agilent Technologies, USA.

Waveguide Filter Amplifier Integration using Coupling Matrix Technique

Yang Gao, Jeff Powell, Xiaobang Shang, *IEEE, Member*, Michael J. Lancaster, *IEEE, Senior Member*

***Abstract*—This letter introduces a novel integrated waveguide filter-amplifier component. The component is a combined filter and amplifier using a novel resonator based input and output matching structure. An *N*+4 active coupling matrix is proposed for the first time to describe the topology mathematically. To illustrate the concept, high-Q waveguide resonators are featured in the design of an X-band filter-amplifier, achieving simultaneous matching at both input and output. Easy integration of the transistor with waveguide resonators is carried out through filter synthesis, where a hybrid waveguide/microstrip structure is implemented for the impedance conversion. An X-band waveguide filter-amplifier is constructed as a demonstrator, but the technique is more valuable at higher terahertz frequencies where waveguide is widely utilized for its low loss.**

***Index Terms*—Active coupling matrix, transistor, resonator, waveguide filter amplifier.**

VI. Introduction

Filters and amplifiers are often designed separately with a common 50-Ω impedance and then assembled. Planar matching circuits are required with a microstrip amplifier in order to attain the 50-Ω impedance. If a waveguide system is ultimately the goal, then a conversion from the waveguide to 50-Ω impedance of a coaxial connector or microstrip is required. Clearly, there is loss in these circuits, which can be significant when frequencies rise to submillimetre-wave. Thus, a co-design approach is proposed here where the waveguide filter is integrated as closely as possible to the amplifier using resonators directly coupled to the transistor's input, removing the restriction of having to translate to the common impedance via matching networks. This yields minimized losses and reduced circuit size and complexity.

Here, we propose the structure of a filter-amplifier with resonators matching at both the input and output ports with the whole structure being expressed using an *N*+4 coupling matrix. Complex valued input and output impedances of the transistor are matched simultaneously, achieving specified S_{11} and S_{22} as well as an S_{21} response with gain over the passband. A Chebyshev filtering response is used as an example. Novelty also lies in the use of waveguide resonators coupled to a microstrip based transistor amplifier using the inherent low loss of the waveguide resonators.

Fig. 1 (a) shows the circuit schematically with clear circles representing the source and the load, and solid black circles

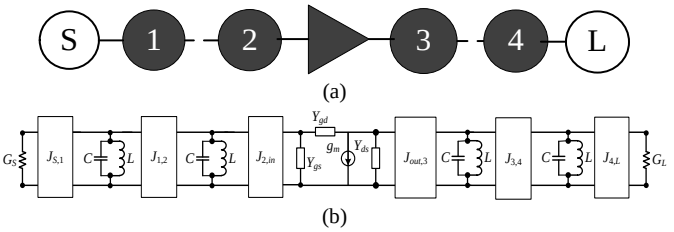

Fig. 1 Lumped circuit and topology of the transistor with input and output resonators matching. (a) Schematic representation of the circuit. (b) Lumped circuit model. G_S and G_L are the source and load conductance; Y_{gs}, Y_{gd}, and Y_{ds} are the admittances between transistor's gate, source and drain; g_m is the transconductance.

denoting the resonators. This can be translated into the small signal lumped circuit with the transistor coupled by *J* inverters to the resonator based filters at the gate and the drain as shown in Fig. 1 (b).

An *N*+4 active coupling matrix, which factors include the parameters of the transistor, is introduced to characterize the performance of the filter-amplifier. Here *N* is the number of the resonators. Given the filter specification and the transistor's parameters, the *S*-parameters response with gain can be predicted using the *N*+4 matrix.

VII. The Active *N*+4 Coupling Matrix

Based on the *N*+2 coupling matrix theory described in [25], and the active *N*+3 coupling matrix synthesized in [2], the *N*+4 active coupling matrix representing the integrated filter amplifier is given by,

$$[m]=\begin{bmatrix} 0 & m_{S,1} & 0 & 0 & 0 & 0 & 0 & 0 \\ m_{1,S} & 0 & m_{1,2} & 0 & 0 & 0 & 0 & 0 \\ 0 & m_{2,1} & m_{2,2} & m_{2,in} & 0 & 0 & 0 & 0 \\ 0 & 0 & m_{in,2} & 0 & m_{in,out} & 0 & 0 & 0 \\ 0 & 0 & 0 & m_{out,in} & 0 & m_{out,3} & 0 & 0 \\ 0 & 0 & 0 & 0 & m_{3,out} & m_{3,3} & m_{3,4} & 0 \\ 0 & 0 & 0 & 0 & 0 & m_{4,3} & 0 & m_{4,L} \\ 0 & 0 & 0 & 0 & 0 & 0 & m_{L,4} & 0 \end{bmatrix} \quad (1)$$

This work was supported in part by the UK Engineering and Physical Science Research Council (EPSRC) under Contract EP/M016269/1. The authors are with the Department of Electronic, Electrical and Systems Engineering, University of Birmingham, Birmingham, B15 2TT, UK (Email: yxg311@bham.ac.uk).

Here we use N=4 representing the circuit shown in Fig. 1, but obviously this can be changed to any value of N. In (1) $m_{i,j}$ is the inter-resonator coupling; $m_{S,1}$=$m_{1,S}$ and $m_{L,4}$=$m_{4,L}$ are the external couplings from the resonators to the source and load; $m_{2,in}$=$m_{in,2}$ and $m_{out,3}$=$m_{3,out}$ are the couplings from the resonators to the transistor's gate and drain. $m_{in,out}$ and $m_{out,in}$ are the couplings between the transistor's input and output and are given in terms of the transistors parameters as [2], [3]

$$m_{in,out} = \frac{\bar{Y}_{gd}}{j}, m_{out,in} = \frac{\bar{Y}_{gd} - \bar{g}_m}{j} \tag{2}$$

The bar on the variable is used to indicate that the transistor's parameters have been normalized to and identity port impedance of 1 Ω. Here the coupling from the drain to gate $m_{in,out}$ is assigned to be zero, as the parasitic parameters between the transistor's gate and drain are usually very small [3], [4]. The terms $m_{2,2}$, and $m_{3,3}$, in (1) correspond to a frequency shift of the resonators adjacent to the transistor, allowing Chebyshev (or other) filter response to be maintained despite the complex impedance of the transistor. Here $m_{2,2}$ and $m_{3,3}$ are calculated by

$$m_{2,2} = -\frac{\mathrm{Im}\left(\bar{Y}_{gs}\right)}{\mathrm{Re}\left(\bar{Y}_{gs}\right)\cdot q_{e2}}, m_{3,3} = -\frac{\mathrm{Im}\left(\bar{Y}_{ds}\right)}{\mathrm{Re}\left(\bar{Y}_{ds}\right)\cdot q_{e3}} \tag{3}$$

q_{ei} is the i^{th} resonator normalized external quality factor [26]. Couplings between the transistor and the resonators are given by

$$m_{in,2} = m_{2,in} = \sqrt{\frac{\mathrm{Re}^2\left(\bar{Y}_{gs}\right)+\mathrm{Im}^2\left(\bar{Y}_{gs}\right)}{\mathrm{Re}\left(\bar{Y}_{gs}\right)\cdot q_{e2}}}$$
$$m_{out,3} = m_{3,out} = \sqrt{\frac{\mathrm{Re}^2\left(\bar{Y}_{ds}\right)+\mathrm{Im}^2\left(\bar{Y}_{ds}\right)}{\mathrm{Re}\left(\bar{Y}_{ds}\right)\cdot q_{e3}}} \tag{4}$$

The other elements in [m] can be calculated in the normal way from the standard filter g values according to [26].

As an example, 2-pole Chebyshev filters are implemented before and after the transistor. A center frequency f_0 of 10 GHz, a bandwidth of 500 MHz (fractional bandwidth FBW=0.05) and a passband return loss of 20 dB is used. According to the filter specification and the normalized transistor's parameters in Table 1, the normalized N+4 coupling matrix [m] can be calculated as

$$[m] = \begin{bmatrix} 0 & 1.2264 & 0 & 0 & 0 & 0 & 0 & 0 \\ 1.2264 & 0 & 1.6621 & 0 & 0 & 0 & 0 & 0 \\ 0 & 1.6621 & -8.2104 & 3.4219 & 0 & 0 & 0 & 0 \\ 0 & 0 & 3.4219 & 0 & 0 & 0 & 0 & 0 \\ 0 & 0 & 0 & 6.75+3.4812j & 0 & 1.6216 & 0 & 0 \\ 0 & 0 & 0 & 0 & 1.6216 & -3.4800 & 1.6621 & 0 \\ 0 & 0 & 0 & 0 & 0 & 1.6621 & 0 & 1.2264 \\ 0 & 0 & 0 & 0 & 0 & 0 & 1.2264 & 0 \end{bmatrix} \tag{5}$$

Referring to [25] and [2], the S-parameters response calculated using the coupling matrix in (5) as shown in Fig. 2, which shows Chebyshev responses for S_{11} and S_{22} with S_{21} showing a gain as expected.

TABLE III
VALUES OF THE NORMALIZED TRANSISTOR'S SMALL SIGNAL PARAMETERS

Y parameters	Value	Normalized Y parameters	Value
$\bar{Y}_{ds}$	**0.2752+ 0.6367*j***	$\bar{g}_m$	**3.4812- 6.7500*j***
$\bar{Y}_{gs}$	**0.2528+ 1.3799*j***	$\bar{Y}_{gd}$	**0**

All parameters are calculated from the data sheet [29] as the transistor operating at 10 GHz.

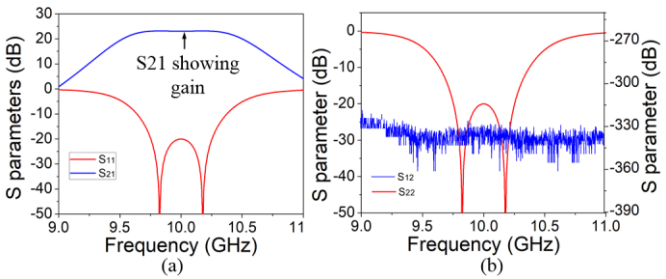

Fig. 2 Calculated filter-amplifier responses using the coupling matrix formulation. (a) S_{11} and S_{21}. (b) S_{22} and S_{12}.

VIII. PHYSICAL DESIGN OF WAVEGUIDE FILTER-AMPLIFIER

The design of the physical structure is comprised of the waveguide resonators and the transistor mounted on a printed circuit board (PCB) and is illustrated in Fig. 3. The transistor PCB is placed on a platform in the middle of the waveguide which is reduced in height and beyond cut-off. The feeding structures on the PCB, coupling Resonator 2 and Resonator 3 to the transistors' gate and drain, are probes of length l_1 and l_2 on the end of feed lines of lengths s_1 and s_2. The waveguide filters are formed of four TE_{101} waveguide cavities. value of this external Q of Resonator 1 and Resonator 4, are calculated from the couplings matrix (5) by

$$Q_{e1} = \frac{1}{FBW \cdot m_{S,1}^2}, Q_{e4} = \frac{1}{FBW \cdot m_{L,1}^2} \tag{6}$$

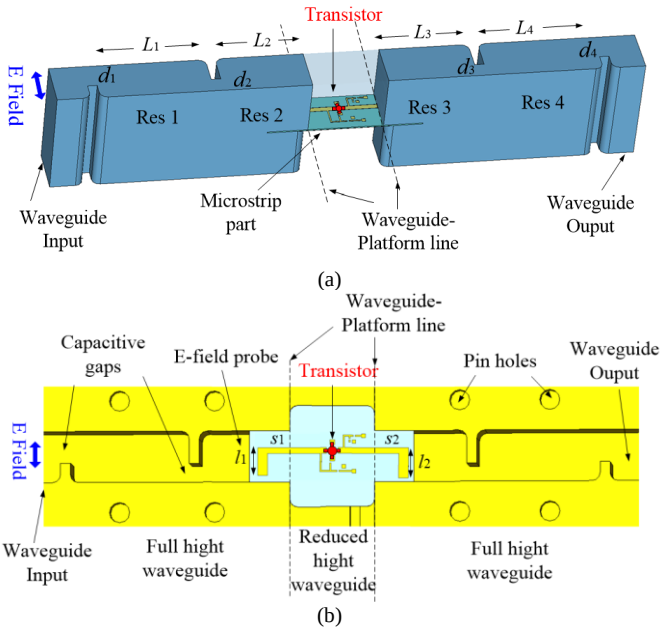

Fig. 3 Illustration diagrams of waveguide filter-amplifier. (a) 3D view of the internal waveguide with the microstrip circuit. (b) Sectional view of the waveguide filter and on-chip transistor circuit.

The gaps d_1 and d_4, which determine external couplings can be determined by extracting the external Q [26]. In this case Q_{e1}=Q_{e4}=13.297, and sizes of d_1, d_4 can be found from the graph of d_1, d_4 versus Q_e shown in Fig. 4 (a).

The length of l_1, l_2, s_1 and s_2 can be determined by extracted external Q of the resonator coupled to transistor's input and output impedances. This assembles to the design of a conventional filter [2]. The external Q of the Resonator 2 coupled with transistor input and Resonator 3 coupled with transistor output are given by Q_{e3}=Q_{e1}=13.297 and Q_{e3}=Q_{e1}=13.297 [2]. The design requires that the resonators 2 and 3 are kept at the 10 GHz center frequency of the filter, and this is done by adjusting the lengths of the resonator L_2 and L_3. The appreciated lengths of l_1, l_2, s_1, and s_2 can be found from the graph of Q_e versus interconnection length s_1, s_2 in Fig. 4(b).

The couplings between Resonators 1 and 2 and Resonators 2 and 3 are determined the by sizes of irises, where the dimensions can be extracted from the graph of d_2, d_3 versus coupling coefficient $M_{i,j}$ shown in Fig. 4(a).

The whole structure is simulated in CST using the initial value extracted above. Then, the optimization is performed by the EM simulator, and the results are shown Fig. 4(c) and (d). It should be noted that the optimized results are close to the initial results showing the accuracy of the technique.

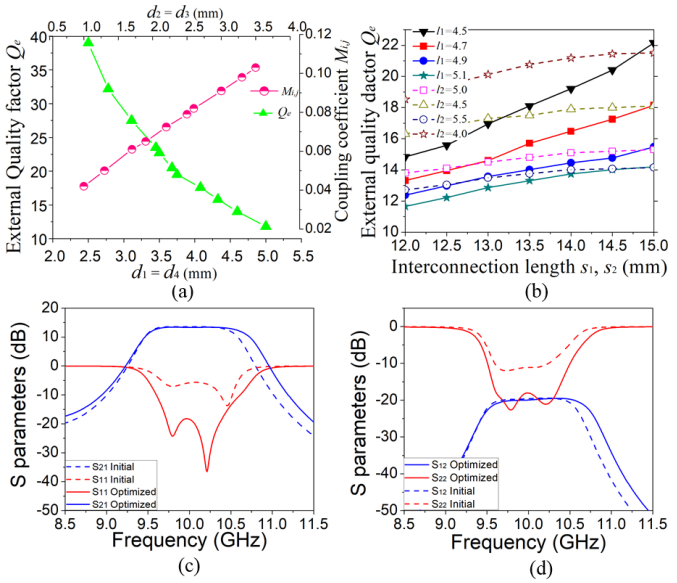

Fig. 4 (a) External quality factor Q_e versus dimension d_1, d_4; Coupling coefficient versus dimension d_2, d_3. (b) External quality factor Q_e versus dimension s_1, s_2. (c) Simulation response with initial and optimized values S_{11} and S_{21}. (b) S_{22} and S_{12}.

IX. Fabrication and Measurements

The waveguide parts are made of aluminum (AL5400), and Duroid RT/5870 is utilized as the PCB substrate for the microstrip. Fig. 5 shows the photo of microstrip sandwiched by the two split-block waveguides. Measurement results are presented in Fig. 6, together with the CST EM simulations. The measurement result shows two reflection poles in both S_{11} and S_{22} responses providing evidence of the two pole filter designs operating well. The measured S_{21} shows a filtering response

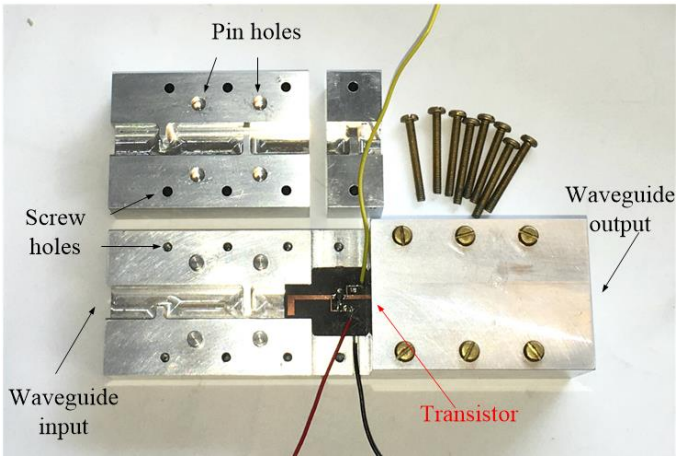

Fig. 5 Photograph of the fabricated waveguide filter-amplifier device.

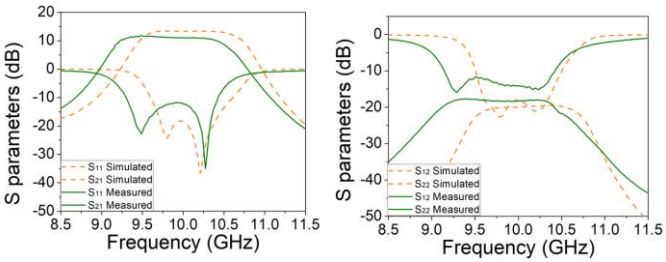

Fig. 6 Simulation (dashed lines) and measurement (solid lines) results. (a) Scattering parameters S_{11}, S_{21}. (b) Scattering parameters S_{22}, S_{12}.

with a gain of around 10 dB across the passband. The generally good agreement between measurement and simulation validates the methodology of the co-design of the filter-amplifier.

X. Conclusion

This letter introduces a novel active N+4 coupling matrix describing the entire filter-amplifier component. The N+4 matrix describes complex impedance conversion and the active elements as well as achieving the Chebyshev response at the two ports including gain. Appropriate initial dimensions of the physical structure are found from the coupling matrix and can be used for final optimization. By the co-design approach, the conventional planar matching network, to a common impedance, can be eliminated by the waveguide resonators, shrink the overall size of the device and remove additional loss. As waveguide technology is widely utilized in terahertz systems, where on-chip losses can be substantial, the technique is expected to be of advantage at these higher frequencies.

References

[1] R. J. Cameron, R. Mansour and C. M Kudsia, *Microwave Filters for Communication Systems: Fundamentals, Design and Applications*. 1st. New York, NY, USA: Wiley, 2007.

[2] Y. Gao, J. Powell, X. Shang, M. J. Lancaster, "Coupling Matrix based Design of a Novel X-band Filter Amplifier", unpublished.

[3] I. Bahl, Fundamentals of RF and Microwave Transistor Amplifiers. Hoboken, N.J.: Wiley, 2009.

[4] D. Pozar, *Microwave engineering*. Hoboken, NJ: Wiley, 2012.

[5] J. S. Hong and M. J. Lancaster, *Microstrip Filters for RF/Microwave Applications*. New York, NY, USA: Wiley, 2001.

[6] California Eastern Labotatories (2004, July). CEL Corp., CA. [Online]. Available: http://www.cel.com/pdf/datasheets/ne3210s1.pdf